Synthesis, Characterization and High Pressure Propene Oligomerization Over Heteropoly Acids, SAPO-11 and MeAPSO-11 molecular sieves

By

James Stuart Vaughan BSc (Chem. Eng.)

Submitted to the University of Cape Town in fulfillment of the requirements for the degree of

DOCTOR OF PHILOSOPHY

Department of Chemical Engineering

University of Cape Town

Rondebosch

Cape Town

South Africa

26th August 1993

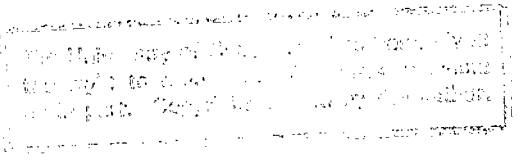

Acknowledgements

I would like to thank to my supervisors Professor Cyril O'Connor and Dr Jack Fletcher for all their assistance and guidance without which this thesis would not have been possible. My thanks also go to Professor Mark Dry for his time and effort in proof reading and commenting on the oligomerization sections of this thesis.

A special thanks also to the old guard, Stefan, Bo, Alex, Miles, Rein and Martin who imparted not only their knowledge but also valued friendship. Thanks to all the other catalyst guys (and girls), Jannie, Sarah, Tony, Gary, Ansgar, for some great times. Thank you also to Barry for all his help with the FT-IR work.

Dear Connie and Leslie, many thanks for all your help, I shall miss you both. Thanks also to Pam for all your help with ordering equipment and numerous other things.

I would like to thank all the members of staff for their help throughout my stay in the department, especially Prof. B.D.A. Paddon and Dr. Jim Petrie.

A big thank you to Steve Langford, my old buddy, may "Nige" (the best F1 driver ever to have lived) keep on going strong.

I would also like to thank Klaus for his help with so many things, the department is lucky to have you. Thanks also to Bill, Tony, Peter, Rob, Granville, James, John and Martin in the workshops for all their hard work and for the manufacture of some fine pieces of equipment.

I would like to thank Mintek for funding me throughout my post-graduate studies and I would also like to thank the FRD, SASOL, AECI and other sponsors of the CRU at UCT.

Last but not least to my parents, Gordon and Vanessa, and my sister and brothers Sammy, Graeme, Gavin and Nanu-Nanu and my wife Monique, thanks for being the best friends I could ever wish for.

SYNOPSIS

Heteropoly acids, HPAs, and SAPO-11 and MeAPSO-11 molecular sieves have been proposed to be active for the oligomerization of propene to high quality distillate fuels. In this study these catalysts have been synthesized, characterized, modified and screened for the oligomerization of propene to distillate fuels.

Heteropoly acids consist of high molecular weight poly-oxoanions, counter cations and water of hydration and are strongly acidic. The following salts of 12-tungstophosphoric acid, a 12-type HPA with the Keggin anion structure, were synthesized: Al, Fe, Ce, Ni, Co, Cu, K and NH_4, as well as the Al and NH_4 salts of 12-tungstosilicic acid. Physicochemical characterization of the HPA salts revealed that, depending on the counter cation, these salts exhibited different thermal characteristics and surface areas. The salst were calssified into two types, *viz.*:

Type A:- low surface area salts, typically less than 15m^2/g, with multiple endothermic mass losses (e.g. Al, Fe, Ce, Ni, Co, Cu) and;

Type B:- high surface area salts, typically 35-150 m^2/g, with a single endothermic mass loss (e.g. K and NH_4).

The Type A salts were multi-crystalline, consisting of more than one phase, and exhibited a non-uniform morphology. The Type B salts, on the other hand, were uniformly crystalline and consisted of small rounded cubic crystallites. Ammonia desorption, monitored by both TCD and FT-IR, revealed that both the Type A and B salts were strongly acidic with the majority of the ammonia being released only upon decomposition of the salt. However, as ammonia and other polar molecules are known to readily absorb into the bulk of HPAs, the ammonia TPD results did not correlate with catalytic activity for surface type reactions such as alkene isomerization and oligomerization. The Type B salts were active for cracking and skeletal isomerization reactions which suggested strong acid sites were present on their surface. The Type A salts only exhibited double bond shift isomerization activity, suggesting sites of only weak to medium acid strength.

Heteropoly acids, and more specifically the Al salt of HPW, were found to be particularly active for the oligomerization of propene, but many of the salts deactivated rapidly due to the formation of Type II polyaromatic coke. The activity order for oligomerization at 230-240°C, WHSV = 12 h^{-1} and 5 MPA, decreased in the order: AlPW >> CoPW > NH4PW ≃ NiPW > CuPW ≃ HPW > CePW ≃ FePW > KPW. Sand dilution dramatically increased the oligomerization activity and lifetimes of all the catalysts, primarily by improving heat transfer from the catalyst into the bulk. This reduced the formation of local hot spots which initiated the formation of deactivating Type II coke. In addition to studying the pure catalysts, modifications such as supporting on high surface area supports were also investigated. The activities of supported HPW and HSiW were higher than their unsupported forms but with increasing shelf time the activity of HPW on α-alumina decreased. Since HPAs are strongly acidic they are affected by the presence of any residual basic material and, hence, supports such as alumina result in gradual decay of the HPA.

The activity of AlPW was sensitive to both water present in the feed and to steaming, both of which resulted in the deactivation of the pure undiluted catalyst. Sand diluted AlPW did not deactivate when steamed or when water was added to the feed.

The major product of propene oligomerization was the trimer. Cetane numbers of unfractionated hydrogenated liquid products were in the region of 25-40. As expected these values increased after fractionation. Increasing the reaction temperature from 230-310°C resulted in a lower selectivity to distillate products.

The SAPO-11 molecular sieve is a medium-pore silicoaluminophosphate which is mildly acidic. Substitution of metals into the framework of SAPO-11, i.e. to form MeAPSO-11 sieves, is proposed to modify the sieves' acidity. SAPO-11 and MeAPSO-11 (where Me = Co, Mn, Ni and Fe) sieves were synthesized according to the relevant patents. Characterization showed that the SAPO-11 and MeAPSO-11 materials contained varying degrees of extra-framework metal species. All the sieves were mildly acidic and addition of Co and Mn to the SAPO-11 synthesis gel resulted in an increase in the number of acid sites versus that of SAPO-11. This is consistent with Me^{2+} substitution for Al^{3+} in the framework of SAPO-11. Ni

and Fe were proposed not to enter the framework of SAPO-11 but rather to occupy either ion-exchange positions or exist in iron-aluminium phosphate/iron oxide phases (Fe^{3+} in octahedral coordination), respectively. The location and state of these extra-framework correlates with the catalytic activity of these materials as was shown by probe reaction studies. Extra-framework species prevented access of reactant (2-methyl-2-pentene) to acid sites thereby reducing catalytic activity. In the case of FeAPSO-11 extra-framework species were believed to be responsible for the formation of large quantities of disproportionation products during *m*-xylene isomerization.

A number of post-synthesis modifications were made in order to possibly improve lifetimes and to investigate the effect of metals on catalytic activity. These modifications included:

(i). **acid washing** to remove extra-framework species from the pores.

(ii) **silanization** to reduce external acidity and reduce coke formation on the outer surface.

(iii) **ion-exchange** to remove extra-framework cations/metals and increase acidity.

(iv) **metal impregnation** to investigate the effect of metals in extra-framework positions.

(v) mild and severe **steaming** to reduce acidity and study the effects of hydrothermal treatment

Characterization of these modified sieves indicated reduced pore volumes and, in the case of acid washing, silanization and steaming, a reduction in the number of acid sites. The SAPO-11 sieves were not resistant to acid attack. Ion-exchange with ammonium nitrate resulted in phosphorous extraction from the framework or removal of extra-framework phosphorous species from the sieves. Metal impregnation did not reduce the number of acid sites.

Except in the case of Mn, metal addition to the SAPO-11 synthesis gel reduced the oligomerization performance of the resulting catalysts as per SAPO-11 ≃ MnAPSO-11 > CoAPSO-11 ≃ FeAPSO-11 > NiAPSO-11 (250°C, WHSV = 12h^{-1} and pressure = 5 MPa). It was proposed that the MeAPSO-11 sieve deactivated due the inability of product oligomers to desorb from pores constricted with extra-framework species. SAPO-11 deactivated due to "hard" coke formation which was proposed to constrict the pores thus preventing access of propene to the acid sites and/or the desorption of product oligomers from the pores.

All of the post-synthesis modifications, except steaming, resulted in reduced oligomerization performance. Mild and severe steaming improved the catalyst performance compared to SAPO-11 and mild steaming increased the cetane number of the distillate product.

Commercial processes have been developed for the oligomerization of olefins to distillate type fuels over ZSM-5 and solid phosphoric acid (CATPOLY) catalysts. AlPW produces a distillate fuel of similar quality to these catalysts but with a lower distillate yield compared to ZSM-5. SAPO-11 produces a distillate with a higher cetane value than ZSM-5 and CATPOLY. However, the yield of distillate is very low making the use of this catalyst in industry unlikely.

TABLE OF CONTENTS

LIST OF FIGURES

List of Tables

Chapter 1
Introduction

1. INTRODUCTION

1.1 SYNTHETIC FUELS

The origin of synthetic fuels production in South Africa lies in the formation of the South African Coal, Oil and Gas corporation (SASOL) in 1950. SASOL produces liquid fuels via the Fischer-Tropsch (FT) process, first reported in 1923 by Franz Fischer and Hans Tropsch, and involves the conversion of CO and H_2 (syngas) to hydrocarbons using an alkylized iron catalyst [Dry, 1981].

The first commercial FT plant in South Africa, SASOL 1, was commissioned at Sasolburg in 1955. This was followed by the construction of two much larger plants, namely SASOL 2 and 3, a direct result of the OPEC oil crisis in 1973. The general layout of SASOL 3 at Secunda is shown in Figure 1.1. More recently the discovery of natural gas deposits at Mossel Bay has prompted the construction of another FT plant (MOSSGAS) to convert natural gas to liquid fuels.

The primary products of (high temperature) FT are olefins, whereas the major end product requirements of the SASOL plants are ethene, gasoline and diesel [Dry,, 1982a, 1982b]. At present the propene and butenes and some of the C_5 olefins from FT are oligomerized to form gasoline and diesel via the CATPOLY process. A plant at Secunda has been constructed to convert propene to higher value polypropylene [Dry 1990]. Plans are also under way to utilize the C_4-C_6 olefins to form higher value products (e.g. isomerization of 1-butene to isobutene for MTBE production and the recovery of 1-pentene and 1-hexene for sale as comonomers in polyethylene production) and to convert SASOL 1 into a high value chemicals plant, mainly for the production of waxes. Tables 1.1 and 1.2 show the composition of the products from the SASOL fixed bed and Synthol reactors. As can be seen for the higher temperature Synthol reactors less than 50% of the products fall in the gasoline and diesel range and substantial amounts of C_3 and C_4 alkenes are also produced. The situation is even less favorable for the low temperature fixed bed reactors which produce less than 32% of the products in the gasoline and diesel range.

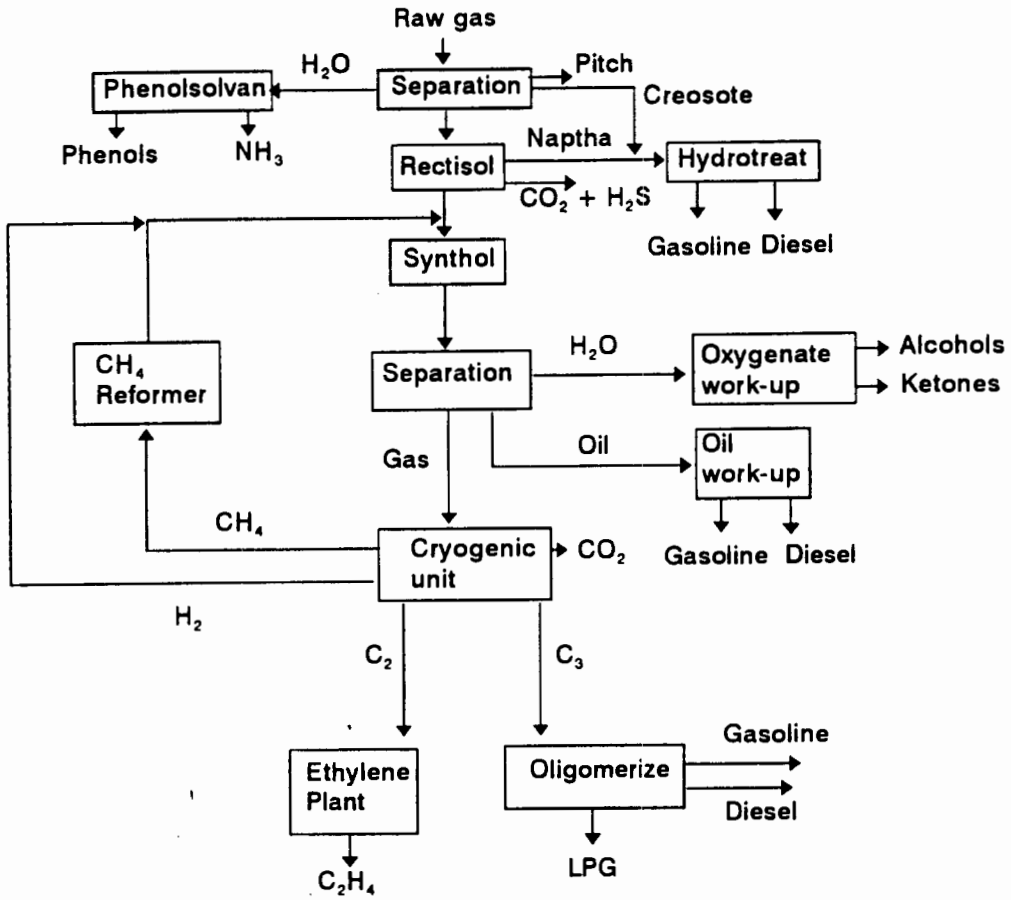

Figure 1.1 Flow sheet of SASOL 3.

Table 1.1 Products of the SASOL Fixed Bed and Synthol Reactors. [Dry, 1982b]

Product	Composition % carbon atom	
	Fixed Bed (493K)	Synthol (598K)
CH_4	2.0	10
C_2H_4	0.1	4
C_2H_6	1.8	4
C_3H_6	2.7	12
C_3H_8	1.7	2
C_4H_8	3.1	9
C_4H_{10}	1.9	2
C_5 to C_{11} (Gasoline)	18	40
C_{12} to C_{18} (Diesel)	14	7
C_{19} to C_{23}	7	-
C_{24} to C_{35} (Medium Wax)	20	4
> C_{35} (Hard Wax)	25	-
Water soluble non-acid chemicals	3.0	5
Water soluble acids	0.2	1

Table 1.2 Properties of Products from SASOL Reactors. [Dry, 1982b]

Product Cut	Property	Arge Fixed Bed[1]	Synthol
Gasoline C_5-C_{11}	Olefins	32	65
	Paraffins	60	14
	Aromatics	0	7
	Alcohols	7	6
	Ketones	0.6	6
	Acids	0.4	2
	n-Paraffins	95[2]	55[2]
	RON[3] (Pb free)	*ca.* 35	88
Diesel C_{12}-C_{18}	Olefins	25	73
	Paraffins	65	10
	Aromatics	0	10
	Alcohols	6	4
	Ketones	<1	2
	Acids	0.05	1
	n-Paraffins	93[2]	60[2]
	Cetane No	75	55
Medium Wax C_{24}-C_{35}	Olefins	10	

1. wt% of cut except for RON and Cetane No.
2. % of paraffins which are straight chained.
3. Research octane number.

There are a number of problems associated with fuel production via the FT process. As can be seen from Table 1.2, at low temperatures the majority of the products are linear 1-alkenes, alkanes, alcohols and aldehydes. While the linearity of these products provides the waxes with a unique combination of high melting point and low viscosity and the diesel cut with a high cetane number (75) and zero aromatics content it produces a gasoline that requires extensive upgrading. Such upgrading involves the isomerization of C_5 and C_6 alkenes and platforming the C_7-C_{11} fraction. This gasoline can then be blended with that obtained from the CATPOLY oligomerization plant to provide a lead free fuel with a RON = 93 [Brink and Swart, 1982]. The diesel product from the oligomerization plant is too branched and the hydrogenated products only yield a cetane number of 33-35. Blending the oligomerization diesel with Synthol diesel results in a product that has a cetane number of 46 [Brink and Swart, 1982]. Although this conforms to South African standards, SASOL are concerned about the poor quality of South African diesel. At higher oligomerization reaction temperatures secondary reactions occur (e.g. aromatization), which

increases the gasoline octane number but further decreases the cetane number of the blended diesel fraction.

Another associated problem of the SASOL FT process is connected to the South African market forces. The market demands a gasoline to diesel ratio of about 1:1 [Dry, 1990]. The Synthol reactors typically produce a ratio of *ca.* 3:1. This ratio cannot be simply increased since the FT process is limited to a maximum of about 25% diesel fraction according to the Schulz-Flory distribution [Jager *et al.*, 1982]. To increase the diesel yield SASOL can employ two secondary processes, namely olefin oligomerization (CATPOLY) and wax cracking, both of which are not as economically viable as upgrading the starting materials to higher value products (e.g. polypropylene) or as valuable as the products themselves (as in the case of the waxes).

The SASOL process is therefore not optimal. Firstly the demands on the market place cannot be easily met and secondly the gasoline produced is of poor quality while the blended diesel fuels have less than desired cetane numbers. Hence there is a great demand for alternative routes to liquid fuels, particularly in the distillate range and some of these routes are briefly mentioned below.

1.1.1 Low temperature fixed bed Fischer-Tropsch (FT) process

Tables 1.1 and 1.2 show that the Arge Fixed bed reactors produce far better diesel fuels that the Synthol reactors. By varying reactor conditions it is possible to vary the gasoline to diesel ratios between 3:1 to 6:1 with cetane numbers of approximately 65.

1.1.2 Methanol conversion

Methanol has recently become an important feedstock for the production of high quality gasoline. In combination with the existing technology available for the conversion of coal, natural gas and biomass to methanol, these processes have provided the final link in a new route for the production of liquid fuels using zeolite molecular sieve catalysts [Tabak and Yurchak, 1990]. This new route is illustrated in Figure 1.2 and the methanol to

gasoline (MTG) and methanol to olefins (MTO) processes are discussed below.

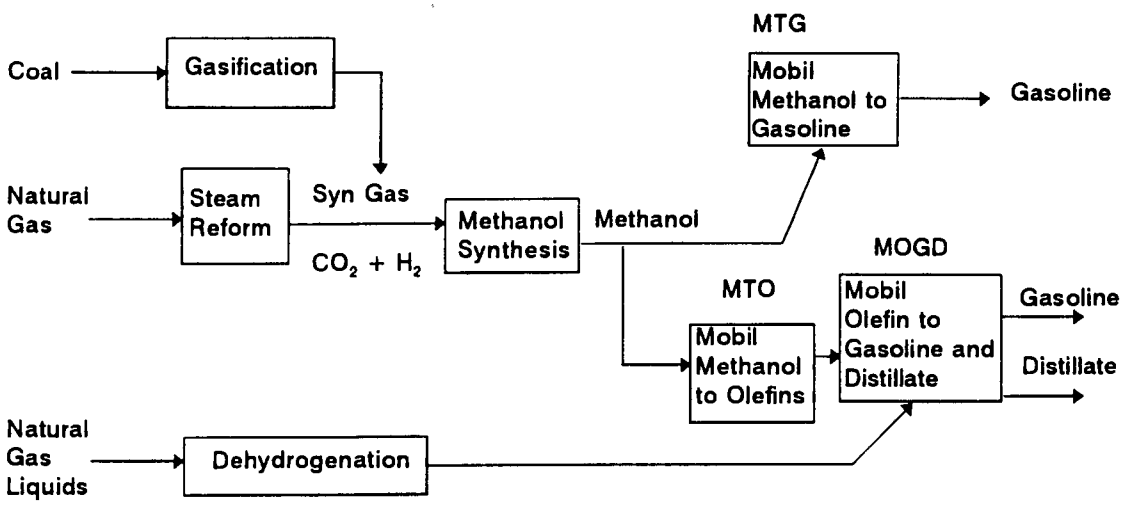

Figure 1.2. Reaction pathway for converting coal, syngas and biomass into liquid fuels via methanol conversion.

1.1.2.1 Methanol To Gasoline Process (MTG)

The MTG process was developed by researchers at Mobil in the late 1970's and involves the use of the molecular sieve catalyst ZSM-5, first synthesized in the early 1970's [Argauer and Landolt, 1972]. In New Zealand a commercial methanol to gasoline (MTG) plant has been in operation since 1985 and satisfies a third of the countries' gasoline demand. The process in New Zealand involves converting crude methanol, containing 17% water, firstly into an equilibrium mixture of dimethyl ether (DME) and water over a non zeolite catalyst (γ-alumina) and then converting DME into hydrocarbons and water using a ZSM-5 catalyst. The reaction is split into two stages primarily to control reactor bed temperatures as the reaction is exothermic. A recycle stream is combined with the DME and water stream entering the second stage, this acts as a quench coolant and also increases the degree of branching and aromatic content of the hydrocarbon product. Increasing the degree of branching and the aromatic content increases the octane number of the gasoline product.

1.1.2.2 Methanol To Olefins Process (MTO)

In this process methanol is converted at high temperatures (470-515°C) into light olefin products, mainly propene and butenes. The MTO catalysts can be divided into two main groups: "small pore", such as erionite and ZSM-34, and "medium pore", such as ZSM-5. The major difference between the two classes of catalysts seems to be a result of shape selectivity (to be discussed in Section 1.5). The initial products formed are light olefins, which can undergo various reactions to form either higher olefins or aromatics (MTG type products). The selectivity to low olefins is favoured up to a point by higher temperatures and by co-feeding water. The selectivity is also effected by changes in the WHSV [Chang *et al.*, 1984]. Generally however catalyst and process variables which increase methanol conversion decrease olefin yield [Avidan, 1988].

Table 1.3. A comparison of the Methanol to Olefins (MTO) and Fischer-Tropsch (FT) yields. [Avidan, 1988]

	MTO Product[1]	FT (Synthol) Product
C_1	1.4	10.0
C_2	0.3	4.0
C_3	2.3	2.0
C_4	3.9	2.0
$C_2^=$	5.0	4.0
$C_3^=$	31.8	12.0
$C_4^=$	19.6	9.0
Gasoline C_5-C_{11}	35.7	40.0
Diesel C_{12}-C_{18}	-	7.0
Heavy product $C_{18}+$	-	4.0
Water soluble oxygenates	0.3	6.0
	100	100
Total light saturates C_1-C_3	4.0	16.0
Total light olefins $C_2^=$-$C_4^=$	56.3	25.0

1. 482°C 102 kPa methanol partial pressure

The process operates at almost 100% conversion and hence no recycle is required. The process at 482°C produces *ca.* 56% light olefins ($C_2^=$-$C_4^=$) and about 36% gasoline (C_5-C_{11}). The low ethene content is quite advantageous as ethene is not a preferred feedstock for the MOGD process. Table 1.3 shows a comparison of MTO and FT product yields.

1.1.3 Mobil Olefin to Gasoline and Distillate Process (MOGD)

The Mobil Olefins to Gasoline and Distillate (MOGD) process involves the conversion of light olefins ($C_2^=$-$C_4^=$) to gasoline and diesel using a ZSM-5 catalyst [Owen *et al.*, 1984]. The ZSM-5 catalyst has a Si:Al ratio of $\simeq$35 and for industrial purposes the catalyst is extruded with 35 wt% alumina binder. The reactor is of fixed bed configuration and reaction conditions are typically 190-310°C, 4-10 MPa and a WHSV of 0.5-1.0 h^{-1} for distillate production. To produce high quality distillate type products low temperatures and high pressures are used. In this mode it is possible to obtain 80 wt% diesel product with a cetane number of >55. To produce acceptable quality gasoline with a RON of 92, higher temperatures (285-375°C) and lower pressures (0.3-4 MPa) are employed.

MOGD diesel has a low density, however its low pour point and low sulphur content make an exceptionally good blending stock [Tabak and Yurchak, 1990]. Due to the isoparaffinic nature and low aromatic content of the MOGD product it also makes an excellent quality jet fuel. One of the advantages of the MOGD process is its flexibility to produce both gasoline and diesel to satisfy the market demands. The gasoline and diesel yields from the two modes of operation are shown in Table 1.4 and the fuels characteristics in Table 1.5.

Table 1.4. Mobil Olefins to Gasoline and Distillate (MOGD) process yields. [Avidan, 1988]

	Distillate mode	Gasoline mode
C_1-C_3	1	4
C_4	2	5
C_5-165°C Gasoline	15	-
165°C$^+$ Distillate	82	-
C_5-200°C Gasoline	-	84
200°C$^+$ Distillate	-	7

Table 1.5. Mobil Olefins to Gasoline and Distillate (MOGD) product characteristics. [Tabak *et al.*, 1986]

	Distillate	
	Raw	Hydrogenated
Specific gravity 15°/15°	0.79	0.78
Bromine no.	79	4.0
Aromatics, vol.%	-	3.0
Pour point, °C	<-50	<-50
Viscosity, cs @ 40°C	-	2.5
Cetane number (engine)	33	56
Sulphur, wt%	<0.002	<0.002
90% B.P., °C	333	343
	Gasoline	
Specific gravity 15°/15°	0.73	
Octane no.		
RON	92	
MON	79	

1.1.4 Alkene oligomerization

In South Africa olefin/alkene oligomerization has satisfied the shortfalls in diesel supply that arise from the FT spectrum. The CATPOLY process (phosphoric acid on kieselguhr) has been employed at SASOL, however the diesel produced, up to 75%, is highly branched and has a low density and viscosity (1.8 cSt at 40°C) [Dry, 1990]. The CATPOLY process produces reasonably good gasoline but the cetane number of the diesel product is low, as mentioned earlier (Section 1.1). Zeolites with intermediate pore size and channel structures have been shown to be excellent oligomerization catalysts (MOGD section). They have a low propensity for coking and are able to operate at high reaction temperatures, good for gasoline production. MOSSGAS (Section 1.1) is also utilizing a zeolite-based system to oligomerize propene and butenes. A semi-commercial scale plant (210 bbl/day) at the Mobil refinery in Paulsboro, Germany has also been in operation [Maxwell and Stork, 1991]. Recently however heteropoly acids [Ratnasamy and Sivasanker, 1990] and SAPO-11 [Long *et al.*, 1985] molecular sieves have been proposed to produce good quality distillate fuels from low olefin oligomerization. Alkene oligomerization will be discussed in more detail in the next section, 1.2.

1.2 ALKENE OLIGOMERIZATION

Oligomerization can be defined as polyolefin chain formation from *n* reacting molecules, where $2 < n < 5\text{-}10$. Polymerization occurs when $n > 100$. Alkene oligomerization is an important industrial source for detergent builders, resins, dyes, plasticisers and medicines. However, as mentioned in Section 1.1.3, in South Africa motor fuel production via olefin oligomerization is of major significance. Since olefin oligomerization at certain temperatures also favours the production of aromatic free fuel this has focused increased attention towards olefin oligomerization as an attractive source of environmentally friendly motor fuels.

Alkene oligomerization may be carried out by both heterogeneous or homogeneous catalysis. The different catalytic routes are discussed below as well as some of their advantages and disadvantages. Several recent reviews on olefin oligomerization are available [e.g. O'Connor and Kojima, 1989; Skupinska, 1991].

1.2.1 Oligomerization by heterogeneous catalysts

1.2.1.1 Zeolites

There are at present two commercially available processes for the production of gasoline and distillate fuels from olefins using zeolite based catalysts. These being the MOGD process and the Shell Polygasoline Kero Process (SPGK). As mentioned previously in the MOGD section ZSM-5 has shown itself to be an excellent oligomerization catalyst, producing both good quality gasoline and distillate fuels by simply varying the operating conditions. The SPGK process produces both gasoline and mid-range distillates and is based on a modified zeolite system [Maxwell and Stork, 1991].

1.2.1.2 Amorphous acid catalysts

1.2.1.2.1 Phosphoric acid

This catalyst, supported on kieselguhr, is used in the CATPOLY process to convert lower alkenes primarily into gasoline [Ipatieff, 1935]. The reaction

typically takes place at 200°C and 3 MPa. Increasing the acid concentration from 92 to 109% results in a product shift from trimers to tetramers [Bethea and Karchmer, 1956]. The disadvantages of this catalyst are that it is corrosive and produces poor quality distillate fuels as mentioned in Section 1.1.

1.2.1.2.2 Heteropoly acids

To date little work has been completed investigating the oligomerization of olefins over heteropoly acids (HPAs). Verstappen and Waterman (1955a) have shown that 12-tungstosilicic acid (HSiW) was active for the oligomerization of propene and produced more tetramer than the phosphoric acid on kieselguhr catalyst (CATPOLY process). The product mainly consisted of branched olefins. Supporting HSiW on a Bauxite support dramatically increased the lifetime of the catalyst, most probably due to decreased coking [Verstappen and Waterman, 1985b]. The catalyst was found to be sensitive to the type of support and the calcination temperature. One of the advantages of the HPA system compared to CATPOLY system is that no water has to be co-fed with the olefin feed mixture. The major disadvantage of the HPA system is the higher price of the HPA catalyst compared to the CATPOLY catalyst.

Recently Ratnasamy and Sivasanker (1990) has suggested that HSiW on a silicotungsten support is an excellent catalyst for the oligomerization of olefins to middle distillates. After oligomerization of a light olefin stream (14% C_2H_4, 44.1% C_3H_6 and 23.8% C_4H_8) at 220°C, 4MPa and a WHSV = 0.4 h^{-1} the product, consisting of mainly C_{12}-C_{21} olefins, is hydrogenated at 300°C and 4 MPa. The final yields and properties of the hydrogenated products are given in Table 1.6 below.

Table 1.6. Yields and compositions of olefin oligomerization products over HSiW on silicotungsten support. [Ratnasamy and Sivasanker, 1990]

Yields (wt %)	
Kerosene	65
Diesel	30
Heavies	5
Properties	
Kerosene (140-250°C)	
sp. gravity	0.78
Smoke point, mm	25
Sulphur, ppm	20
Diesel (250-370°C)	
SP. gravity	0.80
Pour point (°C)	2
Sulphur, ppm	25
Cetane no.	52

1.2.1.3 Aluminophosphate ($AlPO_4$-n) type molecular sieves

Long *et al.* (1985) have suggested interesting olefin oligomerization properties for SAPO-11. Pellet *et al.* (1988) have also reported that $ALPO_4$-n type sieves are active for the oligomerization of olefins, SAPO-11 being the most promising. FAPO-11 and MnAPO-11 were shown to have increased skeletal isomerization products compared to SAPO-11 for hexene isomerization. One of the major advantages of $AlPO_4$-n type sieves compared to zeolite systems for oligomerization is the reduction in hydride transfer and cracking reactions. This is due to their medium acidity (discussed in Section 1.5) and results in a product containing less aromatics. Thomson *et al.* (1990a) have studied propene oligomerization over SAPO-5, -11 and -34. They found that SAPO-5 (large pore) and SAPO-34 (small pore) deactivated rapidly due to coke formation and produced mainly C_4-C_5 olefins. SAPO-11 (medium pore) showed no signs of deactivation and produced predominantly the dimer fraction (C_6). The high selectivity to dimers and lack of deactivation were attributed to the medium acid strength and unique pore dimensions of SAPO-11.

1.2.2 Oligomerization by homogeneous catalysts

The Shell Higher Olefin Process (SHOP) utilizes a homogeneous non-Ziegler nickel ligand-based catalyst to oligomerize ethene to form over one million

tons of linear α-olefins per annum [Bauer *et al.*, 1972]. The reaction occurs at 80-120°C under pressures of 7-14 MPa in a polar solvent immiscible with the alkene products. The final product mixture contains mainly C_4-C_{20} α-olefins according to a Schulz-Flory distribution. The major drawback of homogeneous routes such as the SHOP process are the difficulties involved in product separation as well as the thermal and chemical instability of the products.

1.2.3 Mechanism of alkene oligomerization

Olefin oligomerization over Brönsted acid sites, or cationic oligomerization, is thought to occur via the formation of a carbenium ions [Pines, 1981]. These carbenium ions are then available for further reaction with other olefins to propagate and form oligomers. The oligomerization process proceeds via Markownikoff addition and is consequently dependent on the stability of the carbenium ion which decreases as shown below:

Tertiary > Secondary > Primary

When the olefin in question is propene the primary product is 2-methylpentene. Invariably oligomerization is not the only reaction occurring since other reactions such as cracking, isomerization, cyclization and hydrogen transfer are known to occur concurrently [McMahon *et al.*, 1963]. As can be imagined oligomerization is therefore not a simple straightforward reaction and in most cases is a combination of the above-mentioned reactions. Tabak *et al.* (1986) have proposed the model shown alongside as being representative of propene oligomerization:

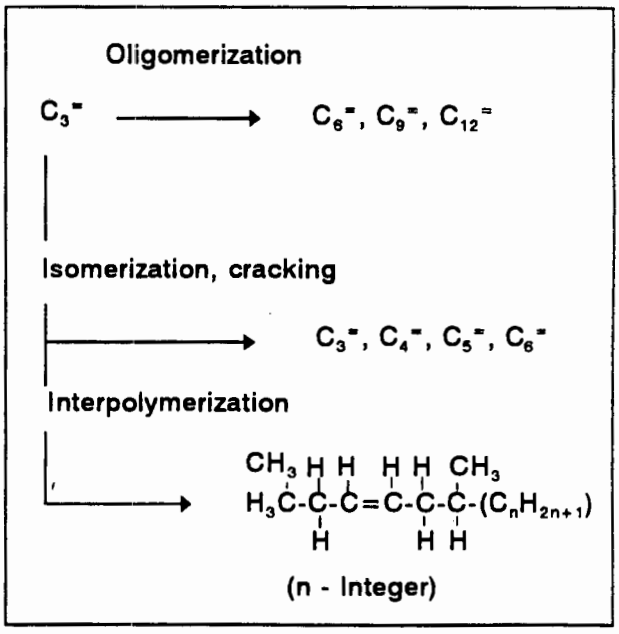

The products formed will not only depend on the stability of the carbenium ion but also shape selective effects in the case of microporous materials (see later section on shape selectivity). Quann *et al.* (1988) have shown that for ZSM-5 the preferred product at 232°C and 5.5 MPa is the trimer. The increased trimer content compared to the dimer content was ascribed to the greater stability of the tertiary carbenium ion of the dimer as opposed to that of the secondary carbenium ion of the monomer. The dimer consequently stands a greater chance of oligomerizing with another monomer, hence favouring trimerization over dimerization. This has also been observed for CATPOLY at 200°C and 3 MPa. Due to their shape selective properties, molecular sieves have been shown to produce less branched products, with ZSM-5 producing less 2,3-dimethylbutene than the expected equilibrium value.

1.2.4 Thermodynamics of oligomerization

Complications arise when trying to investigate the thermodynamics of olefin oligomerization, primarily due to the large number of possible isomer products and secondly due to the lack of available thermodynamic data of the higher molecular weight olefin isomers. Although there are only 18 $C_6^=$ isomers the number increases dramatically to an estimated 895 for $C_{10}^=$ and a massive 12.7×10^9 for $C_{25}^=$ [O'Connor and Kojima, 1989; Reid, 1976]. It is not surprising therefore that many models have relied on lumping or grouping the thermodynamic properties of these oligomers [Smith, 1959; Tabak *et al.*, 1986]. Alberty (1987) on the other hand has proposed a model which includes a 30-step reaction mechanism that encompasses all the possible reactions of the oligomer groups.

1.2.5. Effect of reaction conditions

Quann *et al.* (1988) have reported olefin distributions, based on a restricted isomer group extrapolation, with carbon numbers ranging from C_2-C_{50} (Figure 1.3). The isomers of butene, pentene and hexene were assumed to be at equilibrium. As has been found in practice, high temperatures and low pressures favoured lighter olefin production and lower temperatures and higher pressure favoured higher molecular weight olefins.

1.2.6. Effect of acidity and morphology

Molecular sieve type catalysts with weak acid sites have reduced cracking activity and as a result the product has more clearly defined oligomer groupings. The location of the acid sites and their effect on activity has also been shown to effect the activity and selectivity for olefin oligomerization. By selectively poisoning the external acid sites of ZSM-23 more linear oligomers are produced [Skupinska, 1991]. Wilshier (1987) has also suggested increased linearity of oligomers when the external surface of ZSM-5 was poisoned with 4-methylquinoline or hexamethyldisilazane. The reduction in external surface acidity also decreases the coking rate (coke exists mainly on the external surface of the ZSM-5 crystallite) and hence increases the lifetimes [Suzuki, *et al.*, 1988], although Wilshier (1987) found that poisoning the external surface dramatically reduced the conversion rate.

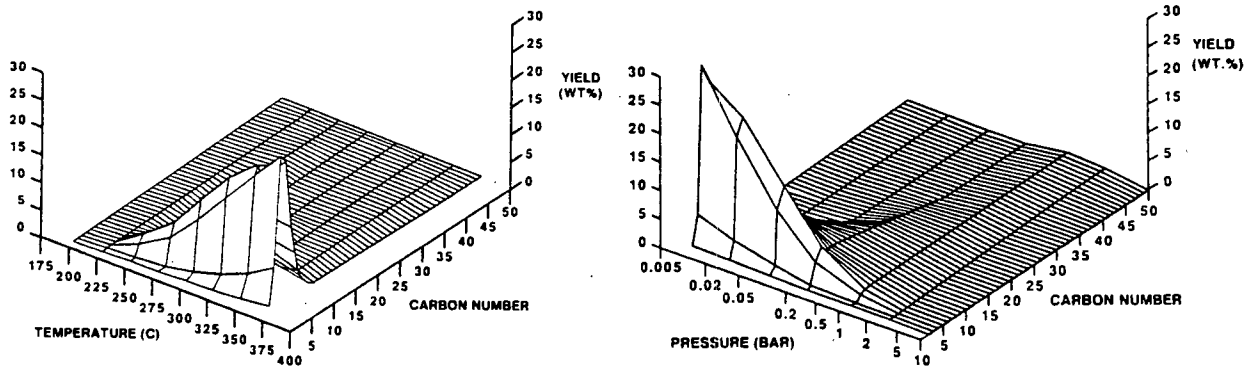

Figure 1.3 Effect of temperature and pressure on the olefin equilibrium distribution. [Quann, 1988]

Schwarz *et al.* (1989) have shown that for a range of Si:Al ratios that ZSM-5 with a Si:Al of *ca.* 40 (intermediate ratio) resulted in the longest lifetimes for propene oligomerization (200-280°C, 5 MPa, WHSV = 12 h^{-1}). Schwarz *et al.* (1991a) have also investigated the effect of varying crystallite size on olefin oligomerization activity. The concept of a depth of effective reaction surface was proposed to explain the increased activity of small crystallite (0.5 μm) ZSM-5. Since oligomerization was assumed to occur only within a certain depth from the crystallite surface (due to diffusion limitations) the

large crystallites would have much of their pore volume inactive. Wilshier (1987) has also concluded that the propene oligomerization reaction occurs mainly on the external surface of ZSM-5 or near the pore mouth.

Olefin oligomerization is also effected by the molecular sieve pore structure and size. Chain branching has been shown to be a function of the pore size [Skupinska, 1991]. The degree of branching increased with increasing pore size, i.e. boralite < offretite < ZSM-5 < mordenite < HY < omega, zeolite omega having the greatest pore diameter of 10Å. Large cages within the pores also allow for the formation of highly branched hydrocarbons (as in the case of ZY). The bulky hydrocarbons become trapped and thereby block the pores or restrict access to acid sites. For molecular sieves with unidimensional pore systems pore blockage or constriction is even more detrimental to the activity.

effect of extruding and pelletizing

Schwarz *et al.* (1991b) have shown for propene oligomerization over ZSM-5 that extrudates (30 wt% Al:70 wt% catalyst) were as active as pure powder and that they produced much less coke. Pellets on the other hand were not as active and produced more hard coke than the powder. Increasing the pelletizing pressure decreased the activity further. Al migration from the binder to the zeolite (Si:Al = 1600) has been reported by Shihabi *et al.* (1985) which increased cracking rates of n-hexane due to increased acidity of Al into the framework.

1.2.7 Catalyst deactivation

Coke formation is the most frequent cause of catalyst deactivation in acid-catalyzed hydrocarbon reactions [Karge, 1991]. The deposit of carbonaceous compounds inside the pores or on the outer surface of zeolites is believed to be the main cause of their deactivation during hydrocarbon reactions [Guisnet and Magnoux, 1992]. Coke removal by combustion can restore activity but as combustion is often incomplete production capacity is decreased and sometimes more severe reaction conditions are required. Often regeneration by combustion destroys the catalyst (as is the case for HPAs) and other methods of regeneration are required, such as liquid extraction.

Coke is generally viewed as very bulky polyaromatic systems, even graphite-like structures. However this view is a bit too narrow as deactivation is often caused by olefinic, and to some extent paraffinic, hydrocarbon species. Karge (1991) has put forward a general definition of coke as follows; *"Coke consists of carbonaceous deposits which are deficient in hydrogen compared with the coke-forming reactant molecule(s)"*.

The suppression of coke formation is a subject that has attracted much interest, but there still exists a need to obtain a better understanding of mechanisms of coke formation. Coke formation is generally viewed as a complex combination of catalyst properties, process chemistry and operating conditions. There are various techniques available to determine type and amount of coke and these have been reviewed by Karge (1991) and Guisnet and Magnoux (1989).

Mechanisms of deactivation

There are basically 2 types of deactivation mechanisms; firstly active site poisoning by irreversible coke adsorption (applicable to porous and non-porous acid catalysts) and secondly pore blockage in molecular sieve-type catalysts. For zeolites these effects can act separately or in combination depending on catalysts' structure, nature of reactants and reaction conditions. The pathway of coke formation in zeolites is shown in Figure 1.4.

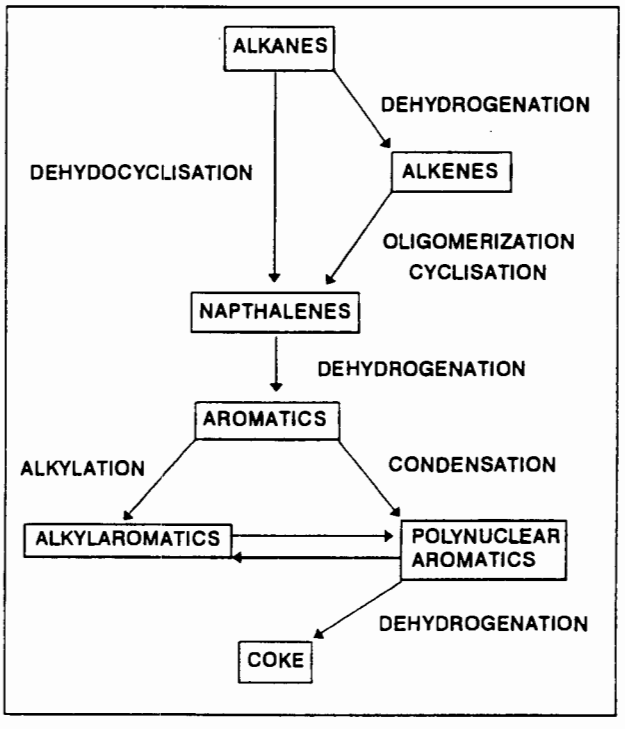

Figure 1.4 Current view of the pathways of coke formation in zeolites.

Molecular sieve type systems

Localization of coke deposits

Usually the question arises as to the location of the coke, i.e. whether inside the pores or external of the crystallite. In some cases even more detailed information is required when cavities (cages) within the pore structure are the possible loci of the coke species.

Effect of pore size and shape

The rate of coke formation in molecular sieve-type catalysts has been shown to be a function of the pore geometry. Large pore sieves tend to deactivate much more rapidly since there are no steric restraints and bulky coke precursors can form. Likewise sieves with cavities often deactivate rapidly due to coke formation within these cavities (causing pore blockage). Medium pore sieves often have a low propensity for coking simply because the coke precursors cannot form in the pore system. Unidimensional pore systems are more likely to be affected by pore blockage more than three dimensional (3D) pore systems.

Effect of acidity

The relationship between coke formation and acidity is far from evident and at present there exists no general correlations between both phenomena [Karge, 1991]. However, coking rate is strongly affected by the catalysts acidity, NaY, which is weakly acidic, showed for example no coke formation, indicating the importance of OH groups on the formation of coke. Coke formation is also affected by acid site density, as oligomerization, cyclization and dehydrogenation which lead to coke formation are bimolecular mechanisms.

IR coke

IR spectroscopy was one of the first techniques employed to investigate the nature of the carbonaceous deposits. The appearance of a predominant band at 1600 cm^{-1} (CH deformation) after the reaction of 1-hexene over Z-Y was ascribed to highly unsaturated carbonaceous residues, most probably

polyolefins. At low temperatures reactions involving olefins lead to the formation of bands at 2960 cm^{-1}, 2930 cm^{-1} and 2860 cm^{-1}. On heating to higher temperatures the band near 1600 cm^{-1} (*ca.* 1585 cm^{-1}) appeared. The in-situ IR results suggest discrimination between two types of coke species, *viz.* so-called Type I coke (low temperature coke, "soft" coke or "white coke") constituted of mainly paraffinic and to a lesser extent olefinic or polyolefinic species. Type II coke (high temperature coke T > 500K) consists of polyalkenes, but is predominantly alkylaromatics and polyaromatics [Karge, 1991].

In summary it can thus be concluded that deactivation due to coke formation is a complex interaction between catalyst type, reaction conditions/type and run time.

1.3 HETEROPOLY ACIDS (HPAs)

In 1826 Berzelius first synthesized and characterized the HPA compound ammonium 12-molybdophosphate [Tsigdinos, 1978]. It was only in 1862, when Marignac, synthesized 12-tungstosilicic acid, that these compounds were recognized as a distinct class of compounds and not simply double salts. The first systematic attempt to understand the nature of heteropoly compounds was made by Miolati in 1908, who suggested a structure based on the ionic theory and Werner's coordination theory. Since then Miolati's theory has been extensively developed and applied by Rosenheim and his co-workers. Heteropoly compounds are classified according to the ratio of number of central atoms to number of peripheral atoms, Table 1.7 illustrates the elements capable of acting as central atoms and Tables 1.8 and 1.9 list the principle series of heteropolymolybdates and heteropolytungstates respectively. The following section detail the structure and properties of HPAs.

1.3.1 Structure of HPAs

HPA compounds in the solid state are composed of heteropoly anions, counter cations (H^+, and metals or onium ions) and water of hydration. **Heteropoly anions** are the **primary structures** and the three dimensional arrangement of the polyanions, counter cations and water of hydration is regarded as the **secondary structure**. The primary and secondary structures will be discussed in the following sections.

1.3.1.1 Primary Structure

A variety of HPA structures are known to exist of which the 1:12 heteropoly anions with the so-called **Keggin** structure are the most common. The structure of the Keggin anion is shown in Figure 1.5. The simplest way to represent the anion, or primary structure, is by polyhedra that share corners, edges or faces with one another (as shown in Figure 1.5). In the case of the Keggin anion of $[PW_{12}O_{40}]^{3-}$ twelve WO_6 (W being the peripheral atom) octahedra surround a central PO_4 (in this case P is the central atom) tetrahedron. There are four different kinds of oxygen atoms: 4 O_i (internal oxygens connecting P and W), 12 O_e (edge-sharing oxygens connecting W's), 12 O_c (corner-sharing oxygens connecting W_3O_{13} units) and 12 O_t

(terminal oxygens bonding to 1 W atom). Each W atom is displaced 0.3-0.4Å from the centre of the WO_6 octahedron giving the W-O_t bond (1.43Å) a double-bond character. The longest W-O bond is the W-Oi bond (2.49Å) which makes the bond weak.

In addition to the Keggin type (α-type) there are geometric isomers (β, γ type).

Table 1.7 Elements capable of acting as central (heteroatoms) atoms in heteropoly compounds. [Tsigdinos, 1978]

Periodic Group	Element[1]
I	H, Cu^{2+}
II	Be^{3+}, Zn^{2+}
III	B^{3+}, Al^{3+}, Ga^{3+}
IV	Si^{4+}, Ge^{4+}, Sn^{4+}(?), Ti^{4+}, Hf^{4+}, Ce^{3+}, Ce^{4+} and other rare earths
V	N^{4+}(?), P^{3+}, P^{5+}, As^{3+}, As^{5+}, V^{4+}, Sb^{3+}(?), Bi^{3+}
VI	Cr^{3+}, S^{4+}, Te^{4+}, Te^{6+}
VII	Mn^{2+}, Mn^{4+}, I^{7+}
VIII	Fe^{3+}, Co^{2+}, Co^{3+}, Ni^{2+}, Ni^{4+}, Rh^{3+}, Pt^{4+}(?)

1. Some of these elements form heteropoly compounds only with molybdenum or only with tungsten. A question mark after the element denotes doubtful existence of a heteropoly anion.

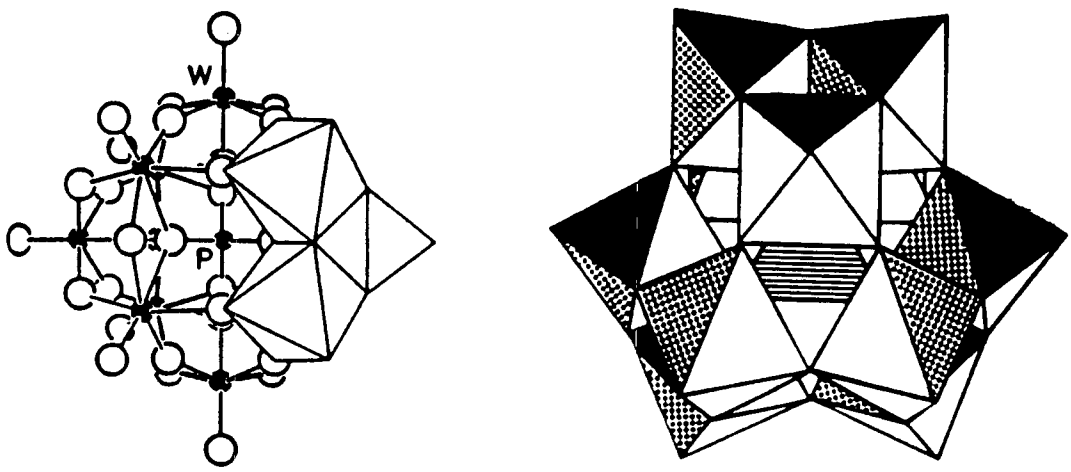

Figure 1.5 Structure of the $PW_{12}O_{40}^{3-}$ Keggin anion.

Table 1.8 Principal series of heteropolymolybdates. [Tsigdinos, 1978]

Number of atoms X:P[1]	Principle central atoms[2]	Typical formulas	Central group	Structure by X-ray
1:12	*Series A*: N^{5+}(?), P^{5+}, As^{5+}, Si^{4+}, Ge^{4+}, Sn^{4+}(?), Ti^{4+}, Zr^{4+}	$[X^{n+}Mo_{12}O_{40}]^{-(8-n)}$	XO_4	Known
	Series B: Ce^{4+}, Th^{4+}, U^{4+}	$[X^{n+}Mo_{12}O_{40}]^{-(12-n)}$	XO_{12}	Known
1:11	P^{5+}, As^{5+}, Ge^{4+}	$[X^{n+}Mo_{11}O_{39}]^{-(12-n)}$	-	Unknown
1:10	P^{5+}, As^{5+}, Pt^{4+}(?)	$[X^{n+}Mo_{10}O_x]^{-(2x-60-n)}$	-	Unknown
1:9	Mn^{4+}, Ni^{4+}	$[X^{n+}Mo_9O_{32}]^{-(10-n)}$	XO_4	Known
1:9	P^{5+}	$[X^{n+}Mo_9O_{31}(OH)_3]^{-(11-n)}$	XO_6	Known
1:6	*Series A*: Te^{6+}, I^{7+}	$[X^{n+}Mo_6O_{24}]^{-(12-n)}$	XO_6	Known
	Series B: Co^{3+}, Al^{3+}, Cr^{3+} Fe^{3+}, Rh^{3+}, Ga^{3+}, Ni^{2+}	$[X^{n+}Mo_6O_{24}H_6]^{-(6-n)}$	XO_6	Known
2:10	Co^{3+}	$[X_2^{n+}Mo_{10}O_{38}H4]^{-(12-2n)}$	XO_6	Known
2:17	P^{5+}, As^{5+}	$[X_2^{n+}Mo_{17}O_x]^{-(2x-102-2n)}$	-	Unknown
2:5	P^{5+}	$[X_2^{n+}Mo_5O_{23}]^{-(16-2n)}$	XO_4	Known
1m:6m (m unknown)	Co^{2+}, Mn^{2+}, Cu^{2+}, Se^{4+} P^{3+}, As^{3+}, P^{5+}	$[X^{n+}Mo_6O_x]_m^{-m(2x-36-n)}$	-	Unknown
4:12	As^{5+}	$[H_4As_4Mo_{12}O_{50}]^{4-}$	Cavity	Known
1:1	As^{3+}	$[(CH_3)_2AsMoO_{14}OH]^{2-}$	AsO_4	Known

1. X = Central atom, P = Peripheral atom (Mo)
2. (?) denotes doubtful existence of heteropoly anion

Table 1.9 Principal series of heteropolytungstates. [Tsigdinos, 1978]

Number of atoms X:P[1]	Principle central atoms[2]	Typical formulas	Central group	Structure by X-ray
1:12	P^{5+}, As^{5+}, Si^{4+}, Ge^{4+}, Ti^{4+}, Co^{2+}, Co^{3+}, Zn^{2+}, Cu^{+}, Cu^{2+}, Ga^{3+}(?)	$[X^{n+}W_{12}O_{40}]^{-(8-n)}$	XO_4	Known
1:10	Si^{4+}, Pt^{4+}	$[X^{n+}W_{10}O_x]^{-(2x-60-n)}$	XO_4	Known
1:9	Be^{2+}	$[X^{2+}W_9O_31]^{-6}$	-	Unknown
1:6	*Series A*: Te^{6+}, I^{7+}	$[X^{n+}W_6O_{24}]^{-(12-n)}$	XO_6	isomorphous with 6-molybdates
	Series B: Ni^{2+}, Ga^{3+}	$[X^{n+}W_6O_{24}H_6]^{-(6-n)}$	XO_6	Isomorphous with 6-molybdates
2:18	P^{5+}, As^{5+}	$[X_2^{n+}W_{18}O_{62}]^{-(16-2n)}$	XO_4	Known
2:17	P^{5+}, As^{5+}	$[X_2^{n+}W_{17}O_x]^{-(2x-102-2n)}$	-	Unknown
2:4:18	X = P^{5+},As^{5+} Z = Mn^{2+}, Co^{2+}, Ni^{2+}, Cu^{2+},Zn^{2+}	$[X_2^{n+}Z_4^{m+}W_{18}O_{70}H_4]^{-(28-2n+m)}$	XO_4	Known
1m:6m (m unknown)	As^{3+}, P^{3+}	$[X^{n+}W_6O_x]_m^{-m(2x-36-n)}$	-	Unknown

1. X = Central atom, P = Peripheral atom (W)
2. (?) denotes doubtful existence of heteropoly anion

Detailed structural information can also be obtained from the vibrational spectra of the Keggin anion, which have characteristic bands with assignment shown in Table 1.10.

Table 1.10 IR bands characteristic of the Keggin Anion, α-$XM_{12}O_{40}$ (cm^{-1}). [Rocchicciolini-Deltcheff *et al.*, 1976]

	$PW_{12}O_{40}$	$PMo_{12}O_{40}$	$SiW_{12}O_{40}$	$SiMo_{12}O_{40}$
X-O	1080-1081	1062-1068	920-928	899-904
M-O_t [1]	976-995	954-975	967-981	940-957
M-O_c-M	890-900	869-880	878-894[2]	855-868
M-O_e-M	805-810	785-810[2]	780-810	770-795

1. Shoulder peaks sometimes appear at *ca.* 10 cm^{-1} higher than the main peak are included in the wavenumber range.
2. In some cases, α-$SiW_{12}O_{40}$ and α-$PMo_{12}O_{40}$ show a doublet.

1.3.1.2 Secondary structure

The secondary structure has been determined from a number of single crystal and powder XRD studies. As an example, the secondary structure of $H_3PW_{12}O_{40}.6H_2O$ or $[H(H_2O)_2]_3PW_{12}O_{40}$ is shown in Figure 1.6. In this case the polyanions (Keggin type) constitute 2 sets of 3-D networks in which the polyanions are connected by $H_5O_2^+$ (hydronium ions) bridges. The two sets of networks penetrate each other so that the arrangement of the polyanions leads to the formation of the most dense secondary structure, bcc type (lattice constant, *ca.* 12Å, Z=2), commonly denoted as type A. Other types B, C and D are known which contain a greater amount of water molecules.

The secondary structure of the Caesium salt of $H_3PW_{12}O_{40}$ was presumed to be the same as shown in Figure 1.6 except in this case Cs^+ ions replace the $H_5O_2^+$ ions.

As can be seen from Figure 1.6 when the polyanions pack together the interstices are very large compared to either water molecules or simple cations. Therefore in most heteropoly compounds there are no direct linkages between the polyanions, as was shown for $K_6[P_2W_{18}O_{62}].14H_2O$. These compounds are joined by hydrogen bonding through some molecules of water.

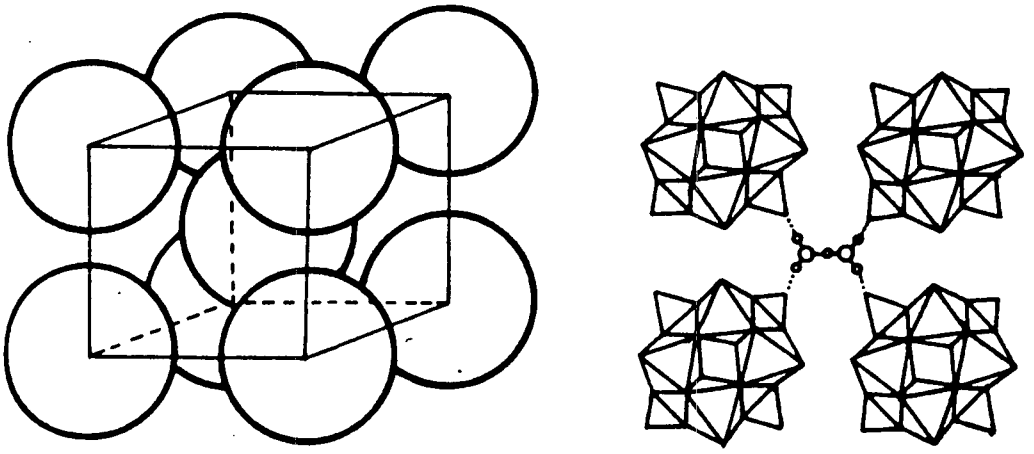

(A) (B)

Figure 1.6 Secondary structure of $PW_{12}O_{40}\cdot 3H_2O$, the bcc packing of the polyanions is illustrated in A. Each $H_5O_2^+$ bridges four polyanions as shown in B.

In the solid state the primary structure is rather stable while the secondary structure is quite variable. The flexible nature of the secondary structure is an important feature of heteropoly compounds when they are used as solid acid catalysts. The flexibility is dependent on the nature of the countercations and environment conditions, as is described later.

1.3.2 Synthesis of HPAs

HPAs are polymeric oxoanions which are formed from the condensation of more than two different types of oxoanions in solution (eqn. 1). Polyanions consisting of one kind of oxoanion are called isopolyanions (eqn. 2).

$$12WO_4^{2-} + HPO_4^{2-} \rightarrow (PW_{12}O_{40})^{3-} + 12H_2O \quad (1)$$

$$7MoO_4^{2-} + 8H^+ \rightarrow (Mo_7O_{24})^{6-} + 4H_2O \quad (2)$$

When the central atom is not a transition element a soluble molybdate or tungstate may be dissolved with a soluble salt containing the central atom in the appropriate oxidation state. This mixture is then acidified to an appropriate pH range. Free acids can be prepared in several ways:

1. by mixing of appropriate quantities of the simple acids;
2. by double decomposition of salts (e.g. sulfuric acid and a barium salt);
3. by extraction with ether from acidified aqueous solutions;
4. by ion exchange from heteropoly salts;
5. from mixed or aprotic solvents.

Salts of free heteropoly acids are always made in solution.

e.g. $H_3PW_{12}O_{40}(aq) + 1.5\ (NH_4)_2CO_3(s) \rightarrow (NH_4)_3PW_{12}O_{40}(s) + 1.5\ CO_2(g)$

An extensive study on the synthesis of HPMo, HSiMo and their metal salts has been prepared by Tsigdinos (1974, 1976).

1.3.3 Physicochemical Properties of HPAs.

Listed below are some general characteristics of heteropolyanions in solution:

1. Free acids and most of their salts with small metal ions are extremely soluble in water and polar solvents. For example 700 g of $H_4SiMo_{12}O_{40}$ will dissolve in 100 ml of water at 25°C. Salts with large ions (Cs^+, NH_4^+ and Ag^+) are insoluble or slightly soluble; this property is often used to determine phosphorous contents by precipitation as $(NH_4)_3[PMo_{12}O_{40}].2HNO_3.xH_2O$.

2. In aqueous solution heteropoly anions are stable at low pHs, at higher pHs they tend to hydrolyze as shown below for the $PW_{12}O_{40}^{3-}$ anion:

$$WO_4^-,\ PO_4^{3-} \rightleftarrows \underset{(PW_9)}{PW_9O_{63}^{5-}} \overset{\text{pH 7-8}}{\rightleftarrows} \underset{(PW_{11})}{PW_{11}O_{39}^{7-}} \overset{\text{pH 2}}{\rightleftarrows} \underset{(PW_{12})}{PW_{12}O_{40}^{3-}}$$

3. Free acids are usually very strong acids.
4. Heteropolyanions are multielectron oxidants and those having Mo of V as peripheral atoms are strong oxidants.

The following sections detail the properties of HPAs in the solid state.

1.3.3.1 Thermal stability, water content and surface area

Changes in HPCs upon heating have been extensively studied by TG-DTA, FT-IR and XRD. Free acids are normally obtained with large amounts of water of crystallization. The majority of this water, known as water of crystallization, is released below 100°C. Decomposition occurs between 350 and 600°C and is believed to occur as shown below:

$H_3PMo_{12}O_{40} \rightarrow 1/2\ P_2O_5 + 12MoO_3 + (3/2)H_2O$ [Misono, 1987] for HPMo and

$H_3PW_{12}O_{40} \rightarrow HPW_{12}O_{38.5} + H_2O$ [Hodnett and Moffat, 1984] for HPW.

Quinwei and Jingfa (1989) have proposed however that HPW decomposes as shown below:

$H_3PW_{12}O_{40} \rightarrow HPW_{12}O_{39} + H_2O$

Typical TG-DTA results are shown in Figure 1.7. The thermal behaviour of the salts of HPAs can be divided into two groups, firstly those which consist of the salts of small cation such as Cu^{2+} and Na^+ and that are water soluble and then the type that are insoluble in water such as the NH^{4+} and Cs^+ salts. These two groups were assigned as Type A and Type B respectively [Niiyama *et al.*, 1981].

The thermal behaviour of the Type A salts resembles that of their respective parent acids in several respects. Both release water at *ca.* 100°C (water of crystallization) as well as between 200-300°C. The higher temperature water loss is believed to be the loss of water associated with protons, i.e. $(H_2O)_2H^+$ species, or of water being lost from coordination binding with metal cations. The Type B salts have low water contents of which all is released below 100°C and is assumed to be "zeolitic" in nature.

Thermal stability

Tsigdinos (1978) has reported that thermal stability data of HPCs should be viewed with caution, as often stabilities of as high as 400°C have been reported for $H_3PW_{12}O_{40}$ and 300°C for $H_4SiW_{12}O_{40}$. These temperatures were determined from dynamic TG-DTA systems and are in fact too high as

these HPAs decompose at much lower temperatures. Meaningful thermal stability data should be supplied with accompanied solubility data as well as information about the length of heating [Tsigdinos, 1978]. By using the above method to determine thermal stabilities of $H_3PMo_{12}O_{40}$ and some of its salts the results are shown in Table 1.11 The thermal stability of $H_4SiMo_{12}O_{40}$ and its salts are lower than those of $H_3PMo_{12}O_{40}$ and it has been shown that 12-molybdosilicic acid decomposes slowly even at room temperature.

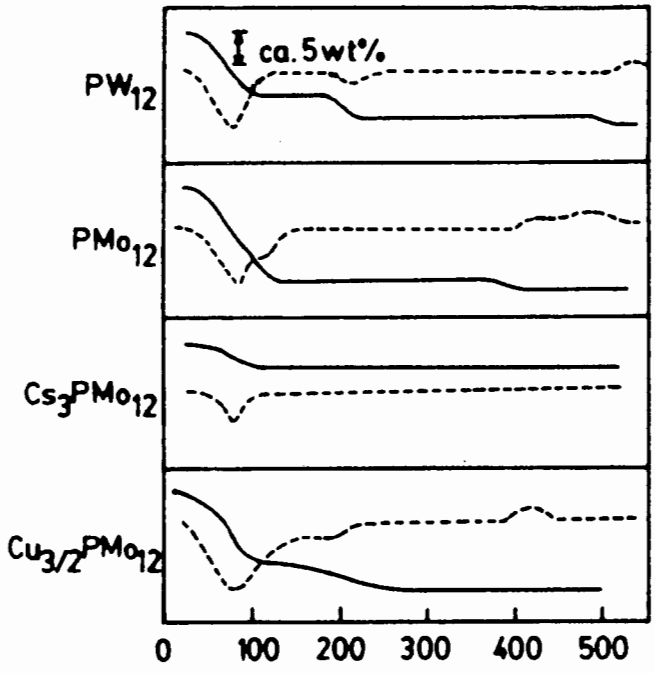

Figure 1.7 TG-DTA spectra for several 12-type heteropoly compounds.

Table 1.11 Thermal stabilities of $H_3PMo_{12}O_{40}$ and some of its salts[1]. [Tsigdinos, 1978]

Compound	Maximum thermal stability (°C)
$H_3PMo_{12}O_{40}.16H_2O$	350
$La[PMo_{12}O_{40}].10H_2O$	300[2]
$Cu_3[PMo_{12}O_{40}]_2.25H_2O$	350
$Mn_3[PMo_{12}O_{40}]_2.17H_2O$	300
$Ni_3[PMo_{12}O_{40}]_2.34H_2O$	300[2]
$Co_3[PMo_{12}O_{40}]_2.34H_2O$	300[2]

1. Samples heated in air at specified temperatures. Heated materials were dissolved in water to ascertain extent of decomposition.
2. These materials begin to show decomposition at 350°C.

Of course the above method cannot be used for Type B salts since they are initially insoluble in water. In general the thermal stability trend of the 12-heteropoly compounds are W > Mo and P > Si:

$$HPW > HSiW \simeq HPMo > HSiMo$$

and the Type A salts are normally less stable than there parent material and both are less stable than the Type B salts. $K_3PW_{12}O_{40}$ is stable up to 700°C before it starts to melt.

The thermal stability of HPAs is also dependent on the environment, in a reducing atmosphere HPAs decompose much more rapidly. The coexistence of oxygen and water vapour enhances the stability at high temperatures and sometimes causes reformation of the HPA structure [Serwicka and Grey, 1990; Tsigdinos, 1974; Stencel *et al.*, 1986]. The reformation of the Keggin ions after contact with water vapour has often resulted in misleading conclusions about the thermal stability of these compounds.

The thermal stability of SiO_2 supported HPAs is a subject that has attracted much attention lately. Certain workers [Moffat and Kasztelan, 1988; Kasztelan and Moffat, 1987, 1989] have suggested increased thermal stability, whereas Fricke and Öhlmann (1986a,b) and Rocchiccioli-Deltcheff *et al.* (1990) believe that the thermal stability decreases. The latter workers have also suggested that the decomposition not only occurs at lower temperatures but also at a slower rates than in the unsupported case. The results reported by Moffat and Kasztelan (1987, 1988, 1989) are believed to be a result of reformation of the Keggin anions after washing the spent catalyst and not increased thermal stability as suggested [Serwicka and Grey, 1990].

Effect of temperature on primary and secondary structure

The secondary structure of the Type A salts is variable and depends to a large extent on the degree of hydration. Often HPA and their salts exist as multi hydrates, the XRD of which are not well defined. Careful pretreatment to ensure single hydrate type materials results in an XRD that is sharper and more indicative of single phase material. The secondary structure of the Type B salts is more rigid and does not change on heating. The primary

structure is quite stable with increasing temperature, however some features such as doublet formation and reduction in band height indicate slight loss of structure.

Surface Area

The surface areas of HPAs vary considerably between the two groups, Type A and B. The Type A salts have low surface areas, typically below 15 m^2/g. The Type B salts on the other hand have surface areas ranging from 100-200 m^2/g. The high surface areas of these Type B salts is most likely due to their very small crystallite size [Misono, 1987] however McMonagle and Moffat (1984) and Taylor *et al.* (1985), have claimed that Type B salts (K^+, NH_4^+, Cs^+) of HPW, HSiW and HPMo contain micropores. These micropores, unlike those of zeolites/microporous materials are not uniform and are 8-13Å in diameter. As yet the length of these micropores has not been determined.

1.3.3.2 Acidity

The acidic properties of HPCs in the solid state are sensitive to counter cation type, constituents of the polyanion, calcination temperature and environment. NH_3- and pyridine-TPD, together with catalytic orders for hydrocarbon reactions, indicate that the acid strengths reflects those in solution i.e.

$$HPW > HSiW > HPMo > HSiMo$$

Free HPAs are strong Brönsted acids containing two types of acidic protons; free ranging/nonlocalized and fixed/bulk nonhydrated type [Misono, 1987]. Five mechanisms have been proposed for the origin of acidity in HPCs in the solid state.

1. Protons in the acidic salts (by deviation from stoichiometry), e.g.

$$H_3PW_{12}O_{40} + (x/2)Cs_2CO_3 \rightarrow H_{3-x}Cs_xPW_{12}O_{40}$$

The above is commonly called partial salt formation [Highfield and Moffat, 1984a,b]. The residual protons have been detected by Py-IR and NH_3-IR. It

has been reported that stoichiometric salt formation is almost impossible [Misono *et al.*, 1984] hence most salts will have this residual free acid material as a source of acidity. Black *et al.* (1987) have shown for $K_{2.5}H_{0.5}PMo$ that a separate H_3PMo phase existed on the surface of a pure K_3PMo phase.

2. Partial hydrolysis during the preparation step, e.g.

$$PW_{12}O_{40}^{3-} \rightarrow PW_{11}1O_{39}^{7-} + WO_4^{2-} + 6H^+ \rightarrow HPO_4^{2-} + 12\ WO_4^{2-} + 23H^+$$

As mentioned in Section 1.3.3 the anions are sensitive to pH. If the pH of the synthesis solution rises above 2 the HPA dissociates.
3. Acidic dissociation of coordinated water as shown below:

$$Ni(H_2O)_m^{2+} \rightarrow Ni(H_2O)_{m-1}(OH)^+ + H^+ \text{ or}$$

$$Al(H_2O)_m^{2+} \rightarrow Al(H_2O)_{m-1}(OH)^+ + H^+$$

Such phenomena have been used to explain the higher activity of Ni and Al containing salts for *o*-xylene isomerization compared to their parent acids. The activity increased even further when the catalysts were steamed or wet *o*-xylene feed was used [Baba *et al.*, 1983].

4. Lewis acidity of metals (counter cations) themselves. Highfield and Moffat (1984a,b) has shown by Py:IR that Lewis sites exist for AlPW.

5. Protons from reduction of metal ions, e.g.
$Ag^+ + 1/2\ H_2 \rightarrow Ag^0 + H^+$ and $Cu^{2+} + H_2 \rightarrow Cu^0 + 2H^+$

The above redox mechanism has been shown to be reversible. Baba *et al.* (1982, 1983, 1992) have shown that by pretreating in hydrogen or introducing hydrogen with the hydrocarbon feed there was an increase in activity.

Based on Hammet indicators the acidity of various HPAs are shown in Table 1.12.

Table 1.12 Acidity of various HPAs as determined by Hammet indicators. [Hayashi and Moffat 1982, 1983a]

Heteropoly Acid	Calcination Temperature (°C)[1]	Acid strength[2] H_o +1.5	-3.0	-5.6	-8.2
HPW	-	+	+	-	-
	70(air)	+	+	+	-
	150(air)	+	+	+	-
	300	+	+	+	+
	400	+	+	+	+
	450	+	+	+	(-)
HPMo	-	+	(-)	x	x
	350	+	+	x	x
HSiW	-	+	+	-	-
	400	+	+	+	-
NaPW	400	+	-	-	-
CaPW	400	+	(+)	-	-
ZnPW	400	+	+	-	-
MgPW	400	+	+	(+)	-
AlPW	400	+	+	+	-
BPW	400	+	+	+	-
ZrPW	400	+	+	+	-

1. Calcined in He unless otherwise stated, - corresponds to fresh acid
2. + acidic colour, - basic colour, () vague, x not measurable

Effect of counter cation

Table 1.12 shows the effect of countercation on acid strength. In general the salts have weaker and less acidity (as measured by Hammet indicators) than their parent materials.

Effect of calcination temperature and environment

Table 1.12 also shows the effect of calcination temperature on strength of acid sites (measured by Hammet indicator method). Increasing the calcination temperature to 400°C increased the acid strength. Calcination above 450°C resulted in weakening of acidity. This was not surprising since HPAs are known to decompose at these high temperatures. Little difference in acidity was observed between calcination in an air or helium environment. Calcination in a reducing atmosphere severely reduced the acidity, most probably due to destruction of the Keggin structure.

Baba *et al.* (1983) have shown increased activity for *o*-xylene isomerization when AlPW was steamed and when CuPW and AgPW were pretreated in a hydrogen atmosphere. The latter result is in contradiction with all previous finding which show decreased acidity for HPAs calcined in a reducing atmosphere. The increased acidity/activity is due to the effect outlined in 4. in the acidity of HPA section on page 30.

Acidity determination by Pyridine and ammonia adsorption

Some authors have used the thermal desorption of pyridine to determine amount and strength of acid sites present [e.g. Serwicka *et al.*, 1991]. Note that the acidity measured will be the "bulk acidity", since the homogeneous or stoichiometric pyridinium salts would result from pyridine absorption. Typical results are shown in Figure 1.8.

Other TPD studies have shown similar results with ammonia being the preferred basic molecule since absorption of pyridine takes longer to reach equilibrium [Highfield and Moffat, 1984b].

Acidity determination by reaction studies (probe reactions) will be discussed later in Section 1.5.

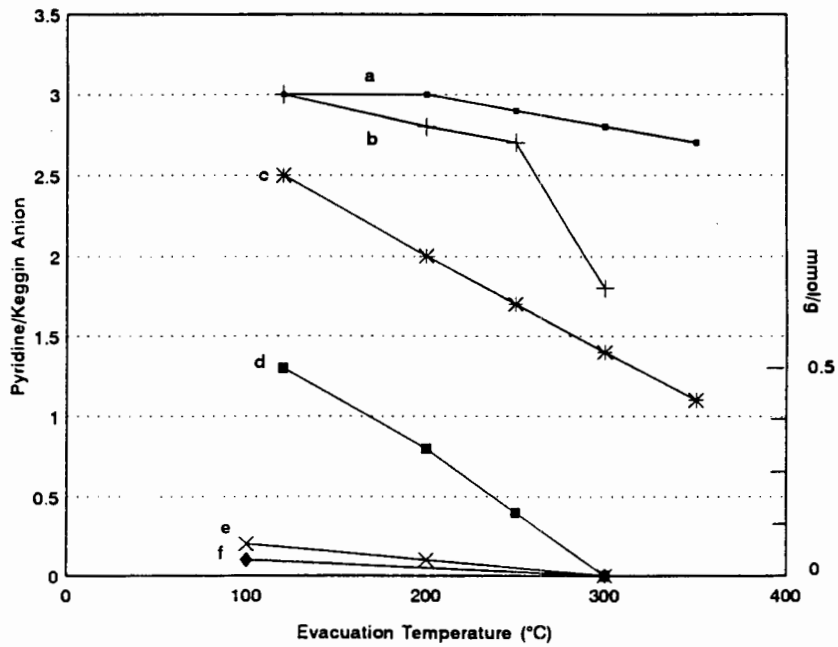

Figure 1.8 Thermal desorption of pyridine from several 12-HPAs and SiAl. Evacuated at each temperature for 1 hour: a. $H_3PW_{12}O_{40}$, b. $H_3PMo_{12}O_{40}$, c. $NaH_2PW_{12}O_{40}$, d. $Na_3PW_{12}O_{40}$, e. $Cs_3PW_{12}O_{40}$, f. SiO_2-Al_2O_3.

1.3.3.3 Pseudoliquid phase behaviour

It has been reported that due to the flexibility of the secondary structure of the Type A HPA compounds polar molecules such as alcohols and amines are readily adsorbed into the bulk of the heteropoly acid. This absorption takes place by substitution for water or by expanding the interscies of the polyanions. This is not diffusion into micro- or macropores since the amounts adsorbed corresponded to 10 to 100 times more than required for monolayer coverage. The absorption of pyridine is shown in Figure 1.9.

After 60 minutes several molecules of pyridine per polyanion were absorbed, which after evacuation became 6 per polyanion. After evacuation to 130°C the number of pyridine molecules corresponds well to the agreed number of protons. Similar behaviour has been observed for other HPAs and absorbed bases. IR showed that pyridine had replaced water molecules and that a homogeneous pyridinium salt had formed.

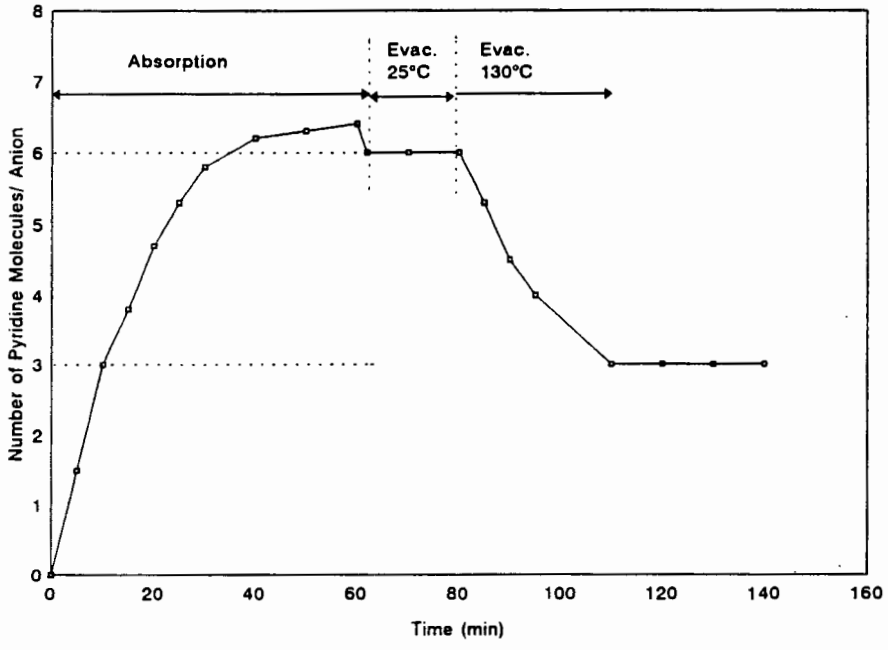

Figure 1.9 Absorption of pyridine (21 Torr) at 25°C by $H_3PMo_{12}O_{40}$ and subsequent desorption at 25°C and 130°C under vacuum.

This effect has been called **"pseudoliquid phase behaviour"**. The tendency to form a pseudoliquid phase depends on the kind of HPC, particularly the countercation, and on the molecules to be absorbed. Acid forms extensively

absorb polar molecules such as alcohols and amines, but non-polar molecules like hydrocarbons are adsorbed only on the surface. For the Type B salts the secondary structure is quite rigid and even polar molecules do not absorb. The temperature, partial pressure and molecules coexisting in the system are also influential.

The rate of absorption varies according to the basicity or polarity of the molecule and by the molecular size [Misono *et al.*, 1985]. The rate is also dependent on the degree of hydration, for example HPA that are calcined at 300°C (and hence are anhydrous) absorb polar molecules only very slowly compared to those that have residual water present. Furthermore there is often a critical partial pressure at which the rate changes abruptly.

1.3.3.4 Catalytic activity

HPAs have found use in industry as both heterogeneous and homogeneous catalysts and have quite a long history. Only recently however have studies revealed that for well characterized HPAs their activity is often much higher than that of zeolites and silica-alumina based catalysts. The following sections describe some of the catalytic processes reported in the current open literature.

Homogeneous

Kozhevnikov and Matveev (1982) have completed a review on homogeneous acidic and oxidative catalysis using HPAs. Oxidation reactions that have been studied include the oxidation of sulfur compounds, bromination of alkenes, oxidation of hydrocarbons and the epoxidation of olefins. Acid-type homogeneous reactions include the hydration and esterification of olefins, decomposition of isopropylbenzene hydroperoxide as well as other types of acid-type reaction.

Heterogeneous

Acid-type catalysis (Bulk vs surface type)

The superior performance of HPCs is often a result of conditions favouring pseudoliquid phase behaviour. Hence some surprising catalytic activities and

unique selectivities have been reported for reactions involving polar molecules such as alcohols. HPAs are also active for alkylation and transalkylation, but deactivation during reaction is often quite significant.

Acid catalysis over HPAs can be divided into two groups; **"Bulk type I"** (pseudoliquid phase-type) and **"Surface type"**. The activity for the former correlate well with their bulk (total) acidity as was shown for alcohol dehydration over $Na_xH_{3-x}PW$ ($3 < x < 0$) [Misono, 1987]. As x increased (to 3) the activity increased accordingly. Unique selectivities for "Bulk type I" reactions often arise due to the different absorption characteristics of the product/reactant molecules. The activity of "Bulk type I" reactions are also less susceptible to variations in calcination temperature. The activity of the later, "Surface" type, are more susceptible to changes in calcination temperature and their reactions proceed on the surface as is the case for any ordinary solid acid catalyst. Figure 1.10 illustrates the "Surface type" vs "Bulk type I" reaction mechanism.

Bulk Type I reactions

HPA catalysts are very effective for the dehydration of alcohols, HPW is 2000× more active than Z-Y in spite of its low surface area ($\simeq 3$ m^2/g). Many examples exist in the literature containing examples of "Bulk type I" mechanisms. Selectivities are usually a function of partial pressure due to the absorption effect.

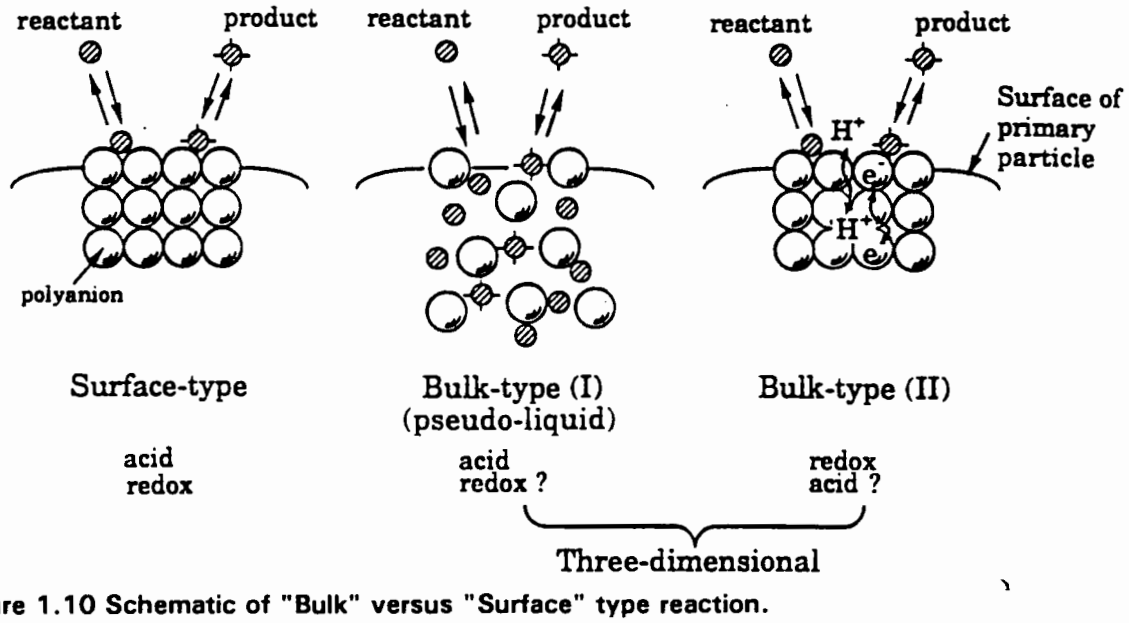

Figure 1.10 Schematic of "Bulk" versus "Surface" type reaction.

Surface type

The activity of HPAs for surface type reactions are not only dependent on the surface area available for reaction but also on calcination temperatures and to the nature of the counter cation and peripheral atoms present. This is not surprising since these parameters are known to effect the acidity (Section 1.3.3.2).

Baba *et al.* (1983) have shown that for *o*-xylene isomerization AlPW was more active than CuPW and AgPW. Matsuda *et al.* (1981) have shown that increasing the calcination temperature from 150°C to 300°C of HPMo and some of its metal salts for butene isomerization increased the formation of the trans isomer indicating the formation of stronger acidity. They also found a linear relationship between trans/1-butene ratio and electronegativity of the countercations. These results have been explained by the formation of acid sites via water interactions with metal countercations (HPA acidity section 1.3.3.2).

HPW, HSiW, HPMo and their ammonium salts have been shown to strongly catalyze double bond shift and cis/trans isomerization of hexene, heptene and octene in the liquid phase at low temperatures (Nayak and Moffat, 1988). No skeletal isomerization was observed.

The activity for hexane cracking of the ammonium salts of the above parent acids and ZSM-5 has also been compared by Nayak and Moffat (1989). The activity order was as follows: ZSM-5 >> NH_4PW >> NH_4SiW > NH_4PMo. Increasing the calcination temperature beyond 748K reduced the activity of NH_4PW to a lower steady state value. The major difference in selectivities between NH_4PW and ZSM-5 was in the formation of aromatics. NH_4PW produced less aromatics with increasing conversion whereas ZSM-5 produced aromatics exponentially with increasing conversion. NH_4PW has been shown to posses superacid sites since it was active for cumene cracking and toluene alkylation (Nowinska, 1990). Supporting HPA on high surface area supports increased the rate for butene isomerization, which suggested that the reaction rate was proportional to the surface area available for reaction [Misono *et al.*, 1978].

Supported HPAs

HPAs have been dispersed on many supports such as silica gel, kieselguhr, activated carbon and aluminas. Supports which show surface basicity like alumina often bring about decomposition of the polyanions [Izumi *et al.*, 1983; Misono, 1987]. Such decomposition may only occur with increasing shelf life of the catalyst. In general however the strongly acidic HPAs are the most affected by residual basic material on alumina supports. For kieselguhr, a low surface area support the majority of the polyanions may simply exist as a mechanical mixture with the support [Misono, 1987].

HPMo supported on alumina has been proposed to form an active AlPMo layer on the surface of the alumina support [Cheng and Luthra, 1988]. Similarly, Ehwald *et al.* (1987) have reported aluminium salt formation for HSiW on alumina. Nowinska *et al.* (1991) have shown for HPW supported on alumina that higher loadings (58 wt% and above) are required to give comparable hexane cracking activities to silica supported HPAs (38 wt%) as excess HPW is required to form the aluminium salt before the H^+ rich HPW phase is present on the surface.

Izumi *et al.* (1983) have investigated supported HPAs for the alkylation of benzene with ethylene, esterification of acetic acid with ethanol and the dehydration of 2-propanol. Silica supported HPA were reported to be the most active. The activity for benzene alkylation, a surface type reaction, increased with increasing HPA loading (on Si) before levelling at 20 wt% HPA loading. Surprisingly for the later reactions, both "Bulk-type I" since they are absorbed into the bulk of HPAs, the trend was similar in that the conversions increased with increasing loading before levelling at 20-25 wt% HPA loading. They proposed that the reactions were principally occurring on the surface of the supported HPA crystallites, since the increase in the effective amount of surface protons subsided with increasing size HPA crystallites. The increasing crystallite size was observed by XRD of the supported catalysts, above 15-20 wt% the diffraction lines of HPW were detected. For the Bulk type I reactions the ceiling was slightly higher (20-25 wt%) suggesting that not only the surface of the HPAs played a part but also the first few surface layers.

Oxidation catalysis

As mentioned in Section 1.3.2 HPAs in solution containing Mo/V as peripheral atoms are strong oxidants. The same applies for HPAs in the solid state. Commercial plants exist for the partial oxidation of isobutyraldehyde/isobutene to methylmethacralate/methacrylic acid using HPMoV type catalysts supported on a diatomaceous earth carrier [Otake and Onoda, 1980; Nakamura and Ichihashi, 1980]. As with acid type catalysis there exists two types of oxidation catalysis, **"Surface type"** and **"Bulk type II"**. The later is unique in that the redox cycle occurs within the bulk of the HPA by virtue of rapid migration of protons and electrons. In this type of mechanism the rate determining step is the formation of water in the bulk. Typical oxidation reactions over HPAs include those shown in Table 1.13.

Table 1.13 Oxidation reactions catalyzed by HPCs. [Misono, 1991]

Reaction	Catalyst	Yield (%)	Temperature (°C)
Isobutene → Methacrylonitrile	$Mo_{10}PBi_3Fe_6K_{0.06}$	74	420
Butene → Maleic anhydride	$Mo_{12}PBi_{0.36}Mn_{0.52}$	63	400
Crotonaldehyde → Furan	PMo_{12}	40	-
Methacrolein → Methacrylic acid	Mo,P,V,Cs,K,Cu,Sb	70	285
	Mo,P,V,Na,K,As,Cu,Al	92	300
	Mo,P,V,Cu,Hg,Pb	79	325
	Mo,P,V,Cu,As,Ni	78	320
	Mo,P,V,(pyridine)	80	300
Isobutyric acid → Methacrylic acid	$PMo_{10}V_2$	69	302
Isobutyl aldehyde → Methacrylic acid	$PMo_{10}V_2$	70	310
Isopropyl methyl ketone → isopropenyl methyl ketone	$PMo_{10}V_2$	48	270

In summary it can be seen that Mo and V containing HPAs are good oxidation-type catalysts whereas those containing W are better acid-type catalysts. The acidity of the HPA follows the trend HPW > HSiW-HPMo > HSiMo. HPAs have been shown to be excellent catalysts for acid-type reactions involving "Bulk Type I" reactions whereas for "Surface type" deactivation due to coke formation is often excessive. In the following study of propene oligomerization the reaction is considered to be "Surface" type since propene is not absorbed into the bulk of HPAs and their salts.

1.4 ALUMINOPHOSPHATE ($AlPO_4$-n) MOLECULAR SIEVES

In the early 1980's workers at Union Carbide Corporation succeeded in synthesizing a novel class of crystalline microporous aluminophosphate molecular sieves [Wilson *et al.*, 1982]. These represented the first family of framework oxide molecular sieves synthesized without silica. These materials, designated as $AlPO_4$-n, where ***n*** is an arbitrary number denoting the structure type, presently include about 20 three-dimensional framework structures of which at least 14 are microporous and 6 are two-dimensional layer type materials. Their frameworks are neutral and are moderately hydrophilic. They have pore sizes in the range 3Å to 8Å.

The addition of silicon into the $AlPO_4$-n framework resulted in the discovery of SAPO-n type molecular sieves [Lok *et al.*, 1984a,b] where silicon is substituted either for phosphorous or an aluminophosphate pair. A number of these materials are isostructural with known zeolites such as chabazite (SAPO-34), faujasite (SAPO-37) and A (SAPO-42). SAPO molecular sieves are mildly acidic and some have unique pore selectivity properties. Incorporation of metals into $AlPO_4$-n or SAPO-n framework results in the formation of MeAPO-n and MeAPSO-n molecular sieves respectively. These materials are also mildly acidic and have pores similar to those of SAPO's. The complete aluminophosphate molecular sieve family is illustrated in Figure 1.11.

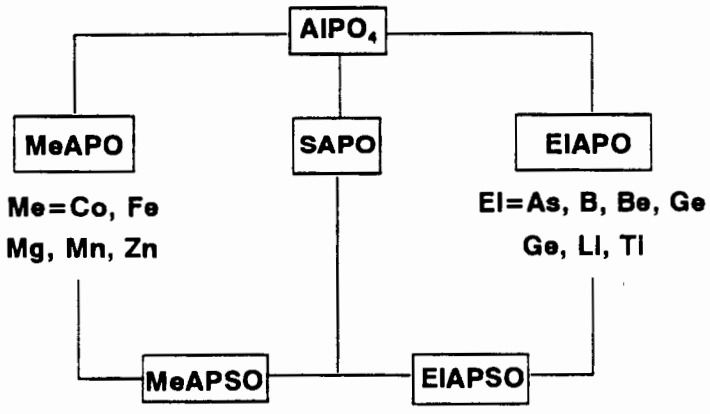

Figure 1.11 The $AlPO_4$-n based family of molecular sieves.

1.4.1. Structure of $AlPO_4$-n based molecular sieves

The concept of primary and secondary building units (SBU's) may be used to describe the different molecular sieve framework topologies. The primary building units consist of small cations (e.g. P^{5+}, Si^{4+}, Al^{3+}, Fe^{3+} etc.) in tetrahedral coordination with four oxygen atoms (shown below in Figure 1.12).

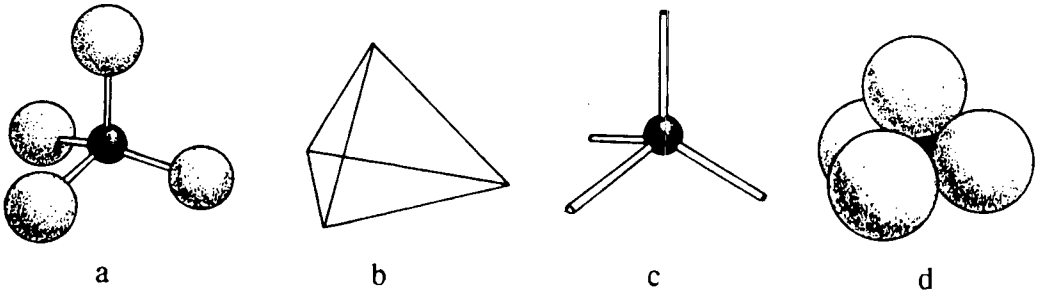

Figure 1.12 Methods of representing primary building units; TO_4 tetrahedra. [Breck, 1984]

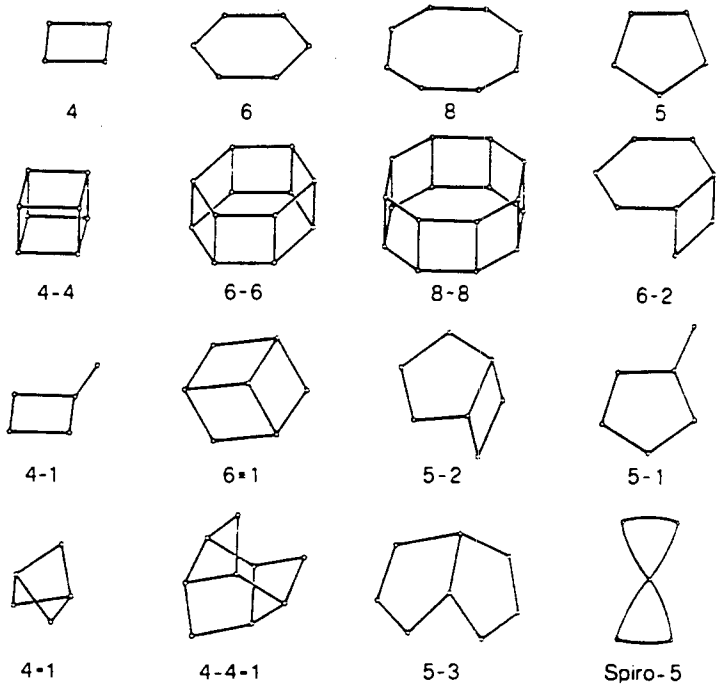

Figure 1.13 Secondary building units. The small circles represent the tetrahedrally coordinated cations and the linking oxygens are shown as straight lines.

SBU's were proposed by Meier, (1968) primarily to help visualize the framework construction on the assumption that a particular framework may only be built by only one SBU, although some frameworks do require two SBU's to describe their structure [van Koningsveld, 1991]. Structural subunits, which are more complex than SBU's, have also been developed to describe various framework topologies. Listed below are some of the zeolites and their SBUs (Table 1.14).

Table 1.14 Selected zeolites and their secondary building units. (SBU's) [Breck, 1984]

Zeolite	SBU	Zeolite	SBU
A	4-4	Analcime	4
Bikitaite	5-1	Brewsterite	4
Chabazite	4,6-6	Dachiaridite	5-1
Edingtonite	4-1	Epistilbite	5-1
Erionite	6.6-6	Faujasite	6-6
Ferrierite	5-1	Gismondine	4
Gmelinite	6-6	Heulandite	4,4=1
Sodalite	6	L	4,6-6
Levynite	6,6-6	Mordenite	5-1
Offretite	6,6-6	Stilbite	4,4=1
X	6-6	Y	6-6

There are over two dozen three-dimensional structures of the $ALPO_4$-n based family of molecular sieves. As mentioned earlier some of these structures are topological analogues of the zeolite molecular sieve family but a large number are novel structures. Among the novel structures, those of $AlPO_4$-5, -11, -14, -16, -33, -46 and -50 and MgAPO-36, SAPO-40, MgAPO-43, CoAPO-44 and CoAPSO-47 have been determined by X-ray diffraction.

Table 1.15 lists the typical structures of the $AlPO_4$-n molecular sieves arranged according to pore size. It can be seen that the $AlPO_4$-n molecular sieves exhibit a similar pore size range to that of the zeolites. There are five large pore size materials that have pore sizes similar to large pore zeolite Y or L, with four of them having novel structures. The intermediate pore materials all have novel crystalline form. Recently the framework topology of the first 14-ring molecular sieve, $AlPO_4$-8, has been reported. $AlPO_4$-8 exhibits a unidimensional, 14-membered ring, pore channel system with pore dimensions of 7.9 × 8.7Å. In addition to the structures of $AlPO_4$-n

materials listed in Table 1.15, SAPO type materials also have several new crystal types such as SAPO-40, -41 and -44.

Table 1.15 Selected structures of $AlPO_4$-n based molecular sieves. [Flanigen *et al.*, 1986]

Species	Structure Type	Pore Diameter (Å)	H_2O Pore Volume (cm^3/g)
Very large pore			
VPI-5	Novel, detm.	12.5	0.35
Large pore			
5	Novel, detm.	8.0	0.31
36	Novel	8.0	0.31
37	Faujasite	8.0	0.35
40	Novel, detm.	7.0	0.33
46	Novel	7.0	0.28
Intermediate pore			
11	Novel, detm.	6.0	0.16
31	Novel	6.5	0.17
41	Novel	6.0	0.22
Small pore			
14	Novel, detm.	4.0	0.19
17	Erionite	4.3	0.28
18	Novel	4.3	0.35
26	Novel	4.3	0.23
33	Novel	4.0	0.23
34	Chabazite	4.3	0.30
35	Levynite	4.3	0.30
39	Novel	4.0	0.23
42	Linde Type A	4.3	0.30
43	Gismondine	4.3	0.30
44	Chabazite-like	4.3	0.34
47	Chabazite-like	4.3	0.30
Very small pore			
16	Novel	3.0	0.30
20	Sodalite	3.0	0.24
25	Novel	3.0	0.17
28	Novel	3.0	0.21

Hasha *et al.* (1988) have studied the crystal structure of SAPO-20 (sodalite structure) and showed evidence that there are no Si-O-P linkages in the framework of the molecular sieve. They have also discovered that silicon atoms are found to have silicon and/or aluminium neighbours while phosphorous is surrounded exclusively by aluminium atoms. These findings have been observed by other workers for other SAPO-n sieves [Flanigen *et al.*, 1986,1988; Kuhl and Schmitt, 1990]. It is therefore possible to conclude that, in terms of substitution mechanisms, Si^{4+} can substitute for

P^{5+}, and vice versa, and Si-O-Si can substitute for Al-O-P, and vice versa. The presence of silicon-rich aluminosilicate domains have been reported in SAPO-5, -11 and -37 [Martens *et al.*, 1990; Man *et al.*, 1991]. Si and metal substitution into the framework is discussed in more detail in Section 1.4.4.

1.4.1.1 Structure of SAPO-11 and AEL structure types

SAPO-11, isostructural with $AlPO_4$-11, has the AEL (IUPAC Zeolite structure code) structure-type and consists of 6-2 SBU's with a framework density of 19.1 T/1000Å^3. The crystal structure is orthorhombic (Imma) with unit cell dimensions of a = 13.5Å, b = 18.7Å and c = 8.4Å and $\alpha = \beta = \eta = 90°$. The pore structure of SAPO-11 consists of nonintersecting elliptical 10-membered rings with maximum and minimum diameters of 6.3Å and 3.9Å respectively (Figure 1.14). The structure of MnAPO-11 has also been determined and the crystal structure is orthorhombic (Icm2), a = 13.472Å, b = 18.712Å, c = 8.4431Å and a unit cell volume of 2128.4Å^3.

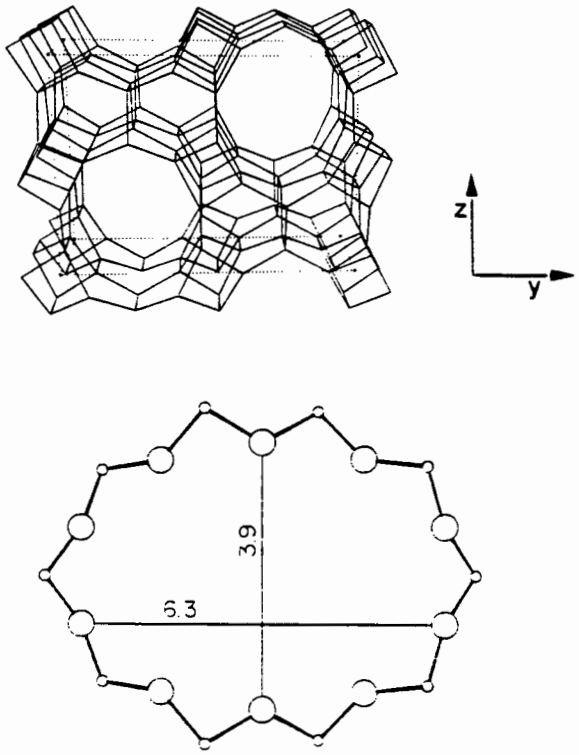

Figure 1.14 Framework and pore structure of SAPO-11 viewed along the [100] plane. [Bennet *et al.*, 1987]

According to sorption data [Barrer, 1988] it was estimated the SAPO-11 has an effective pore diameter of 6Å.

1.4.2. Synthesis of $AlPO_4$-n type molecular sieves

$AlPO_4$-n type molecular sieves are synthesized hydrothermally between 100-250°C under autogenous pressure and crystallization times ranging from 2 hours to several days. The reaction mixtures contain reactive sources of aluminium, phosphorous and additional framework elements (Si, and Me = Co, Mn and Fe etc.) as well as an organic amine or quaternary ammonium salt (R) and water. Typically equimolar amounts of aluminium and phosphorous are used. The reactive gel compositions for most SAPO-n sieves is illustrated in Figure 1.15 below.

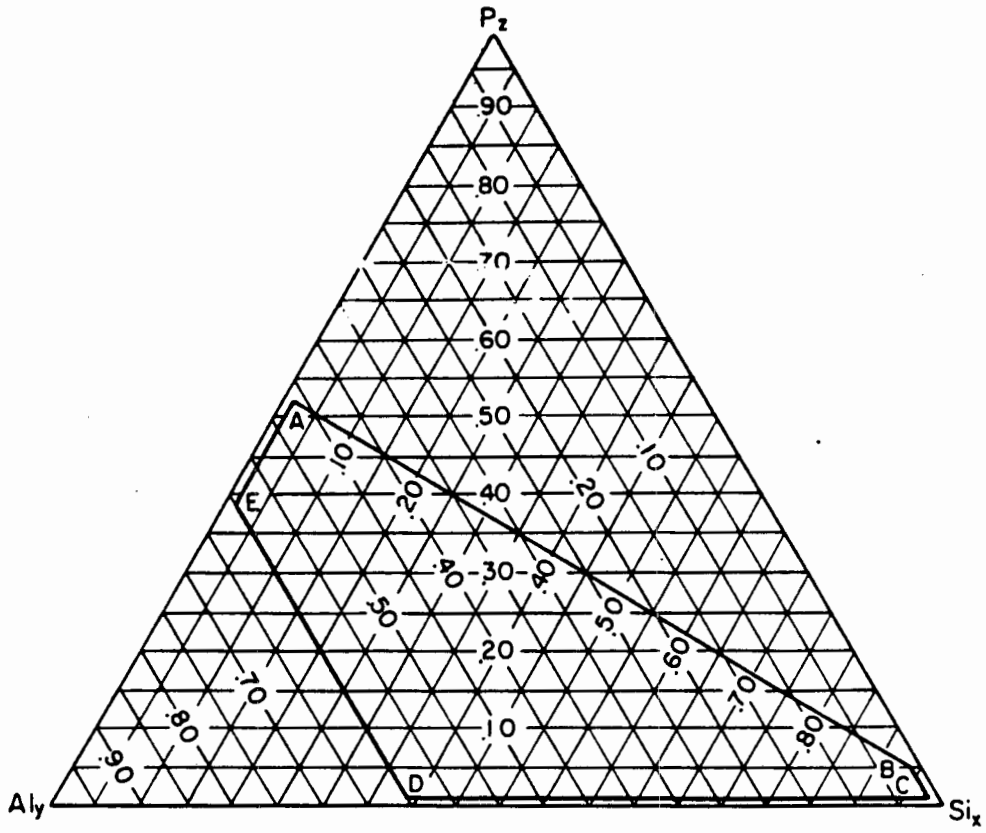

Figure 1.15 Ternary diagram of the chemical compositions of the reaction gel for the synthesis of SAPOs. [Lok *et al.*, 1984b]

The chemical compositions of the various members of the $AlPO_4$-n family are outlined below:

$AlPO_4$: [xR] Al_2O_3 (1.0 ± 0.2) $P_2O_5 \cdot yH_2O$.

The quantities x and y represent the amounts of R (R = organic amine or quaternary ammonium salt) and H_2O needed to fill the microporous voids within the neutral $AlPO_4$-n framework.

MeAPO: [mR] $(Me_xAl_yP_z)O_2$ (anhydrous basis).
The value of x, the mole fraction of Me (Me = Co, Mn, Fe, Zn, Mg), typically varies from 0.01-0.25 and the value of y, the mole fraction of Al, varies from 0.25 to 0.5. The value of z, the mole fraction of P, remains constant at 0.5 and the value of m, the mole fraction of R varies between 0 and 0.3.

SAPO: [mR] $(Si_xAl_yP_z)O_2$ (anhydrous basis).
Where the value of m, the mole fraction of R varies between 0 and 0.3. The possible values of x, y and z are represented below in Figure 1.16.

MeAPSO: [mR] $(Me_wAl_xP_ySi_z)O_2$ (anhydrous basis).
Where the value of m, the mole fraction of R varies between 0 and 0.3. Me = Co, Mn, Fe, Zn, Mg. The possible values of w, x, y and z are given below in Figure 1.17

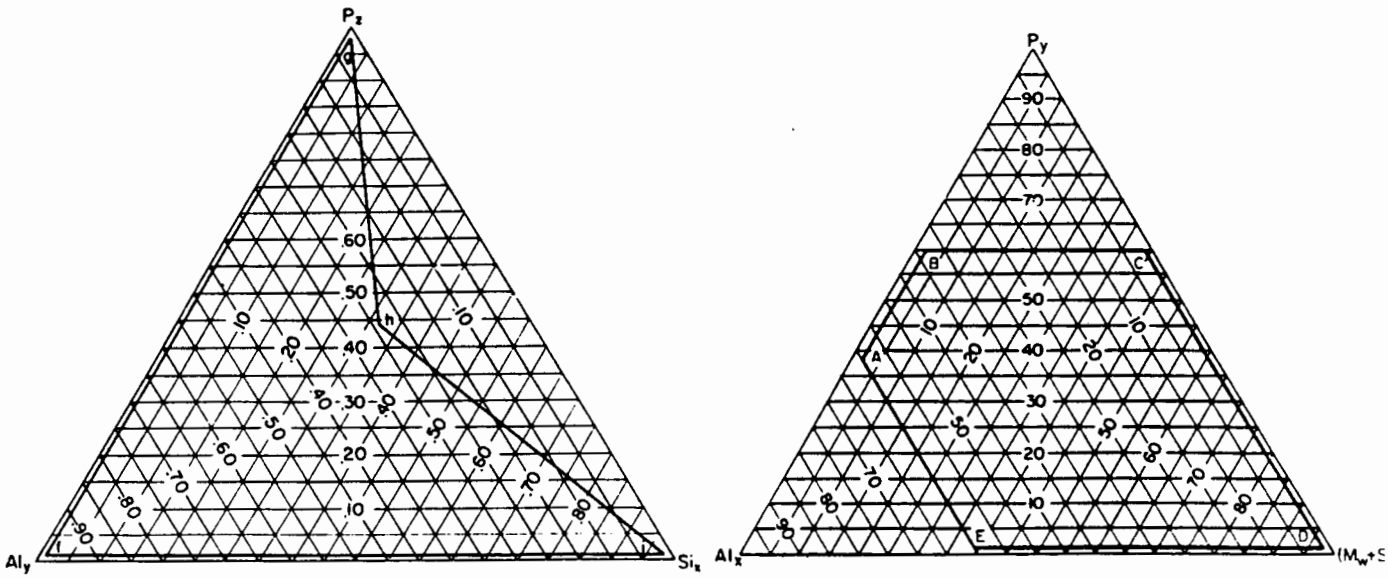

Figure 1.16 Ternary diagram of the chemical compositions of as-synthesized SAPOs. [Lok *et al.*, 1984b]; Figure 1.17 Ternary diagram chemical compositions of as-synthesized MeAPSOs. [Lok *et al.*, 1985]

The most common reactive sources of Si, Al, Me and P are:
Si: Fumed silica, colloidal silica solution (e.g. Ludox HS-40)
Al: Aluminium isopropoxide, pseudoboehmite (hydrated Al_2O_3)
P: Orthophosphoric acid
Me: Metal acetates, nitrates, chlorides, sulfates.

Listed and discussed below are some of the most important variables that influence the synthesis of $AlPO_4$-n type molecular sieves. More detailed information about synthesis variables and their effects on the final product have been published in some excellent articles and reviews [Ren *et al.*, 1991; Wilson, 1991; Wilson *et al.*, 1984; Wilson and Flanigen, 1989, Flanigen *et al.*, 1986,1988].

1.4.2.1 Effect of template

The organic template appears to play a critical structure-directing role and becomes entrapped or clathrated within the crystalline product [Pluth and Smith, 1989]. Over 100 amines and quaternary ammonium salts have been used successfully as crystallization templates, including primary, secondary, tertiary and cyclic amines and alkanolamines.

The degree of template-structure specificity varies from the crystallization of $AlPO_4$-5, with 23 templates, to the formation of $AlPO_4$-20 with only 1 template. The most common templates are shown in Table 1.16. As can be seen from Table 1.16, one template can be responsible for many different structures. In these cases the structure is controlled by varying synthesis variables such as template concentration, gel oxide composition, temperature, crystallization time, stirring rate and pH, which will be discussed in the Sections below.

The influence of the template is both steric and electronic and commonly exhibits neat stoichiometric and space filling characteristics. In some cases two templates are required to produce a certain structure type, in these cases one template performs a structure directing role and the other establishes the correct pH.

The effect of the template type and concentration used in the synthesis of $AlPO_4$-5 and SAPO-5 has been investigated [Weyda and Lechert, 1990;

Wilson *et al.*, 1984]. It was shown that the type of template affected the crystallization rates and induction period. Crystallization with Pr_3NH, Et_3NH and diethylamine proceeded much faster than for TPAOH. Higher concentrations of Pr_3NH template resulted in faster crystallization rates and shorter induction periods. This indicated that at higher template concentrations more nuclei were being formed. At low concentrations of template (and consequently low pH values of the gel), dense aluminophosphate phases such as tridymite, cristobalite, metavariscite and $AlPO_4$(quartz) are formed [Wilson, 1991]. Jahn *et al.* (1989) have since suggested that the role of the template (triethylamine) in the formation of $AlPO_4$-5 is to stabilize the newly created tetrahedral Al in the synthesis gel and to prevent its conversion to octahedral Al by shielding it from attack by water.

Table 1.16 Typical templates used for $AlPO_4$-n synthesis. [Wilson and Flanigen, 1989]

Structure Type	Template
Large pore	
5	tetraethylammonium hydroxide (TEAOH)
	tetrapropylammonium hydroxide (TPAOH)
	tri-n-propylamine (Pr_3NH)
	piperidine
	methylpyridines
	cyclohexylamine
36	Pr_3NH
37	TPAOH
	TPAOH and tetramethylammonium hydroxide (TMAOH)
46	di-n-propylamine (n-Pr_2NH)
Intermediate pore	
11	n-Pr_2NH
	isopropylamine
	Pr_3NH
	n-dibutylamine
	n-dipentylamine
31	n-Pr_2NH
41	n-Pr_2NH
Small pore	
14	isopropylamine
17	quinuclidine
18	TEAOH
34	TEAOH
35	quinuclidine
44	cyclohexylamine
Very small pore	
20	TMAOH

For the synthesis of $AlPO_4$-11 sieves, Tapp *et al.* (1988b) have suggested that even if the amine template was capable of stretching or bending to the required c-dimension of $AlPO_4$-11 (c=8.44Å) the amine would not necessarily be a successful template. For example, primary amines such as n-hexylamine and n-butlyamine were not successful templates for $AlPO_4$-11/SAPO-11 synthesis. This suggested that the amine plays not only an important templating role but also an important electronic role. Balakrishnan and Prasad (1990) have recently reported that long chain secondary amines such as $(n\text{-}C_5)_2NH$ (c=14.2Å) are capable of templating $AlPO_4$-11. This suggested that the steric property of the template in structure direction by itself is not likely to be the main criterion. They proposed that the amine appears to act primarily as an optimum pH stabilizer.

1.4.2.2 Effect of synthesis gel composition/preparation

The preparation of the reaction mixtures and their composition has an important influence especially on nucleation and the induction period and rate of crystallization as well as on the products obtained.

Composition

Water is the most common reaction mixture solvent, although alcohols, such as water immiscible n-hexanol, have been used for biphasic syntheses [Martens *et al.*, 1989a,b]. Increasing the water content of $AlPO_4$-n synthesis gels beyond a certain value generally reduces the crystallinity of the final product [Weyda and Lechert, 1990]. In some cases, however, high water contents are used to assist in the synthesis of large single crystals [Kessler, 1989; Finger *et al.*, 1991; Muller *et al.*, 1989]. By increasing the water content SAPO-5 and $AlPO_4$-5 crystals with varying lengths and aspect ratios have been synthesized [Finger *et al.*, 1991; Muller *et al.*, 1989]. Qui *et al.* (1991) have reported similar findings.

The presence increased Si content reduces the crystallization rates of SAPO-5 and beyond a certain critical Si content (Si > 0.4) the crystallinities decrease [Weyda and Lechert, 1990]. The critical Si content varies depending on the structure type. For example the most crystalline SAPO-11 products have been obtained with Si contents of < 0.14 [Mertens *et al.*, 1990]. Khouzami *et al.* (1988) has shown that the most crystalline SAPO-11

product was obtained with a Si content of 1 Si per unit cell and that increasing the Si content decreased the crystallinity. Addition of metals to the synthesis gel also reduces crystallization rates and product crystallinity [Lechert *et al.*, 1991], hence longer synthesis times are often required for pure crystalline products. Excess metal ions in the synthesis of MeAPSO-5 sieves tends to result in the crystallization of denser phosphate phases or to cristobalite or tridymite phases [Lechert *et al.*, 1991].

Using aluminium and phosphorous sources other than those suggested in the patent literature results in poor crystals and other undesirable products being formed. In the synthesis of $AlPO_4$-n sieves increasing the Al:P ratio above one gives rise to the formation of amorphous alumina species. To improve the chances of preparing a pure product the Al and Si concentrations are usually chosen to be limiting, since they are the least soluble [Wilson, 1991]. Syntheses with Al:P ratios less than 1 usually require more template to be added to counteract the effect of excess phosphoric acid.

Different aluminium sources can produce a product with different morphologies, for example, Tapp *et al.* (1988b) have shown that syntheses with aluminium isopropoxide results in an $AlPO_4$-11 consisting of hexagonal rods and syntheses with pseudoboehmite result in an $AlPO_4$-11 consisting of polycrystalline aggregates. Ernst *et al.* (1988) have also shown that using different aluminium sources can lead to different products. For example, aluminium isopropoxide (Al(iso)) yields CoAPSO-50 and pseudoboehmite yields CoAPSO-46. By omitting the Si from the synthesis gels, CoAPO-11 was formed. Weyda and Lechert (1990) have shown that using Al(iso) a less crystalline SAPO-5 product is obtained compared to synthesis with pseudoboehmite. The lower crystallinity of the Al(iso) SAPO-5 synthesis was attributed to the presence of isopropanol in the gel (formed when Al(iso) is added to H_3PO_4), as was proved when isopropanol was added to the synthesis gel dense phases (the crystalline impurities) were obtained. Lok *et al.* (1983) suggest that the use of Al(iso) as opposed to boehmite results in the possible formation of amorphous material or substantially slower crystallization rates.

Addition of HF to $AlPO_4$-n and SAPO-n synthesis gels has been investigated by Kessler, (1989) and Qui *et al.* (1991). The fluorine acts as a mineralizer

and causes growth of larger crystals. Surprisingly the HF had little effect on the gel pH and the products did not contain fluorine. The addition of NaOH and NH_4OH to a CoAPO-5 synthesis gel resulted in increased impurity levels but promoted large single crystal growth [Shiralkar *et al.*, 1989].

Preparation

Although the effects of order of addition of the components is not well understood, it is clear that the mix order can affect the mix rheology and pH. Pretreatment conditions such as gel ageing have also been suggested to result in more crystalline pure products but the general desirability of an ageing step has not yet been comprehensively demonstrated.

Tapp *et al.* (1988a,b) has shown that route C (90°C pretreatment before addition of template and synthesis at 200°C) and D (90°C pretreatment of synthesis gel with template before synthesis at 200°C) yielded a more crystalline $AlPO_4$-11 product, free of any condensed phases. The 90°C pretreatment was proposed to form a poorly crystalline metavariscite/variscite reactive intermediate which precludes the formation of crystalline microporous $AlPO_4$-11. Substitution into this intermediate may be the critical step for the synthesis of substituted $AlPO_4$-11 type sieves. Gel ageing with stirring has also been shown to be important factor during the synthesis of pure SAPO-37 [Ojo *et al.*, 1991].

1.4.2.3 Effect of pH

The initial gel pHs in most cases are weakly acidic (pH 3-5) facilitating the successful incorporation of the hydrolyzeable metal cations into the frameworks and thus inhibiting their precipitation as spurious hydroxides or oxides. In the synthesis of SAPO-5 the changes in pH with synthesis time has been investigated and the results are shown in Figure 1.18.

An explanation for such a result may be that a rearrangement of the hydrogel takes place during the crystal growth thus reducing the number of free OH^- groups at the surface of the growing crystals and the gel particles.

SAPO-5 can be synthesized with the starting gel at a pH of between 4 and 7. At pH lower than 4 crystallization is poor although this could be due to

the high Cl^- concentration since HCl was added to starting gel to reduce the pH. At pHs below 3 dense aluminophosphates phase crystallize out [Weyda and Lechert 1990; Wilson, 1991].

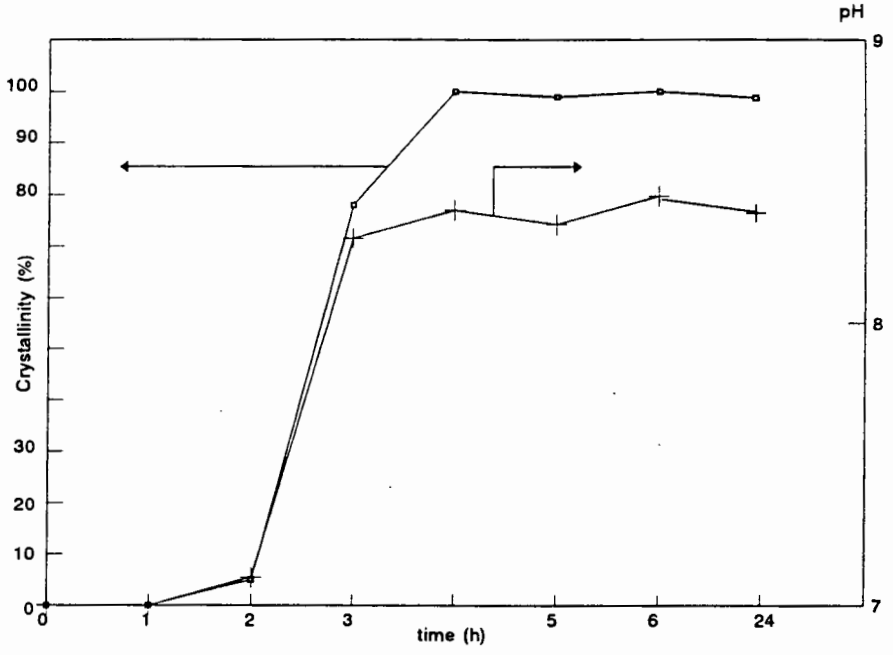

Figure 1.18 Changes in pH with synthesis time of a SAPO-5 synthesis gel. [Weyda and Lechert, 1990]

The initial gel pH for SAPO-11 synthesis depends on the aluminum source used, aluminium isopropoxide yielding higher pH values (9-10) than pseudoboehmite (pH 4-5) [Mertens *et al.*, 1990]. The pH of the final mixtures was between pH 8-10 (i.e. remains constant for Al(iso)). The pseudoboehmite apparently reacts less than the Al(iso) during the initial preparation, giving mixtures with lower pH values [Wilson, 1991]. Al(iso) reacts rapidly with phosphoric acid, probably producing different precursor species, resulting in a synthesis gel with a higher pH value.

1.4.2.4 Effect of synthesis temperature

$AlPO_4$-n and SAPO-n tend to crystallize at temperatures above 125°C whereas MeAPOs and MeAPSOs can be crystallized below 125°C. Temperature plays an important role in the rate of crystallization of SAPO-5. Increasing the temperature from 150-225°C decreases the crystallization time from 6 to 4 hours. In some instances increasing the synthesis

temperature results in the formation of different structures [e.g. Wilson *et al.*, 1984].

1.4.2.5 Effect of synthesis time

Rajic *et al.* (1990) have shown that in the preparation of CoAPSO-34 at 125°C there was no crystalline material present after 14 days. However, after 35-45 days a crystalline product comprising 90% CoAPSO-34 was obtained. Wohlrab *et al.* (1992) showed that increasing the reaction time from 12 to 24 hours transformed FeAPO-5 to FeAPO-34, suggesting that FeAPO-34 was thermodynamically more stable than FeAPO-5. Maistriau *et al.* (1989) have shown that the yield of SAPO-37 attained a maximum after a synthesis time of 24 hours and decreased with increasing synthesis times thereafter. The decrease in SAPO-37 yield was accompanied by the formation of SAPO-40. Ojo *et al.* (1991) have since suggested that longer synthesis times favour the co-crystallization of SAPO-5 and/or SAPO-40 along with SAPO-37. Therefore the crystallization process appears to be a competitive one between that of SAPO-37 and SAPO-5/SAPO-40.

With increasing synthesis time Jahn *et al.* (1990) have suggested that SAPO-11 becomes more Al enriched. The changes in chemical composition of their SAPO-11 was consistent with that of an aluminium uptake rather than a P loss from the crystalline product. It was proposed that the Al atoms were incorporated onto the SAPO-11 crystal lattice by condensation with P-OH groups localized in the neighbourhood of single Si atoms.

1.4.2.6 Effect of stirring

In the preparation of SAPO-37 rapid stirring (300 rpm) in an autoclave produced pure SAPO-37. Slow (30 rpm) or no stirring resulted in a mixture of SAPO-37 and SAPO-40 [Maistriau *et al.*, 1990]. It has also been observed that smaller crystals are produced under faster stirring conditions, most probably because more nucleation centres are created by achieving greater homogeneity of the gel. No work has been done to date investigating the effect of stirring on the synthesis of $AlPO_4$-11 type sieves.

In summary it can be concluded that the synthesis of pure/crystalline $AlPO_4$-n type sieves is not simple and depends on a variety of factors as listed

above. One of the most important factors however is the template type and concentration, followed closely by the gel composition and preparation procedure.

1.4.3 Post-synthesis modifications

1.4.3.1 Acid washing

Mineral acids are often used for dealumination purposes. $AlPO_4$-n molecular sieves have been suggested to be mildly resistant to acid attack [Barrer, 1988] whereas most zeolites are acid resistant. Acid washing removes aluminium from the pores. Hampson *et al.* (1989) have shown that crystallinity of $AlPO_4$-5 decreases when the calcined sieve was exposed to mineral acids. The order of lattice attack increased for HCl > HNO_3 >> H_3PO_4. The loss in crystallinity was proposed to occur via leaching of phosphorous from the framework. Choudhary *et al.* (1988) have shown that at pHs below 1.0, $AlPO_4$-5 completely dissolves, and that milder acid treatments result in decreases in pore volume and % crystallinity. Zeolites with high aluminium content (Zeolite-Y) are also non-resistant to acid attack and since $AlPO_4$-n sieves have high Al contents this may be the reason for their low resistance to acid attack.

1.4.3.2 Silicon treatments

Silanization is most commonly used to poison external acid sites which results in decreased coking (Section 1.2.7). Treatment of zeolites with $SiCl_4$ vapour may also result in the replacement of aluminium framework atoms by Si [Beyer and Belenykaja, 1980], decreasing the acidity. The majority of work for $AlPO_4$-n sieves has centered around silicon incorporation into the framework, which should increase the acidity. Little work exists on silanization of the external surface of $AlPO_4$-n type sieves other than by $SiCl_4$ treatments.

Silanization of $AlPO_4$-5 with $SiCl_4$ at 300-600°C has resulted in Si-substituted $AlPO_4$-5 formation without significantly affecting the crystal structure [Choudhary *et al.*, 1989]. During silanization both Si substitution for Al and Al:P was proposed (up to 10% Si for Al). The former mechanism is highly unlikely since this would result in the formation of Si-O-P bonds

and a positive framework. These sieves had strong acid sites and were active for the conversion of iso-octane and *o*-xylene isomerization. Theocharis *et al.* (1989) have suggested that upon treatment of $AlPO_4$-5 with $SiCl_4$ that fewer but stronger acid sites are produced compared to $AlPO_4$-5. They proposed that Si substituted for P only. They also proposed that some adsorption sites were lost and mesoporosity developed. The reaction occurred preferentially at inter crystalline regions and at intercrystalline defects i.e. defects in the pore structure. Brinen *et al.* (1990) have also treated $AlPO_4$-5 with $SiCl_4$ and shown increased ammonia and pyridine retention but no increased activity for cumene cracking. The xylene product distribution was similar to that expected from a Friedel-Crafts type alkylation. Their pyridine IR showed only Lewis bound pyridine. More severe treatments leave silicon-rich residue in the pores which decreases reaction rates and ammonia retention. Li and Davis (1992) suggest that $SiCl_4$ treatment significantly reduces pore volume by deposition of amorphous material. Treatment of SAPO-5 with $SiCl_4$ vapour dealuminates the SAPO-5 silicoaluminium region only. Their thermochemical calculations revealed that the reaction of $AlPO_4$-n sieves with $SiCl_4$ is unlikely.

1.4.3.3 Hydrothermal treatments

Hydrothermal treatment of zeolites results in the removal of aluminium from the framework. Unlike in acid washing these extra-framework aluminium species remain within the pores. Severe steaming usually results in decreased activity whereas mild steaming often increases activity [Lago *et al.*, 1986]. Anderson (1991) has also shown increased hexene oligomerization activity after mild hydrothermal treatments of ZSM-5. The reason for the increased activity is proposed to be due to the formation of strong/superacid sites. Deep bed (DB) calcination often allows a very mild form of steaming to occur (profile in bed as bottom catalyst will be more steamed). The water is desorbed between 100-250°C (water of hydration). $AlPO_4$-n and SAPO-n molecular sieves have been reported to be very stable to hydrothermal treatment [Wilson *et al.*, 1982; Lok *et al.*, 1984a; Barrer, 1988]. Barger (1992), for example, has shown hydrothermally treated SAPO-34 (700°C, 100% steam), which has less acidity and increased ethylene and propene selectivity for methanol conversion (also less paraffins), still retains 80% crystallinity. Van Niekerk (1992) has shown that steaming reduced the activity of SAPO-34 for methanol conversion but that

deep bed calcination resulted in increased activity compared to shallow bed calcination. Choudhary *et al.* (1988) have shown that $AlPO_4$-5 underwent no phase transformations during steaming (35 mm Hg, t=6-168 hs) but the crystallinity decreased with increasing steam time. Accompanied with the losses in crystallinity were losses in pore volume (determined by N_2 adsorption).

1.4.3.4 Metal impregnation

Metal impregnated molecular sieves have been widely studied since these catalysts are used extensively for industrial reactions [Rabo, 1976]. Often the major objective is to introduce bifunctional catalysts with shape selective properties and not simply to use the molecular sieve as a high surface area support.

Metal impregnation of $AlPO_4$-5 by chemical vapour deposition (CVD) of Ni or $NiNO_3$ impregnation has shown that Ni resided exclusively on the external surface of the crystallites since pore volumes (measured by n-butane adsorption) were not effected by impregnation [Kraushaar-Czarnetzki and Van Hooff, 1989]. Often metal impregnation leads to pore blockage. Co impregnated $AlPO_4$-n type sieves have been shown to exert strong interactions between the $AlPO_4$-n framework and the extra-framework Co. Whether Co was introduced into the synthesis gel or by impregnation of the sieves the Co effected the P-NMR to same extent.

1.3.3.5 Ion-exchange

Zeolites are often synthesized in the Na and hence non-acidic form. To transform the Na form to the acidic H form the zeolites are ion exchanged in NH_4 solution and then deammoniated. Since $AlPO_4$-n molecular sieves are synthesized without Na the acid form is simply obtained by calcining the template form in air to remove the template. Ion-exchange is also commonly used as a method of impregnating metals or exchanging various cations into or out of the zeolite. Ion exchange is usually achieved by placing the sieve in a solution containing the required anion/cation.

Hampson *et al.* (1989) have investigated the stability of the $AlPO_4$-n framework in aqueous salt solutions and found that the framework degrades

via the leaching of Phosphates into solution. The extent to which the framework was attacked increased with increasing salt concentration and also depended on the nature of the anion (OH^- > I^- > $S_2O_3^{2-}$ > Br^- > Cl^-). The stability of the frameworks followed the order of $AlPO_4$-11 ≃ $AlPO_4$-25 > $AlPO_4$-5.

Montes *et al.* (1990) have also observed phosphorous loss after ion exchanging calcined CoAPO-5. They have suggested that extra-framework phosphorous species may exist (such as $H_2PO_4^-$), similar to those found in $AlPO_4$-52 [Bennet *et al.*, 1988], and these are removed during IX. Kuhl and Schmitt, (1990) have also shown that phosphates were occluded in the sodalite cages of SAPO-42. The $H_2PO_4^-$ species were proposed to be chargebalancing for extra-framework Co^{2+} which was also exchanged from CoAPO-5. The effective pore diameter of CoAPO-5, less than that of $AlPO_4$-5, increased after ion-exchange which suggested that these extra-framework P and Co species were occluded within the pores.

Lee *et al.* (1991) studied the location and adsorbate interaction of Cu^{2+} ion exchanged in H-SAPO-11. Reductions in crystallinities were observed after calcination and subsequent ion-exchange. The amount of Cu^{2+} exchanged was very low (<0.1 %). The ion exchanged Cu^{2+} was proposed to occupy the sites shown below in Figure 1.19.

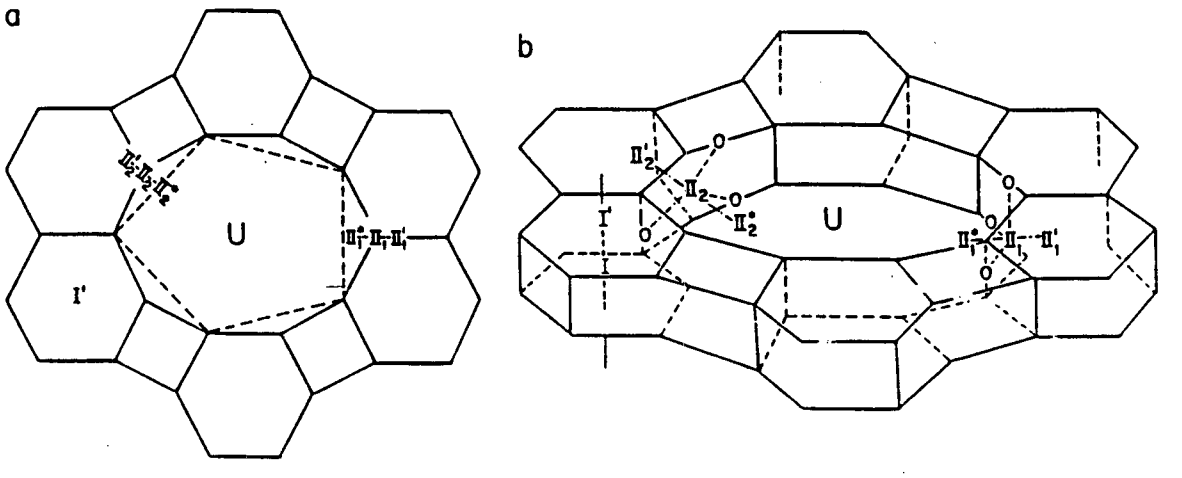

Figure 1.19 Possible locations of Cu^{2+} in ion-exchange sites in H-SAPO-11.

Kraushaar-Czarnetzki and Van Hoof (1989) have attempted to ion-exchange Ni into $AlPO_4$-5 using $NiNO_3$ but found very little Ni had been ion-exchanged (0.05%). Due to the electronic neutrality of $AlPO_4$-n the driving forces for ions to migrate internally are small and hence this was not unexpected.

1.4.4 Silicon and Metal substitution into $AlPO_4$-n framework

Since silicon (Si) and metal incorporation into the $AlPO_4$-n framework is proposed to give rise to acidity, the location and state of the Si and Me are of obvious importance. The current views on Si and metal location and their effect on acidity as well as the techniques used to determine their location and state will be discussed in the following sections.

1.4.4.1 Si substitution

As mentioned in Section 1.4.1, Si substitutes for either P or an Al:P pair. Tapp *et al.* (1988a) have shown that for Si content of less than 2% there exists a good correlation between amount of Si incorporated and the number of acid sites generated in SAPO-5. This suggests a substitution mechanism of Si for P. At Si concentrations above 2% the relationship falls away primarily due to the substitution mechanisms changing with the formation of not only SAPO domains but Si and SiAl rich domains [Martens *et al.*, 1990; Mertens *et al.*, 1990]. Si substitution is mainly monitored by Si-NMR. Martens *et al.* (1990) suggest that for SAPO-11 there exist SAPO domains with little or no Si and that the majority of the Si is located in SiAl domains (Si/Al ratio ranging from 2-9). The activity for decane cracking was related to the presence of SiAl and SiAl-SAPO interface type acid sites. SAPO-5 on the other hand has Si rich SiAl domains and SAPO domains with appreciable amounts of Si. The activity of SAPO-5 for decane cracking was related therefore to SAPO-type acid sites.

1.4.4.2 Metal substitution

Metals substitute preferentially for Aluminium. Kraushaar-Czarnetzski *et al.* (1991a,b) have found that for CoAPO-5, -11, -16 and -34 that for metal concentrations of less than 2% there exists a good correlation between the number of acid sites generated and the amount of Co present. The percentage of framework metal at which the relationship deviates is also

dependent on the structure type and decreases in the order $CoAPO_4$-5>-11>-16>-34. At higher concentrations the relationship falls away with the concurrent formation of extra-framework Co species as well as framework Co.

Of all the work on metal substituted $AlPO_4$-n type sieves the majority of studies have focused on Co containing systems. The most commonly used methods for the detection of framework substituted Co are spectroscopic techniques such as ESR, EPR, IR, UV-VIS and XPS. The presence of acid sites in CoAPO-n sieves has been confirmed, showing that Co^{2+} must predominantly substitute for Al^{3+} [Tapp *et al.*, 1985]. The intense blue colour of these sieves further indicates that Co is in a tetrahedral environment [Cotton and Wilkinson, 1987]. However the degree of substitution depends on the structure type and amount of Co added to the synthesis gel. Above 14 mol% Co addition an amorphous cobalt aluminium phosphate impurity phase was formed and at levels above 35 mol% Co no crystallization was observed for CoAPO-5 [Shiralkar *et al.*, 1989].

A detailed spectroscopic investigation by Schoonheydt *et al.* (1989), revealed that the diffuse reflectance spectra (DRS) of CoAPO-5 showed structural Co only and that after air calcination some of the Co^{2+} was partially oxidized to Co^{3+} which still remained in the framework but with strongly distorted symmetry. This Co^{3+} could be completely reduced back to Co^{2+} by reduction in hydrogen at 500°C. These observations have lead to the study of the redox chemistry of Co in the lattice of molecular sieves.

Montes *et al.* (1990), in their study have also indicated that framework Co^{2+} is oxidized to framework Co^{3+} after air calcination. The colour of the sieve after air calcination was yellow-green and returned to blue (the as-synthesized colour) after reduction in hydrogen at 500°C, suggesting reduction of Co^{3+} to Co^{2+}. Contacting calcined CoAPO-5 with methanol or acetone also reverted the colour back to blue indicating that methanol or acetone may also act as reducing agents. Iton *et al.* (1989) have also reported that after methanol adsorption the colour of calcined CoAPO-34 and CoAPSO-34 reverts to blue. A free radical mechanism for the redox involving methanol was proposed and is shown below. The first step involves a one-electron transfer,

$CH_3OH + Co^{3+} \rightarrow CH_3O\cdot + Co^{2+} + H^+$

followed by a second one-electron transfer

$CH_3O\cdot + Co^{3+} \rightarrow H_2CO + Co^{2+} + H^+$

Support for this mechanism was shown by an increase in the hydroxyl region, but no reaction products were collected by Montes *et al.* (1990) or Iton *et al.* (1989) to substantiate their redox proposals.

Kraushaar-Czarnetzki *et al.* (1991a,b) have proposed that the redox mechanisms for CoAPO-5 and CoAPO-11 type sieves are completely reversible, whereas the mechanisms for CoAPSO-16 and CoAPO-34 show reduced crystallinity and a loss in framework Co after each redox cycle. Their results showed that both framework and non-framework Co existed and that the amount of framework Co (and hence potential Brönsted acid sites) could be determined from electron absorption spectroscopy. Changes in the cation exchange capacity and number of acid sites were also observed when the Co in the framework underwent redox.

Further work by Kraushaar-Czarnetzki *et al.* (1991a,b) showed changes in Lewis and Brönsted acidity after redox (the number of Brönsted and Lewis increases after reduction) and the formation of formaldehyde was detected after reduction using methanol. They proposed the same redox mechanism as Iton *et al.* (1989) for the redox mechanism involving methanol but have not yet fully investigated the reaction mechanism involving the $CH_3O\cdot$ radicals.

Recently further spectroscopic studies [Chen *et al.*, 1992; Chao *et al.*, 1992] have been published that confirm the previous authors findings and have also suggested that Co is driven out of the framework after air calcination and these species become chemically anchored to the framework as $Co(II)O_6$ octahedra.

The redox ability of Co containing sieves has been brought into question by Perriera *et al.* (1992), who have suggested that the change in colour may simply be due to the distortion of the tetrahedral environment of Co^{2+} to a pseudo-octahedral one. These authors did not detect any oxidation products

after calcination or any reduction products after reduction with 2-propanol and suggest that their UV-vis and ESR results are not conclusive enough to substantiate that Co^{3+} is in a tetrahedral environment. Kustov *et al.* (1991) have also suggested that from their UV-vis and ESR results that Me^{3+} ($Me = Ti^{3+}$ and Zr^{3+}) ions were in distorted tetrahedral coordination.

Reaction data to support the redox ability of Co containing $AlPO_4$-n molecular sieves has been published by Prasad and Balakrishnan (1991). Iton *et al.* (1989) also noted that these sieves showed the capacity to oxidatively homologate methane conversion to higher hydrocarbons at temperatures < 400°C. As yet however there exists little direct evidence that these sieves are active redox catalysts.

Mn substitution for Al has been supported by NMR and ESR [Goldfarb, 1989], XPS and luminescence spectroscopy [Kuperman and Ozin, 1992], ESEM [Brouet *et al.*, 1991] and XRD studies [Pluth *et al.*, 1988]. Goldfarb (1989) has suggested that at Mn contents of 0.029 and 0.085, MnAPO-5 has both framework and nonframework Mn^{2+} present. The later species were detected by ESR and showed Mn^{2+} to have octahedral coordination. After calcination it was proposed that extra-framework Mn migrated towards the framework as evident by the coalescence of the NMR spectra towards one line. The NMR spectra of Mn-impregnated $AlPO_4$-5 also showed anisotropy, but not as large as for MnAPO-5, indicating some interaction between extra-framework Mn and the $AlPO_4$-5 framework. By comparison of ESEM and ESR results of water interactions with Mn-impregnated $AlPO_4$-11 and MnAPO-11 (< 0.1 mol% Mn) significant differences were observed to indicate framework substitution of Mn^{2+} for Al [Brouet *et al.*, 1991]. Detailed XRD studies of MnAPO-11 [Pluth *et al.*, 1988] with 10% Mn indicated substitution of Mn for Al only.

Ni (loaded) containing $AlPO_4$-n molecular sieves have been reported [Inui, 1990a,b, 1991] but as yet little information exists to confirm the presence of Ni^{2+} in the framework. Xu *et al.* (1989) have synthesized NiAPO-5 using NiCl and HF addition and claimed that Ni is incorporated into the framework of $AlPO_4$-5. However Lechert *et al.* (1991) have shown that no Ni was incorporated into the $AlPO_4$-5 or SAPO-5 framework when NiO was used as the Ni source. The results of Lechert *et al.* (1991) have been verified by Mavrodinova *et al.* (1991) who suggested that Ni acetate rather than NiO

was the preferred Ni source. These workers tentatively suggested that with, NiAc as a Ni source, Ni was partially incorporated into the framework. Rajic *et al.* (1991) have provided evidence of Ni being incorporated into the framework of NiAPO-21 and NiAPO-12, but only in octahedral coordination. It was proposed that Ni replaced the hexavalent Al species. The principal reason for Ni replacing octahedral aluminium whereas Co^{2+} replaced tetravalent Al (in CoAPO-21) was most likely due to the greater tendency of Ni^{2+} to form octahedral rather than tetrahedral complexes.

Fe substitution into the framework of $AlPO_4$-n sieves has been studied primarily by ESR and ^{57}Fe-Mössbauer. This is discussed further in Section 1.5.

1.4.5 Acidity and catalytic activity of $AlPO_4$-n type molecular sieves

1.4.5.1 Acidity

$AlPO_4$-n molecular sieves appear to contain strictly alternating AlO_2^- and PO_2^+ tetrahedra and are consequently electrically neutral and isoelectronic with SiO_2. Counter cations are thus not required and Brönsted acidity does not occur. It is possible however that due to local electronegativity differences between Al^{3+} and P^{5+} the surface hydroxyl groups (Al-OH and P-OH respectively) may possess some residual hydrophilic and acidic character [Derouane *et al.*, 1989; Hunger *et al.*, 1993; Sauer, 1988, 1989].

For SAPO sieves the substitution of silicon for phosphorous in the lattice gives rise to an anionic framework with a net negative charge coupled with exchangeable cations and Brönsted sites. The substitution mechanism may vary from structure to structure. For example in SAPO-37 which has a faujasite structure the number of Al atoms equals the total of P and Si atoms [Martens *et al.*, 1990]. In SAPO-11 the amount of (Si+P) is slightly larger than that of Al and the sieve consists of one-dimensional channels of elliptical cross-section. Like zeolites the acidity of $AlPO_4$-n based molecular sieves is dependent on both the framework composition and the structure type.

In general to date there does not appear to be any unifying concept as regards the nature of the acidity of $AlPO_4$-n molecular sieves.

1.4.5.2 Catalytic activity

Due to the fact that $AlPO_4$-n sieves have little or no acidity these materials do not have any significant catalytic activities. The catalytic activities of SAPO and MeAPSO molecular sieves have however been studied for a wide variety of reactions and some of these are discussed below.

Alkane cracking

n-Butane cracking activities are good indicators of strong acidity (Section 1.5) and Figure 1.20 shows some typical activities for selected structures and compositions. In general this data shows that the incorporation of heterovalent elements into the $AlPO_4$-n framework generates a range of weak to strong acid sites. Small pore types with chabazite structure and large pore structures have strong acidity whereas medium pore types have weak acidity. It should be noted however that because of the steric constraints that may exist in the cracking reaction due to the formation of bulky transition state complexes, the medium pore data may not be truly indicative of the intrinsic Brönsted acidity.

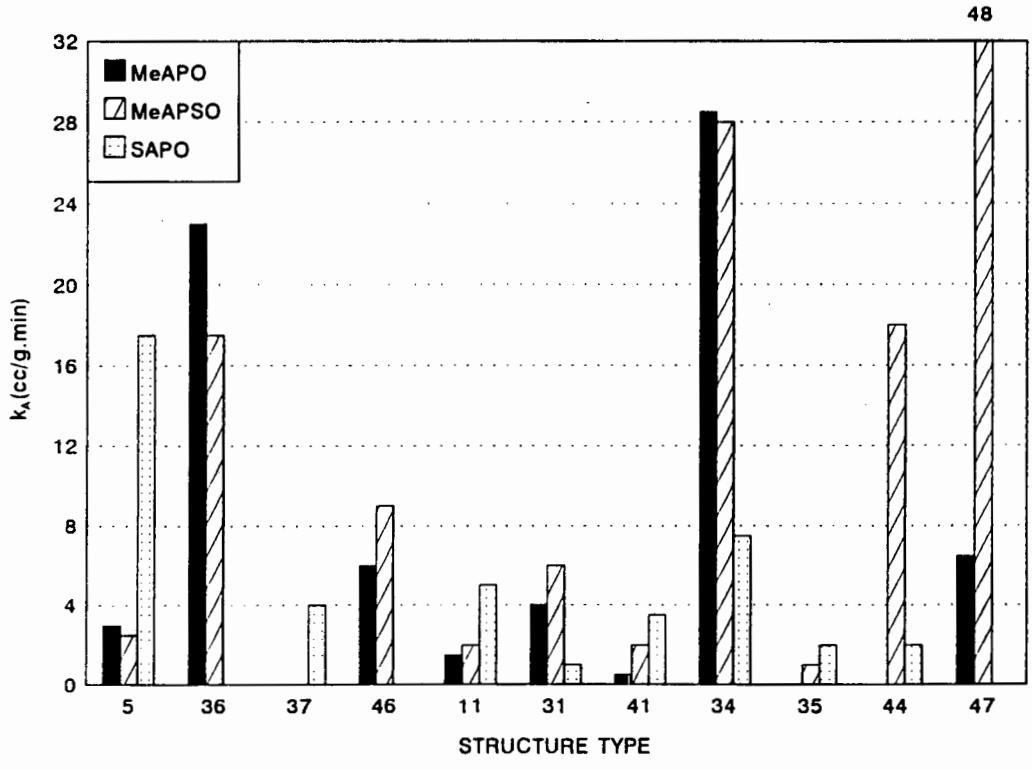

Figure 1.20 Butane cracking activities of various $AlPO_4$-n sieves.

Methanol to olefins

The catalytic conversion of methanol to lower alkenes is a process that is currently enjoying much attention. Ideally a small pore size zeolite or molecular sieve is required so as to inhibit the formation of aromatics. Most such zeolites investigated for this reaction however showed rapid deactivation which could be reduced by using a catalyst of intermediate to low acidity. SAPO-34 has been shown to be an excellent catalyst in this regard.

Marchi and Froment (1991) in a study of the conversion of methanol on SAPO-34 obtained selectivities of 90-95% alkenes in the hydrocarbon product with the yields of ethene and propene being the highest. No aromatics or branched products were produced. They did however observe a fairly rapid deactivation rate and under most operating conditions the catalytic activity decreased rapidly after 3 hours. Van Niekerk *et al.* (1992), in a similar study, obtained essentially the same selectivities but with catalyst lifetimes 2 to 3 times longer. These longer lifetimes are accompanied by significantly reduced formation of methane and a greater production of ethene. The shape selectivity behaviour of SAPO-34 is well illustrated by comparing its activity and selectivity with that of SAPO-11 under similar conditions. The latter catalyst has a pore size of 6Å as opposed to that of 4.3Å for SAPO-34. SAPO-11 produced significant amounts of aromatics and branched isomers.

Olefin reactions

As mentioned in Section 1.2.1.4, $AlPO_4$-n type sieves are active and selective for propene oligomerization. Rabo (1988) has investigated the effect of different SAPO-n sieves and their activity for propene oligomerization and hexene isomerization.

Tables 1.17 and 1.18 indicate that medium pore sieves, particularly SAPO-11, are the most promising oligomerization catalysts. The hexene isomerization results also indicate quite unique selectivities for FAPO-11 and MnAPO-11, which produced significantly more skeletal isomerization products than SAPO-11.

Recently a Patent has been published [Gadja, 1992] suggesting that SAPO-11 and FAPO-11 produce more isobutene and 1-butene respectively with less undesirable by-products than the conventional zeolite system for the butene isomerization process (feed *ca.* 95% 2-butenes).

Table 1.17 Vapour phase propene oligomerization over $AlPO_4$-n type sieves. [Rabo, 1988]

Molecular sieve	SAPO-5	SAPO-11	SAPO-31	SAPO-34	LZ-105
Pore size, Å	8	6	7	4.3	6
Temperature, °C	371	371	371	371	371
Pressure, MPa	0.17	0.17	0.24	0.17	0.17
WHSV, h-1	0.98	0.94	1.04	0.53	0.90
TOS[1], h	4.3	4.2	5.5	2.33	3.5
$C_3^=$ conversion	0	86.3	76.2	41.6	81.6
C_5+ selectivity[2]	-	77.0	82.7	19.5	37.2

1. Time on stream
2. C_5+ selectivity = (C_5+ yield, wt%)/($C_3^=$ conversion, wt%) × 100

Table 1.18 Hexene isomerization[1] over $AlPO_4$-n based molecular sieves. [Rabo, 1988]

Molecular sieve	SAPO-5	SAPO-11	FAPO-11	MnAPO-11
Pore size, Å	8	6	6	6
Total Conv., %	85.1	84.5	90.1	89.6
Selectivities				
DBI[2]	79.1	46.2	22.1	28.0
SI[3]	10.9	41.9	70.6	63.6
Oligomerization	5.6	4.3	2.4	0.9
Cracking	3.2	3.3	1.5	1.9

Molecular sieve	SAPO-31	FAPO-31	MnAPSO-11	LZ-105
Pore size, Å	7	7	7	6
Total Conv., %	86.0	89.1	94.5	93.7
Selectivities				
DBI	82.2	42.5	43.2	2.4
SI	14.3	52.8	44.6	12.2
Oligomerization	1.7	0.9	4.1	55.1
Cracking	0.9	1.3	2.6	25.6

1. Temperature = 343°C, pressure = 0.27 MPa, WHSV = 5.5 l/h
2. Double bond shift isomerization
3. Skeletal isomerization

Aromatic reactions

In a study of toluene methylation over SAPO molecular sieves and ZSM-5 it was shown that the medium pore SAPOs showed superior methylation selectivity relative to the large pore SAPO-5 catalyst. The latter sieve showed very high methyl group disproportionation selectivity similar to the performance of ZSM-5 at comparable temperature.

Pellet *et al.* (1988) have shown that as the pore size of the SAPO increases the conversion due to disproportionation increases. This is consistent with the concept of transition state shape selectivity where the bulky bimolecular interaction between two xylenes to form toluene and trimethylbenzene is difficult to achieve in the 6Å channels of the medium pore sieves (possible in the 8Å pore sieves). Experiments were also carried out to investigate the catalytic performance of medium pore SAPOs with an ethylbenzene and *m*-xylene feed. All the molecular sieves yielded *p*-xylene in amounts equivalent to thermodynamic equilibrium (Table 1.19). CoAPSO-31 and MnAPSO-31 yielded higher *p*-xylene and lower *o*-xylene selectivity than did SAPO-31. Their high selectivities were probably a result of pore constriction, either due to metal in the framework or in extra-framework species (product shape selectivity).

Table 1.19 *m*-Xylene/Ethylbenzene reactions[1] over medium pore $AlPO_4$-n sieves. [Rabo, 1988]

Molecular Sieve	Para/Ortho Xylenes	%Para-xylene	%Disproportionation Ethylbenzene	
SAPO-11	0.97	96	9.9	23.2
SAPO-11 (Al^{3+} exchanged)	1.15	102	6.6	20.1
SAPO-11 (steam treated)	1.52	63	0.2	6.0
SAPO-31	0.78	100	31.6	56.3
SAPO-31 (steam treated)	1.56	102	1.7	10.4
MnAPSO-11	0.88	104	5.0	23.3
CoAPSO-11	1.81	91	0.0	7.7
MnAPSO-31	3.59	120	1.7	17.7
CoAPSO-31	3.06	111	1.7	23.0
LZ-105	0.99	100	23.6	58.5

1. Temperature = 427°C, Pressure = 0.68 MPa, WHSV = 5.6 l/h

Reactions with hydrogen

The mild acidic nature of the aluminophosphate molecular sieve family renders them selective for a number of rearrangement reactions as seen above. This property and their apparent low disproportionation activity suggested that they may exhibit advantageous behaviour for bifunctional reactions. In a set of experiments in which the feed was 17% ethylbenzene and 83% *m*-xylene (typical of a C_8 aromatic cut from reformate gasoline) SAPO-11, to which 0.4% Pt was added, showed itself to be an excellent catalyst for converting ethylbenzene to xylenes. The selectivity for this reaction was 75% with the remaining 25% consisting of the products of disproportionation reactions. Almost no ring-opening reaction occurred.

Conclusion of acidity and catalytic activity

$AlPO_4$-n materials have no acidity and their application is mainly in the area of adsorption. The SAPO-n molecular sieves and those materials in which metals are incorporated into the framework have weak to strong acidity and have been shown to be catalytically active for a wide range of reactions. In particular SAPO-34 shows much promise as a catalyst for converting methanol to lower alkenes especially ethene, and SAPO-11 shows promise for alkene oligomerization, isomerization and aromatic type reactions.

The catalytic activity is effected by acidity and shape selectivity. It is obvious therefore that the acidic and shape selective properties need to be well characterized. Probe reactions have shown promise and will be discused in the next section.

1.5 CHARACTERIZATION OF ACIDITY AND SHAPE SELECTIVITY USING PROBE REACTIONS

The acidity and the porosity of molecular sieves can be modified by numerous treatments as mentioned in Section 1.4.3 With such a large number of factors affecting the acidity and porosity of the molecular sieve there exists a need for a simple yet powerful set of tools to probe these properties of the molecular sieve. The main characteristic of molecular sieve catalysts are their remarkable "shape selective" properties. This property is due to the fact that their acid centres are predominantly internal and that their pores and cavities are more or less the same size as organic molecules. Hence the shape selectivity of molecular sieves will be determined not only by the characteristics of their acid sites but also by the geometrical characteristics of the diffusion path of reactant molecules towards the active centers or of the product molecules towards the external surface of the crystallites. The size and shape of the space available near the active sites will also be important.

1.5.1 Shape Selectivity

Three main types of shape selectivity have been defined

1. Reactant selectivity
2. Product selectivity
3. Restricted transition state selectivity.

Figure 1.21 illustrates an example of each type of selectivity.

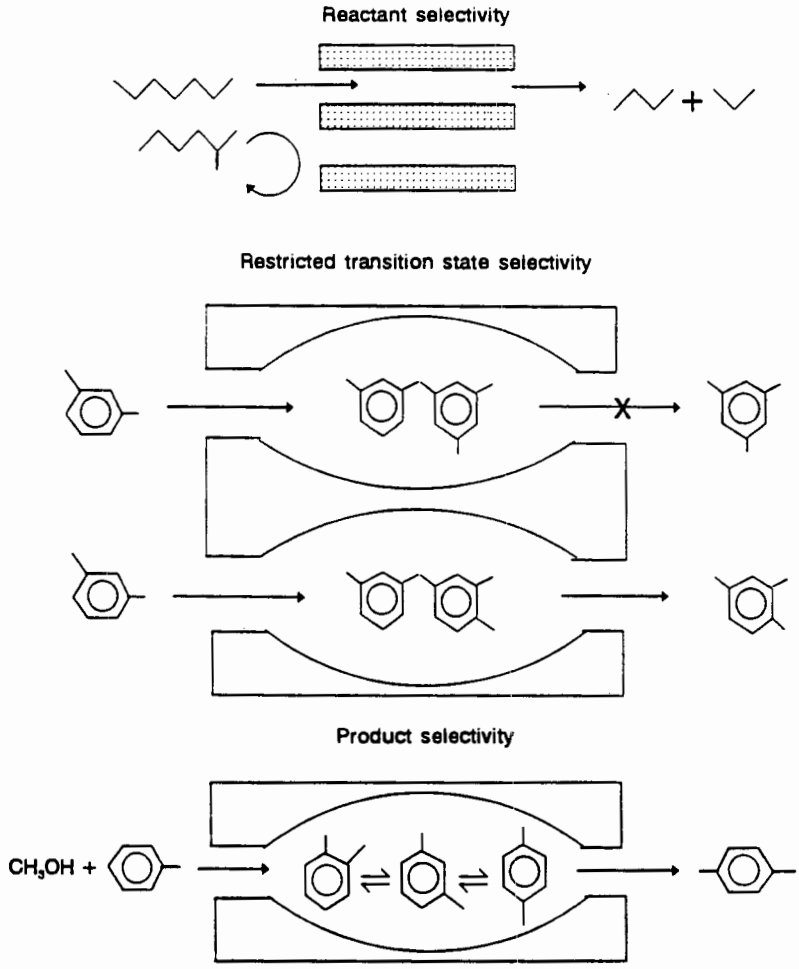

Figure 1.21 Shape selectivity by reactant, transition state and product selectivity.

The following sections outline the most common current methods used to determine acidic and shape selective properties and discuss their limitations. The characterization of the acidic centers and porosity (shape selectivity) of the molecular sieves by probe reactions and their limitations will also be highlighted.

1.5.2 Current Methods of Probing Acidity and Porosity

1.5.2.1 Acidity

The most common tools for probing the acidity of molecular sieves involves the chemisorption of basic molecules onto the molecular sieve and thermally desorbing the base. The easiest method (NH_3-TPD) does not distinguish between protonic (Brönsted) and electrophilic (Lewis) sites. IR spectroscopy allows the distinction between adsorption on Lewis or Brönsted acid sites of bases such as ammonia and pyridine, via the band at 1450 cm^{-1} corresponding to Lewis sites and 1540 cm^{-1} corresponding to Brönsted

sites. Both methods are time consuming and often performed at conditions far removed from those experienced during reaction (e.g. under vacuum for IR studies). Sometimes these methods provide data that does not correlate well with catalytic data. Neither of these tests can determine the density of acid sites, which is often very important in some catalytic reactions (e.g. butane cracking).

1.5.2.2 Porosity

The most common method used to determine the pore size and geometry is by the adsorption of specific molecules, e.g. N_2 BET, and detailed crystal XRD. Both methods are tedious and the later requires detailed computation work.

1.5.3 Determining Acidity by Probe Reactions

In order to determine the acidity of molecular sieves using probe reactions the probe molecule must have easy access to the active sites and the production of reaction intermediates must not be inhibited. Reactions that produce water and alcohols may be able to modify the catalyst (e.g. transformation of Lewis to Brönsted acid sites by water) and hence the probe reactions that have been used to determine acidity are exclusively hydrocarbon reactions.

Bourdillon *et al.* (1990) have probed the acidity of Zeolite Y using the following reactions:

1. Skeletal isomerisation of 3,3,-dimethyl-1-butene
2. Isomerisation and cracking of 2,2,4-trimethylpentane, 2,4,-dimethylpentane and n-hexane
3. Isomerisation and disproportionation of *o*-xylene and 1,2,4-trimethylbenzene.

The strength of the site was estimated by the catalysts capacity to retain a basic molecules (pyridine). The changes in the rates of the reaction as a function of the desorption temperature of pyridine enabled the classification of the acid sites of minimum strength to catalyze the reaction. The reactions chosen represented a group that required a wide range of acid strengths.

The idea currently accepted is that the more difficult the reaction the stronger are the acid sites required for it to proceed. Hence the isomerisation of 3,3-dimethyl-1-butene at low temperatures, which occurs rapidly on weak acid catalysts such as alumina, was used to probe for weak acid sites. The transformation of n-hexane on the other hand, which occurs at higher temperatures and/or on very strong acid sites, such as ZSM-5 was used to probe for strong acidity.

The study showed that it was possible to use the above theory and that the rates of various reactions can give complementary information concerning the number of active centers present, i.e. acid site distributions can also be obtained.

Kramer and McVicker (1986) have shown that the isomerization of 2-methylpent-2-ene can be used as a reaction to probe the relative acidity of solid acid catalysts of moderate strength. Olefins can convert to a large number of products whose relative rates of formation are expected to reflect the relative freedom of cationic intermediates. The conversion of 2-methylpent-2-ene to 4-methylpent-2-ene and 3-methylpentenes can be proposed as proceeding via protonation to form a *tert*-cation which rearranges by 1,2 hydride shift to a secondary ion which experiences either a proton loss or methyl migration. The proton loss and methyl migration are then competing reactions of a common intermediate over varied energy surfaces. The stronger the acid site the more readily methyl migration would occur and the ratio of the rates for alkyl migration to double bond shift would be expected to rise. By comparing the methyl shift to double bond shift ratio and the MAT number (a measure of the extent of conversion of an East Texan gas oil under specific conditions) a linear relationship was evident.

1.5.4 Probing Shape Selectivity by Catalytic Reactions

As mentioned above three parameters can govern the selectivity of a reactant transformation on shape selective catalysts. Firstly, the characteristics of the catalytic sites which determine the nature of the intermediates and their fate. Secondly, the size and the shape of the space near the active sites which can bring steric constraints to bear on the formation of transition states. Finally the characteristics of the diffusion path

which fix the residence time and the evolution of the reactants and of the intermediates. In order for the molecular sieve catalyst to be characterized with the aid of probe reactions the determining factor must be understood. The ideal conditions for this kind of characterization are that acid sites are well characterized and that the collected information only involves one of the later two mentioned above.

To characterize the diffusion path it is best to use reactions involving monomolecular intermediates so as to limit the influence of steric constraints. An example of such a reaction is the isomerisation of *m*-xylene. Characterization of the space available in the vicinity of the acid sites requires the size of the reactants and products as well as the conditions of the reaction to be chosen so that diffusional limitations can be neglected. The disproportionation of *m*-xylene to 1,2,3-, 1,2,4- and 1,3,5-trimethylbenzenes is often used for such purposes.

1.5.5 Probing the Acidic and Shape Selective Properties of SAPOs and HPAs

1.5.5.1 SAPOs

Khouzami *et al.* (1988) have investigated the acidic and catalytic properties of SAPO-11 molecular sieves by conventional methods such as NH_3-TPD and also by probe reactions. Their NH_3-TPD and pyridine adsorption (FT-IR) experiments suggested that SAPO-11 exhibited both Brönsted and Lewis acidity of medium strength which resulted in poor catalytic activity for alkane cracking. However the SAPO-11 catalysts were active for methanol conversion, isopropanol dehydration and double bond shift isomerisation of 1-butene. Alkane cracking is usually used to determine the amount of strong Brönsted acid sites. Halik *et al.* (1989) and Meusinger *et al.* (1991) have studied alkane cracking and dehydrogenation over SAPO-5 and MeAPO-5 sieves. The higher activity of MgAPO-5 and CoAPO-5 compared to SAPO-5 was attributed to the accessible metal cations and not strong acid sites. ZnAPO-5 showed only dehydrogenation activity.

Choung and Butt, (1990) have studied the acidic and shape selective properties of SAPO-11 and Pd/SAPO-11 using 1-hexene conversion as a probe reaction. They compared their results with those for ZSM-5 and

mordenite catalysts. The results indicated that at lower temperatures (150-175°C) the predominant reaction pathway was double bond shift (DBS) isomerization and the product selectivity was not influenced by the type of catalyst. At higher temperatures significant changes in selectivity were observed from DBS to cracking and skeletal rearrangement depending on the type of catalyst. Mordenite maintained DBS activity even up to high temperatures (450°C), ZSM-5 produced significant quantities of cracked alkenes and SAPO-11 was intermediate. The incorporation of Pd into SAPO-11 increased the DBS activity and reduced the production of cracked alkenes. NH_3-TPD studies also showed that the incorporation of Pd reduced the amount of strong Brönsted acid sites. From TPD studies it was concluded that the LTD peak was representative of Lewis acidity and the two HTD peaks represented Brönsted acid sites.

Thomson *et al.* (1990b) have studied CO hydrogenation over Pd supported SAPO-5, -11 and -34. The differences in product distributions were attributed to acidity and shape selectivity effects.

Acidity and diffusion in SAPO-11 has been studied by Yang *et al.* (1991) who compared their results with SAPO-5 and ZSM-5. Selective alkylation of toluene with methanol and *p*-xylene isomerization were used as probe reactions. The former contains water as a reaction product which may cause changes to the acidity and pore structure as mentioned in Section 1.4.3.3. The diffusivity of *p*-xylene in SAPO-11 was similar to that in ZSM-5. Due to weaker acidity the concentration of *p*-isomers are greater than that expected for equilibrium cases.

Hoffmeister and Butt (1992) have investigated the selectivities in methylcyclopentane and n-hexane conversion on some metal (Pt/Pd) loaded SAPO-11 catalysts. The results obtained indicated that both confinement and shape selective factors were important in the determination of the observed product distributions.

1.5.5.2 Probing surface acidity of HPAs

As mentioned in Section 1.3.3.4 there are two types of acid-type reactions, *viz.* **Surface-type** and **Bulk-type I**. Butene isomerization [Matsuda *et al.*, 1981], cumene cracking [Nowinska, 1991], *o*-xylene isomerization [Baba *et*

al., 1983], hexane cracking [Nayak and Moffat, 1989] are all examples of surface type reactions that have been used to probe the surface acidity of HPAs.

In summary by using specific probe reactions the acidic and shape selective properties of a catalyst and a molecular sieve can be characterized in such a way that useful information on their catalytic activity for other reactions can be inferred. This complements classical methods, such as TPD, BET, etc., which often do not predict catalytic activity.

1.6 CHARACTERIZATION OF METAL CONTAINING CATALYSTS BY TPR

The success or otherwise of catalyst preparation or modification depends on the availability of suitable characterization techniques available for this purpose. These techniques include X-ray powder diffraction, SEM, photoelectron spectroscopy and infrared spectroscopy. However none of these techniques have proved to be wholly reliable or generally applicable to the characterization of catalysts under working conditions. Temperature programmed reduction (TPR) is a technique first applied by Robertson *et al.* (1975), which is highly sensitive and which does not depend on any specific property of the catalyst other than that the species under study be in a reducible condition. A comprehensive review on the basic concepts of the TPR technique, including many experimental profiles, has been reported by Hurst *et al.* (1982). Soon afterwards a paramagnetic sensitivity and estimation of kinetic parameter study was completed by Monti and Baiker, (1983).

In the following sections a brief overview of the thermodynamics, kinetics and mechanisms of reduction are discussed as well as a description of the apparatus used. The usefulness of the TPR technique will be illustrated by examples of TPR studies of supported and unsupported metallic catalysts.

1.6.1 Thermodynamics and kinetics

The reaction between metal oxide (MO) and hydrogen to form metal (M) and water vapour can be represented by the general equation shown below:

$$MO(s) + H_2(g) \rightarrow M(s) + H_2O(g)$$

The standard free energy change for reduction ΔG^o is negative for a number of oxides (Figure 1.22) and thus for these oxides the reductions are thermodynamically feasible. However since

$$\Delta G = \Delta G^o + RT\log(P(H_2O)/P(H_2))$$

it may still be possible for the reduction to proceed even when ΔG^o is positive. The TPR experimental method is such that the water vapour is constantly removed from the reaction zone as soon as it is formed. Thus if

$P(H_2O)$ is lowered sufficiently at elevated temperatures, it is possible that the term $RTlog(P(H_2O)/P(H_2))$ could be sufficiently negative to nullify a positive ΔG^o. Thus it has been possible to obtain TPR profiles for oxides of vanadium, tin and chromium which, at the reduction temperatures, have approximate positive ΔG^o values (kJ/mol) of 45, 50, and 100, respectively.

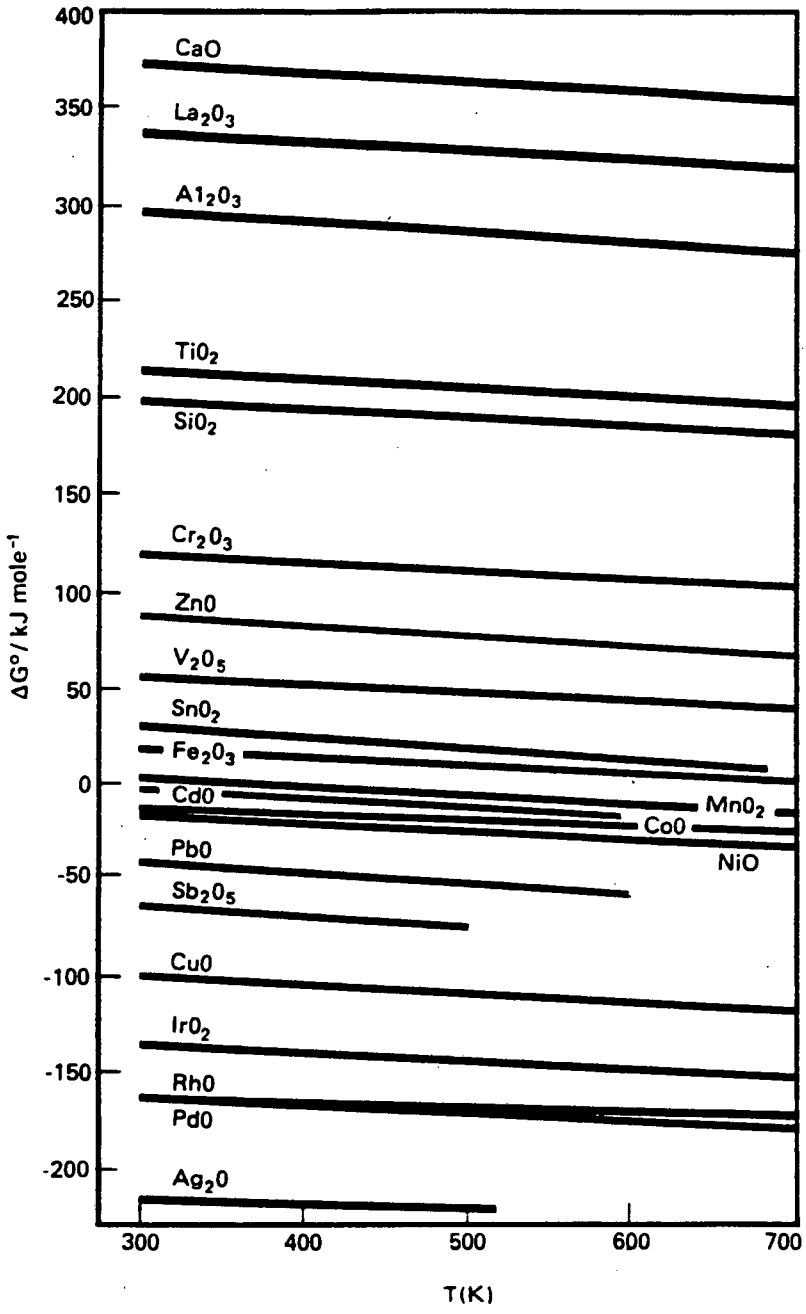

Figure 1.22 Standard free energy change (ΔG^o) as a function of temperature for the process: Metal oxide + H_2 → metal + H_2O.

Kinetics and mechanisms

The most common method used to observe rates of reduction is by monitoring the degree of reduction (α) as a function of time, t, for various temperatures and pressures of hydrogen. This data constitutes the kinetics which have been interpreted in terms of the mechanism by which the reduction has occurred. There are two types of reduction models, the **nucleation** and **shrinking core** model. The former is characterized by a sigmoidal α versus t plot and the latter by an inverse exponential α versus t plot. (Figures 1.23 and 1.24). It is common practice to analyze experimental data in terms of chemical or diffusion control and if the results do not correspond exactly then to infer some kind of mixed control. However the problem of increasing the complexity of the model is that many variables may be introduced which will inevitably lead to a fit of the model without, however, any real mechanistic significance.

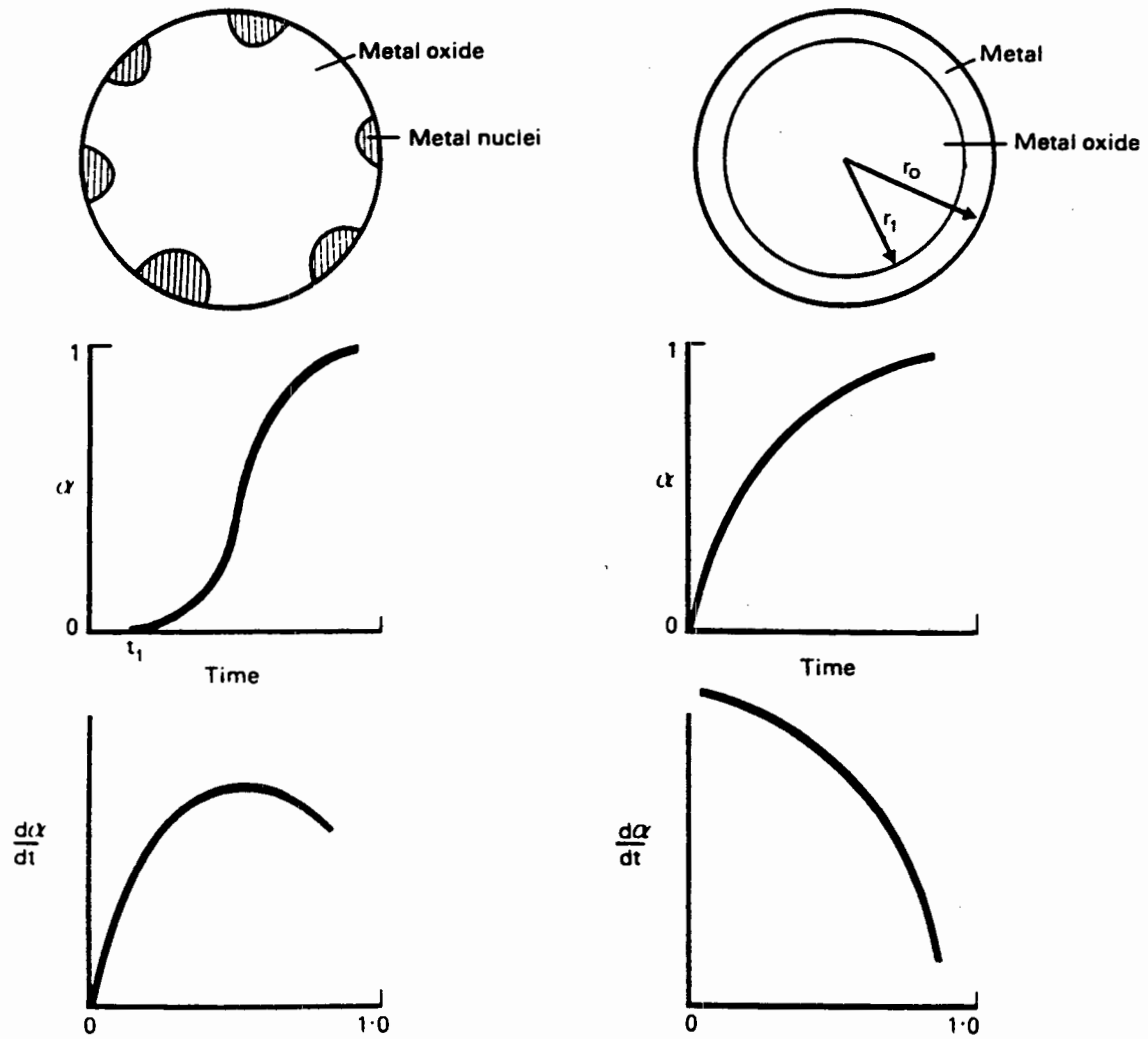

Figures 1.23 and 1.24 Mechanisms of reduction, nucleation and shrinking core model.

A parametric sensitivity and estimation of the kinetic parameters has been discussed by Monti and Baiker (1983) and a study of the effect of experimental parameters by Gentry *et al.* (1979). Monti and Baiker (1983) have put forward a characteristic number, K, which is defined to facilitate selection of the most appropriate operating variables.

$$K = S_o/(V^*.C_o)$$

For commonly used heating rates, 0.1-0.3 K/s the limiting values are $55 < K < 140$ s.

1.6.2 Bulk oxides

The TPR profiles of bulk oxides have been reported by many authors. Often differences in the reduction peak temperatures are due to different experimental conditions. The reduction profiles of many bulk oxides are illustrated in the review by Hurst *et al.* (1983).

1.6.3 TPR of Supported oxides

Metal oxides supported on inert carriers such as γ-alumina and SiO_2 exhibit different reduction behaviours compared with the unsupported oxides. Reduction can be hindered or promoted depending on the nature of the oxide/support interaction. Supported metal oxides may be homogeneously distributed across the surface of the support or exist as islands of oxide separated by uncovered support. Islands of metal oxides may be expected to reduce in a similar manner to unsupported oxide, in which case the support may act purely as a dispersing agent and promote the reduction. Under these conditions the reduction kinetics observed for the supported oxide are the same as for the bulk oxide. For example both bulk and supported CuO reduce with sigmoidal α versus t plots which is characteristic of a nucleation or autocatalytic reduction. The supported CuO is also found to reduce more easily.

Bulk NiO also shows a sigmoidal reduction isotherm, while supported NiO, which is more difficult to reduce than the bulk oxide, which shows a reduction isotherm which is characterized by constantly decreasing rates of reduction as shown for the contracting sphere model. The concept of a

contracting sphere model would seem inappropriate in the case of a homogeneously distributed metal oxide. The reduction may rather involve instantaneous nucleation across the whole area of the supported oxide.

Many TPR studies have focussed on the reduction behaviour of Ni containing catalysts. Unmuth *et al.* (1980) have shown for Ni on SiO_2 that there are three reductions, α at 262°C, corresponding to a reduction of NiO and the endothermic phase transformation. β at ca. 310°C and γ at 390°C. The β peak is NiO being reduced to Ni and the shoulder peak, γ, the result of strong support interactions, possibly the formation of nickel silicates.

Metal atoms and crystallites are known to be mobile on the surface of supported metal oxides so that under certain appropriate conditions the reduction of a homogeneously supported metal oxide may proceed with the reduction of individual metal ions, followed by surface diffusion to form metal crystallites which in turn may diffuse and combine to form particles of the reduced phase. Such a reduced phase may have an autocatalytic effect on the reduction.

The TPR of bulk CoO/Co_3O_4 and Al_2O_3, TiO_2 and SiO_2 supported has been investigated by Van't Blik and Prins (1986), Martens *et al.* (1986) and Van't Blik *et al.* (1986). Their results show that for Co on alumina several Co species exist. These are: (i) Co spinels that are formed during reduction which results in the loss of Co metal to form cobalt-aluminates, (ii) Co in octahedral sites of the support and/or (iii) "bulk-like" Co_3O_4. The reduction of Co on TiO_2 (and Al_2O_3) proceeds via Co_3O_4 to CoO then to Co^0. Cobalt silicate species were suggested to form for the Co on SiO_2 system.

The reduction of 5 wt% Fe_2O_3 on SiO_2 was studied by Unmuth *et al.* (1980). The reduction profiles consisted of two peaks at ca. 580K and 720K which corresponded to:

$$3\alpha\text{-}Fe_2O_3 + H_2 \rightarrow 2Fe_3O_4 + H_2O$$

$$Fe_3O_4 + 4H_2 \rightarrow 3\alpha\text{-}Fe + 4H_2O.$$

Kock *et al.* (1985) have also suggested that reduction of 25 wt% Fe on γ-Al_2O_3 occurs via the sequence α-$Fe_2O_3/Fe_3O_4/Fe_{1-x}/\alpha$-Fe. Mössbauer and IR

studies of reduced 25 wt% coprecipitated Fe-containing Al_2O_3 catalysts have provided evidence that the reduction to α-Fe proceeds via the sequence α-FeOOH/Fe_3O_4(spinel)/$Fe_{1-x}O$ structure [Wielers *et al.*, 1989]. 20 wt% Fe on SiO_2 does not reduce via the Fe_3O_4 structure but rather via the formation of Fe(II)silicate which is partially reduced to α-Fe with some Fe(II)silicate remaining after reduction to 820K.

These results indicate that the reduction behaviour is not only dependent on the reduction conditions but also on factors such as the catalyst metal loadings and preparation and pretreatment procedures.

1.6.4 TPR of Zeolites and molecular sieves

Zeolites containing reduced metal, whether atomically dispersed or existing as small clusters within the pore structure, are of great value to the petrochemical industry as hydrocracking and reforming catalysts [Rabo *et al.*, 1978; Minachev and Isakov, 1976]. The activity of these catalysts is critically dependent on both the degree of dispersion and the location of the metal, which are in turn dependent on the method of reduction and pretreatment. Thus an understanding of the kinetics and mechanism of reduction is particularly valuable in the preparation of these catalysts.

The reduction of a metal ion in a zeolite is generally achieved by using hydrogen; the overall reaction stoichiometry may be written as follows:

$$M^{n+} + (n/2)H_2 \rightarrow M^0 + nH^+$$

The protons react with the zeolite lattice to produce hydroxyl groups whose presence has been established by IR spectroscopy:

$$nZO^- + nH^+ \rightarrow nZOH$$

The reduction of transition metals in zeolites has been reviewed by Uytterhoeven *et al.* (1978), who observed a correlation between reducibility and standard electrode potential. His data along with more recent TPR results are reproduced in Table 1.20. Care should be taken in comparing the results of different authors since it is known that the TPR peak positions are sensitive to experimental conditions (Section 1.6.1). A more recent review

on dispersed metal particles in zeolites has been published by Delafosse (1986).

Table 1.20 Reducibility of Transition Metal ions in Zeolites X and Y. [Hurst *et al.*, 1982]

Reduction process	Standard electrode potential (V)	Temperature (K) of first major reduction maximum (minor in parentheses) Zeolite Y	Zeolite X
Pd^{2+}/Pd^{0}	+0.83	290	250
Ag^{+}/Ag^{0}	+0.80	393	-
Cu^{2+}/Cu^{+}	+0.16	440;520	550;540
Cu^{+}/Cu^{0}	+0.52	700;.773	730;773
Ni^{2+}/Ni^{0}	-0.23	773;(600) 950	(600) 900; (570) 830
Co^{2+}/Co^{0}	-0.28	a	a
Cd^{2+}/Cd^{0}	-0.40	a	a
Fe^{2+}/Fe^{0}	-0.41	a	700
Cr^{3+}/Cr^{2+}	-0.41		650
Cr^{3+}/Cr^{0}	-0.74		
Zn^{2+}/Zn^{0}	-0.76	a	a
Mn^{2+}/Mn^{0}	-1.03	a	a

a. No reduction observed.

Jacobs *et al.* (1979) have studied the reduction of nickel in NiY and shown that after incomplete dehydration the degree of reduction increased with temperature up to 100% at 873K. After more thorough dehydration it was found that the reduction was restricted to about 30% at 873K, suggesting that water enhanced the reduction process. The following mechanistic steps were proposed: (1) activation of hydrogen at some surface site, (2) diffusion of Ni^{2+} towards the active site, (3) regeneration of the site as the rate determining step, and (4) the formation of charged clusters, estimated to be Ni_3^{2+} or Ni_4^{2+}

Briend-Faure *et al.* (1978) studied the reduction of Ni^{2+} in both zeolite X and Y zeolite. In NiY they observed three distinct kinetic regimes dependent on both the initial level of exchange and the degree of reduction, and they correlated these reduction regimes to the initial distribution of Ni^{2+} ions. Suzuki *et al.* (1989) have studied the reduction of Ni in Z-Y and proposed that Ni^{2+} exists in three kinds of exchanged sites which were discriminated by reduction peaks at 793, 913 and 1093K respectively. The reducibility of these Ni species was enhanced by replacing Na^{+} cations with Ca^{2+} or Sr^{2+}.

All the foregoing work on Ni^{2+} zeolite systems have found Ni^{o} as the only reduction product. Garbowski *et al.* (1977a,b), however, using EPR and electron spectroscopy, have observed Ni^{+}. TPR, at relatively high hydrogen pressure, was able to identify a two step mechanism and hence it must be assumed that the concentration of Ni^{+} is low and that further reduction to Ni^{o} is rapid.

TPR of Fe containing zeolites/silicates have shown reduction of α-Fe_2O_3 to β-Fe_3O_4 followed by reduction to Fe at high temperatures [Kan *et al.*, 1991].

In conclusion it may be drawn from the literature that:

1. The ease of reduction of different ions follows the standard electrode potential series, although unexpected oxidation states may be stabilized by the zeolite lattice.

2. The ease of reduction is dependent on the chemical composition of the zeolite (i.e. Si/Al ratio and nature of cation) and on the location of the ion in the following order:

supercage > sodalite cage > hexagonal prism

3. Reduction is often affected by different pretreatment conditions.

4. The rate determining step is generally associated with the migration of ions to reduction sites.

5. Reduction is frequently limited to less than 100% with the formation of electron-deficient clusters.

6. Although reduction is most frequently carried out in hydrogen atmosphere it is possible for metal ions to be reduced by metal Na vapour, NH_3, CO and by atomic H at low temperatures.

1.7 IRON (Fe) COORDINATION BY MÖSSBAUER SPECTROSCOPY

^{57}Fe Mössbauer spectroscopy offers many advantages for the study of Fe species in zeolite frameworks. Firstly there is no form of Fe that is Mössbauer-silent in a solid (unlike EPR). Moreover the observed spectrum is the weighed sum of the different sub-spectra corresponding to iron in different environments. In general Mössbauer spectra are interpreted via analogy with spectra of well-characterized model iron containing compounds.

The most important feature of Mössbauer is the ability to distinguish between framework and non-framework sites [Meagher *et al.*, 1988]. Fe in the framework is necessarily in the tetrahedral oxygen coordination, whereas Fe in nonframework sites is probably occluded as iron oxides, e.g. α-Fe_2O_3, which exist in the octahedral coordination. To distinguish between tetrahedral and octahedral the isomer shift (I.S.) parameter is used. This parameter is of course commonly used to distinguish between Fe^{2+} and Fe^{3+}. Garten *et al.* (1970) have indicated that for room temperature Mössbauer, I.S. < 0.3 mm/s is indicative of iron in a tetrahedral coordination and I.S. > 0.3 mm/s octahedral. Because of the effect known as the second order Doppler shift the I.S. value increases at lower temperatures. A value of 0.35 mm/s for cronstedtite, a silicalite material, has been quoted for tetrahedral coordination and 0.47 mm/s for octahedral coordination (α-Fe_2O_3) from 4.2 K Mössbauer.

It is possible, however, that the occluded iron oxide is in the tetrahedral coordination as for γ-Fe_2O_3 in ZSM-5. Fortunately Mössbauer can distinguish between tetrahedral iron present in iron-oxides (magnetically ordered) and the dilute iron in the framework (paramagnetic). This is done via magnetic hyperfine interactions.

1.7.1 Magnetically ordered iron oxides

Magnetically ordered materials generally give rise to a six-line (sextet) ^{57}Fe Mössbauer spectrum where the splitting of the lines is proportional to the hyperfine field B_{hf}. In the bulk different iron species can be identified via there different hyperfine fields. For small particles there are two complicating effects: collective magnetic excitations and

superparamagnetism. The former causes smaller values of B_{hf} to be observed whereas the later results in the replacement of the sextet with a quadrapole doublet at a temperature called the blocking temperature, T_B. For particles of a given structure the blocking temperature often varies linearly with the particle volume and this behaviour is often used in characterizing small particles in catalyst systems.

1.7.2 Dilute paramagnetic framework iron

Dilute paramagnetic ferric (Fe^{3+}) iron can also give rise to an apparent sextet at low temperatures due to the electronic relaxation times becoming longer than the Mössbauer measuring time. At higher temperatures the absorption lines become broader and then collapse into a broad singlet or unresolved doublet. This behaviour is known as paramagnetic hyperfine splitting (PHS), but is rarely reported in zeolite studies.

Therefore one can see that two quite different cases can give rise to very similar spectra. To differentiate between the two a strong magnetic field is usually applied and if PHS exists then the spectra should become much sharper (the line widths will decrease). If magnetically ordered iron oxides exist the spectral lines should broaden or double. Also if PHS exists then a reduction in the sextet component should be compensated by an increase in the central singlet or doublet..

1.7.3 Previous studies of iron in zeolites and $AlPO_4$-n type molecular sieves.

There has been a lot of interest in the use of Mössbauer spectroscopy for the characterization Fe-ZSM-5, unfortunately quite different interpretations have been assigned to quite similar spectra. According to Meagher (1989) this was due to misinterpretation of data by Calis *et al.* (1987). Meagher (1989) has since urged the adoption of the room temperature isomer shift value as a good indicator of tetrahedral/octahedral coordination after Garten *et al.* (1970).

Lazar *et al.* (1991) have studied the effect of ion exchange of Li^+ for H^+ and the effect on framework Fe^{3+} in Fe-ZSM-5 and have shown that effect depends considerably on the type of charge compensation (300K, I.S. = 0.23 mm/s for as-synthesized and I.S. = 0.22 and 0.31 mm/s for

calcined). Brönsted acidic bridged H^+ ions induced greater asymmetry around the framework Fe^{3+} than that generated by charge compensating Li^+. The framework Fe^{3+} was reduced to extra-framework Fe^{2+} but the reduction was decreased after Li^+ ion-exchange. The symmetry of the environment was in strong correlation with the Q.S. value.

Only Fe containing $AlPO_4$-5 sieve has been investigated to date. Li *et al.* (1988), from room temperature and 4.2K Mössbauer spectroscopy, suggested that the majority (*ca.* 74%) of the Fe was Fe^{3+} paramagnetic and in the framework in as-synthesized form (295 K I.S. = 0.4 mm/s, Q.S. = 0.73 mm and line width = 0.55 mm/s). From 4.2 K Mössbauer spectroscopy, 54% was found to be paramagnetic Fe^{3+}(framework) (I.S. = 0.5 mm/s, Q.S. = 0.87 mm and line width = 0.49 mm) and 12% was magnetic Fe^{3+} (I.S. = 0.51 mm/s, Q.S. = -0.25 mm and line width 0.52 mm, internal magnetic field = 52.6 T).

Schubert *et al.* (1989) have since studied the effects of varying calcination temperature on the above mentioned FAPO-5. Depending on the calcination temperature there were three different types of iron species present. After calcination in air no Fe^{2+} species existed which suggested that Fe^{2+} had oxidized to Fe^{3+}. Calcination to 400°C showed 65% of the Fe^{3+} was in the framework. Calcination to 500°C revealed that only 55% of the Fe was in the framework which suggested that the framework Fe^{3+} was being removed with increasing calcination temperature. Calcination to 600°C shows two sets of subspectra, one due to small α-Fe_2O_3 particles and the other a magnetically inhomogeneous Fe^{3+} species whose hyperfine splitting parameters are close to Fe^{3+}-phosphate. XRD after 600°C indicated that the tridymite structure was present which indicated a phase transformation from FAPO-5 to Fe-Tridymite. After calcination to 700°C the Fe species present were, α-Fe_2O_3 (25%), Fe^{3+}phosphate clusters (40%) probably occluded within the FAPO-5 framework and Fe^{3+} in a site with tetrahedral coordination and high structural symmetry. Ojo *et al.* (1989) have reported similar findings to the above authors. Pang *et al.* (1989) suggested that the Fe^{3+} in the framework of $AlPO_4$-n molecular sieves is more stable than that in ferosilicates.

The results of Li *et al.* (1988) have since been challenged as they attributed a Fe species with an I.S. = 0.4 mm/s value to be framework tetrahedral Fe,

when this is much higher that the I.S. < 0.3 mm/s requirement for tetrahedral coordination as stated by Meagher *et al.* (1988). Cardile *et al.* (1990) have suggested that the Fe species in question is rather that of an iron aluminium phosphate. Their results show very little framework Fe exists.

1.8 RESEARCH OBJECTIVES

It has been proposed that certain heteropoly acids (HSiW) and $AlPO_4$-n type molecular sieves are active and selective for the formation of distillate fuels from propene oligomerization but as yet no detailed study has been completed on their activity and selectivity for this reaction.

The aims and objectives of this study were:

(i). To synthesize and characterize various salts of 12-tungstophosphoric acid, 12-tungstosilicic acid and 12-tungstophosphoric acid;

(ii). To investigate the effect of the heteropoly acid countercation, central atom and peripheral atom on the activity, selectivity and lifetime of these catalysts for propene oligomerization;

(iii). To investigate the effect of supporting heteropoly acids on α-alumina on their activity, selectivity and lifetime for propene oligomerization;

(iv). To synthesize and characterize SAPO-11 and MeAPSO-11 (where Me = Ni, Co, Mn and Fe) molecular sieves;

(v). To determine the location and state of the metals in the MeAPSO-11 molecular sieves;

(vi). To investigate the effect of the addition of metals to the SAPO-11 synthesis gel on the activity, selectivity and lifetime of the sieves for propene oligomerization;

(vii). To investigate the effect of post-synthesis modifications, *viz.* steaming, acid washing, metal impregnation and silanization on the activity, selectivity and lifetime of these molecular sieves for propene oligomerization;

(viii). To determine the reaction conditions required for optimum catalyst performance;

(ix) To compare the propene oligomerization activity, selectivity and lifetimes of the HPA, SAPO-11 catalysts with ZSM-5 and solid phosphoric acid (CATPOLY) catalysts.

Chapter 2
Experimental

2. EXPERIMENTAL

2.1 CATALYST SYNTHESIS AND MODIFICATION

2.1.1 Heteropoly acid synthesis

Materials

The parent acids, 12-tungstophosphoric acid (HPW), 12-tungstosilicic acid (HSiW) and 12-molybdophosphoric acid (HPMo) were obtained as analytical reagents from Merck. These materials were used without further purification. The following compounds were used in the synthesis of the HPA salts: the nitrates of nickel (BDH), aluminium (Riedel-de-Haen), cerium (Mintek), iron (BDH) and cobalt (BDH), the carbonates of nickel (BDH), potassium (Merck) and ammonium (Holpro) as well as copper acetate (Merck) and aluminium isopropoxide (Fluka). Acid washed quartz sand (AR) was obtained from Merck and α-alumina (AR) from Aldrich.

Synthesis Procedure

The salts were prepared as desribed by Tsigdinos (1974) from an aqueous solution of the parent acid to which the required stoichiometric amount of the carbonate, nitrate or acetate salt of the counter cation was added. Typically 10 g of $HPW{\cdot}20H_2O$ was added to 50 ml of distilled water and to this solution the stoichiometric amount of the countercation containing carbonate/acetate/nitrate was added. This aqueous salt solution was stirred and held at 80°C for 30 minutes. The Type A salts (Section 1.3.2) were crystallized out of solution by evaporating to dryness in an air oven at 80°C. The Type B salts (K^+ and NH_4^+) formed as precipitates as these salts are water insoluble, and were centrifuged from the mixture and washed with distilled water three times before being dried at 80°C in an air oven.

The aluminium salts were also prepared by reacting aluminium isopropoxide with the respective parent acid in diethylether (referred to hereafter as AlPW:ether). These salts were either crystallized directly from the diethylether solution or recrystallized from an aqueous solution (referred to hereafter as AlPW:ether/water).

All of the dried salts were crushed and sieved to a size fraction less than 250 μm before being stored. The salts synthesized and their nomenclature for the remainder of the thesis are outlined in Table 2.1

Table 2.1 HPAs synthesized and nomenclature

Catalyst name	Solvent	CC Salt[1]	Chemical formula	Nomenclature
tripotassium-12-tungstophosphate	H_2O	K_2CO_3	$K_3PW_{12}O_{40}$	KPW
triammonium-12-tungstophosphate	H_2O	$(NH_4)_2CO_3$	$(NH_4)_3PW_{12}O_{40}$	NH_4PW
nickel-12-tungstophosphate	H_2O	$Ni(NO_3)_2$	$Ni_{3/2}PW_{12}O_{40}$	NiPW
nickelmonohydrogen-12-tungstophosphate	H_2O	$Ni(HCO_3)_2$	$NiHPW_{12}O_{40}$	NiHPW
cobalt-12-tungstophosphate	H_2O	$Co(NO_3)_2$	$Co_{3/2}PW_{12}O_{40}$	CoPW
copper-12-tungstophosphate	H_2O	$Cu(Ac)_2$	$Cu_{3/2}PW_{12}O_{40}$	CuPW
iron-12-tungstophosphate	H_2O	$Fe(NO_3)_3$	$FePW_{12}O_{40}$	FePW
cerium-12-tungstophosphate	H_2O	$Ce(NO_3)_3$	$CePW_{12}O_{40}$	CePW
aluminium-12-tungstophosphate	H_2O	$Al(NO_3)_3$	$AlPW_{12}O_{40}$	AlPW:nitrate
	ether	Al(iso)[2]	$AlPW_{12}O_{40}$	AlPW:ether
	ether/water	Al(iso)	$AlPW_{12}O_{40}$	AlPW:ether/water
	H_2O	$Al(NO_3)_3$	$Al_{2/3}HPW_{12}O_{40}$	AlPW1
	H_2O	$Al(NO_3)_3$	$AlPW_{12}O_{40}$	AlPW2[3]
	H_2O	$Al(NO_3)_3$	$Al_{4/3}(NO_3)PW_{12}O_{40}$	AlPW3
tetra-ammonium-12-tungstosilicate	H_2O	$(NH_4)_2CO_3$	$(NH_4)_4SiW_{12}O_{40}$	NH_4SiW
aluminium-12-tungstosilicate	H_2O	$Al(NO_3)_3$	$(Al)_{4/3}SiW_{12}O_{40}$	AlSiW

1. Counter cation containing salt, water of hydration not included in the formula
2. Al(iso)-Aluminium isopropoxide
3. AlPW2 is equivalent to AlPW:nitrate

2.1.2 Heteropoly acid modifications

HPA sand dilution and supporting on α-alumina

Quartz sand diluted HPA catalysts were prepared by intimately mixing a 1:10 mixture of pure catalyst to acid washed quartz sand (150-212 μm). The α-alumina supported catalysts (20 wt% HPA) were prepared by the incipient wetness technique. Typically 2 g of HPA was dissolved in 5 ml of water and added to 8 g of α-alumina and stirred into a paste. This paste was dried at 80°C in an air oven before being crushed and stored.

Synthesis of HSiW on silicotungsten support

The silicotungsten (SiW) support was synthesized according to the procedure illustrated in the patent of Ratnasamy and Sivasanker (1990). HSiW (20 wt%) was supported on the SiW support by the incipient wetness technique outlined above for the α-alumina supported HPAs.

In-situ steaming of AlPW:nitrate

AlPW was steamed *in-situ* before propene oligomerization. The steam partial pressure was *ca.* 60 Torr H_2O at 100 ml/min nitrogen flow for 60 minutes. The temperature of the second stage of the double stage saturator was set at 42°C ($\Delta T = 10°C$).

2.1.3 SAPO-11 and MeASPO-11 synthesis

Materials

Aluminium and phosphorous sources for all of the syntheses were aluminium-isopropoxide (Fluka) and 85 wt% H_3PO_4 (BDH) respectively. Two silicon sources were used, *viz.* Ludox HS-40 (DuPont) and Fumed Silica (Merck). For the MeAPSO-n syntheses the acetates of cobalt(II), nickel(II) and manganese(II) (BDH), and the nitrate of iron(II) (Merck) were used as the metal sources. The organic template for all of the syntheses was n-dipropylamine (Aldrich).

Synthesis procedure

SAPO-11 and MeAPSO-11 (where Me = Co, Fe and Mn) molecular sieves were synthesized according to examples given in the relevant patents [Lok *et al.*, 1984b, 1985] and NiAPSO-11 was synthesized by substitution of Ni for Mn. The synthesis procedure was as follows: 85 wt% H_3PO_4 and deionized water were added to finely ground aluminium-isopropoxide and stirred vigorously until a homogeneous mixture was obtained (roughly 10-15 minutes). During this period propanol evaporated from the mixture. The Si source was then added to this mixture which was stirred for a further 10 minutes before the template, di-propylamine, was added dropwise while stirring. The pH of this mixture was approximately 10. For MeAPSO

syntheses the metal salt was dissolved in deionized water and added to the synthesis mixture after addition of the silicon source. Finally, the reaction mixtures were sealed in Teflon lined stainless steel autoclaves which were either mechanically (400 rpm) or magnetically (80 rpm) driven (Figures 2.1 and 2.2). After reaction the products were centrifuged and washed thoroughly before being dried in an air oven at 80°C. The dried as-synthesized samples were crushed and sieved to a -150 μm size fraction and stored for further use. The syntheses conditions, molar oxide ratios and catalyst nomenclatures are shown in Table 2.2. $AlPO_4$-11 was synthesized simply by excluding Si from the recipe for S11(1).

Deep bed calcination

Modifications, unless otherwise stated, were made to samples that had been deep bed calcined. The deep bed calcination (10 cm bed height) was carried out at 500°C in nitrogen for 12 hours before changing to air for a further 24 hours (the deep bed calcined samples will be assigned the suffix DB).

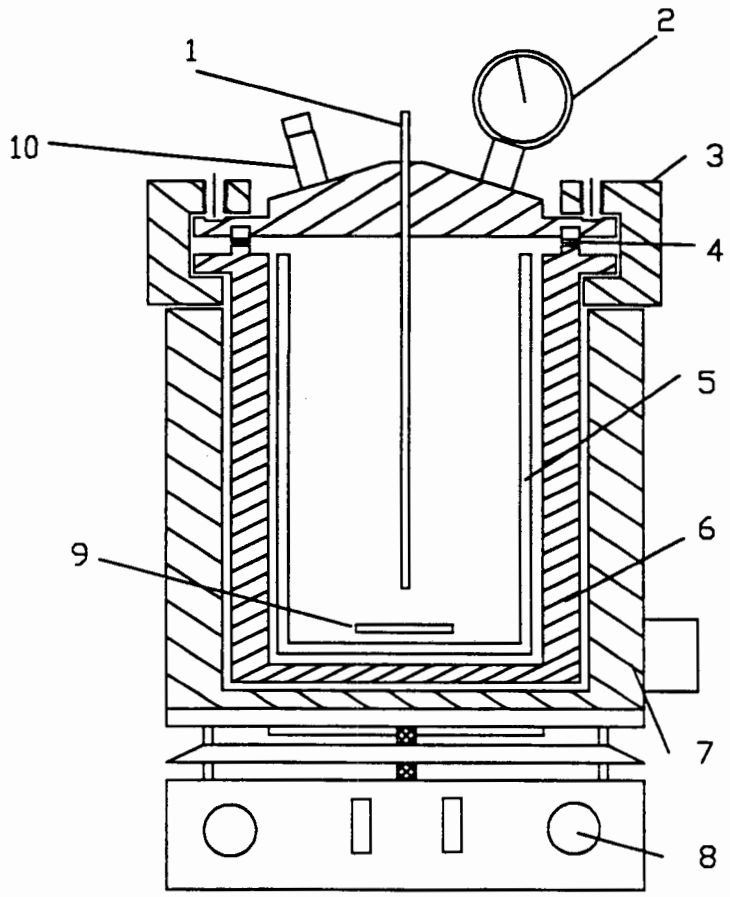

1. Thermowell
2. Pressure gauge
3. Clamp
4. Teflon seal
5. Teflon beaker
6. 316 SS autoclave body
7. Heating mantle
8. Stirrer speed control
9. Magnetic Teflon coated stirrer bar
10. Pressure relief valve

Figure 2.1 Magnetically stirred autoclave.

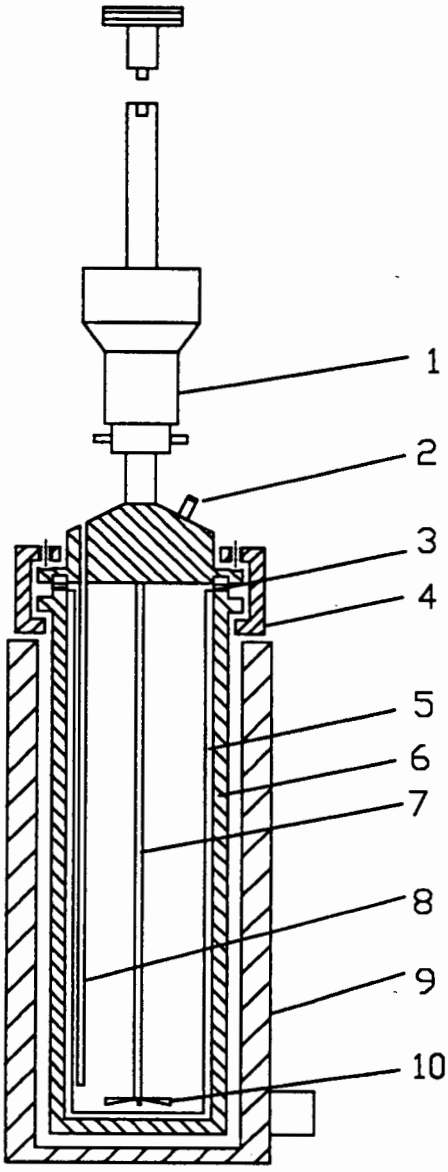

1. Magnidrive
2. Pressure relief valve
3. Teflon seal
4. Clamp
5. Teflon beaker
6. 316 SS autoclave body
7. Impeller shaft
8. Thermowell
9. Heating mantle
10. Impeller

Figure 2.2 Mechanically stirred autoclave.

2.1.4 SAPO Modifications

The following post-synthesis modifications of S11(3)DB were carried out:

Metal impregnation: Ni and Co impregnation was achieved using the incipient wetness technique (*ca.* 4 wt% metal loading). As an example, 0.687 g of $Ni(NO_3)_2 \cdot 6H_2O$ was dissolved in 10 ml of water and added to 5 g of S11(3)DB. This mixture (a thick paste) was well mixed and allowed to stand for 6 hours at room temperature before being dried at 80°C in an air oven.

Table 2.2 SAPO-11 and MeAPSO-11 Synthesis Data and Nomenclature

Synthesis conditions	S11(1)	S11(2)	S11(3)	S11(4)	S11(5)	S11(6)	S11(7)	NiS11(1)	NiS11(2)	CoS11	FeS11	MnS11
Temperature (°C)	150	150	150	150	150	200	200	150	150	150	150	150
Synthesis Time (h)	133	133	133	133	133	48	48	133	133	96	133	96
Autoclave	mag[1]	mag	mech[2]	mag	mag	mag	mag	mag	mech	mag	mag	mag
Charged masses (g)												
Al(iso)[3]	30.23	30.23	181.38	30.23	30.23	30.23	34.00	30.23	180.06	30.01	30.01	30.03
H_3PO_4(70%)	17.1	17.1	102.6	17.1	17.1	17.1	19.3	17.1	101.64	14.40	14.40	16.94
Water	53.3	53.3	319.98	52.0	52.0	53.3	13.8	68.3	409.8	68.28	60.02	68.32
Fumed Silica	0.467	0.467	2.802	-	-	0.467	-	-	-	-	-	-
Ludox(40% SiO_2)	-	-	-	1.17	2.34	-	7.6	2.45	14.7	2.45	2.45	2.45
$(Pr)_2NH$	7.4	7.4	44.4	7.4	7.4	7.4	6.9	8.24	49.44	8.24	8.24	8.25
$Ni(Ac)_26H_2O$[4]	-	-	-	-	-	-	-	4.06	24.36	-	-	-
$Co(Ac)_26H_2O$	-	-	-	-	-	-	-	-	-	4.07	-	-
$Mn(Ac)_26H_2O$	-	-	-	-	-	-	-	-	-	-	-	4.00
$Fe(Ac)_26H_2O$	-	-	-	-	-	-	-	-	-	-	4.24	-
Yield[5] (g)	12.4	14.7	90.0	15.0	11.7	16.5	23.6	16.3	115.0	18.5	18.0	16.8

1. mag = magnetically stirred autoclave (80 rpm)
2. mech = mechanically stirred autoclave (400 rpm)
3. Al(iso) = Aluminium isopropoxide
4. (Ac) = acetate
5. Yield = mass of dried (80°C in an air oven) catalyst product in g

Acid washing: 5 g of the calcined catalyst, S11(3)DB, was placed in 50 ml of 0.01N HNO_3 and stirred at 80°C for 4 hours. The mixture was then filtered and washed three times with hot distilled water before being dried in an air oven at 80°C. This sample will be abbreviated hereafter as AcidS11(3).

Steaming: Steaming was performed *in-situ* using 1 g of calcined catalyst. Steaming conditions were as follows: ***Mild steaming***, 60 Torr H_2O ($T_{sat}=42°C$), 100 ml/min nitrogen at 500°C for 2 hours or 6 hours, abbreviated hereafter as MS(2)-S11(3) and MS(6)-S11(3) respectively. ***Severe steaming***, 250 Torr H_2O ($T_{sat}=69°C$), 100ml/min nitrogen at 500°C for 6 hours, and 120 Torr H_2O ($T_{sat}=50°C$), 100 ml/min nitrogen at 500°C for 12 hours, abbreviated hereafter as $SS_{(250)}$-S11(3) and $SS_{(120)}$-S11(3) respectively. The partial pressures of water were set by the temperature of the second stage of the double stage saturator as indicated in parentheses. After steaming the catalysts were dried in flowing nitrogen at 500°C for 2 hours before use.

Silanization: Tetraethoxysilane (TESiOH) was fed via a syringe pump (2.33 g/h) with 100 ml/min nitrogen before entering a reactor containing 2 g of S11(3)DB. The reactor temperature was set at 350°C and the silanization time was 1.5 hrs. Excess TESiOH was flushed from the catalyst at 350°C for 1 hour in nitrogen. The flushed sample was calcined at 500°C in air for 12 hours to burn of any organic residue. This sample will be abbreviated as SilanS11(3)).

Ion-exchange: Ammonium ion-exchange of the deep bed calcined samples was carried out at 80°C in a reflux system containing 2 g of catalyst in 100 ml of 2M NH_4NO_3 for 12 hours (ion-exchanged samples will hereafter be assigned the suffix IX, e.g. CoS11-IX). The samples were washed three times with deionized water after filtration. The filtered and washed samples were dried in an air oven at 80°C. The original filtrate was analyzed for aluminium and metal content by AA and the pH was also recorded.

Extrudates of S11(3)syn (Ext-S11(3)) were made by mixing a 75:20:5 mixture of catalyst:binder:hydroxymethylcellulose and were extruded under 5 tonnes pressure. The binder was α-alumina and the hydroxymethylcellulose was added as a viscosity modifier to ease extrusion.

Pellets of S11(3)syn were pressed under 10 tonnes and then crushed to ±2 mm size fraction. This sample will be assigned as Pell-S11(3).

2.2 CATALYST CHARACTERIZATION

The following sections detail the physicochemical characterization techniques used. Since HPAs and SAPOs are quite different materials often the pretreatment conditions are different for the various techniques, these are mentioned below.

2.2.1 Catalyst composition

Since the parent HPA samples were obtained from commercial vendors their chemical compositions were known. Likewise for their salts all the chemicals used are recovered after crystallization from solution and hence it was assumed that the resulting salts were stoichiometric in their respective elements.

Aluminium, phosphorous and silicon contents of the SAPO-type materials were determined using ICP at Mintek (Randburg, South Africa) and the metal contents determined using atomic adsorption (AA). Si and Al contents were also checked using AA. For metal content determination 0.5 g of deep bed calcined catalyst was dissolved in 10 ml of concentrated HNO_3 and allowed to digest overnight before being diluted to the required level for AA analysis. For Al and Si analysis 0.5 g of catalyst was dissolved in 5 ml 40% HF and digested in a Teflon bomb at 80°C for 2 hours. To this was added boric acid which was then diluted appropriately for AA analysis.

2.2.2 Catalyst structure and morphology

X-ray diffraction (XRD)

Powder X-ray diffractograms were obtained using a Philips X-ray diffractometer using Cu-Kα radiation at 40 kV, 30 mA and a typical 2θ range of 5-45°. For the HPA materials 1°/1° slits were used and for the SAPO materials an automatic diverging slit was in operation.

The pretreated HPA samples (325°C in nitrogen) were stored in a desiccator while in transit to the XRD machine. As little time as possible was spent in the open atmosphere before transferring the samples to the XRD chamber and immediately commencing the XRD.

Relative crystallinities for the SAPO-type sieves were determined by summation of the 5 most intense reflections in the 2θ range 15-25° and normalizing with respect to S11(3)syn for the as-synthesized sieves or S11(3)DB for the deep bed calcined sieves. The five most intense 2θ reflections corresponded to the 130, 002, 231, 141 and 240 [Van Ballmoos, 1990].

Infrared spectroscopy (FT-IR)

FT-IR spectra of the catalysts (*ca.* 1% in KBr) were recorded at room temperature using a Nicolet 5ZDX FT-IR spectrometer at a resolution of 4 cm^{-1}. Unless otherwise stated all the HPA samples were predried in an air oven at 100°C for 2 hours prior to analysis. The as-synthesized SAPO samples were analyzed as is unless otherwise stated, i.e. no predrying.

Mössbauer spectroscopy

Mössbauer spectra of as-synthesized and calcined FeAPSO-11 were recorded in standard transmission geometry at room temperature (20°C) with a ^{57}Co in Cr matrix source (University of Witwatersrand, WITS, Jhb). Isomer shifts were calibrated against α-Fe.

Scanning electron microscopy (SEM)

Electron micrographs were obtained using a Cambridge S200 Scanning Electron Microscope (SEM) with the accelerating voltage set at 10 keV for HPA and 15 keV for SAPO-type sieves. The Stage tilt was set at 30°, working distance = 9-12 mm and the Aperture size = 30 μm. Samples were mounted on aluminium stubs and coated with Au/Pd film.

2.2.3 Thermal stability

Thermogravimetric-differential thermal analysis (TG-DTA) was carried out in a Standton Redcroft STA-780 thermal analyzer. Typically 15 mg samples were heated either in dry flowing nitrogen or air from 20°C to 600°C, at 10°C/min, and held at 600°C for 30 minutes. In some instances the samples were also heated to 700°C.

Thermal desorption of template (TPD-MS)

SAPOs: Template desorption products from the as-synthesized sieves were detected by TPD-MS using an in-house designed system with an attached HP5890 MS detector. The catalysts (0.05 g) were placed in a quartz reactor tube and heated from 70°C to 700°C at 10°C/min in 100 ml/min of He. The ions monitored were M/e=16, 17, 18, 43 and 58 respectively. For S11(3) and CoS11 total ion chromatograms (TIC) were also recorded (M/e 12-200).

2.2.4 Catalyst Acidity

Temperature programmed desorption (TPD) methods

Ammonia TPD was performed in a quartz sample cell containing *ca.* 0.25 g of catalyst.

HPA-TPD procedure: The HPA catalyst was first calcined in flowing helium at 325°C for 4 hours before being cooled in flowing helium to 100°C. Ammonia was then adsorbed from a 4% NH_3 in helium mixture for 60 minutes and the physisorbed ammonia was removed by purging in flowing helium for a further 1-2 hours at 100°C. TPD spectra were recorded by measuring the ammonia desorbed using a thermal conductivity detector (TCD) while increasing the temperature at 10°C/min from 100°C to 600°C and maintaining the final temperature for 30 minutes. Baseline spectra (no ammonia adsorbed) were subtracted from all the HPA ammonia TPD spectra. NH_3 mass balances, checked by titration of the exiting steam, were always better than 95%.

SAPO-TPD procedure: The SAPO catalyst was first calcined at 500°C in flowing air for 240 minutes before being cooled to 100°C in flowing helium. Ammonia was then adsorbed as for the HPA-TPD procedure and the excess ammonia desorbed by flushing in flowing He for 24 hours. The TPD procedure was as for the HPA system. Baseline spectra were not subtracted from the SAPO ammonia TPD spectra.

TPD-MS of HPA: NH_3 desorption was also detected by MS (as opposed to TCD). Calcination and adsorption procedures were the same as for HPA NH_3-TPD procedure above, except the samples were flushed in He for 24 hours at

100°C instead of 2 hours. The ammoniated samples were heated to 700°C at 10°C/min in 100 ml/min He. The ions monitored were M/e=15, 16, 17 and 18.

FT-IR acidity determination

HPA samples were calcined and ammonia adsorbed following the NH_3-TPD procedure except that the catalysts were kept in flowing helium for 24 hours as opposed to 2 hours at 100°C. These ex-TPD samples were then heated at 10°C min^{-1} to 200, 300, 400, 500 and 600°C respectively for approximately 1 hour, before being removed from the quartz sample cell and pressed into KBr discs. The samples were then dried at 100°C for 1 hour before being transferred to the FT-IR for analysis. The area under the 1640 cm^{-1} (NH_4^+) and the area under the 1080 cm^{-1} (P-O) bands were recorded. Since the P-O band is triply degenerate the ratio of NH_3 to Keggin unit, quoted as $A_{(1640)}/A_{(1080)}$, is calculated by taking the ratio of the two areas and multiplying by 3.

2.2.5 Catalyst surface area and pore volume

HPA surface areas were obtained using a multipoint Carlo-Erba sorptometer (AECI, Moderfontein, South Africa) with nitrogen as the sorbate. Prior to adsorption the samples were degassed under vacuum at 250°C. N_2-BET surface areas and micropore volumes of the SAPO-DB materials were obtained using an ASAP 200 (Mintek) and prior to nitrogen adsorption the samples were pretreated under vacuum at 250°C.

Hexane adsorption (SAPO-type)

Prior to hexane adsorption the catalysts were calcined in flowing air at 500°C for 2 hours before being cooled to 70°C in dry flowing nitrogen. The catalysts were then exposed to a flowing hexane in nitrogen stream at a partial pressure of 55 Torr for 120 minutes. The amount hexane adsorbed is given as a weight percent after the two hours.

2.2.6 Reducibility of metal component of the catalyst by temperature programmed reduction (TPR)

TPR was performed in a quartz sample cell containing *ca.* 0.25 g of catalyst. Prior to reduction in a 5% H_2 in nitrogen stream the catalysts were calcined at 500°C in flowing air before being cooled in flowing nitrogen to 100°C. Samples were reduced to either 650°C, 800°C or 1000°C at 10°C/min and held at temperature for 30-45 minutes. The K value (Section 1.6), determined after Monti and Baiker (1983), was between 55 and 70 s^{-1}. Calculations of the K value are given in Appendix VI. The TPR system was calibrated using either nickel acetate or a 7 wt% Ni on silica-alumina catalyst.

2.2.7 Coke analysis

TG-DTA

Samples of the deactivated catalysts (15 mg) were heated in a flowing nitrogen stream to 500°C in the TG balance and held at that temperature for 60 minutes before air was passed over the coked catalyst for a further 120 minutes. This categorization differentiates between high boiling point hydrocarbons, or "soft" coke, and poly-nuclear aromatics, or "hard" coke. This is different to the coke classification of, for example Karge (1991), and is used in the analysis of coke by FT-IR described below.

FT-IR

FT-IR was also used to characterize the type of coke deposited on the catalysts after the various reactions. They were characterized as Type I coke (bands at 2958, 2926, 2860, 2856, 1485, 1468, 1382, 1359 and 1638 cm^{-1}) and Type II coke (bands 3080 and 1540 cm^{-1}). The former bands are characteristic typically of olefinic hydrocarbons and the latter of aromatic hydrocarbons (Section 1.2.7).

2.3 REACTOR CONFIGURATIONS AND EXPERIMENTAL PROCEDURES

The following sections describe the reactor configurations and experimental procedures for the various probe reactions studied as well as propene oligomerization. n-Butane cracking and 1-butene isomerization were used as probe reactions for the HPAs, and 2-methylpent-2-ene and *m*-xylene isomerization were used as probe reactions for SAPO-11 catalysts.

2.3.1 n-Butane cracking

0.5 g of HPA catalyst was packed into the same reactor as that used for oligomerisation studies (see below) and calcined at reaction temperature for 6 hours before n-butane was passed over the catalyst (GHSV = 21600 h^{-1}). The first gas product sample was taken after 3 minutes on stream and analyzed off-line by gas chromatography. Thereafter effluent samples were analyzed every half hour. The GC was equipped with a 1/8" stainless steel packed column, n-octane Porasil C. The GC oven was kept at 50°C for 5 minutes then ramped at 10°C/min to 130°C and finally held at 130°C for 10 minutes.

2.3.2 1-Butene isomerization

Approximately 1 g of HPA catalyst was packed into a quartz reactor (25 cm long, I.D. 10 mm) and calcined at 325°C in flowing nitrogen for approximately 2 hours before being cooled to reaction conditions (225°C, 101 kPa). The feed mixture, consisting of a 1:4 mixture of 1-butene and nitrogen, was then passed over the catalyst (GHSV = 1800 h^{-1}). The first gas product sample was taken after 3 minutes on stream and thereafter samples were taken at 30 minute intervals. Product analysis was carried out by off-line GC analysis using a n-octane Porasil C packed 1/8" stainless steel column. The GC oven was kept at 50°C for 10 minutes and then ramped at 10°C/min to 150°C and finally held at 150°C for 10 minutes. Detailed calculations of conversion and selectivity are shown in Appendix I. Mass balance was assumed to be 100%.

2.3.3. *M*-xylene isomerization

For all of the SAPO probe reactions the catalysts were first calcined *in-situ* in flowing air at 500°C for at least 12 hours.

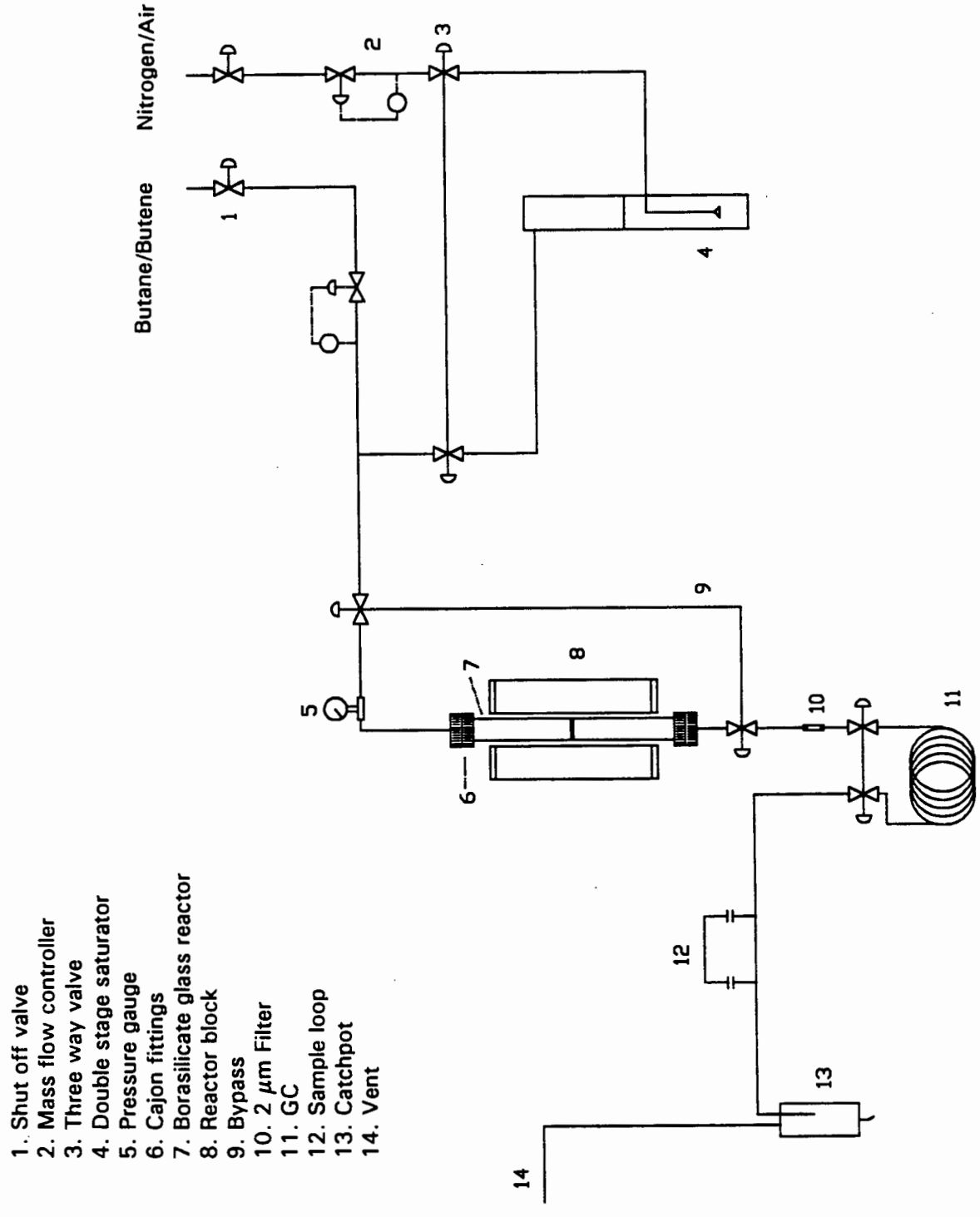

Figure 2.3 Schematic of atmospheric pressure probe reaction apparatus.

The reaction was carried out in a 16 mm I.D. quartz reactor packed with *ca.* 0.5 g of catalyst and the *m*-xylene was fed to the reactor via a double stage saturator (partial pressure = 1 kPa) in a nitrogen stream. The reaction conditions used were 450°C, WHSV = 1.05 h^{-1} and 115 kPa. On-line GC samples were taken after 5 minutes on stream and thereafter at half-hourly intervals. *m*-Xylene product analysis was by on-line gas chromatography (GC). A 30 m Supelcowax 10 capillary column was used to separate the xylene isomers and the other *m*-xylene reaction products. Column conditions were 70°C for 5 minutes and 10°C/min to 180°C and held at 180°C for 10 minutes. Detailed conversion and selectivity calculations shown in Appendix II.

2.3.4 2-Methylpent-2-ene isomerization

The reaction was carried out in a 24 mm I.D. borosilicate glass reactor packed with *ca.* 0.25 g of catalyst and the 2-methyl-2-pentene was fed to the reactor via a double stage saturator using nitrogen as a carrier gas. The partial pressure of 2-methyl-2-pentene was 18 kPa. The reaction conditions used were 200°C, WHSV = 11 h^{-1} and 115 kPa. On-line GC samples were taken 5 minutes after startup and every half hour thereafter. The 2-methyl-2-pentene products were analyzed on-line using a 30 m, 0.352 mm I.D. fused silica megabore column coated with a 1.5 μm film of BD-1 (100 % methylpolysiloxane). For the separation of all 18 C_6 isomers the GC oven was kept at 0°C for 7.5 min and then ramped at 5 °C/min to 250°C and kept at 250°C for 10 minutes. Detailed calculations of mass balance, conversion and selectivity are shown in Appendix III.

2.3.5 Propene oligomerization

Equipment

The propene oligomerisation apparatus used is illustrated in Figure 2.4. The feed mixture (86 wt% propene, 14 wt% propane) was stored in a gas cylinder at 1 MPa. The feed was dried over 3A molecular sieves before being fed via a high pressure diaphragm pump to the reactor. The reactor pressure was held at 5 MPa and the weight hourly space velocity (WHSV) of SASOL feed used was 12-14 h^{-1} unless otherwise stated. Temperature profiles were measured by a thermocouple housed within an axially

positioned thermowell at the centre of the reactor. Typically, 1 g of the catalyst was loaded into the reactor.

HPA start-up procedure: The catalysts were first calcined in flowing nitrogen at 325°C for 2-6 hours before being cooled to 200°C under static nitrogen (5.0 MPa). The propene/propane SASOL feed was then fed over the catalyst and the reactor jacket temperature set so that the catalyst bed temperature remained at 230°C.

SAPO start-up procedure: The catalysts were calcined in flowing air at 500°C before the reactor was cooled to 100°C under static nitrogen (5 MPa). The propene/propane SASOL feed mixture was then passed over the catalyst bed. Once the feed contacted with the catalyst bed the reactor jacket was kept at 100°C for 5 minutes before being heated at 6°C/min to 220°C. Depending on the activity of the catalyst the reactor temperature was then set so that the required catalyst bed temperature was achieved. Unless otherwise stated propene oligomerisation was carried out at 250°C, WHSV = 12 ± 2 h^{-1} and 5.0 MPa for the SAPO system. Gas and liquid product samples where taken every hour for the first 6 hours and thereafter every 5 to 6 hours.

Product analysis and data work-up

Vapour and liquid phase products were analyzed off-line using a 0.352 mm I.D., 50 m long fused silica megabore column coated with a 1.5 μm film of DB-1 (100% methylpolysiloxane). The GC oven was held at 35°C for 2 minutes then ramped at 10°C/min to 250°C and finally held at 250°C for 8 minutes. The products were analyzed according to oligomer groupings, as shown in Table 3.7, and these groupings were assigned on the basis of GC-MS analysis of liquid product samples.

Cetane number: Samples of the liquid product were hydrogenated in a high pressure autoclave at 3 MPa and 165°C for 12 hours under hydrogen. Palladium on activated carbon (Aldrich, 5 wt% Pd) was used as the hydrogenation catalyst and was added in 5 wt% aliquots to the liquid product. H^1-NMR spectra of the hydrogenated unfractionated liquid product were recorded using a 90 MHz Bruker NMR spectrometer. Cetane numbers

were obtained using Gautier's correlation [Gautier, 1988]. This calculation is shown in Appendix V.

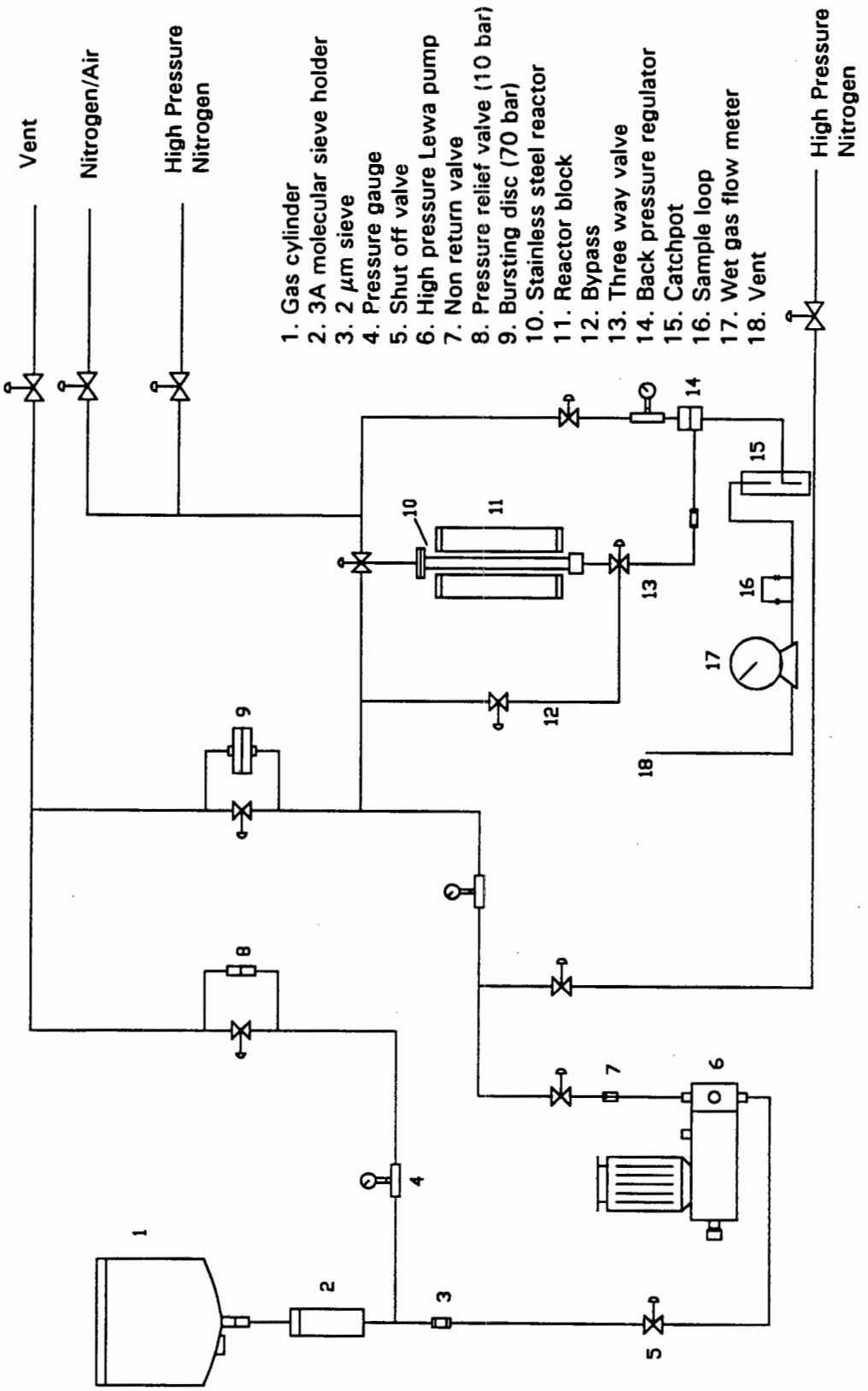

Figure 2.4 Schematic of high pressure propene oligomerization apparatus.

Data work-up

Conversion levels are reported as wt% conversion of propene to liquid product collected in a catchpot kept at 20°C.

% Conversion=(M_L/M_P)x100

M_L=Mass of liquid collected over 1 hour

M_P=Mass of propene passing over catalyst bed in 1 hour

C_{12}+ Selectivity=(M_{12}+/M_L)x100

M_{12}+=Mass of C_{12}+ hydrocarbon in liquid product (determined from GC analysis)

C_{12}+ Yield=(C_{12}+ Selectivity)x(% Conversion)/100

Detailed mass balance, WHSV, conversion, selectivity and yield calculations are shown in Appendix IV.

Catalyst performances were also compared by determining catalyst utilization values (CUVs) over the total run time. CUV is defined as the g•(liquid product)/g•(catalyst).

For all of the reaction studies the **WHSV is quoted per mass of active catalyst**, i.e. the weight of binder or support is not included in the WHSV calculations.

2.4 ERROR ANALYSIS

Due to the duration of many of the analyses (NH_3-TPD take *ca.* 2-3 days) a true statistical analysis was not possible. Hence the majority of the errors listed below are estimates made by the author. Where possible the accuracy of measurements were determined according to the manufacturers claims.

Table 2.3 Error analysis of characterization techniques

Measurement	Units	Technique	Error[1]
Total Al (SAPO)	wt%	AA/ICP	5
Total P (SAPO)	wt%	ICP	5
Total Si (SAPO)	wt%	ICP	20
Water Content	wt%	TD-DTA	5
Crystallinity (SAPO)	ratio	XRD	5
NH_3-TPD peak temp	°C	TPD	5°C
NH_3-TPD total acidity	mmol/g	TPD	7.5
IR	cm^{-1}	FTIR	4 cm^{-1}
Surface area	m^2/g	N_2-BET	10

Table 2.4 Propene oligomerization activity and selectivity data

Measurement	Units	% Error
Conversion	%	5
CUV	g.liquid/g.cat 5	
$C_{12}+$	wt%	10
Cetane no.	no.	5
Pressure	MPa	5
Temperature	°C	±2°C
WHSV	h^{-1}	5

Chapter 3
Results

3. RESULTS

3.1 HPA CATALYST CHARACTERISATION

3.1.1 Surface area and Thermogravimetric Differential Thermal Analysis

The surface areas of HPW and its salts are given in Table 3.1. With the exception KPW and NH_4PW these were between 3 and 15 m^2/g. KPW and NH_4PW had surface areas that were significantly greater than HPW. The surface area values were reproducible to within 5%. The TG-DTA data is also presented in Table 3.1 and the TG-DTA of AlPW:nitrate is shown in Figure 3.1. The results showed that, for the HPAs tested, with the exception of KPW and NH_4PW, there were two distinct endothermic regions, Endo(1) and Endo(2). For AlPW:ether and AlPW:ether/water the second distinct endotherm was Endo(3) and not Endo(2). These endotherms were accompanied by mass losses. HPW and its salts, with the exception of KPW, each had a large exotherm which indicated that decomposition was occurring in the range 570-630°C. A small exotherm at 626°C was also observed for all the salts, except KPW, when heated beyond 600°C. KPW showed no exotherms and was thermally stable up to 600°C. NiPW, FePW and CePW each had a third small endotherm between 300-370°C. These endotherms occurred near the end of their second mass loss.

The aluminium salts exhibited different thermal behaviour depending on their synthesis procedure. The AlPW:nitrate salts had four endotherms, Endo(3) and Endo(4) being small (Figure 3.1). The final endotherm, Endo(4), occurred at the end of the second mass loss. AlPW:ether and AlPW:ether/water each had three endotherms at 140°C, 300°C and 410°C respectively. All the aluminium salts decomposed at approximately 570°C, *ca.* 60°C lower than the decomposition temperature of the parent acid, HPW.

HSiW, HPMo and their salts (except KPMo) were thermally less stable than HPW and decomposed below 500°C. The TG-DTA traces were in general similar to those shown for HPW in Table 3.1

Table 3.1 Surface area and TG-DTA data for HPW and its salts

Catalyst	SA[1] (m^2/g)	Endo(1)[5] (°C)	Endo(2) (°C)	Endo(3) (°C)	Endo(4) (°C)	Exo[6] (°C)	H_a/H_b[3]	n.H_2O[4]
HPW	3[2]	110	240	-	-	626	2.8	24
NH_4PW	37	110	-	-	-	600	-	6
NH_4PW[7]	35	110	-	-	-	600	-	6
KPW	140	105	-	-	-	-		7
NiPW	6	120	250	360	-	600	0.3	8
CoPW	2	115	250	-	-	595	0.3	8
CuPW	2	140	250	-	-	590	0.3	7
FePW	11	120	230	300	-	600	0.8	9
CePW	6	140	230	370	-	600	0.8	11
AlPW:nitrate	2	130	230	280	400	570	1.3	11
AlPW:nitrate	12	130	230	280	400	570	1.0	10
AlPW:ether	5	138	-	300	410	570	1.2	11
AlPW:ether/ water	9	140	-	300	410	570	1.3	12

1. SA = Surface area (m^2/g)
2. From Hayashi and Moffat (1983)
3. H_a/H_b ratio of water of hydration to those associated with acid sites.
4. n = Number of molecules of water
5. Endo(n) = Endotherm, value in brackets indicates order of appearance
6. Exo = Major exotherm
7. Reproducibility

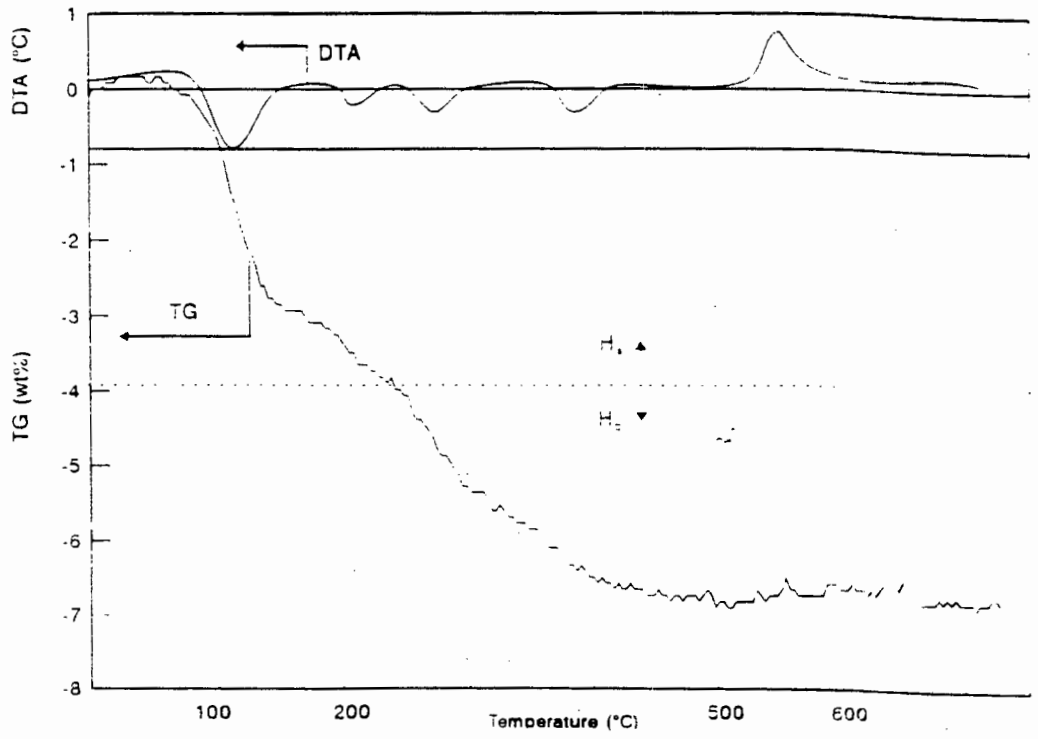

Figure 3.1 TG-DTA spectra of ALPW:nitrate

On the basis of the TG-DTA and surface area data the HPAs were divided into two types, after Niiyama *et al.* (1980), *viz.*:

Type A: low surface area salts with multi-endothermic regions; and
Type B: high surface area salts with a single endotherm at 100°C.

The Type A salts were water soluble and the Type B salts were water insoluble.

3.1.2 FT-IR of primary structure

The infrared spectra of HPW and several of its salts are shown in Figure 3.2 and as can be seen the Keggin unit bands (primary structure) are well defined. The Keggin unit bands of the HPW salts used in this study are listed in Table 3.2. The band that was most affected by the type of counter cation present was the νM-O-M (edge) band.

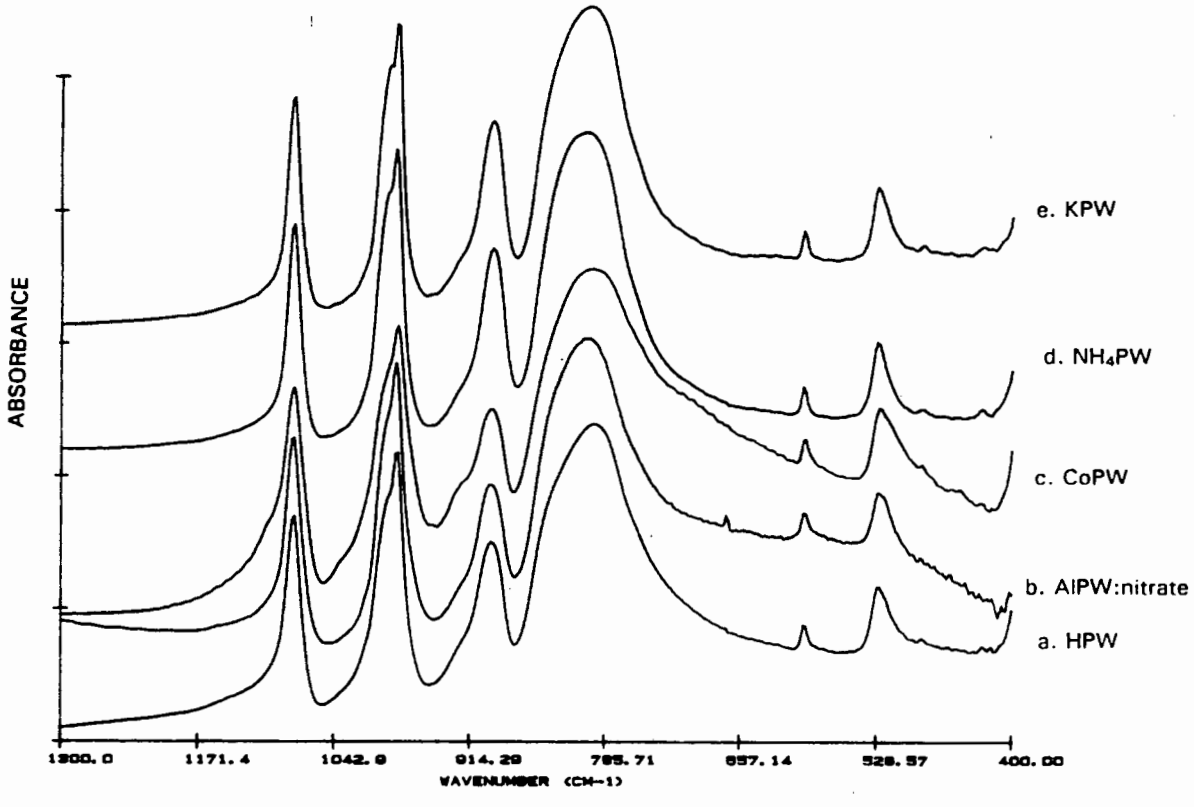

Figure 3.2 FT-IR spectra of a. HPW, b. AlPW:nitrate, c. CoPW, d. NH_4PW and e. KPW.

Table 3.2 FT-IR Keggin ion bands of HPW and some salts (cm^{-1})

Catalyst	HPW	NH_4PW	KPW	CoPW	CuPW	NiPW	FePW	AlPW:nitrate
δO-P-O	595	596	596	595	595	594	595	594
νM-O-M_e	794	809	800	797	793	798	793	792
νM-O-M_c	892	891	891	892	893	892	891	892
νM=O	984	986	985	982	983	984	982	984
νP-O	1081	1081	1081	1081	1081	1081	1081	1081

FT-IR spectra of the other as-synthesized HPA catalysts are shown in Appendix VII.

3.1.3 State of the secondary structure (Crystallinity)

The X-ray diffractogram of fresh HPW is shown in Figure 3.3a. After drying in flowing nitrogen at 325°C the diffractogram had fewer and broader peaks (Figure 3.3b). The Type B salts (Figure 3.3c) had well defined diffractograms that changed little upon drying at 325°C indicating greater thermally stability for this crystalline structure.

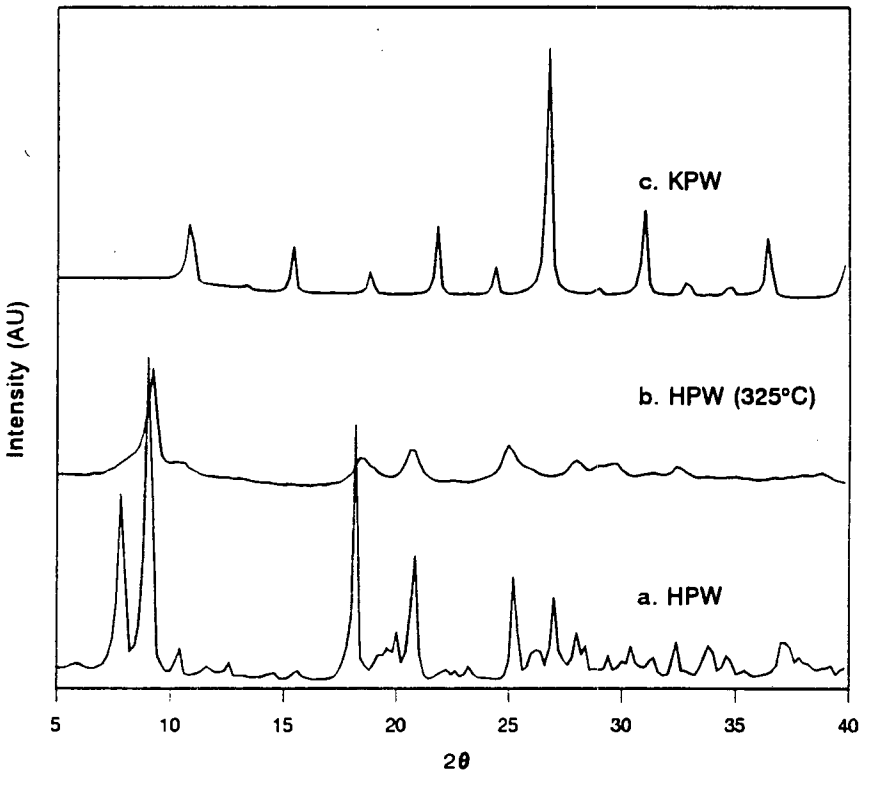

Figure 3.3 XRD spectra of a. HPW, b. HPW(325°C) and c. KPW

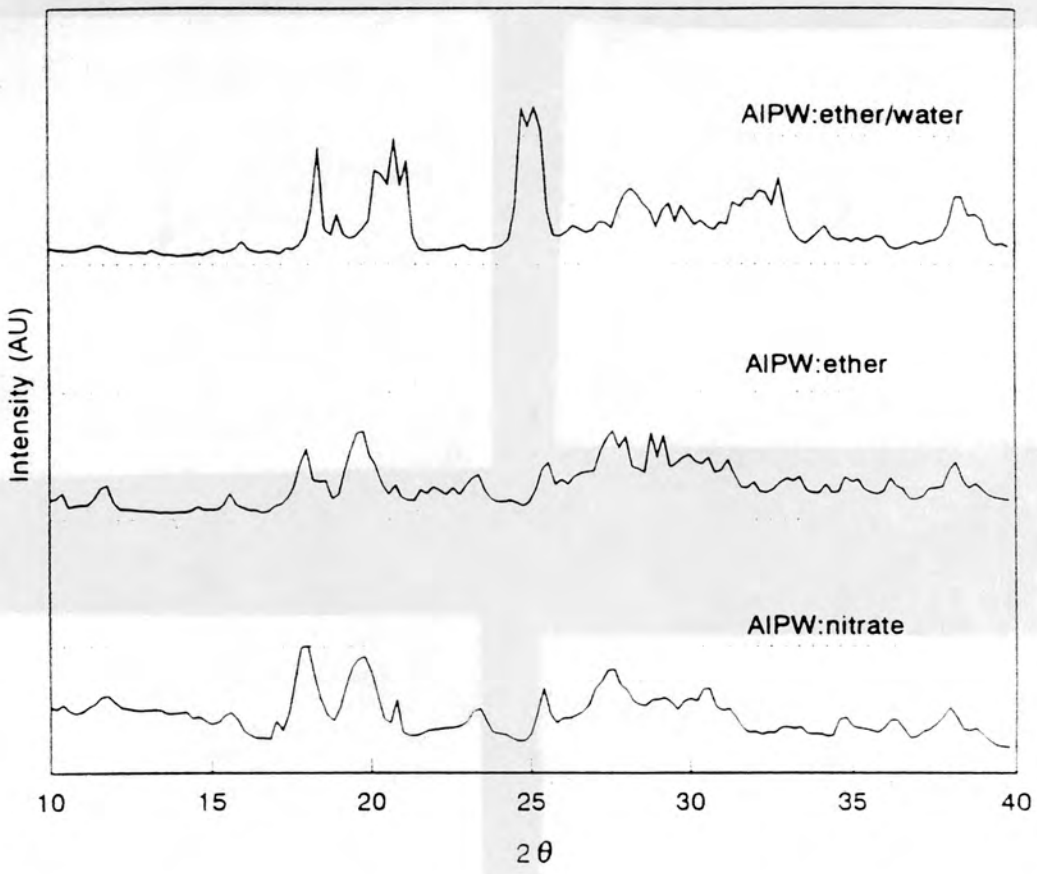

Figure 3.4 XRD spectra of AlPW salts prepared by different synthesis routes

Diffractograms of the aluminium salts of HPW, shown in Figure 3.4, indicated a partly crystalline structure. When the AlPW:ether salt was recrystallized from water the intensity and the sharpness of the peaks increased indicating structural changes were occurring after recrystallization. XRD patterns of all the HPA catalysts synthesized are shown in Appendix VIII.

3.1.4 Crystallite size and morphology

Figure 3.5a shows an electron-micrograph of the parent acid, HPW. This acid consisted of irregularly shaped smooth crystallites, approximately 20 μm in diameter, as well as sponge-like crystallites. AlPW:nitrate (Figure 3.5c), AlPW:ether and AlPW:ether/water on the other hand consisted of irregularly shaped column-like crystallites 10-50 μm long. FePW (Figure 3.5d) and the other Type A salts had similar morphology to the aluminium salts. NH_4PW (Figure 3.5b) and KPW consisted of 50-150 μm agglomerates of well-formed 0.5-2 μm rounded cubic crystallites.

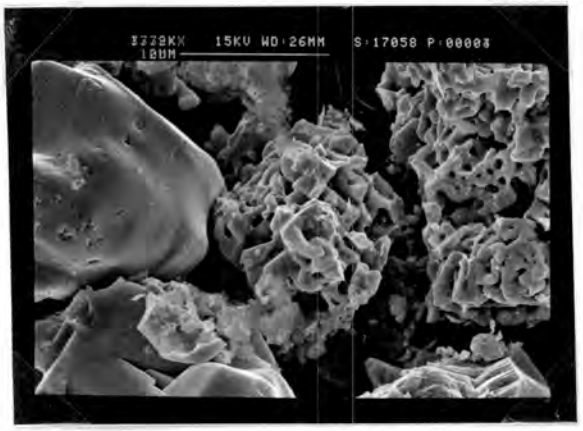

a.

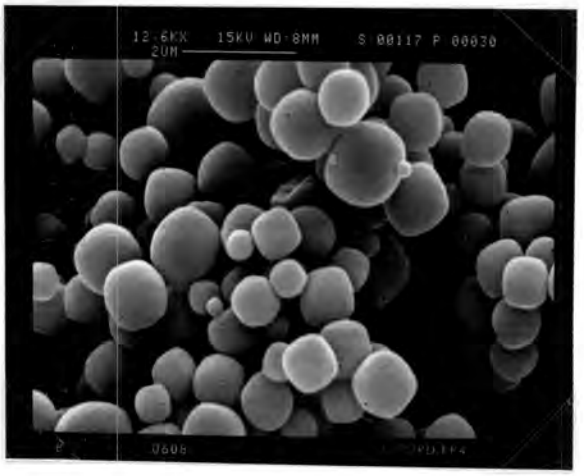

b.

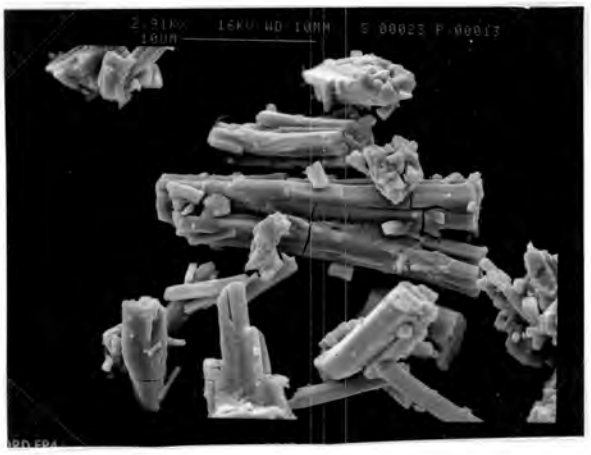

c.

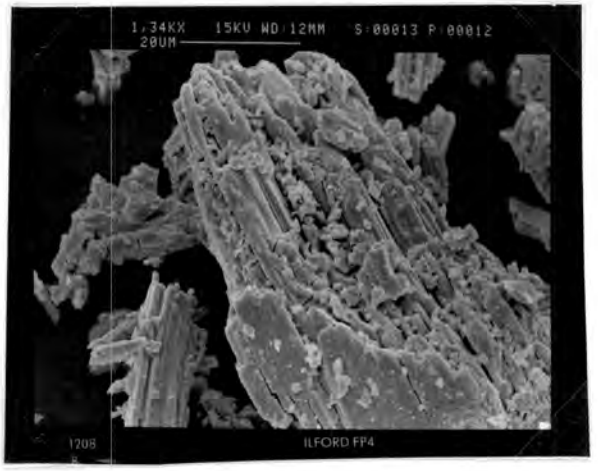

d.

Figure 3.5 Electron-micrographs of a. HPW, b. NH_4PW, c. AlPW and d. FePW

3.1.5 HPA Acidity

NH_3-TPD

Ammonia TPD spectra, shown in Figure 3.6, all exhibited two temperature regions in which ammonia was desorbed. The first desorption (low temperature desorption-LTD) occurred between 100-200°C while the second desorption (high temperature desorption-HTD) occurred between 530-600°C. The temperatures at which desorption occurred and the respective quantities of ammonia desorbed are listed in Table 3.3.

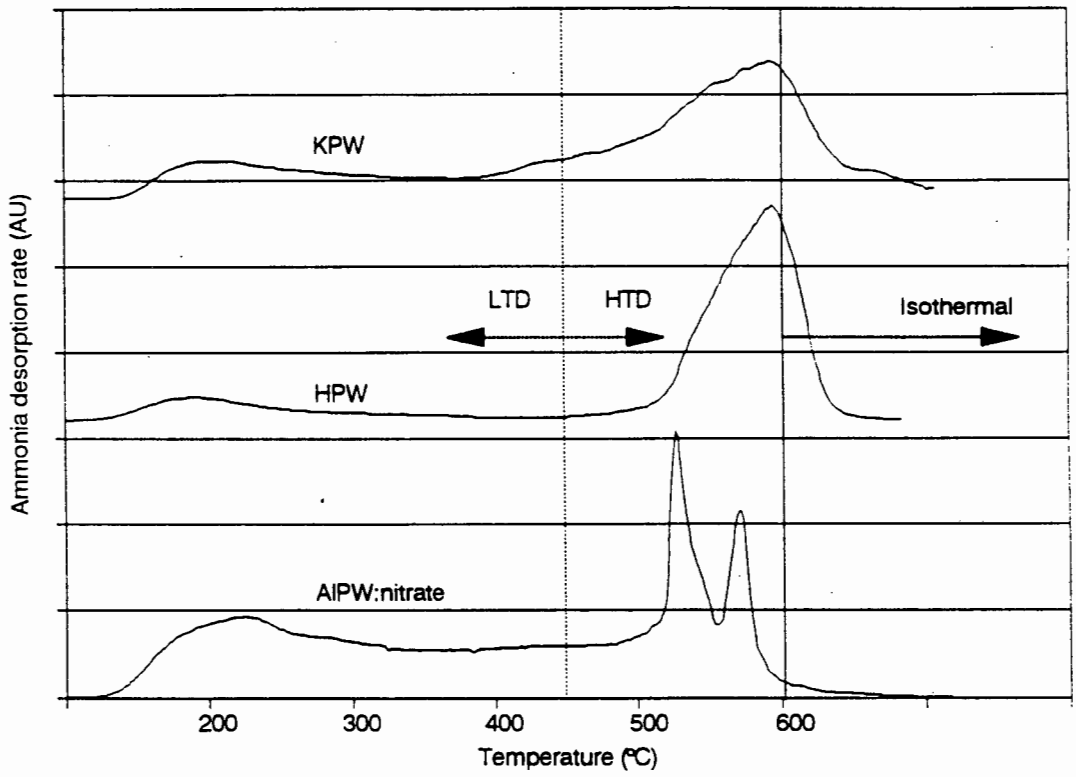

Figure 3.6 NH_3-TPD spectra of HPW, KPW, AlPW, FePW

There was little difference between the TPD spectra of the Type A and B salts with the exception that the Type A salts in general had 2 to 3 times the amount of acidity than did the Type B salts. The baseline spectrum of NH_4PW, i.e. in the absence of adsorbed ammonia, was very similar to the NH_3-TPD spectrum of HPW. The only difference was that the baseline spectra of NH_4PW had no LTD peak. The baseline spectra of AlPW showed two sharp high temperature peaks at 535°C and 575°C and is illustrated in Figure 3.7. These peaks were confirmed to be water by mass spectrometry.

Table 3.3 NH_3-TPD data

Catalyst	LTD (°C)	HTD1 (°C)	HTD2 (°C)	LTD[1] (mmol/g)	HTD1 (mmol/g)	HTD2 (mmol/g)	Total (mmol/g)	Pauling Elec.[2]–
HPW	170	598	-	0.20	0.92	-	1.12	2.20
NH_4PW	170	575	-	0.18	0.28	-	0.46	-
KPW	192	571	-	0.14	0.28	-	0.42	0.82
NiPW	230	585	-	0.35	0.45	-	0.80	1.80
CoPW	257	556	-	0.78	0.56	-	1.34	1.80
CuPW	252	556	-	0.63	1.01	-	1.64	1.90
FePW	194	583	541	0.63	0.51	0.43	1.57	1.80
CePW	193	581	564	0.51	0.20	0.31	1.02	1.10
AlPW:nitrate	223	579	529	0.96	0.46	0.26	1.68	1.61
AlPW:nitrate	283	578	534	0.80	0.53	0.26	1.59	1.61
AlPW:ether	269	575	530	0.88	0.48	0.24	1.60	1.61
AlPW:ether/ water	260	575	528	0.83	0.54	0.27	1.64	1.61

1. LTD = mmol/g ammonia desorbed below 450°C
2. Pauling Electronegativity of the counter cation

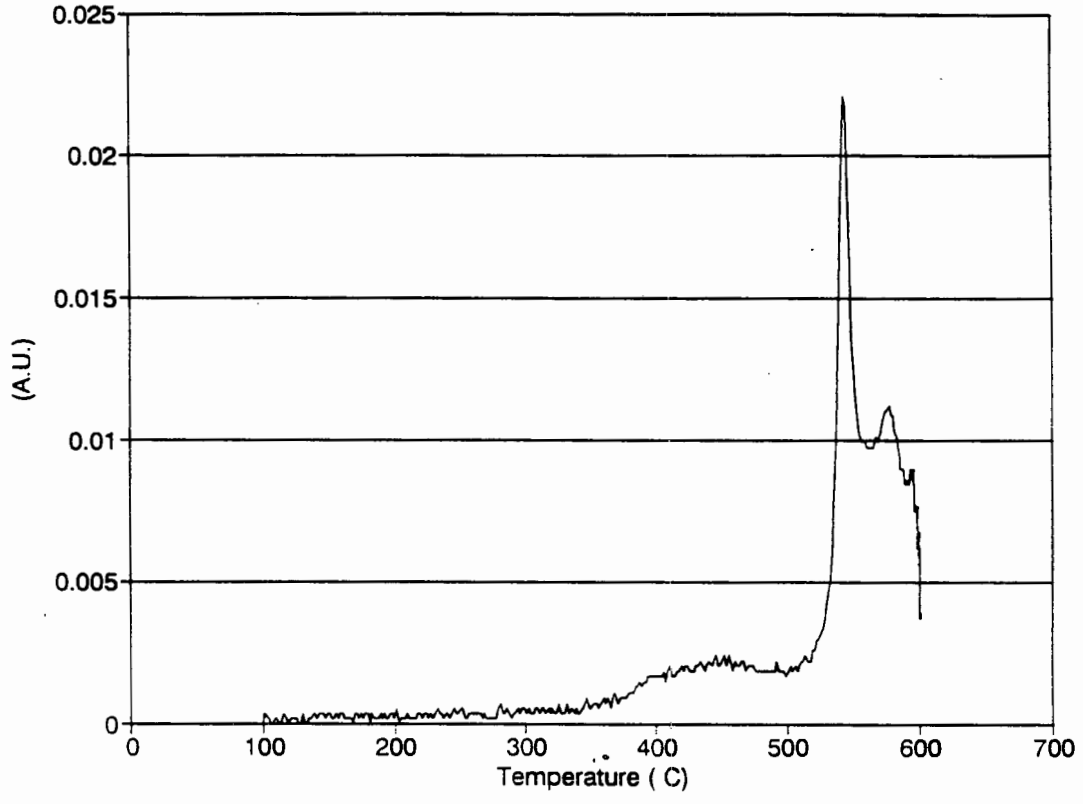

Figure 3.7 Baseline H_2O-TPD spectra of AlPW:nitrate

TPD-MS of AlPW:nitrate indicated that water was desorbed concurrently with ammonia at each HTD peak. In all cases the respective baseline spectra were subtracted from the NH_3-TPD spectra.

FI-IR spectra of samples onto which NH_3 was adsorbed

As can be seen from Figure 3.8 adsorbing ammonia on HPW resulted in the appearance of the NH_4^+ band at 1450 cm^{-1}. This band was present for all the other HPAs tested. For AlPW, KPW and CoPW the 1630 cm^{-1} band was also present, particularly at higher temperatures, which is indicative of ammonia coordinatively bound with metal ions [ref]. The initial ratios of $A_{(1450)}/A_{(1080)}$ for AlPW, CoPW, KPW, NH_4PW and HPW are given in Table 3.4. As the desorption temperature increased this ratio decreased for all catalysts indicating a loss of ammonia. At 500°C the Keggin ions of AlPW:nitrate + NH_3 and CoPW + NH_3 began to decompose whereas the Keggin bands of HPW + NH_3, KPW + NH_3 and NH_4PW + NH_3 remained relatively intact. At 600°C the HPW + NH_3, NH_4PW + NH_3, AlPW + NH_3 and CoPW + NH_3 Keggin bands were essentially nonexistent which indicated complete decomposition of the Keggin anions had occurred. The Keggin bands of KPW + NH_3 were still intact at 600°C which indicated no collapse of the Keggin anions.

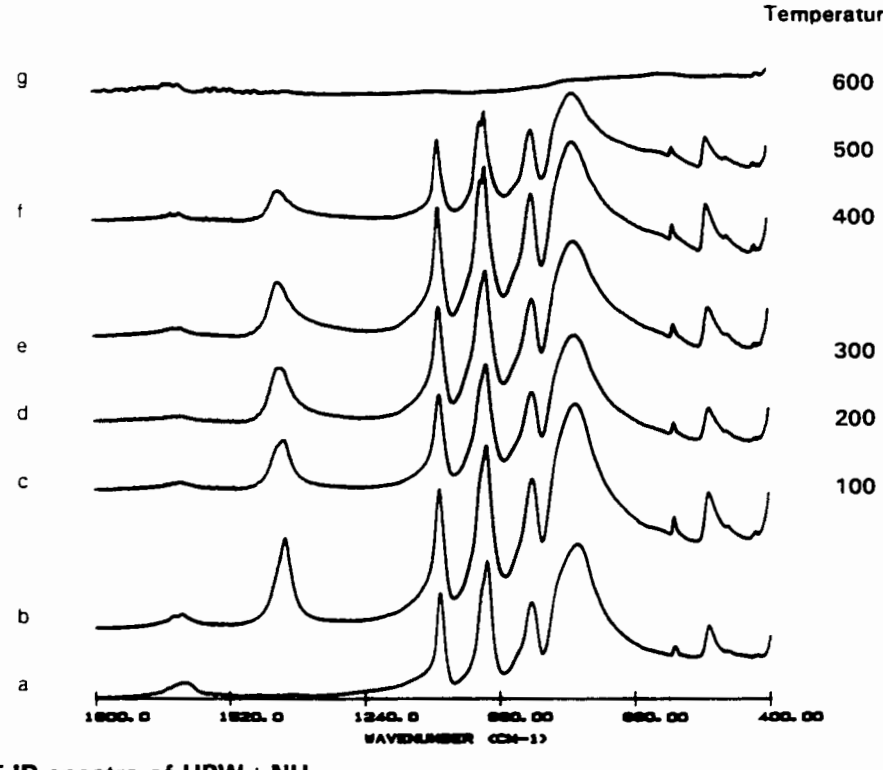

Figure 3.8 FT-IR spectra of HPW + NH_3

Table 3.4 FT-IR $A_{(1420)}/A_{(1080)}$ for HPA + NH_3 after heating to 100, 200, 300, 400, 500 and 600°C.

Catalyst Temperature(°C)	$A_{(1420)}/A_{(1080)}$					
	100	200	300	400	500	600
HPW	3.45	3.06	2.71	2.49	2.34	0.00
NH_4PW	2.82	2.60	2.50	2.27	2.27	0.00
KPW	0.69	0.57	0.52	0.42	0.24	0.09
CoPW	3.00	2.46	2.46	1.53	0.93	0.00
AlPW	1.59	1.53	1.35	0.87	0.86	0.00

Table 3.4 is represented graphically in the Figure 3.9 below and can be compared to that shown for pyridine desorption from various HPAs in Section 1.3.3.2.

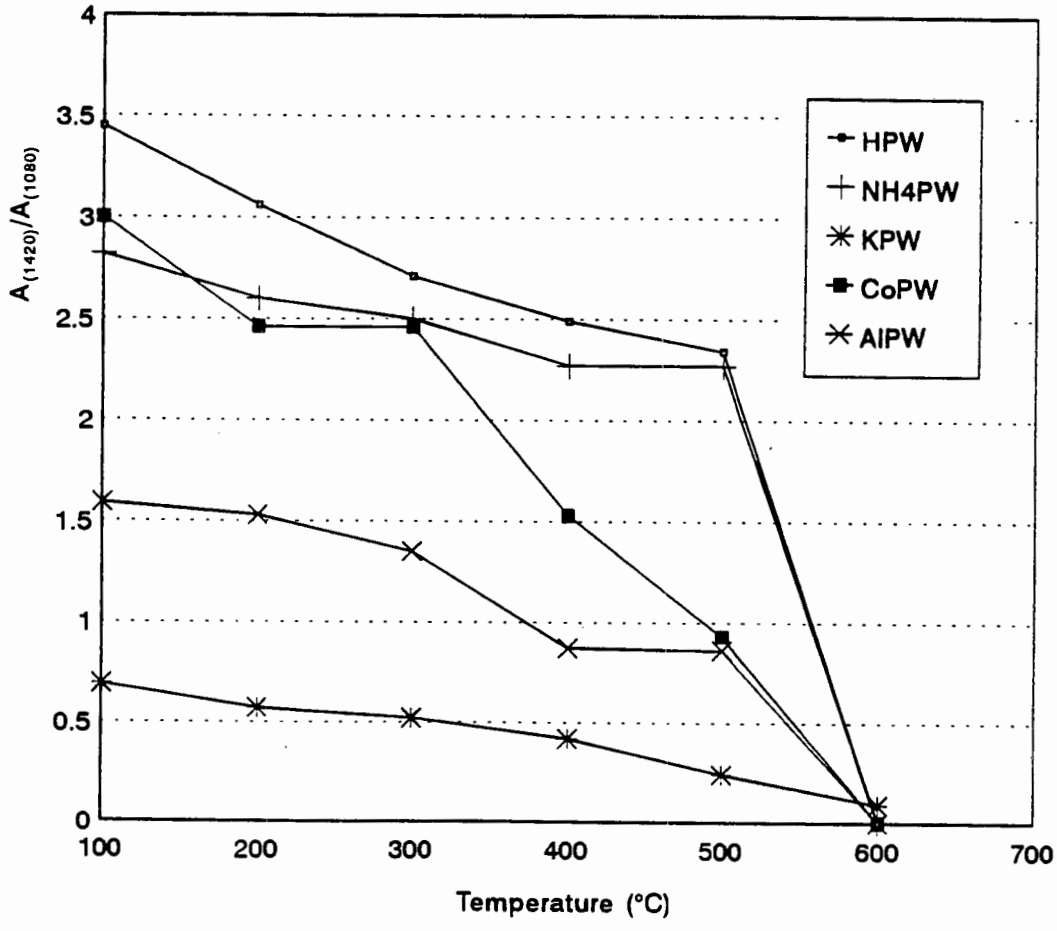

Figure 3.9 Desorption of NH_3 as determined from FT-IR as a function of temperature

3.1.6 n-Butane cracking activity

HPW and AlPW:nitrate(2) (Type A) showed no activity for n-butane cracking between 350 and 450°C. When the catalysts were removed from the reactor, however, they were black in appearance. TG-DTA of these samples indicated that only about 0.4 to 1 wt% "non-graphitic" or "soft" coke (coke that can be desorbed in nitrogen at 500°C) and no "graphitic" or "hard" coke (coke that can only be removed by combustion in air at 500°C) was present. NH_4PW (Type B) was slightly active for n-butane cracking, converting 1.9% n-butane at 400°C (products of reaction included; 1.4 wt% iso-butane, 0.3 wt% propene, 0.1 wt% ethene and 0.1 wt% butenes), but the conversion was far less than that of ZSM-5 (19.7% conversion, major reaction products included; 14.2 wt% propane, 1.1 wt% propene, 1.5 wt% iso-butane, 1.9 wt% ethane and 0.4 wt% methane) at the same reaction conditions. Sand diluted AlPW and HPW (Section 2.1.2) were also inactive for n-butane cracking.

3.1.7 1-Butene isomerization activity

The 1-butene isomerisation results are shown in Table 3.5. Both the Type A and B salts achieved similar conversion levels but their initial product selectivities differed. The Type A salts produced almost exclusively double bond shift products whereas the Type B salts initially produced reaction products typical of cracking and skeletal isomerisation as well as double bond isomerization. As the reaction time increased the products became exclusively double bond isomerization products. No liquid products were collected in the catchpot during the butene isomerization experiments. This indicated that there was no oligomerization of butene occurring.

Table 3.5 1-Butene isomerization data

Catalyst	HPW		AlPW		KPW	
Time (min)	3	30	3	30	3	30
Product	mass%		mass%		mass%	
C_1	0.00	0.00	0.00	0.01	0.05	0.00
C_2	0.00	0.00	0.00	0.00	0.74	0.00
$C_2^=$	0.08	0.03	0.09	0.00	0.74	0.00
C_3	0.33	0.08	0.24	0.06	11.69	0.28
$C_3^=$	0.71	0.64	0.75	0.58	4.27	0.61
1-$C_4^=$	14.24	14.79	14.55	16.57	12.64	17.35
Cis-$C_4^=$	31.42	30.02	31.77	29.97	26.35	28.85
Trans-$C_4^=$	53.21	54.45	52.61	52.82	41.98	52.88
iso-$C_4^=$	0.00	0.00	0.00	0.00	2.03	0.00
Conversion	85.76	85.21	85.45	83.43	87.36	82.65
Selectivities						
Cis/Trans	0.59	0.55	0.60	0.57	0.63	0.55
DBS[1]	98.69	99.12	98.75	99.23	78.21	82.65
Cracking	1.31	0.88	1.26	0.77	19.47	1.12
SI	0.00	0.00	0.00	0.00	2.32	0.00

1. DBS = Double bond shift products (c-/t-2-butene)
2. SI = skeletal isomerization products (isobutene)

3.2 PROPENE OLIGOMERISATION OVER HPA CATALYSTS

Table 3.6 shows the activities of the pure HPW and its salts calcined at 325°C for propene oligomerisation. Conversion is defined as fractional conversion (mass%) of propene to liquid product retained in the catchpot at 20°C and the mass balances obtained for all the runs were better than 95%. The repeatability of the oligomerization runs was very good as shown in Figure 3.10. HPMo, HSiW and NH_4SiW had minimal activity when calcined at 325°C, whereas AlSiW was active when calcined at 325°C. HPW and its corresponding salts were the most active and the low surface area AlPW:nitrate(2) salt exhibited the highest activity. The performance of the HPW salts decreased in the following order (value in parentheses indicates surface area in m^2/g):

AlPW:nitrate ≃ (2)Al:ether(5) > CoPW ≃ AlPW:nitrate(12) ≃ AlPW:ether/water(9) > NH_4PW ≃ NiHPW ≃ NiPW > CuPW ≃ HPW > CePW ≃ FePW > KPW.

3.2.1 Effect of Surface area

As can be seen from Figure 3.10 it was apparent that the performance of the AlPW salts was inversely dependent on their surface areas. AlPW:nitrate(2) and AlPW:ether(5), which had surface areas of 2 and 5 m^2/g respectively, had similar performances. Recrystallizing AlPW:ether(5) in water increased the surface area but the oligomerisation performance more than halved. The oligomerization performance of the higher surface area AlPW:nitrate(12) salt was also almost half that of the lower surface area AlPW:nitrate(2) salt.

3.2.2 Effect of water in feed and steaming of AlPW:nitrate

Figure 3.11 illustrates that the moisture content of the feed (0.1 wt% H_2O) affected the oligomerisation performance of low surface area AlPW:nitrate. Under normal circumstances all oligomerisation runs were completed as indicated in Section 2.3.5, i.e. the feed was dried by passing over 3A molecular sieves. These were the so-called "dry feed" conditions. When "wet feed" (no molecular sieves present) was used the conversion was lower by more than half compared to "dry feed" conversion. Bypassing the molecular sieves, after steady state "dry feed" conversion had been

molecular sieves, after steady state "dry feed" conversion had been reached, and hence changing to "wet feed" conditions, resulted in a sudden increase in conversion followed by a steady deactivation.

Table 3.6 Propene oligomerization performances of HPW salts calcined at 325°C, Reactor temperature = 230°C, WHSV = 12 h^{-1}, pressure = 5 MPa.

Catalyst	Initial % Conversion[1]	1/2 life (h)[2]	Trend[3]	Run Time	SS[4] Conv.	wt% coke	H/S Coke[5]	C_{12}^+ wt%[6]
HPW	17	4	d	4	-	8	0.05	40
NH_4PW	22	-	n	6	21	9	0.15	44
KPW	11	3	d	5	-	7	0.08	55
CuPW	15	6	d	3	-	17	0.13	50
CoPW	28	-	n	6	22	17	0.13	40
NiPW	35	-	n	6	20	10	0.00	41
NiHPW	24	-	n	6	20	13	0.38	44
FePW	11	-	n	6	10	20	0.01	56
CePW	9	-	n	3	7	-	-	51
AlPW:nitrate(2)[7]	42	-	n	33	87	42	0.16	36
AlPW:nitrate(12)	35	-	n	6	40	30	0.30	41
AlPW:ether(5)	34	-	n	8	75	36	0.25	37
AlPW:ether/ water(9)	24	-	n	6	35	29	0.31	40
AlSiW	17	-	n	2	23	-	-	36
HSiW[8]	40		n	12	40	-	-	-

1. Conversion of propene to liquid product after 1 hour on stream.
2. Time to 1/2 maximum conversion, no value indicates no loss of activity during time on stream.
3. indicates whether catalyst is deactivating (d) or not (n).
4. SS = steady state conversion value.
5. H/S represent amounts of "hard" vs "soft" coke as determined by TG-DTA.
6. Determined from GC analysis of the liquid product.
7. Value in parentheses indicates surface area in m^2/g.
8. Calcined at 200°C.

The effect of steam calcining the low surface area AlPW:nitrate(2) at 200°C, 70 Torr water pressure and a steam flow rate of 100 ml/min for one hour after pretreating the catalyst at 325°C in nitrogen, was also studied. The performance of this catalyst, using "dry" feed, was between that of the "dry" and "wet" feed cases.

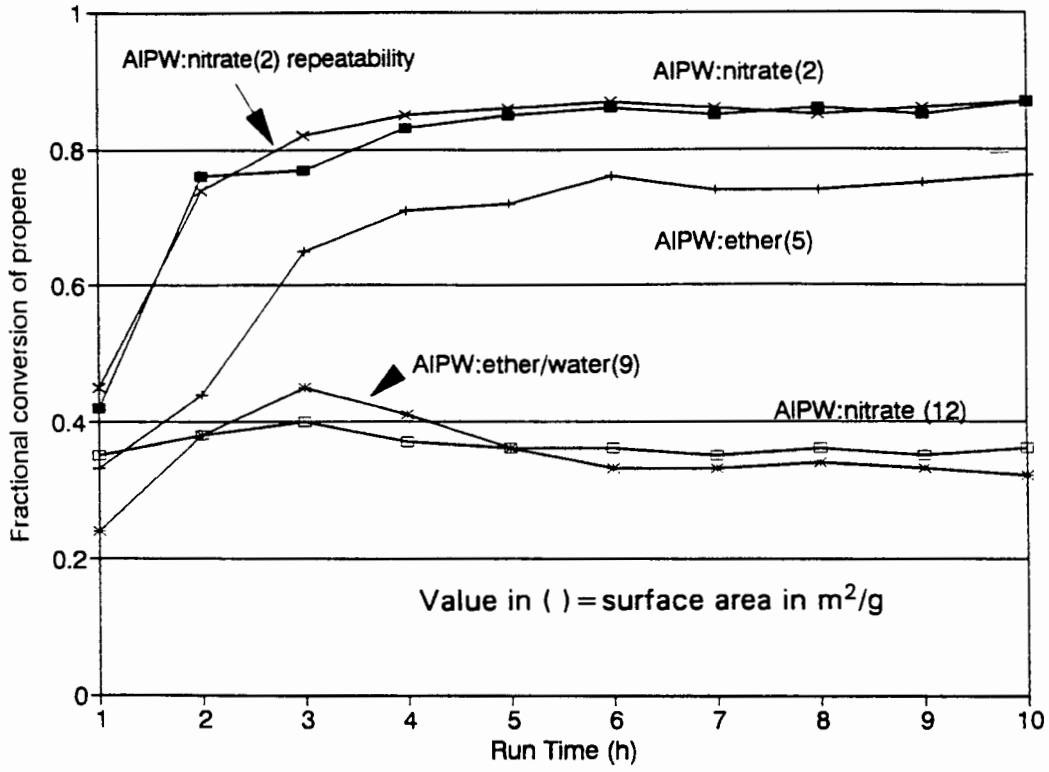

Figure 3.10 Effect of surface area on propene oligomerization performance of pure AlPW.

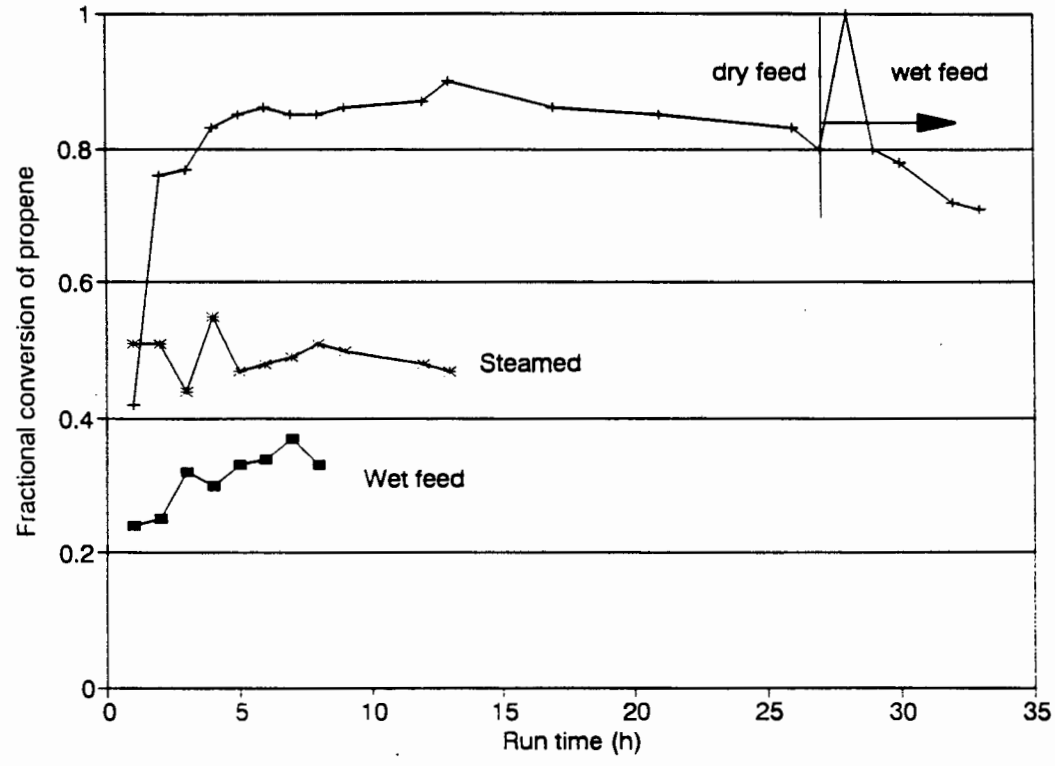

Figure 3.11 Effect of water in the feed and steaming of AlPW:nitrate(2) on propene oligomerization performance.

3.2.3 Effect of calcination temperature

Calcining HPW and AlPW:nitrate(2) in nitrogen at 200°C or 425°C resulted in similar oligomerization performances to those observed after calcination at 325°C. No conversion was observed when HSiW was calcined in nitrogen at 325°C or 425°C. However, the performance of HSiW, when calcined at 200°C, was far greater than that of HPW calcined in the range 200-425°C (Figure 3.16). Calcining AlPW:nitrate(2) in air, as opposed to nitrogen, at 325°C resulted in similar conversion levels.

3.2.4 Propene oligomerisation over catalysts diluted with sand

As propene oligomerisation is an exothermic reaction, acid washed quartz sand (150-212 μm) was added in a 10:1 ratio with the catalyst to dilute the bed and reduce the possibility of temperature runaways and hot spots. These are most likely to occur during the start-up phase. Sand dilution resulted in a dramatic increase in lifetime and conversion (i.e. increased performance) as can be seen from Figure 3.12. This illustrated the need maintain isothermal conditions within the reactor. The catalyst utilization values, or yield trends, for the sand diluted catalysts, however, followed the same performance trends for the pure powder results, *viz.* AlPW:nitrate(2) > CuPW > FePW.

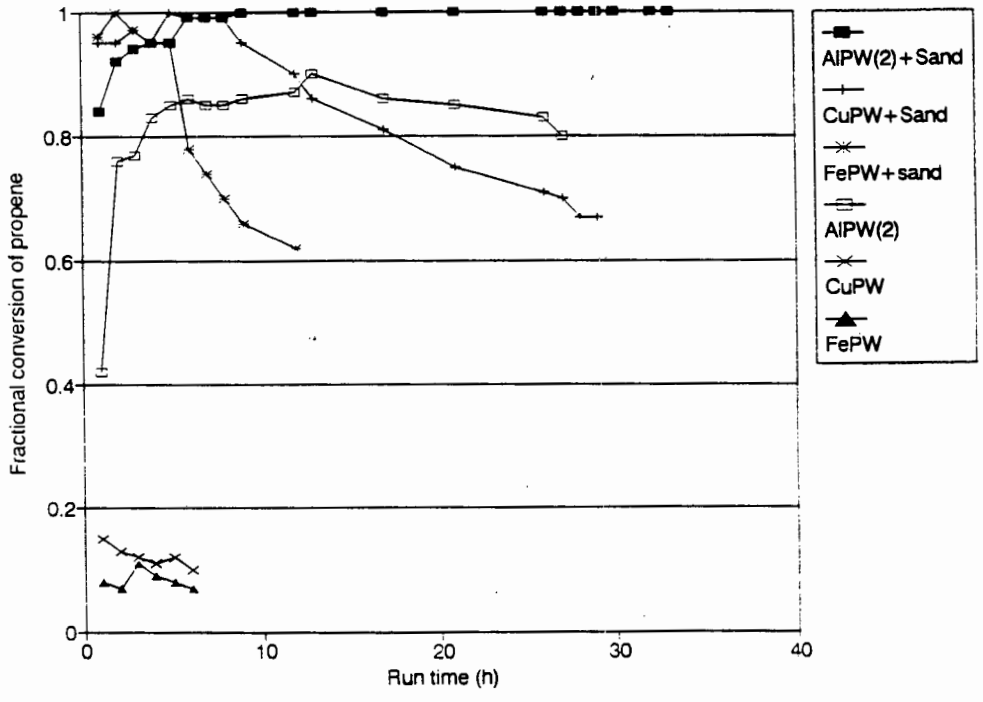

Figure 3.12 Effect of sand dilution on propene oligomerization performance

3.2.5 Coke Analysis

The TG-DTA spectra of ex-reactor AlPW:nitrate catalyst is shown in Figure 3.13 and the wt% coke data for all the HPA catalysts is presented in Table 3.6. This data showed that the mass% coke deposited on the catalysts increased with increasing run time. Although the majority of the coke was "soft" coke, the amount of both "soft" and "hard" coke increased with increasing run time (Section 2.2.7 for definition of "soft" and "hard" coke). In the interpretation of this data it was noted that further polymerization of the olefinic species adsorbed on the HPA may have occurred during the TG-DTA coke analysis procedure, especially given the strongly acidic nature of these catalysts. Sand diluted coke samples had significantly less "hard coke" that the undiluted cases.

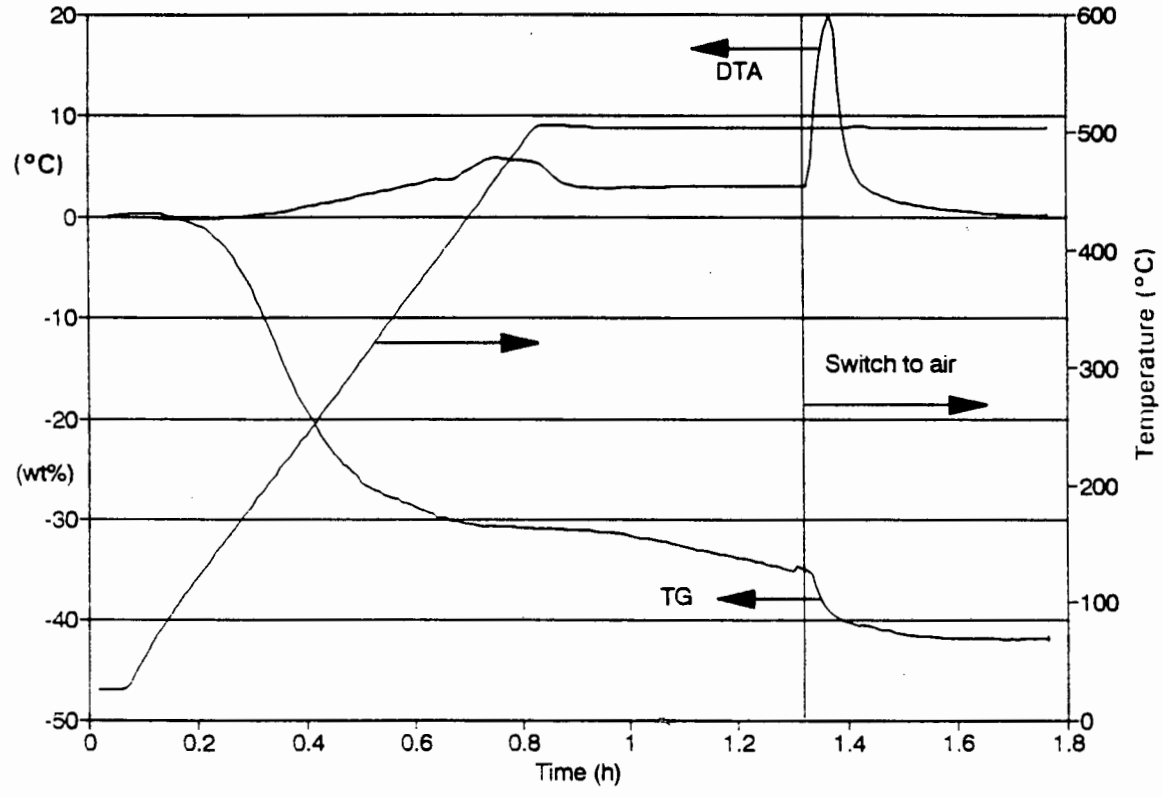

Figure 3.13 TG-DTA spectra of coked AlPW:nitrate

FT-IR showed that when the reactor was operated non-isothermally the Type A salts produced mainly Type I (olefinic) coke but also Type II (polyaromatic) coke (Section 2.2.7 for detailed definition of Type I and II coke). As the run time was increased or when the catalysts began to

deactivate, the amount of Type II coke present increased. In those cases where isothermal conditions were used Type I coke was formed exclusively and only after long run times or when the catalyst deactivated was Type II coke formed. The Type B salts produced both Type I and II coke irrespective of the run time.

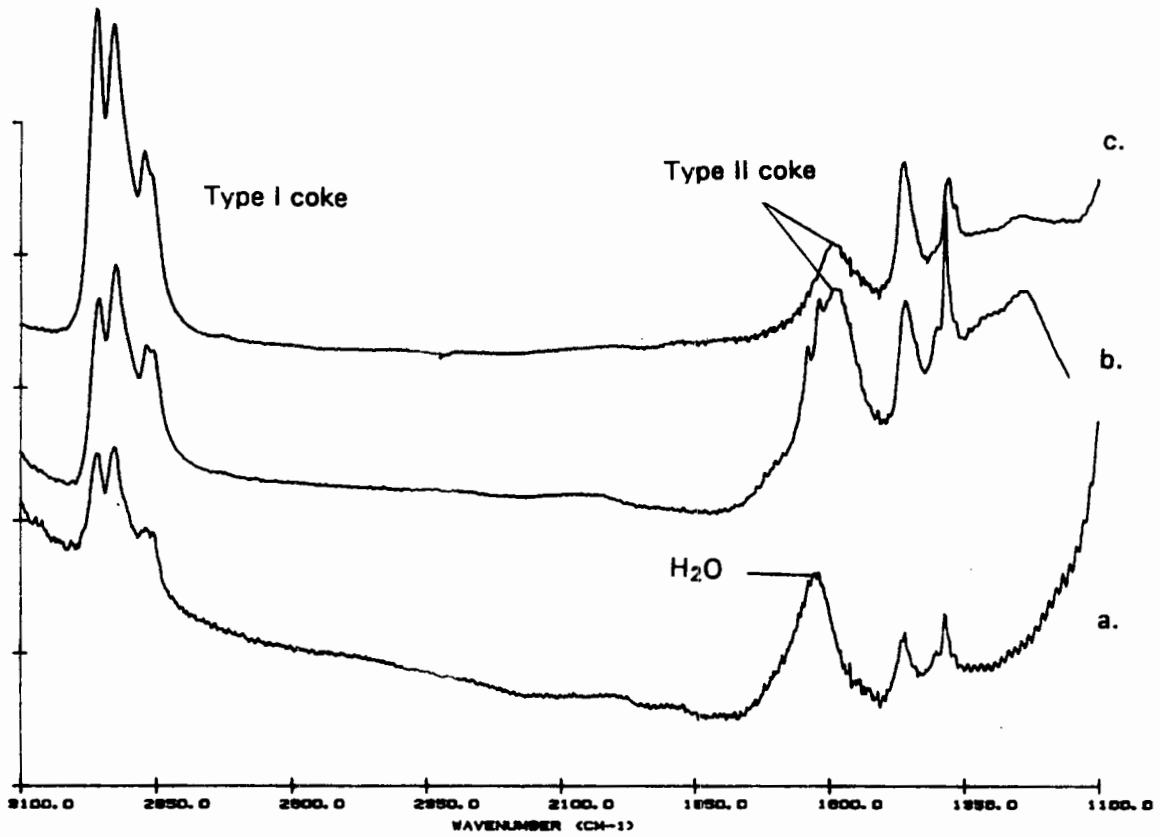

Figure 3.14 FT-IR spectra of a. coked AlPW:nitrate (isothermal 10 h), b. AlPW:nitrate (non-isothermal) and c. AlPW:nitrate (isothermal 150 h)

3.2.6 Supported HPA

3.2.6.1 Effect of α-alumina Support

The effect of supporting HPW and HSiW on α-alumina is illustrated in Figure 3.15. HPW and HSiW supported on α-alumina (25 wt% HPA) had higher conversions and lifetimes compared to their pure acid forms. Supported HSiW was more active than HPW on α-alumina after 3 hours on stream. However, if the catalysts were stored for some time (e.g. 3 months) and then tested again the performance of supported HPW was significantly lower than when the catalyst was freshly prepared. Supported HSiW was

not affected by storage time as much as HPW. This type of loss of performance through ageing has previously been reported for HPAs supported on α-alumina [Izumi *et al.*, 1983].

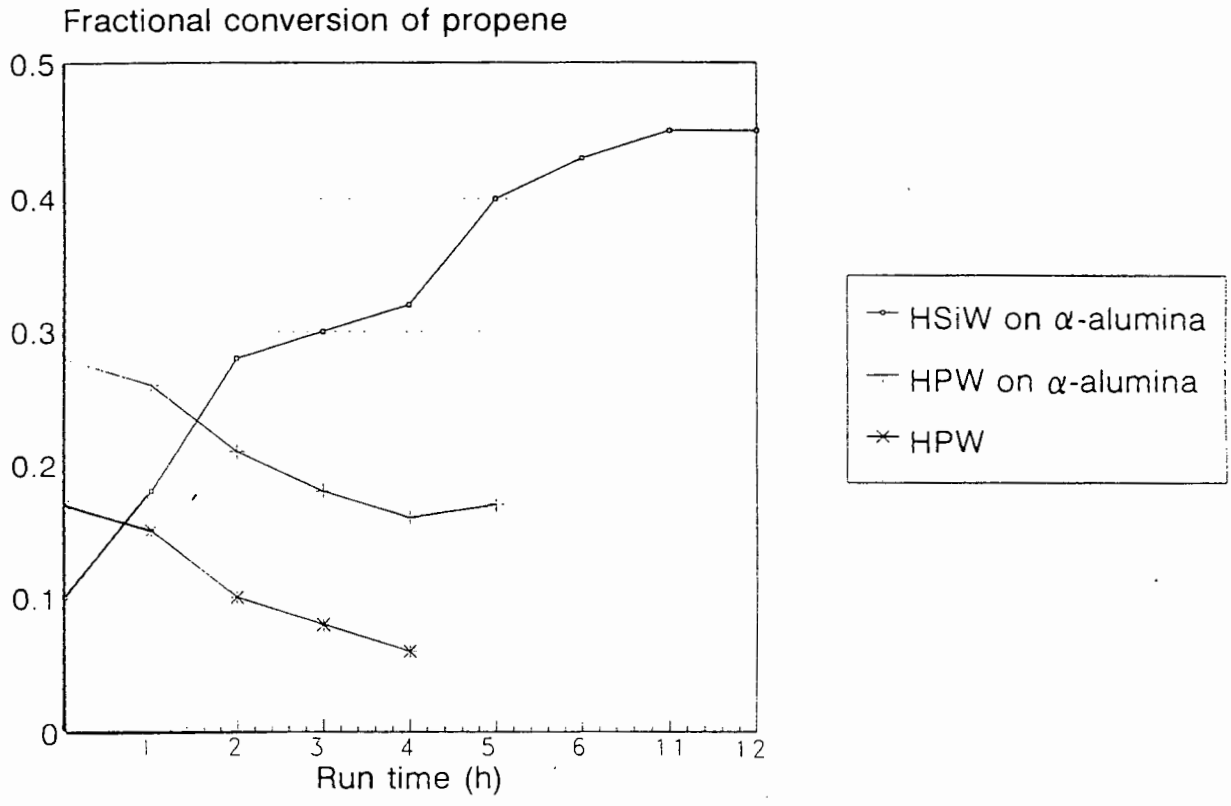

Figure 3.15 Effect of α-alumina support on propene oligomerizing performance

Supporting AlPW:nitrate(2) on α-alumina reduced its oligomerization performance.

3.2.6.2 Effect of SiW support

HSiW supported on silico-tungsten, prepared according to the procedure of Ratnasamy and Sivasanker (1989), resulted in the conversion remaining constant at the initial level, whereas unsupported HSiW deactivated to a lower level before achieving steady state conversion (Figure 3.16).

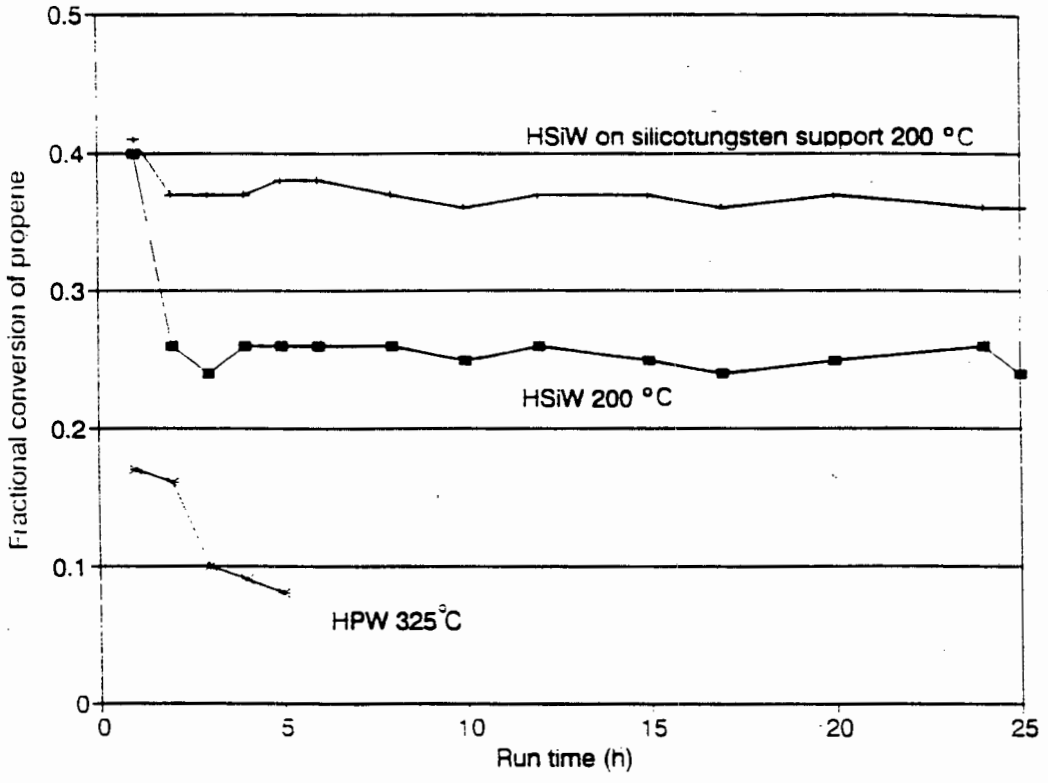

Figure 3.16 Effect of SiW support on oligomerization performance of HSiW

3.2.7 Liquid product selectivity and cetane number analysis

Liquid product selectivity

Table 3.7 presents the GC analysis of the liquid products obtained from propene oligomerization. As selectivities can only be properly compared at similar conversion levels only limited conclusions can be made about possible shape selective effects over these different heteropoly acids. This was especially the case for this study as not only are the conversions quite dissimilar but some of the products of oligomerisation do not condense out at 20°C and would thus exit in the vapour phase (up to 15 wt% of C_6 was at times present in the vapour phase). Thus the salts which had very low conversion levels appeared to have liquid products with relatively more C_{12}^-, whereas, in actual fact, a large proportion of the lighter products exited in the vapour phase. From Figure 3.17 it can be seen that the actual yield of C_{12}^- is a function of conversion and not the type of countercation. In all cases the trimer was the dominant oligomer present in the liquid product. The sand diluted catalysts had similar product selectivities with C_{12}^+ liquid product fractions in the region of 36 to 38 wt%. Increasing the

reaction temperature from 230°C to 310°C reduced the amount of $C_{12}+$ for sand diluted AlPW with an accompanied increase in C_4-C_7 products being formed.

The HPAs supported on α-alumina had liquid products with lower $C_{12}+$ selectivity values compared to their respective unsupported pure acids, but the yield of $C_{12}+$ is greater since they are more active than unsupported HPAs. For HSiW on a silico-tungsten support, however, the C_{12}^+ selectivity was similar to that of HSiW even though their respective conversions were dissimilar.

Cetane number

Cetane numbers were calculated using Gautier's correlation (Appendix V). Table 3.7 lists the cetane numbers of the whole liquid product fraction. The cetane number error margin has been estimated to be ±1.5 cetane units. AlPW:nitrate(2) liquid product fractionated at 180°C yielded a slightly higher cetane number (41) than that of the cetane number of whole liquid product fraction (37) and thus the cetane numbers of the distillate fractions of the liquid products are likely to be about 4 numbers higher than the values given in Table 3.7. As can be seen from Appendix V, which shows the GC spectra of fractionated versus unfractionated product, the liquid product contains no aromatics.

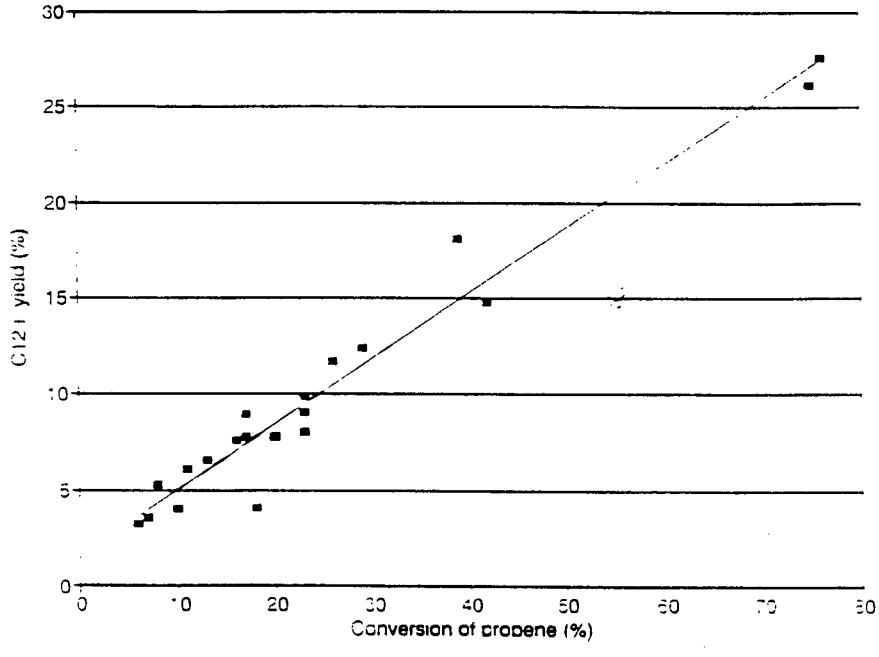

Figure 3.17 C_{12}^+ yield vs conversion to liquid product

Table 3.7 Liquid product selectivities1 (%) and cetane numbers of total hydrogenated product (Reaction conditions T=230°C, WHSV=12h^{-1}).

Catalyst	Dimer C_6-C_8	Trimer C_9-C_{11}	Tetramer C_{12}-C_{14}	Pentamer C_{15}-C_{17}	Hexamer C_{18}-C_{20}	Heptamer+ C_{21}+	Cetane no.[2]	Conv.
HPW	7.2	25.0	24.2	22.1	12.7	8.8	26.0	8
NH_4PW	19.2	36.7	21.6	13.1	5.6	3.8	22.0	23
KPW	10.5	34.5	27.1	15.7	7.6	4.6	-	6
NiPW	19.6	39.9	21.2	11.1	5.1	8.2	-	20
NiHPW	-	-		-	-	-	-	-
CoPW	19.5	39.9	22.8	11.0	4.5	2.4	-	23
CuPW	9.5	38.1	24.5	15.4	7.7	4.8	-	13
FePW	8.7	34.4	25.1	16.3	9.1	6.4	38.0	11
CePW	9.0	39.7	24.2	14.2	7.3	5.5	-	7
AlPW:/ nitrate	25.9	37.8	19.5	9.8	4.3	2.8	38.4	75
AlPW:/ ether	21.8	40.6	19.9	10.0	4.5	3.2	36.0	76
ALPW:/ ether/water	-	-	-	-	-	-	-	-
HSiW	19.0	34.3	21.1	13.5	6.9	5.2	31.6	26
AlSiW	25.4	38.6	17.8	10.7	4.4	3.0	-	23
HPW/ α-Alimina	12.2	40.6	22.7	12.7	7.4	4.3	35.8	17
HSiW/ α-Alumina	17.4	46.3	22.1	9.1	3.3	1.8	39.9	42
HSiW/ SiW	17.4	34.6	22.4	14.1	6.8	4.6	37.0	39
AlPW+ sand	11.9	42.7	25.0	13.3	2.9	0.2	37.0	100
CuPW+ sand	10.0	39.3	23.4	12.6	5.4	2.2	32.6	100
FePW+ sand	14.0	40.0	24.6	13.0	2.3	0.1	36.6	100
AlPW+ Sand[3]	20.5	52.9	21.2	5.3	0.1	0.0	-	100
AlPW+ Sand[4]	25.7	57.2	13.9	3.0	0.2	0.0	-	100
AlPW+ Sand[5]	42.6	51.1	4.1	1.9	0.3	0.0	-	100

1. From GC analysis of liquid product
2. Cetane number calculated from H-NMR data using Gautier's correlation (Appendix V)
3. 250°C
4. 280°C
5. 310°C
6. Conversion after 3 hours on stream

3.3 SAPO PHYSICOCHEMICAL CHARACTERIZATION

3.3.1 Catalyst composition and morphology

Chemical composition

The results of chemical analysis are given in Table 3.8 and for all the sieves shown the (Al+Me) to (P+Si) molar ratios were greater than 1. This was higher than the expected value, *viz.* 1, for the substitution mechanisms suggested by Flanigen *et al.* (1986). Even if Si substituted for an Al:P pair the ratio would have decreased and not increased. The high ratios, especially for CoS11 and FeS11, suggested that there was extra-framework aluminium and/or metal present. The amount of silicon present for the SAPO-11 type sieves of this study was significantly lower than those values given by the Union Carbide Patent [Lok *et al.*, 1984b]. Since the amount of Si was less than 2 wt% it was assumed that Si had substituted for P only [Tapp *et al.*, 1988a]. Metal contents for the MeAPSO-11 sieves were all less than 5.5 wt% and decreased in the order FeS11 > CoS11 > MnS11 > NiS11. The amounts of Fe, Co and Mn corresponded well to those given in their respective examples in the patent [Lok *et al.*, 1985].

Table 3.8a. Chemical analysis data of as-synthesized sieves, molar ratios

Catalyst	Al	P	Si	Me	LOI[1]	Al/P	(Al+Me)/(Si+P)
Patent[2]	1.0	0.90	0.13	0.00	9.4	1.11	0.97
S11(1)	1.0	0.82	0.01	0.00	9.0	1.22	1.21
S11(1)[3]	1.0	0.83	0.01	0.00	9.0	1.21	1.19
S11(3)	1.0	0.80	0.01	0.00	10.0	1.25	1.24
S11(4)	1.0	0.73	0.01	0.00	12.8	1.36	1.35
NiS11	1.0	0.85	0.03	0.08	11.0	1.18	1.23
MnS11	1.0	0.91	0.02	0.09	11.0	1.10	1.18
CoS11	1.0	0.77	0.03	0.09	16.0	1.39	1.36
FeS11	1.0	0.73	0.01	0.14	14.2	1.36	1.52

1. LOI: mass loss on ignition at 600°C in air (wt%)
2. e.g. 15 from Lok *et al.* (1984b)
2. Reproducibility

Table 3.8.b. Chemical analysis data of as-synthesized sieves, mass %

Catalyst	Al	P	Si	Me
Patent	19.5	20.2	2.60	0.00
S11(1)	20.9	19.7	0.40	0.00
S11(1)	21.2	20.2	0.20	0.00
S11(3)	22.1	20.2	0.40	0.00
S11(4)	21.5	18.1	0.40	0.00
NiS11	19.1	18.5	0.60	3.20
MnS11	18.7	19.5	0.30	3.36
CoS11	19.8	17.6	0.60	3.81
FeS11	19.5	16.4	0.30	5.47

Ion-exchange and acid washing

Ammonium ion-exchanging (IX) the calcined MeAPSO-11s in 2M ammonium nitrate solution at 80°C succeeded in displacing *ca.* 30, 45 and 50 wt% of the Ni, Co and Mn respectively from NiS11DB, CoS11DB and MnS11DB, but no Fe could be exchanged from FeS11DB. In all instances the pH of the ion-exchange medium dropped from 4.5 to 3.5 which indicated phosphorous extraction, i.e. the formation of phosphoric acid in solution. Tests for phosphate in the ion-exchange medium proved positive and chemical analysis of the sieves after ion-exchange showed that 7% and 8% of the P was removed from CoS11 and NiS11(2) respectively. In all cases there was less than 1 percent removal of aluminium from the molecular sieves as a result of this procedure. Acid washing in nitric acid removed 8% of the aluminium from S11(3).

Colour changes

Table 3.9 lists the colours of the as-synthesized, air calcined, ion-exchanged and reduced samples (ex-TPR). The brilliant/intense blue colour of CoS11syn has been attributed to tetrahedrally coordinated Co^{2+} [Cotton and Wilkinson, 1989]. All of the as-synthesized MeAPSO-11s, except NiS11(2)syn, changed colour after air calcination and subsequent hydration at room temperature (*ca.* 20 Torr H_2O). CoS11DB reverted to its as-synthesized colour after ion-exchange, hexane adsorption and NH_3-TPD. However, after ion-exchange, the colour remained that of the as-synthesized material (blue), even after the ion-exchanged sample was once again calcined in air. The colour change for CoAPSO-n sieves after air calcination

has been attributed to redox mechanisms (Section 1.4.4) and this will be discussed further in Section 4.3.

Table 3.9 Colour changes of AEL sieves after various treatments

Catalyst	as-synthesized	DB calcined	Ion-Exchanged	Hexane Adsorption	NH_3-TPD	TPR
S11(3)	white	white	white	white	white	white
NiS11(2)	green	green	green	green	green	grey
MnS11	white	pink	pink	pink	pink	white
CoS11	blue	green	blue	blue	blue	grey
FeS11	green	brown	brown	brown	brown	grey

FeS11DB, MnS11DB and NiS11DB did not undergo colour changes after ion-exchange or NH_3-TPD although MnS11DB did revert back to its as-synthesized colour after TPR to 1000°C. It was not surprising that the ex-TPR samples of CoS11DB, FeS11DB and NiS11(2)DB were grey/black since TPR showed reduction had occurred and it would be expected therefore that the ex-TPR samples would have a colour similar to that of their respective metal/metal oxides species.

3.3.2 Catalyst Structure and morphology

Crystallinity (XRD)

According to XRD (Figures 3.18 a, b, c) of the as-synthesized sieves, no crystalline phases were present other than those of the AEL structure type [Bennet *et al.*, 1987; Van Ballmoos 1990]. S11(3)syn was the most crystalline of the sieves and metal incorporation into the synthesis gel reduced the crystallinity of the sieves (Table 3.12). Higher synthesis temperatures, shorter crystallization times, higher silicon gel concentrations and lower water concentrations resulted in a SAPO-11 product that was less crystalline compared to S11(3)syn. After calcination and subsequent hydration (*ca.* 20 Torr H_2O), the crystallinities of all the sieves were approximately 25% lower than their as-synthesized counterparts (Figure 3.18 d.). The reduced crystallinities were also coupled with shifts in the 2θ values of some of the peaks (e.g. 21.1° → 22°). Modifications such as acid washing, steaming, ion-exchanging and impregnating with Co or Ni did not affect the crystallinities of the sieves compared to their "deep-bed" calcined

counterparts. However, after ion-exchange, CoS11-IX, MnS11-IX and FeS11-IX had similar 2θ peak positions (Irna2 or Icmm) to their as-synthesized samples, whereas NiS11(2)-IX and S11(3)-IX had the same 2θ as their "deep-bed" calcined forms. The XRD spectra of all the SAPO-n sieves are shown in Appendix VIII.

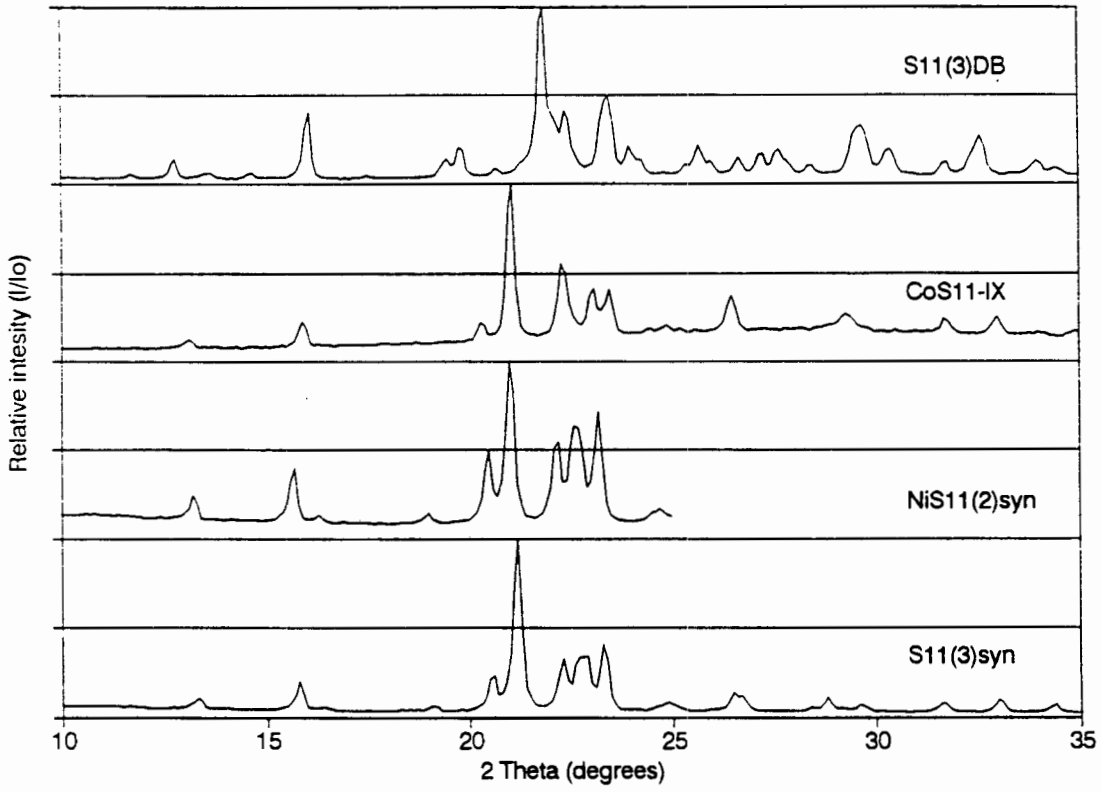

Figure 3.18. a. XRD spectra of S11(3)syn, b. NiS11, c. CoS11-IX and d. S11(3)DB

FT-IR analysis

FT-IR of the as-synthesized sieves were similar to those reported by Szostak (1992), and other workers [Tapp *et al.*, 1990; Burkhardt *et al.*, 1992]. FT-IR spectra of the mid infra-red regions (400-1300 cm^{-1}) of S11(3)(syn), S11(3)DB, NiS11(2)(syn) and CoS11-IX are shown in Figure 3.19. Their absorption bands and those of the other sieves are listed in Table 3.10. Examination of this region showed all the as-synthesized samples to have similar features with a large absorption between 1000-1300 cm^{-1} corresponding to the T-O(internal) asymmetric stretching frequency [Flanigen, 1976]. The bands in the 540-640 cm^{-1} region are assigned to those of the double-ring type vibrations (Section 1.4.1). Other bands in the

spectrum at 460-470 cm^{-1} and 700-715 cm^{-1} were assigned as the T-O bending and symmetric T-O stretching frequencies respectively. The bands most affected by metal addition to the synthesis gel were the T-O(internal) bending (*ca.* 470 cm^{-1}) and T-O(internal) asymmetric stretching frequencies (*ca.* 714 and 1117 cm^{-1}).

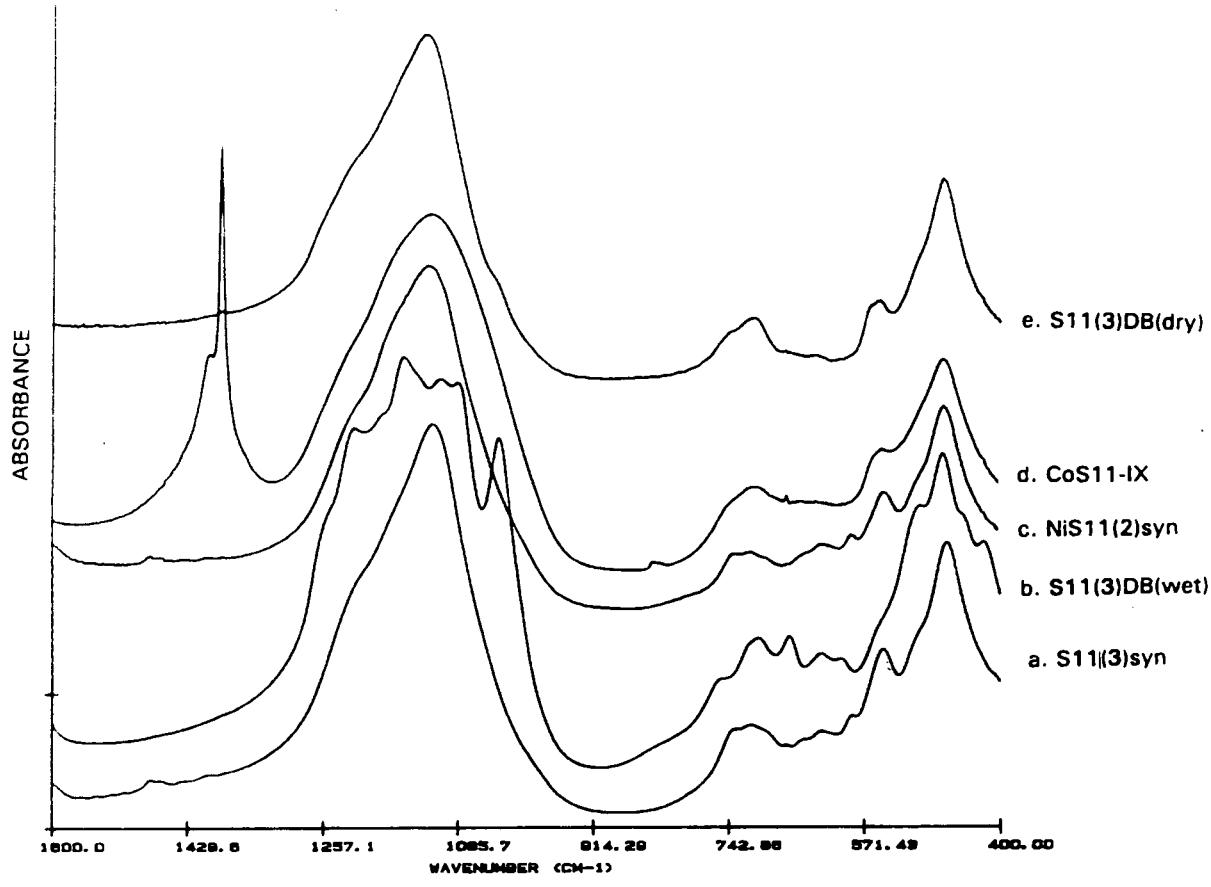

Figure 3.19 FT-IR spectra of a. S11(3)syn, b. S11(3)DB(wet), c. NiS11(2)syn, d. CoS11-IX and e. S11(3)DB(dry)

After calcination and subsequent hydration there were several new distinct features in the T-O asymmetric stretching region, particularly the formation of a strong absorption band at 1033 cm^{-1}. At first it was thought that these absorptions correspond to individual T-O asymmetric stretching frequencies, such as Al-(O-P-O)-Al. Tapp *et al.* (1990), however, have shown that these features were in fact due to the presence of physisorbed water. On heating the present samples to 150°C and removing the physisorbed water the multiple T-O features disappeared and the spectra resembled that of the as-synthesized sieve. This indicates that these multiple features were indeed due to physisorbed water interactions with the T-O tetrahedra.

FT-IR after ion-exchange confirmed the presence of new strong absorptions for FeS11-IX, MnS11-IX and CoS11-IX at 1385, 1399, 3020 and 3141 cm^{-1}. These first two absorptions occurred at lower wave numbers than those expected for NH_4^+ ions in ion-exchange positions (1460, 2860, 3000, 3200 cm^{-1}) and were probably those of the NO_3^- group attached to either metals, i.e. $Co(NO_3)_2$ or to the $SAPO^+$ framework [Ward, 1976; Rabo, 1976]. These NO_3^- features were very small for NiS11(2)-IX and S11(3)-IX, which also showed small features at 1459 cm^{-1} which are typical of NH_4^+ ions associated with Brönsted acid sites [Ward, 1976].

Table 3.10. FT-IR data of SAPO-11 and MeAPSO-11 sieves

Catalyst	δT-O	4DR[4]	6DR	ν_{sym}T-O	ν_{as}T-O	ν_{as}T-O	ν_{as}T-O	
As-synthesized								
S11(1)	468	547	sh[1]	626	712	1119		
S11(3)	466	546	sh	624	714	1117		
S11(4)	467	544	585	625	712	1116		
S11(5)	470	545	585	625	712	1114		
S11(6)	471	535	584	627	713	1128		
S11(7)	471	539	584	625	715	1125		
NiS11(2)	470	545	sh	623	715	1122		
MnS11	468	545	sh	621	709	1117		
CoS11	465	544	sh	625	710	1112		
FeS11	467	545	sh	623	709	1115		
AlPO-11	474	551	sh	621	704	1122		
AlPO-11*	462	545	585	620	705	-		
SAPO-11*	470	550	590	-	710	1125		
"Deep-bed" calcined								
AlPO-11*	470	498	590	620	660	695,712		
S11(3)w[2]	420,471	500,sh	600	624	665	704,750	1033	1085
S11(3)d[3]	469	550	-	631,641	650	710	1124	
NiS11(2)w	420,474	500,sh	599	626	665	704	1034	1085
NiS11(2)IXd	421,474	549	597	632	647,663	708	1037	sh
MnS11w								
CoS11w	422,471	-	600	621	664	703	1034	1106
CoIXd	471	549	-	631	m	712	1125	
FeS11d	470	550	-	630	654,671	710	1122	
FeIX	471	548	618	629	670	709	1121	

1. sh-shoulder peak
2. w-wet sample (20 Torr H_2O)
3. d-dry sample, 100°C in air
*. From Szostak (1992)
4. 4DR, 6DR - double ring vibrations

The multiple absorption band features in the T-O asymmetric region for CoS11DB, MnS11DB and FeS11DB (samples all wet) were nonexistent after ion-exchange whereas those of NiS11(2) and S11(3) were still present. After NH_3-TPD the multiple features of the "deep-bed" calcined catalysts also absent. FT-IR spectra of all the SAPO-n catalysts are shown in Appendix VII.

Fe coordination by Mössbauer Spectroscopy

Room temperature Mössbauer spectra of FeS11(syn) and FeS11(cal) are shown in Figure 3.20. The as-synthesized sample consisted of one Fe^{2+} and two different Fe^{3+} species. After calcination in air at 500°C there were only two species present, both Fe^{3+}. The relative amounts of each species and possible assignments are given in Table 3.11. The Mössbauer data was comparable to that published for the molecular sieve FAPO-5, which also showed that upon calcination all the Fe^{2+} species were oxidized to Fe^{3+} [Schubert *et al.*, 1989].

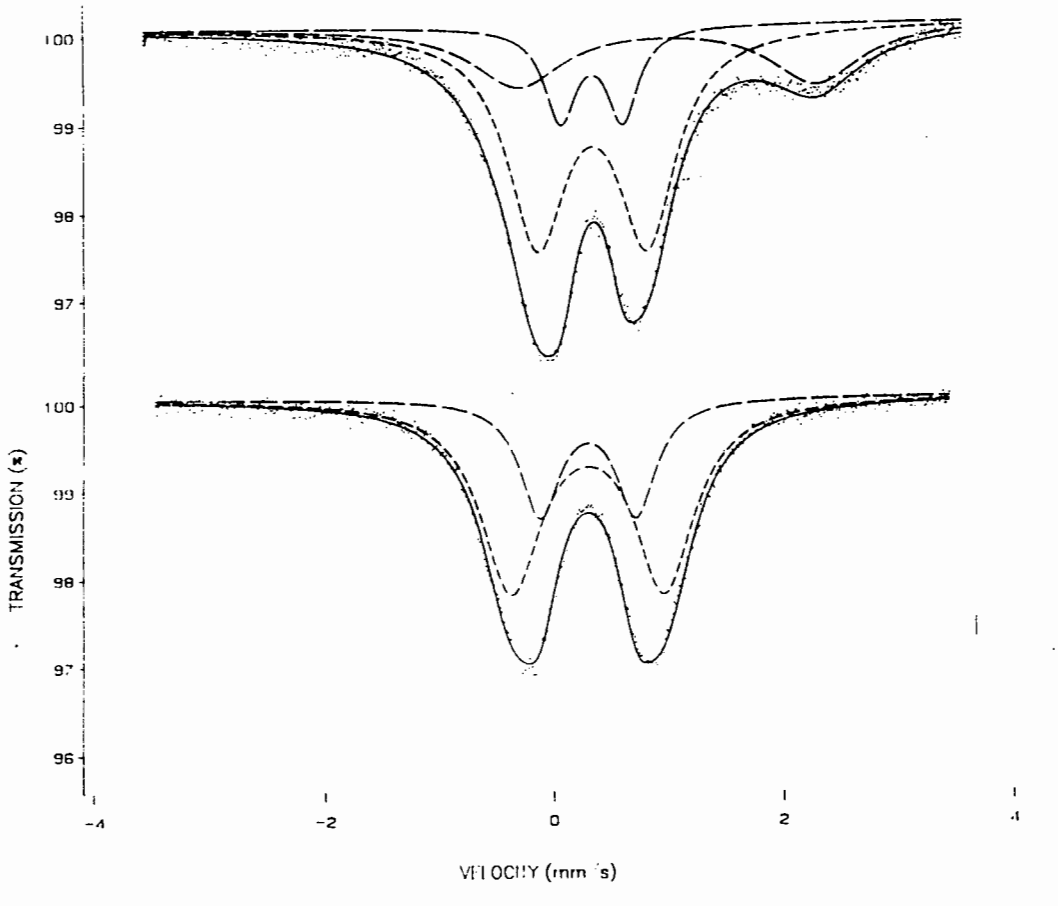

Figure 3.20 Room temperature Mössbauer spectra of a. FeS11(syn) b. FeS11DB.

Table 3.11 Room temperature Mössbauer spectroscopy data

FeS11(syn)			
I.S.[1] (mm/s)	QS[2] (mm)	Area%	Possible assignment
0.44	0.48	59	Fe^{3+}(octa)[3]phosphate
0.44	0.28	26	Fe^{3+} (FeO/FeOH)(octa)
1.10	1.31	14	Fe^{2+} (octa)
FeS11DB (500°C in Air)			
0.39	0.67	55	Fe^{3+} (FeO/FeOH)(octa)
0.39	0.42	45	Fe^{3+}(octa)Phosphate

1. I.S.-Isomer shift, relative to α-Fe
2. QS.-Quadrupole splitting
3. (octa)-octahedral coordination

Catalyst morphology

S11(1)syn, S11(2)syn, S11(3)syn (Figure 3.21a), S11(4)syn and S11(5)syn consisted of spherical (rose bud shaped) agglomerates of rod-like and plate-like crystallites. S11(6)syn (Figure 3.21b) consisted of S11(3)syn type spherical agglomerates, except that the rod-like crystals were not as well defined and there were also *ca.* 5 μm long single rectangular (coffin-like) crystallites present. S11(7)syn (Figure 3.21c) crystallites had a similar morphology to S11(6) crystallites except there were no large single crystallites. CoS11syn (Figure 3.21d) showed three different features, large intertwined rectangular crystallites *ca.* 5-10 μm long, agglomerates of platelets and separate amorphous type material. All the sieves showed no morphological changes after calcination in air at 500°C. The crystallites of FeS11 and MnS11 were similar to those of CoS11 but there was no separate amorphous type material present for MnS11. After ammonium nitrate ion-exchange of CoS11 (Figure 3.21e), MnS11 and FeS11 the previously clean surfaces of the platelets and agglomerates were covered with an amorphous type material. NiS11(2) had a morphology similar to S11(7) and NiS11(2)-IX showed little change from its parent type material.

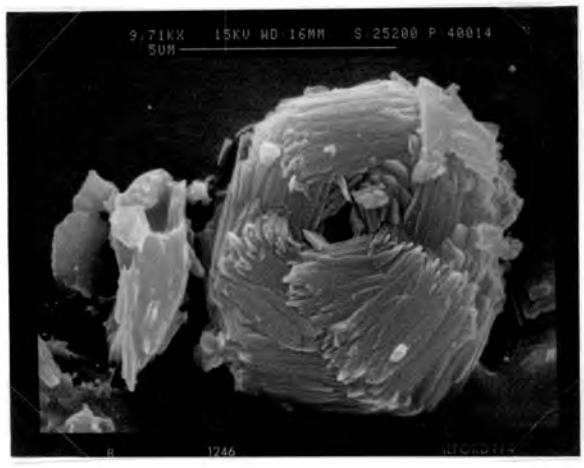

a.

b.

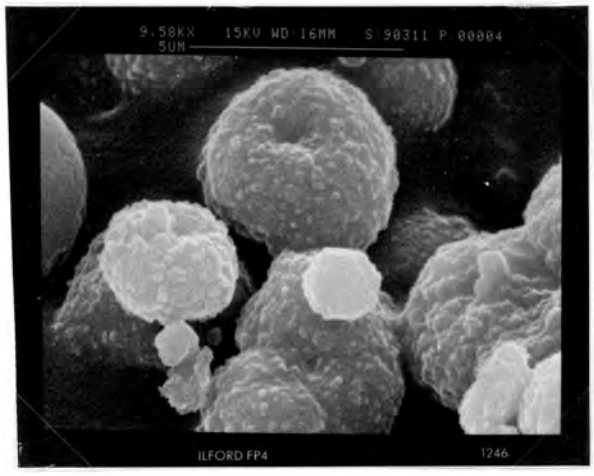

c.

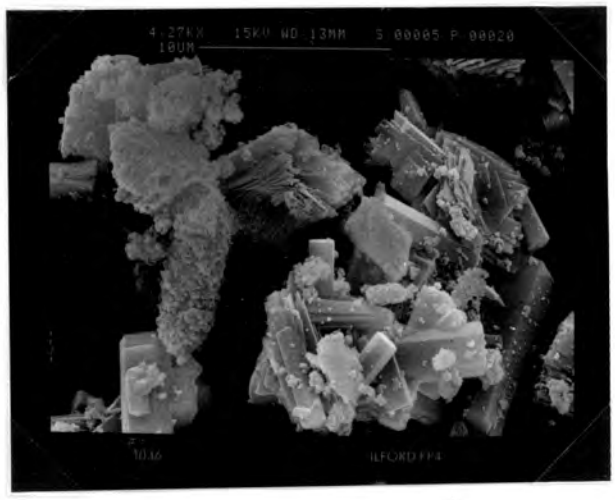

d.

e.

Figure 3.21 Electron micrographs of a. S11(3), b. S11(6), c. S11(7), d. CoS11 and e. CoS11-IX.

3.3.3 Surface area, pore volume and TG-DTA

N_2-BET surface areas, n-hexane and water adsorptions values are given in Table 3.12. Incorporation of metals into the SAPO-11 synthesis gel decreased the surface area and the hexane adsorption capacity of the resulting sieves compared to S11(3). Higher synthesis temperatures, shorter synthesis times, high Si concentrations in the gel, low water gel concentrations, metal impregnation, acid washing, silanizing, steaming and ion-exchanging all decreased the hexane adsorption capacity which indicated pore blockage or constriction by extra-framework species.

Table 3.12 Surface Area, Micropore Volume, Hexane Adsorption, Water adsorption and % crystallinity data

Catalyst	SA[1] (m^2/g)	Micropore volume (cm^3/g)	Hexane[2] wt%	H_2O%[3] wt%	*m*-xylene[4] wt%	crystallinity[5] %
S11(1)	212	-	4.0	7.0	-	100
S11(2)	202	0.0685	-	-	-	94
S11(3)	236	0.0816	4.5	10.4	3.0	100
S11(3)DB*	-	-	-	-	-	72
MS(6)-S11(3)	-	-	3.5	-	-	99
S11(4)	-	-	2.9	-	-	72
S11(5)	-	-	3.0	-	-	75
S11(6)	-	-	3.1	-	-	79
S11(7)	-	-	3.0	-	-	74
Acid-S11(3)	168	0.0559	3.0	11.0	-	99
Silan-S11(3)	-	-	2.1	-	-	98
NiS11(2)	200	0.0567	3.8	11.0	2.0	72
Ni(imp)S11(3)	70	0.0142	1.9	-	-	100
NiS11(2)-IX	137	0.0407	2.5	-	-	64
MnS11	193	0.0634	3.0	9.5	1.8	70
MnS11-IX	-	-	2.0	-	-	72
CoS11	128	0.0274	2.8	8.4	-	60
CoS11-IX	-	-	2.5	-	-	61
Co(imp)S11(3)	89	0.0149	-	-	-	100
FeS11	120	0.0306	2.8	12.0	2.4	61
FeS11-IX	-	-	1.8	-	-	60

1. SA=surface area (m^2/g)
2. 55 Torr Hexane in 50 ml/min N_2, wt% adsorbed at 70°C
3. *ca.* 20 Torr H_2O, wt% adsorbed at 20°C
4. 7.5 Torr *m*-xylene in 50 ml/min N_2, adsorbed at 90°C
5. % crystallinity relative to S11(3)syn for as-synthesized sieves and S11(3)DB for DB calcined modified sieves. * % crystallinity relative to S11(3)syn

The water adsorption values were similar to those reported in the patents [Lok *et al.*, 1984b, 1985]. There was a linear correlation between the BET surface areas and hexane adsorptions as can be seen in Figure 3.22. The N_2-BET surface area for S11(3) was similar to that reported for $AlPO_4$-11 of 200 m^2/g by Tapp *et al.* (1988b).

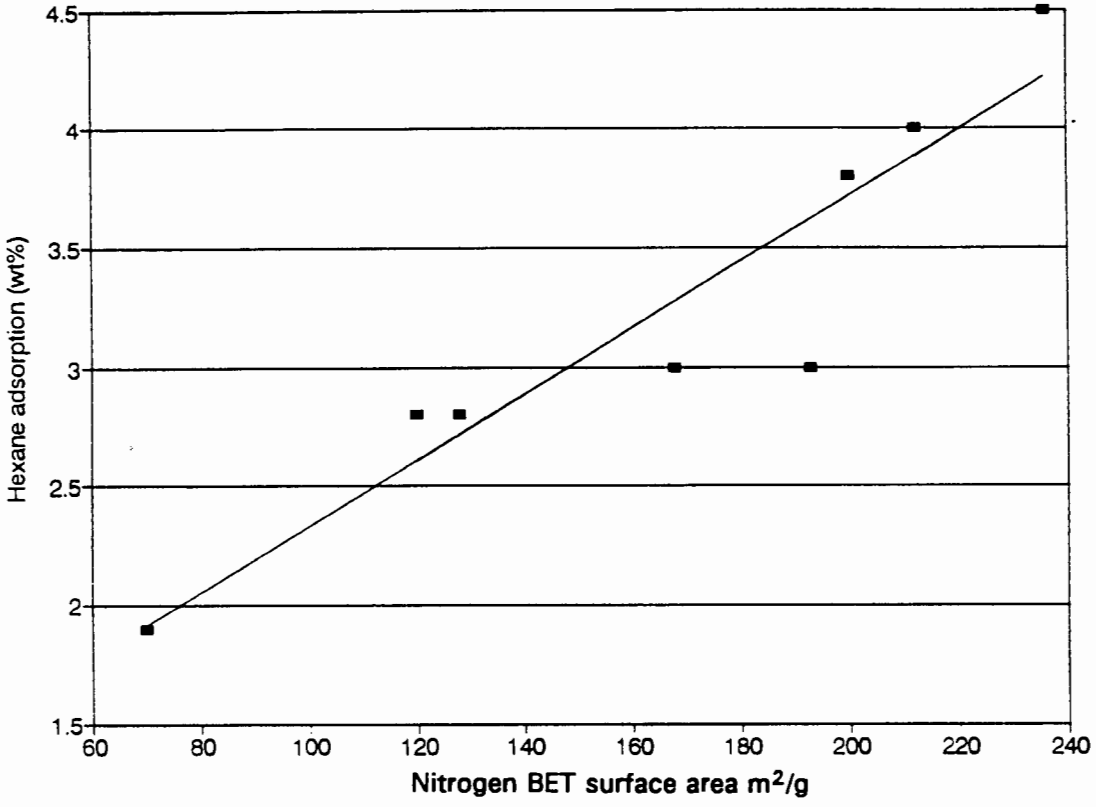

Figure 3.22 BET surface areas versus hexane adsorptions

Template removal

Mass loss on ignition (LOI, 600°C in air) of as-synthesized catalysts (Table 3.8), decreased in the order CoS11syn > FeS11syn > MnS11syn, NiS11syn > S11(3)syn and these values are similar to those given in the patents [Lok *et al.*, 1984b,1985]. TG-DTA data of the as-synthesized MeAPSO's is presented in Table 3.13 and the TG-DTA of S11(3)syn is shown in Figure 3.23. All the sieves experienced two endothermic mass losses and a single exothermic mass loss, except for AlPO-11 for which there was no exothermic mass loss. Endo(1), *ca.* 100°C, and Endo(2), *ca.* 270-290°C, were most probably associated with the desorption of zeolitic

water and intact template respectively. Endo(2) for AlPO-11 occurred at significantly lower temperature than that for the other sieves. Exo(1), *ca.* 370-500°C, was most probably due to decomposition of the remaining template by a Hoffman type elimination reaction [Tapp *et al.*, 1985,1988a], to form ammonia and propene. The above assignments for the various endo- and exothermic losses were supported by the TPD-MS data which is presented in Table 3.13. The TPD-MS spectrum of S11(3)syn, NiS11(2)syn and CoS11syn are also shown in Figure 3.24. For all the as-synthesized sieves, zeolitic water began to desorb at *ca.* 100°C and was completely desorbed by 250°C. Desorption of the intact template began at *ca.* 200°C and was followed by desorption of the decomposition products (ammonia and propene) of the template at *ca.* 300°C. Decomposition was complete by 500°C. There was appreciably more template decomposition type products for CoS11syn, FeS11syn, MnS11syn compared to S11(3)syn. NiS11(2)syn, on the other hand, had significantly more intact template desorbing as opposed to decomposing. A total ion chromatogram TPD-MS of CoS11syn and S11(3)syn revealed that aromatic type products were also formed during template decomposition, a result also observed for FAPO-5 [Park and Chon, 1992].

Table 3.13. TG-DTA and TPD-MS data.

Catalyst	Endo (°C)	Endo (°C)	Exo (°C)	T1[1] (°C)	T2[2] (°C)	T3[3] (°C)	T4[4] (°C)	T5[5] (°C)
S11(3)	100	275	470	110	200	450	120	330
NiS11	100	280	380	130	220	375	170	300
MnS11	100	275	480	160	255	470	220	320
CoS11	100	275	500	155	230	450	205	320
FeS11	100	280	470	150	215	470	170	330
AlPO-11	120	230	-	-	-	-	-	-

1. Water
2. Intact template
3. Template decomposition peak maxima
4. Start of intact template desorption
5. Template decomposition

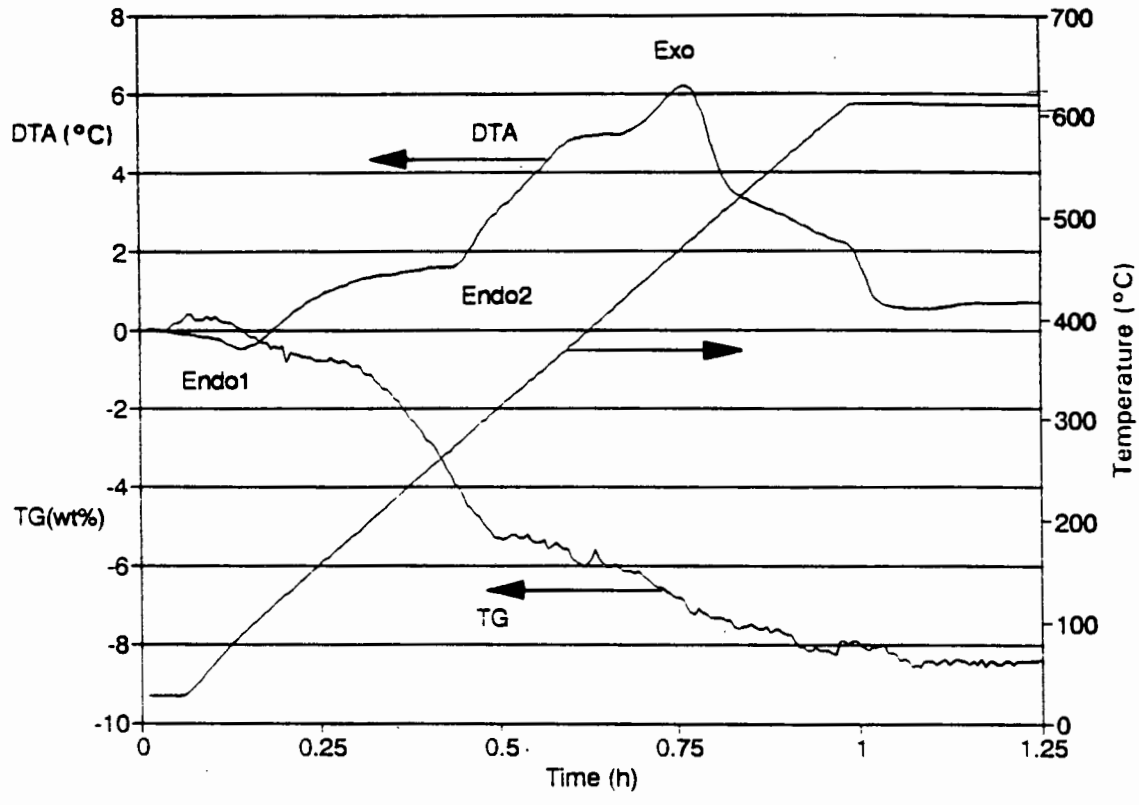

Figure 3.23 TG-DTA spectra of S11(3)syn in air

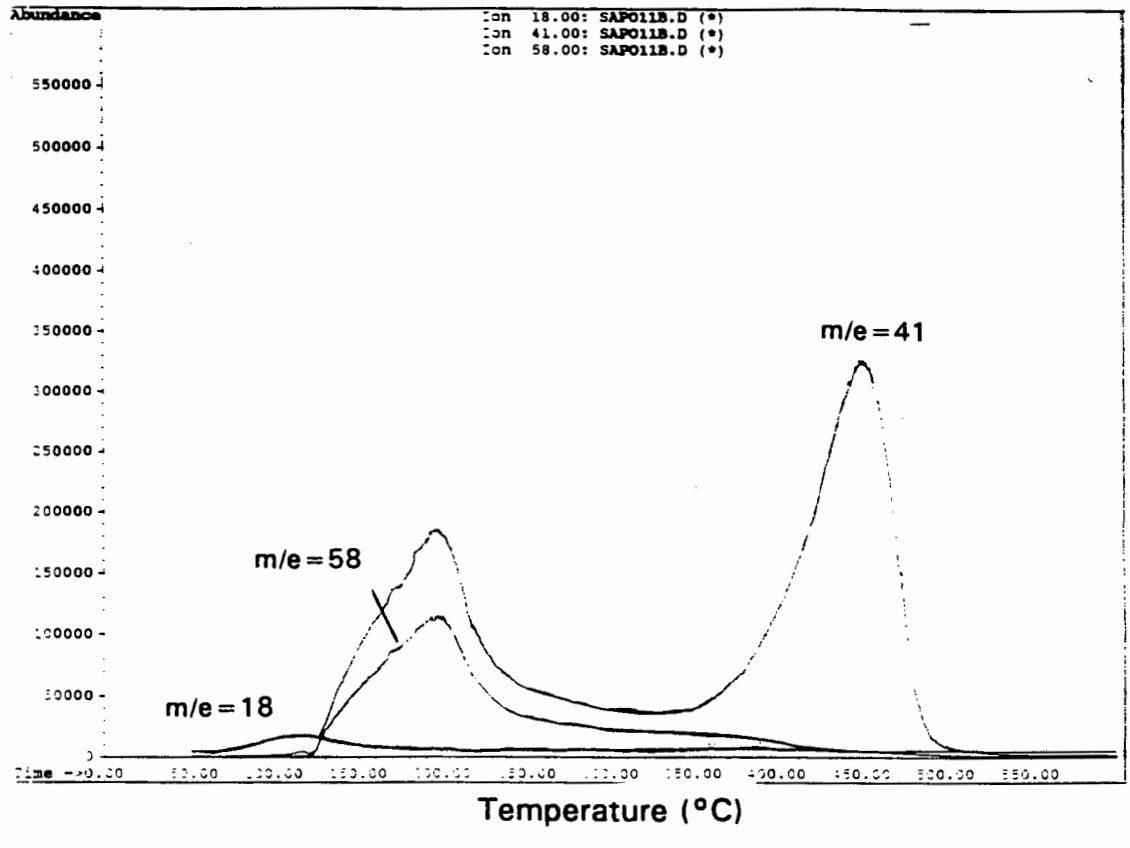

Figure 3.24 a. TPD-MS spectra of S11(3)syn.

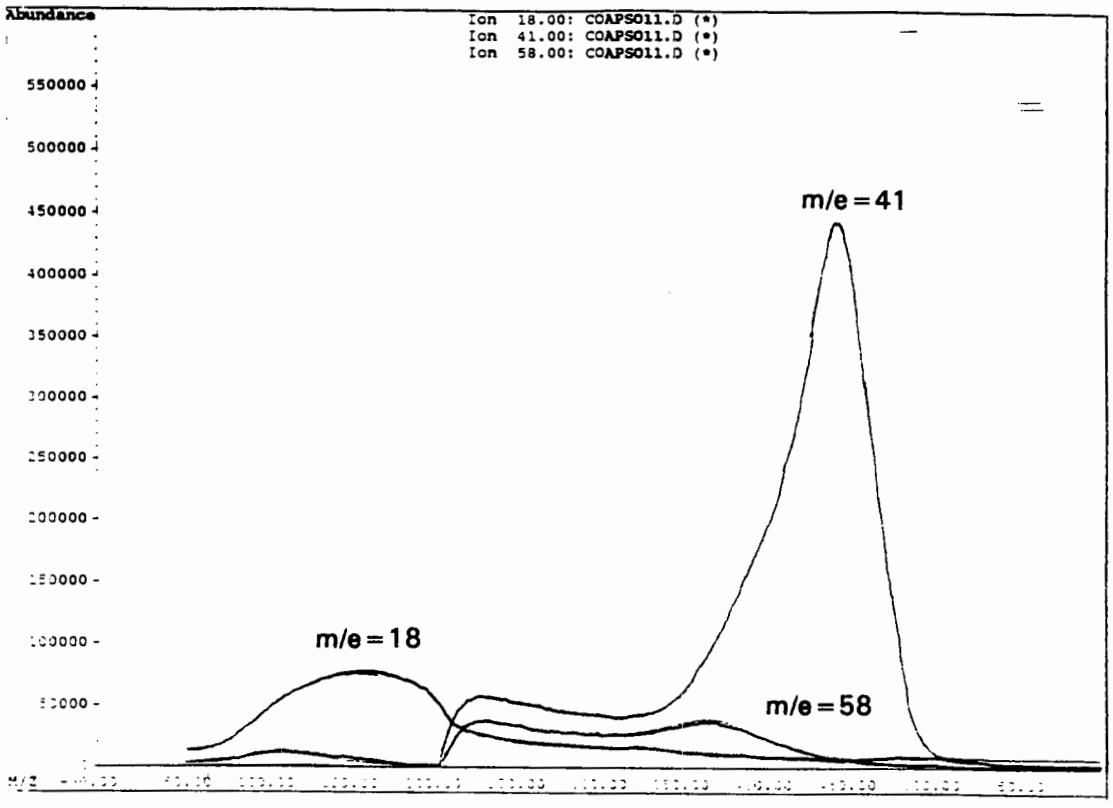

Figure 3.24 b. TPD-MS spectra CoS11syn.

3.3.4 SAPO Acidity

The NH_3-TPD data (Table 3.14, Figure 3.25) showed that the catalysts all possessed mild acidity, with the majority of the ammonia being desorbed between 250-310°C (low temperature desorption-LTD). No catalysts showed any indications of distinct high temperature desorption (HTD) peaks typical of strong acidity. There were however small trailing edge or shoulder peaks as indicated in Table 3.14. When Co and Mn were added to the SAPO-11 synthesis gel the number of LTD acid sites increased compared to S11(3) due primarily to the broadening of the LTD peak and also to the appearance of a distinct shoulder on the trailing edge of the LTD peak for MnS11. Ni and Fe addition to the SAPO-11 synthesis gel had no effect on the number of acid sites compared to S11(3), although the LTD peak shifted to slightly lower temperatures which indicated a slight weakening of acidity. Increasing the synthesis temperature and silicon content of the gel reduced the number of acid sites compared to S11(3). Steaming S11(3) reduced the number of HTD acid sites although some distinct HTD features developed

which indicated that a specific type of strong acid site may have been formed after steaming. Silanized S11(3) had less LTD and HTD acid sites than S11(3) although a small shoulder on the trailing edge of the LTD peak of Silan-S11(3) appeared. Ni and Co impregnation of S11(3) did not reduce the number of acid sites. All of the ion-exchanged samples, except NiS11(2)-IX and S11(3)-IX, showed a loss in the total number of acid sites. After ion-exchange all samples displayed the formation of small HTD features.

Table 3.14 NH_3-TPD data of SAPO-11 and MeAPSO-11 sieves.

Catalyst	LTD[1] (°C)	Shoulder (°C)	HTD (°C)	LTD[2] (mmol/g)	HTD[3] (mmol/g)	Total (mmol/g)
S11(1)	305	450	-	0.23	0.20	0.43
S11(3)	312	481	-	0.24	0.19	0.43
Acid-S11(3)	300	436	-	0.22	0.12	0.34
MS(2)-S11(3)	310	410	590	0.20	0.09	0.29
$SS_{(250)}$-S11(3)	330	420	590	0.20	0.11	0.31
Silan-S11(3)	310	480	s	0.12	0.10	0.22
S11(4)	280	-	-	0.22	0.14	0.36
S11(5)	275	400	-	0.18	0.14	0.32
S11(6)	312	430	-	0.22	0.14	0.36
S11(7)	310	410	590	0.17	0.13	0.30
NiS11(2)	256	-	-	0.23	0.22	0.45
Ni(imp)	317	480	-	0.26	0.16	0.42
NiS11(2)-IX	246	411	590	0.27	0.20	0.47
MnS11	293	405	-	0.32	0.22	0.54
CoS11	310	-	-	0.41	0.22	0.63
Co(imp)	311	500	-	0.23	0.16	0.39
CoS11-IX	296	385	590	0.24	0.19	0.43
FeS11	282	480	-	0.25	0.19	0.44
FeS11-IX	300	-	590	0.18	0.13	0.31

1. LTD = low temperature desorption peak position
2. LTD-amount of ammonia desorbed below 450°C
3. HTD-amount of ammonia desorbed above 450°C

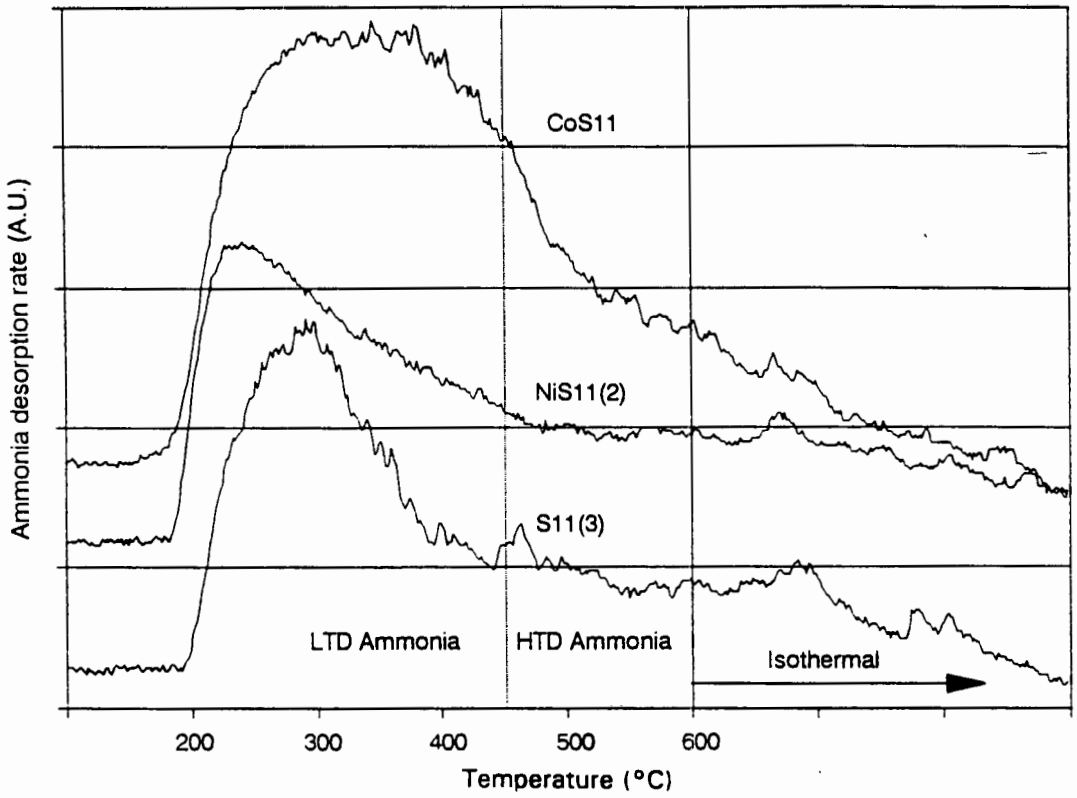

Figure 3.25 NH_3-TPD spectra of S11(3), NiS11 and CoS11.

3.3.5 Metal reducibility by Temperature Programmed Reduction (TPR)

TPR spectra of various MeAPSO-11 sieves showed quite diverse reduction behaviours. The reduction temperatures and amounts of hydrogen consumed for all of the MeAPSOs are given in Table 3.15. As expected TPR of S11(3) showed no reduction peaks and was used for baseline subtraction in conjunction with other spectra. TPR of NiS11(2) exhibited four reduction events. The first reduction, a small low temperature peak at 390°C probably corresponded to the reduction of well dispersed extra-framework NiO species as this peak was present for Ni(imp)S11(3) and occurred at a similar temperature to that of bulk NiO (420°C). The second and third reductions at 640°C and 795°C respectively did not correspond to the reduction temperatures of Ni in impregnation sites (400 and 590°C), but the temperatures corresponded well to those for the reduction of Ni^{2+} in ion-exchange sites of Zeolite Y [Suzuki *et al.*, 1989].

The second reduction peak at 590°C for Ni(imp)S11(3) was probably due to the reduction of Ni species strongly associated with the SAPO support or of

NiO species in macropores, which are more difficult to reduce [Mile *et al.*, 1988]. For NiS11(2)-IX the reduction shoulder at 620-640°C was absent. This suggested that the Ni^{2+} species that were being reduced at 640°C were those that were in exchangeable positions.

A high temperature reduction at 950°C was observed for both Ni(imp)S11(3), NiS11(2) and NiS11(2)-IX. The total amount of hydrogen consumed for these catalysts corresponded to *ca.* 2.2 times the amount required for complete reduction of all the Ni present as determined by AA. Reduction to 800°C corresponded to *ca.* 100% reduction of the Ni present. Re-oxidizing the catalysts after TPR to 1000°C and then completing a second TPR resulted in a shift to lower reduction temperatures and the amount of hydrogen consumed corresponded exactly to the amount required for complete reduction of all the Ni present.

Table 3.15 TPR data.

Catalyst	Metal[1] (mmol/g)	H_2 consumed (mmol/g	% Metal reduced	T_1[3] (°C)	T_2 (°C)	T_3 (°C)	T_4 (°C)	T_5 (°C)
S11	0.0	0.0	-	-	-	-	-	-
NiS11	0.63	1.376	232	390	640	795	950	-
re-NiS11[4]	0.63	0.666	106	360	550	640	-	-
Ni(imp)	0.63	1.346	214	350	400	590	950	-
re-Ni(imp)[4]	0.63	0.652	103	340	550	600	-	-
NiS11(2)IX	0.47	1.086	230	-	-	795	950	-
NiSiAl	1.19	1.203	101	350	510	-	-	-
NiSi	10.0	1.719	100	-	550	-	-	-
NiO	4.23	4.02	105	420	-	-	-	-
MnS11	0.673	0	0	0	-	-	-	-
CoS11	0.65	0.999	155[2]	890(sh)	980	-	-	-
re-CoS11[4]	0.65	0.698	100[2]	320	360	560	780	1000+
Co(imp)	0.68	0.8	118[2]	270	330	770(sh)	850	980
CoO	3.44	3.681	107[2]	280	360	-	-	-
FeS11	1.0	1.858	124[2]	470	610	670	780	930+
re-FeS11[4]	1.0	1.539	102[2]	380	500	770	790	850+

1. Amount of metal (mmol/g)
2. % Co and Fe reduced calculated as Co^{3+} and Fe^{3+}.
3. T_1, T_2 etc.=Reduction peak temperatures
4. re- reduction after reoxidation

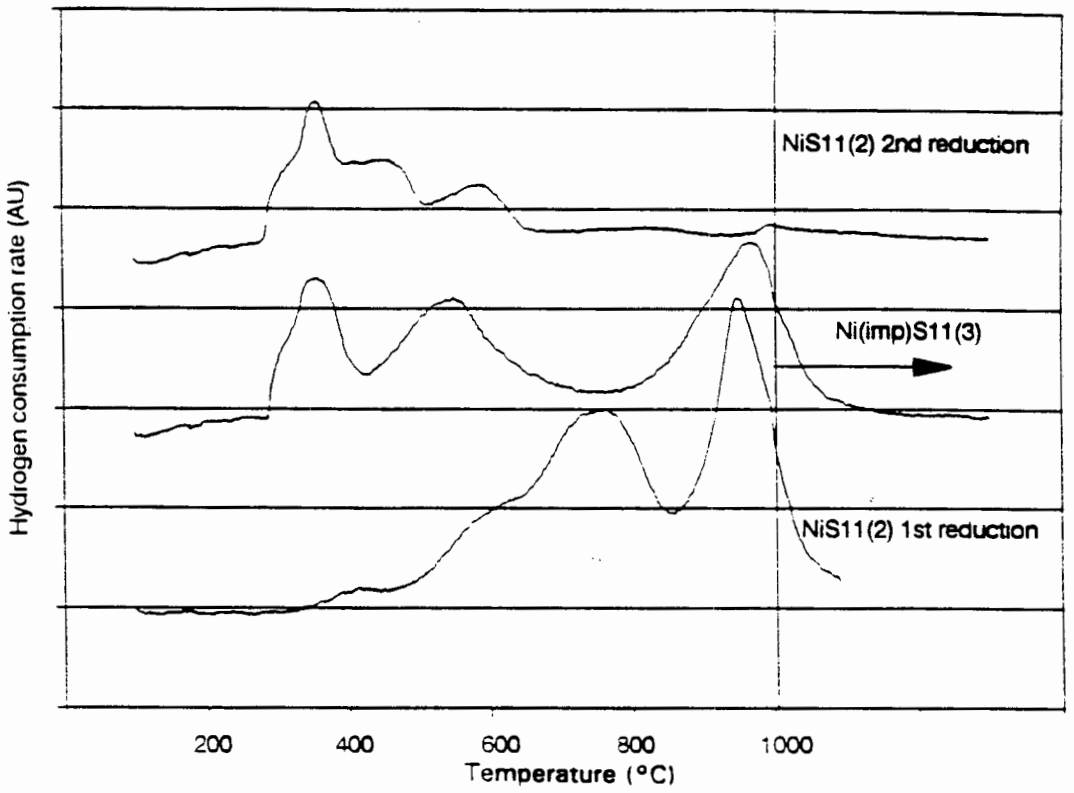

Figure 3.26 TPR spectra of NiS11, Ni(imp) and NiS11 after re-oxidation.

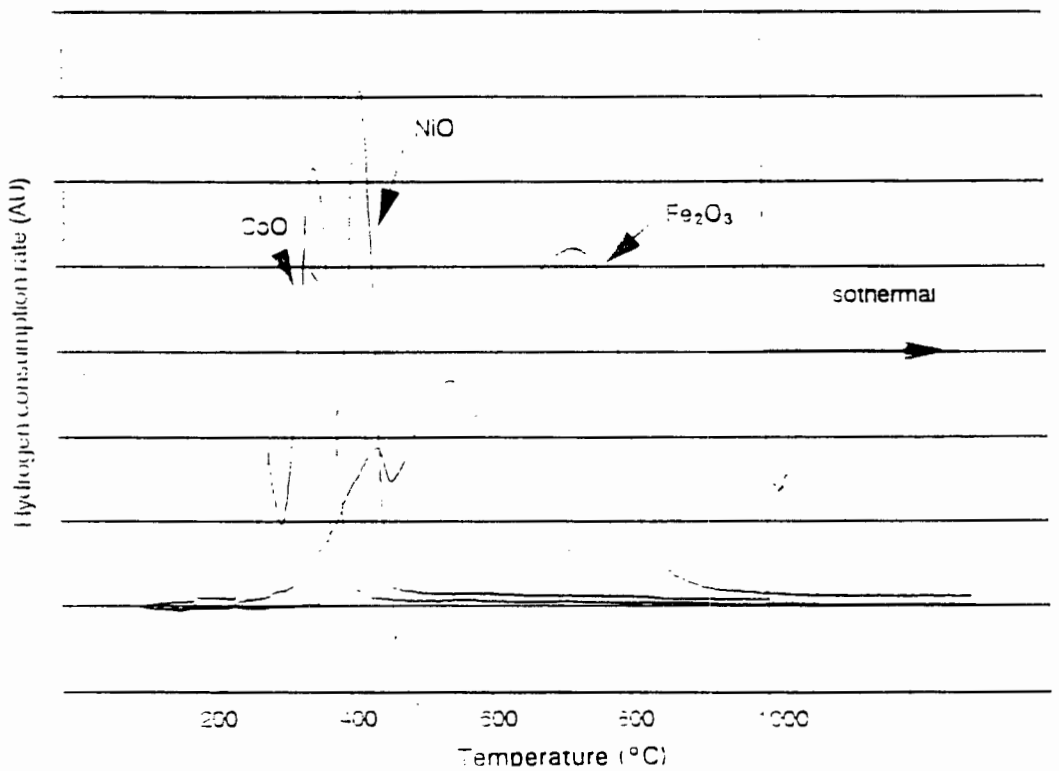

Figure 3.27 TPR spectra of NiO, CoO and Fe_2O_3.

XRD and FT-IR (Appendix VIII and VII) of the ex-TPR (800°C) samples showed no structural loss or collapse. All of the 1000°C ex-TPR samples, except S11(3), showed some loss of the features in the T-O asymmetric stretching region but their XRD remained unchanged. XRD of the ex-TPR (650, 800 and 1000°C) Ni-containing catalysts showed new peaks at 2θ values of 44° and 60° which correspond to those of Ni/NiO species.

TPR of Co(imp)S11(3) and CoS11 to 1000°C both resulted in excess consumption of hydrogen w.r.t. the amount of metal present as determined by AA. The calculations were made for Co^{3+} being reduced to Co^{0}. The major difference between the reduction behaviour of CoS11 compared to Co(imp)S11(3) was the presence of low temperature reductions at 270°C and 330°C for the latter. The leading edge shoulder for Co(imp)S11(3) was also more pronounced and the high temperature reduction started at 600°C compared to 770°C for CoS11(2). The low temperature reductions observed for Co(imp)S11(3) are likely to be those of surface CoO species since the reduction temperatures corresponded well to those of bulk CoO and Co on alumina.

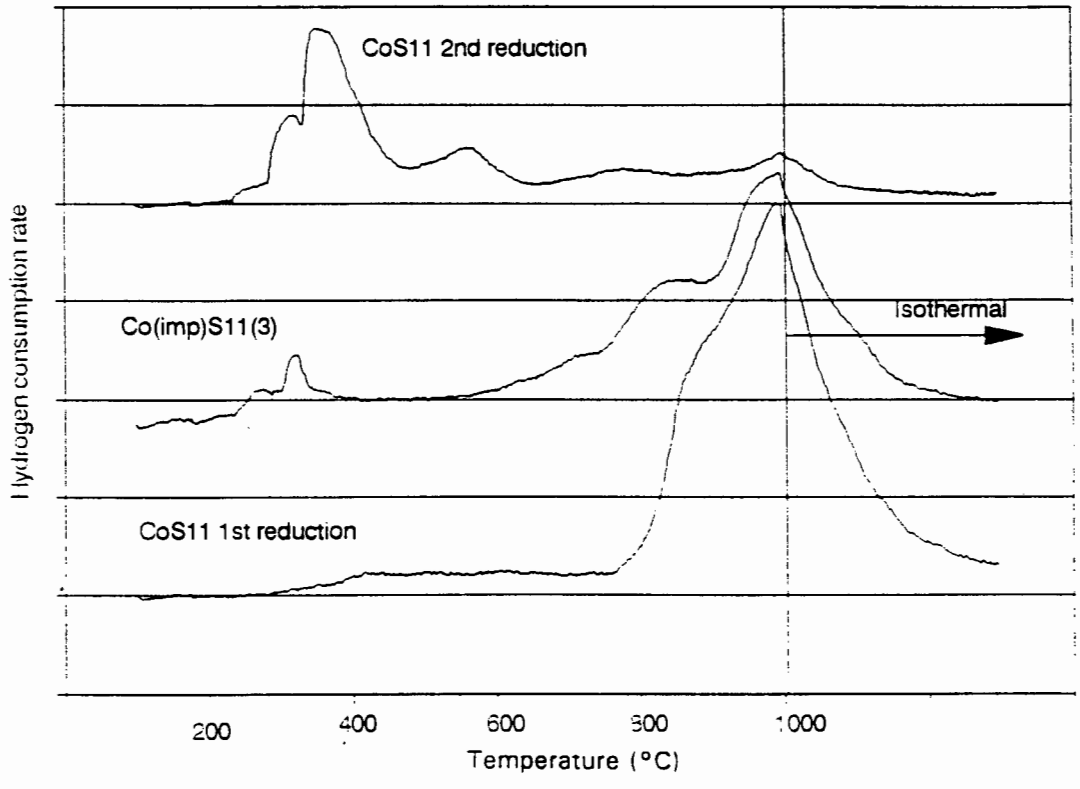

Figure 3.28 TPR spectra of CoS11, Co(imp)S11(3) and CoS11 after re-oxidation.

According to the data in Table 3.15, TPR of FeS11 also showed that excess hydrogen was consumed, but as there was still reduction occurring at 1000°C (Figure 3.29) it is possible that reduction at even higher temperatures and/or longer reduction times would have resulted in even more hydrogen being consumed. Approximately 35-40 wt% of the Fe present (calculated as Fe^{3+} to Fe^{0} on the basis of Mössbauer data) could be reduced by 850°C. The reductions below 850°C occurred at temperatures similar to those observed for Fe^{3+} in framework positions of ZSM-5 or silicalite [Lazar *et al.*, 1991, Kan *et al.*, 1991] and extra-framework Fe_2O_3 on alumina [Tang *et al.*, 1987]. Reduction after reoxidation, shown in Figure 3.29, showed that a small low temperature reduction occurred at 380°C. The remaining reductions occurred at slightly higher temperatures than in the first reduction and the high temperature reduction peak was significantly reduced. The amount of hydrogen consumed for the second reduction corresponded well to the amount of Fe present as determined by AA and assuming reduction from Fe^{3+} to Fe^{0}.

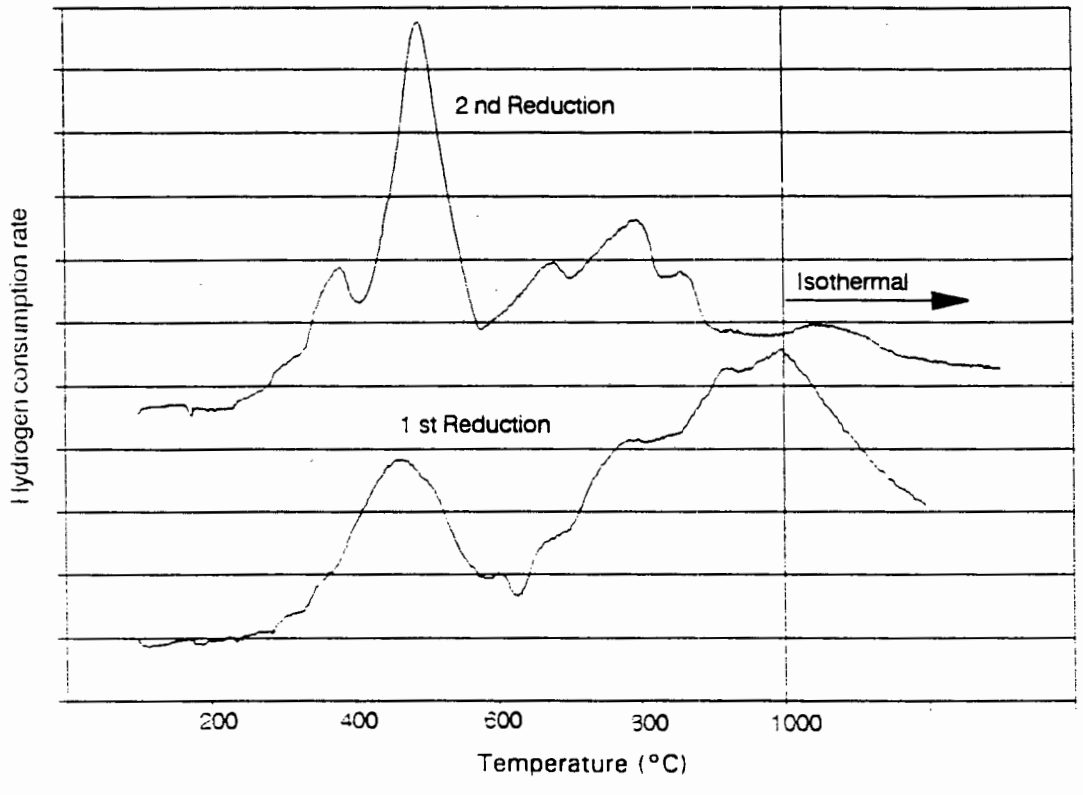

Figure 3.29 TPR spectra of FeS11 and FeS11 after re-oxidation.

No reductions were observed for MnS11 up to 1000°C which indicated that either Mn^{2+} was extremely stable within the framework or that it simply was not reducible. No reductions were observed for Mn in ion-exchange positions in Zeolite X below 700°C (Mahoney *et al.*, 1979).

3.3.6 Probe reaction studies

3.3.6.1 *m*-Xylene isomerization

M-xylene isomerization results are given in Table 3.16. All of the catalysts deactivated with time on stream, with the exception of CoS11 which achieved an optimum after 20 minutes on stream before deactivating. Initial conversions decreased as: FeS11 > MnS11 > CoS11 > S11(3) > Acid-S11(3) > NiS11(3). Steady state (t = 80 min) para-/ortho- ratios were: Co(1.78), S11(3)(1.74), Mn(1.74) > Fe(1.46) > Ni(1.28), Acid(1.2); the value in parentheses indicates the para-/ortho- ratio. From these results it can be seen that the sieves are para-selective since the para-/ortho-xylene ratio is greater than 1. The ratio of disproportionation products to isomerization products decreased with increasing run time for all the sieves to a steady state value except for Acid-S11(3) for which the ratio remained constant. The steady state disproportionation to isomerization ratios decreased as follows: FeS11 > S11(3) ≃ Acid-S11(3) > MnS11 ≃ CoS11. Initially FeS11 produced only disproportionation products.

Table 3.16 *m*-Xylene Isomerization data.

Catalyst	S11(3)		NiS11(3)		FeS11		CoS11		MnS11		Acid-S11(3)	
	Init[3]	SS[4]	Init	SS	Init	SS	Init	SS	Init	SS	Init	SS
p/o[1]	0.9	1.7	0.85	1.25	0.0	1.5	1.4	1.7	0.0	1.9	1.4	1.2
Disp/Isom	[2]2.5	1.3	3.2	0.9	inf	3.1	1.55	1.0	2.3	1.0	1.4	1.4
Conv.	8.0	3.7	6.0	3.9	12.8	4.4	9.8	3.8	10.3	4.0	6.7	3.1
Selectivities												
Isom[5]	29	33	24	52	0	24	39	44	31	48	42	42
Disp[6]	71	67	76	48	100	76	61	56	69	52	58	58
Coke[7]	3.4		2.3		2.2		3.2		-		-	

1. *p/o* = *p*-/*o*-xylene ratio
2. Disp/Isom = ratio of disproportionation products (toluene + benzene + tri- and tetraMB's) to isomerization products (*o*-/*p*-xylenes)
3. Init.-run time = 8 min
4. SS run time = 80 min
5. Isom.-selectivity to isomerization products
6. Disp.-selectivity to disproportionation products
7. Coke-from TG-DTA (wt%)

3.3.6.2 2-Methyl-2-pentene (2M2P) isomerization

2-Methyl-2-pentene isomerization results are shown in Table 3.17. The mass balances for all of the runs shown below were greater than 95%. All catalysts deactivated to a steady state conversion and the oligomerization products were always below 6 wt%. The oligomerization products consisted primarily of C_{12} olefins. The ratio of 2M2P to 2M1P was *ca.* 3.3 which indicated an equilibrium was being established. Initial conversions decreased in the order: S11(3) > MnS11≅NiS11(2) > FeS11≅CoS11 and the ratios of methyl shift to DBS products at steady state decreased as S11(3) > MnS11 > NiS11(2) > FeS11≅CoS11. The ratios of the amounts of skeletal isomerization to (double bond shift+skeletal isomers) is also given in Table 3.17.

Table 3.17 2-Methyl-2-pentene isomerization data

Catalyst	S11(3)		NiS11(2)		MnS11		CoS11		FeS11	
Time(min)	5	80	8	73	11	121	10	117	8	91
Conv.[1]	55.7	40.8	42.8	37.7	42.6	38.0	33.8	28.3	34.4	30.9
Olig.[2]	0.8	0.0	0.0	0.0	1.4	0.7	1.7	0.9	3.4	5.3
R1[3]	1.50	0.78	0.83	0.20	0.83	0.33	0.11	0.10	0.15	0.13
R2[4]	3.3	3.3	3.3	3.3	3.3	3.3	3.3	3.3	3.3	3.3
R3[5]	0.6	0.44	0.45	0.17	0.45	0.25	0.10	0.09	0.13	0.12
Coke[6]	1.6		2.1		4.3		3.9		5.9	

1. Conv.=Conversion of 2M2P to all products
2. Olig.=% hydrocarbons>C_6
3. R1=ratio of methyl shift products (c/t3M2P) to DBS products (c/t-4M2P)
4. R2=ratio of 2-methyl-2-pentene to 2-methyl-1-pentene
5. R3=ratio of (c/t-3M2P/c/t-4M2P+c/t-3M2P)
6. Coke (wt%) determined by TG-DTA.

3.4 PROPENE OLIGOMERIZATION

Repeatability, effect of "deep-bed" calcination and mechanical versus magnetic stirring synthesis conditions

Figure 3.30 shows that the repeatability of the propene oligomerization runs is good. For all runs the mass balance was greater than 95%. The slight differences in initial conversion can be attributed to WHSV fluctuations during the first few hours of the run. Figure 3.30 also shows that "deep-bed" calcination had no effect on the oligomerization performance of S11(3). SAPO-11 and NiAPSO-11 synthesized in mechanically stirred autoclaves [S11(3) and NiS11(2)] were as active as those synthesized in magnetically stirred autoclaves [S11(1) and NiS11(1)] (Figures 3.30 and 3.31). Figure 3.30 also shows that the reproducibility of the synthesis is quite good as the oligomerization performance of S11(1) and S11(2), synthesized under identical conditions, were similar.

Effect of metal and increased Si addition to the synthesis gel (synthesis variations)

The catalytic oligomerization performances of the MeAPSO-11 type sieves is shown in Figure 3.31. With the exception of MnS11, metal addition to the SAPO-11 synthesis gel decreased the oligomerization performance and caused rapid deactivation compared to S11(3). SAPO-11 synthesized at 150°C with LUDOX as the Si source, S11(4), was less active than SAPO-11 synthesized at 150°C with Fumed Silica, S11(3). Increasing the Si content of the SAPO-11 synthesis gel, increasing the synthesis temperature and decreasing the water content of the gel resulted in SAPO-11 sieves that had lower oligomerization performance compared to S11(3) (Figure 3.32).

Effect of Reaction temperature and WHSV

Increasing the reaction temperature from 250 to 310°C increased the conversion of propene and catalyst utilization value (CUV) of S11(3), as shown in Figure 3.33. Increasing the WHSV from 12 h^{-1} to 24 h^{-1} reduced the conversion by half and decreasing the WHSV to 6 h^{-1} increased the conversion to almost 100%.

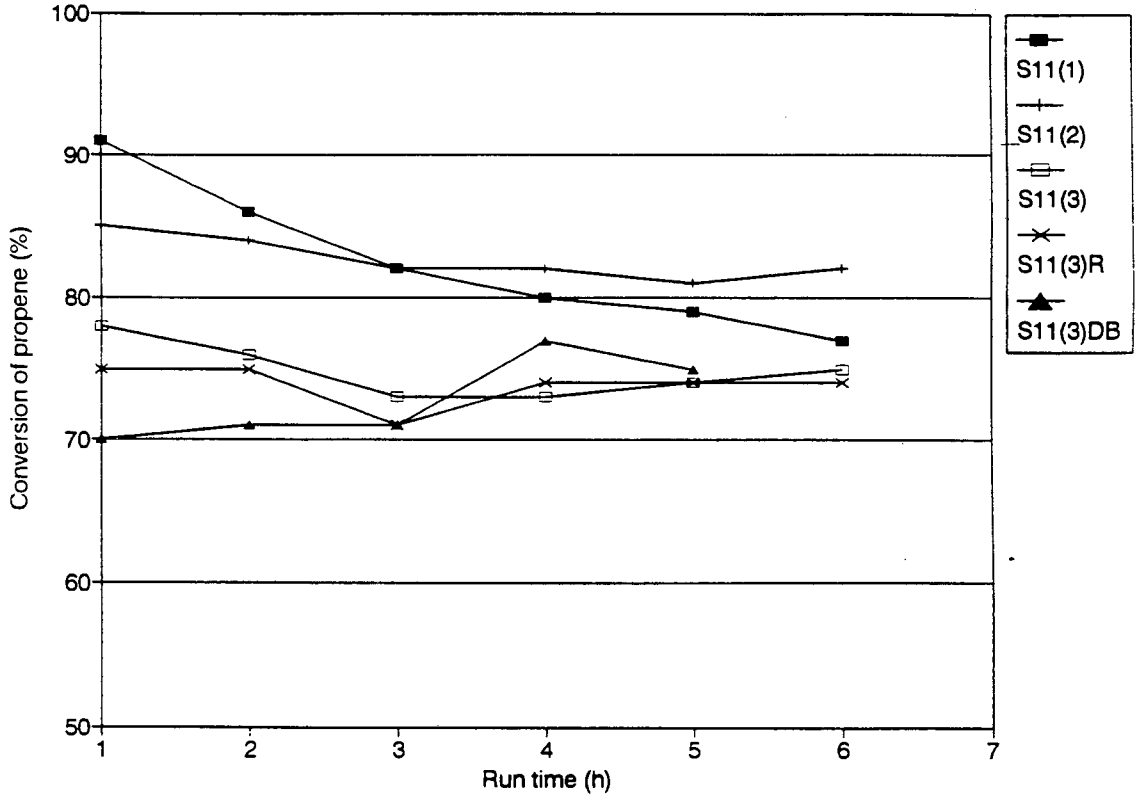

Figure 3.30 Repeatability of propene oligomerization runs for SAPO-11 type catalysts (R = repeat run).

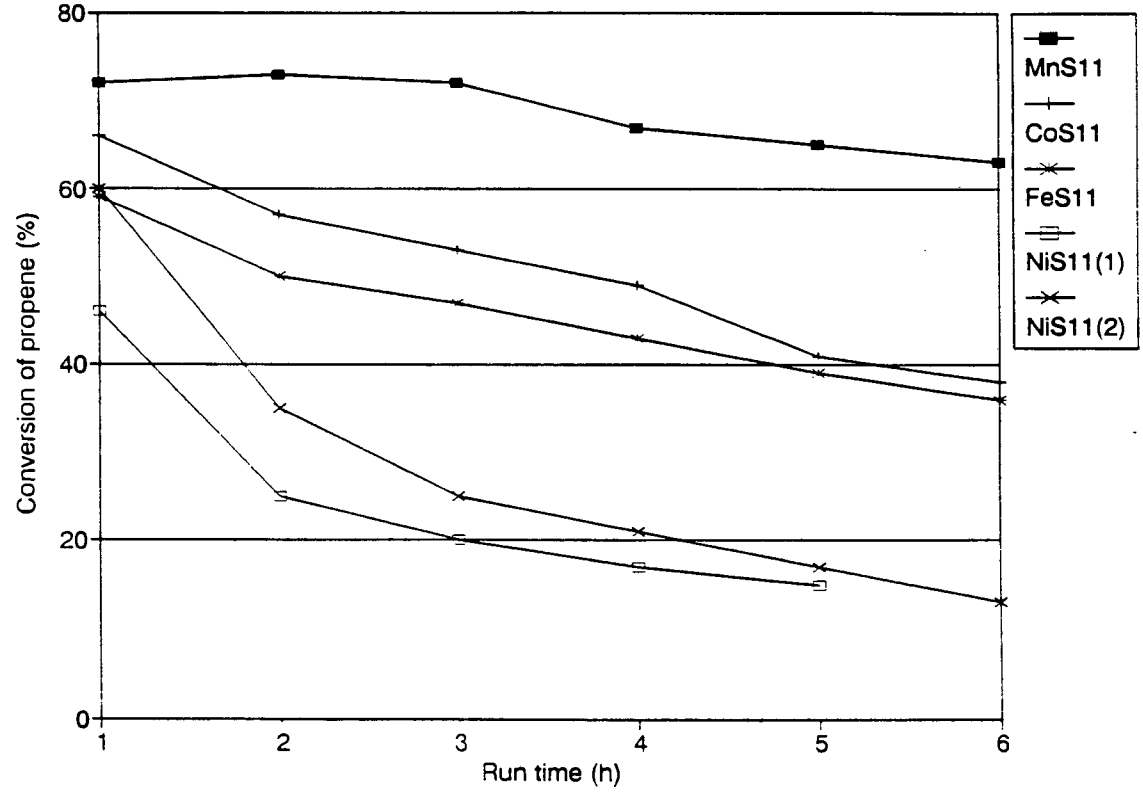

Figure 3.31 Effect of Metal addition to the synthesis gel on the oligomerization performance

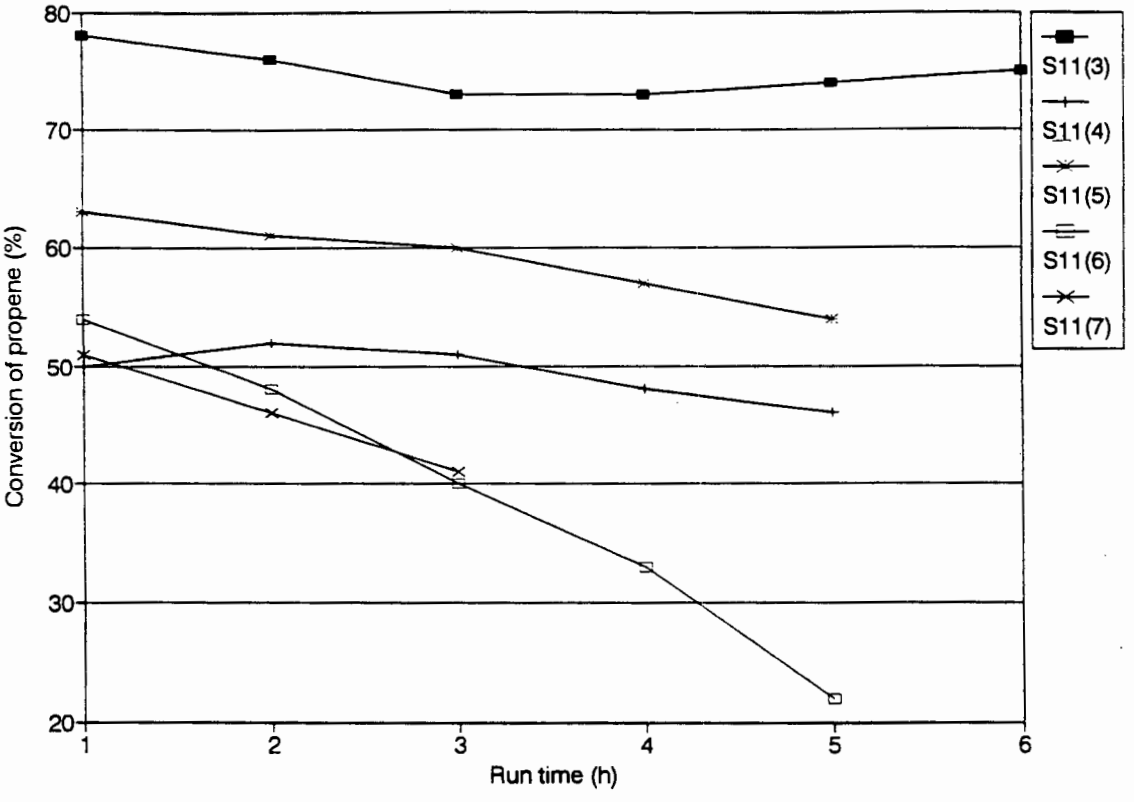

Figure 3.32 Effect of increasing Si content, increasing synthesis temperature and decreasing water content of SAPO-11 synthesis gel on oligomerization performance.

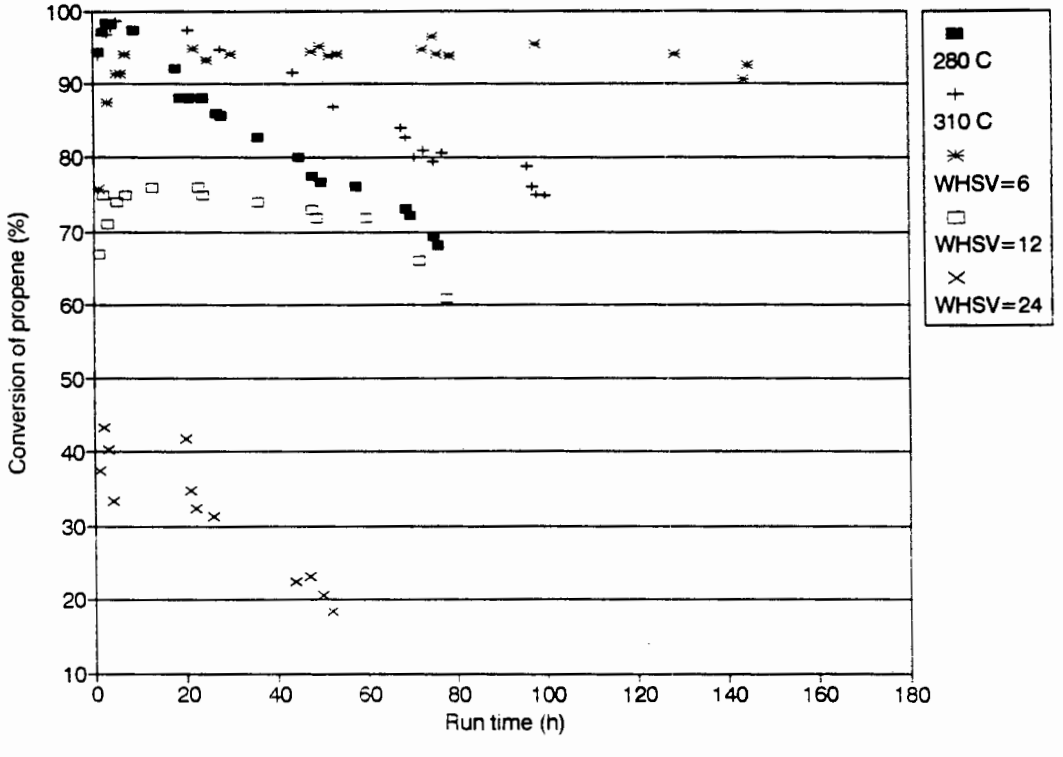

Figure 3.33 Effect of increasing reaction temperature and WHSV on oligomerization performance and lifetime of S11(3).

Effect of post synthesis modification

Silanizing and acid washing both reduced the oligomerization performance of S11(3)DB. The metal impregnated sieves were inactive for oligomerization (no liquid product was formed, although gas analysis showed *ca.* 10 wt% C_6). The ion-exchanged MeAPSO-11 samples had lower activities compared to their parent materials (Figure 3.34).

Effect of Extruding and pelletizing

Figure 3.35 shows the oligomerization performance of extrudates and pellets of S11(3) versus the performance of the pure powder form. The pellets were the most active, more active even than the pure powder form. Extrudates on the other hand did not perform as well as the pure powder form.

Effect of hydrothermal treatment

As can be seen from Figure 3.36 both mild (60 Torr H_2O, 100 ml/min N_2 for 6 hrs) and severe (120 Torr H_2O, 100 ml/min N_2 for 12 hrs) steaming improved the conversion and lifetime compared to S11(3). The CUVs decreased in the order $SS_{(120)}$-S11(3) $\simeq$ MS(6)-S11(3) > S11(3). The data in Table 3.18 shows that increasing the partial pressure of water (from 120 Torr H_2O to 250 Torr H_2O) increases the steady state conversion during the first 6 hours of the run from 89 to 95%. Reducing the steaming time from 6 to 2 hours for mild steaming conditions lowered the performance during the first 6 hours on stream.

The activity data for all of the propene oligomerization runs is listed in Table 3.18.

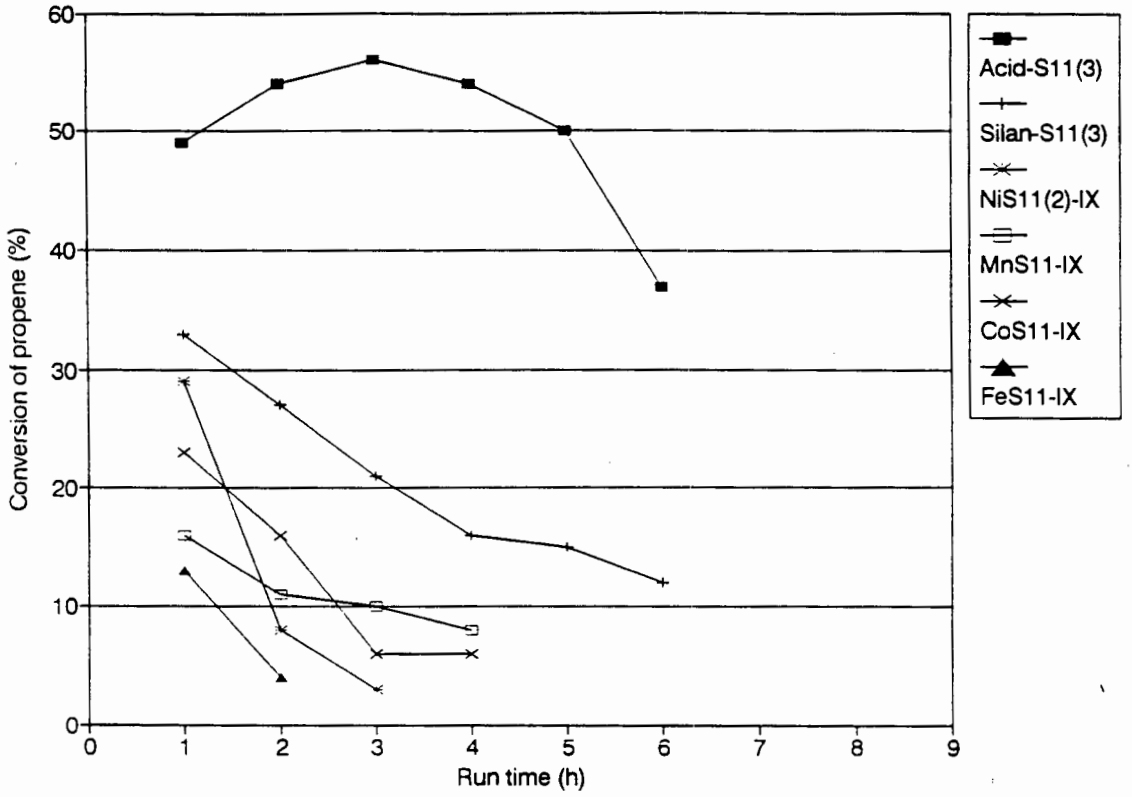

Figure 3.34 Effect of post-synthesis modifications, ion-exchange, metal impregnation, silanization and acid washing on oligomerization performance.

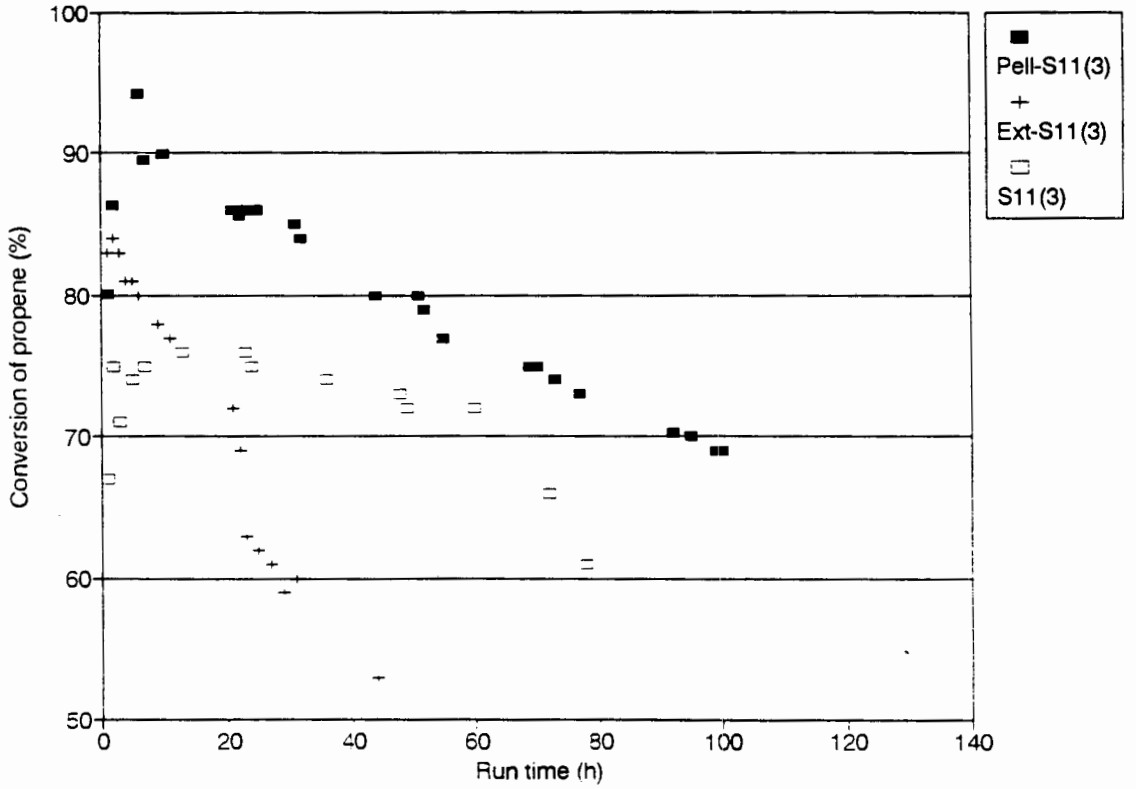

Figure 3.35 Effect of extruding and pelletizing on oligomerization performance and lifetime of S11(3).

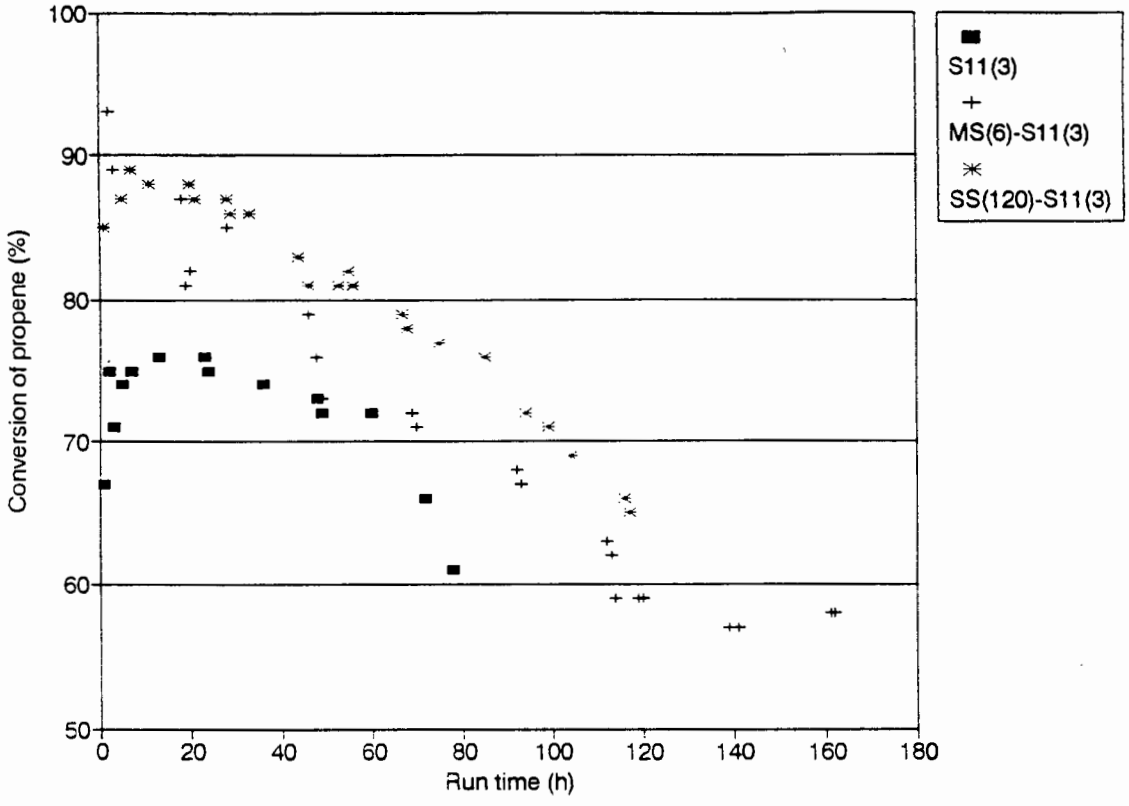

Figure 3.36 Effect of steaming S11(3) on the performance and lifetime for propene oligomerization.

3.4.1 Liquid product selectivity and cetane number analysis

The liquid product distributions are given in Table 3.19 and except for S11(7) and NiS11(2)-IX, the dimer fraction was the major reaction product and accounted for *ca.* 73 wt% of the product in the case of CoS11. Cetane numbers of the fractionated hydrogenated liquid product (+180°C fraction) were in the range of 35-50 and, as can be seen from the H-NMR spectra in Appendix V, no aromatics were present. To compare selectivities the conversions must be similar since the selectivity/yield is related to the conversion as shown in Figure 3.37. This figure shows that with increasing conversion the liquid product consists of heavier oligomers. This explains why the product becomes lighter, i.e. more C_6 olefins are produced, as the run times increase and the catalyst deactivates (Figure 3.38).

Increasing the reaction temperature to 310°C resulted in higher conversions and hence a liquid product with an increased amount of heavier oligomers, particulaly the C_9 fraction, compared to S11(3) at 250°C. Increasing the

reaction temperature also increased the cetane number of the liquid product. Mild steaming for 2 hours did not change the product spectrum of S11(3). However mild steaming for 6 hours (similar performance to S11(3) during the first 10 hours) increased the cetane number of the product of S11(3) from 40 to 49 and the amount of C_9's increased compared to S11(3). Severe steaming resulted in a product with a similar cetane number to S11(3) but consisted of more of the C_6 fraction. The liquid products of Ext-S11(3) and Pell-S11(3) had similar cetane numbers to the parent material, S11(3), but the pellets had more of the C_6 and C_9 fraction than S11(3).

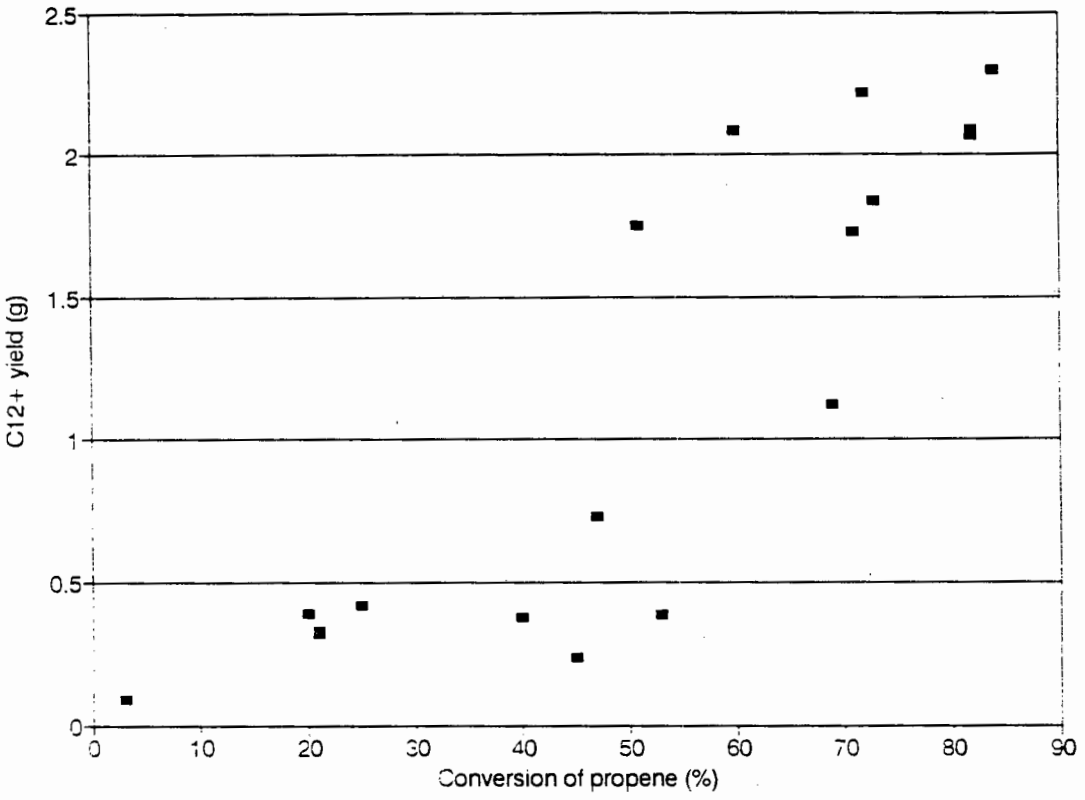

Figure 3.37 $C_{12}+$ yield versus conversion for SAPO-type catalysts

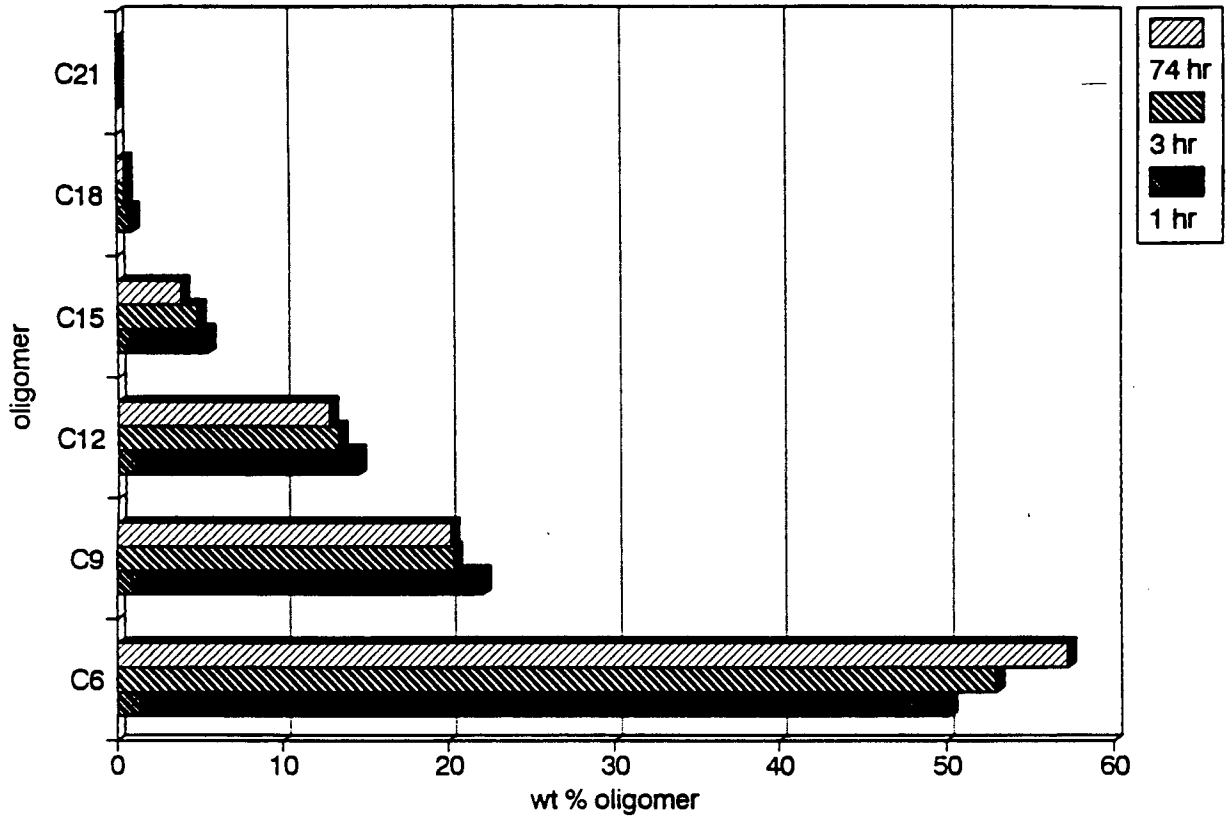

Figure 3.38 Liquid product selectivity versus run time

Table 3.18 SAPO propene oligomerization run data and coke data. Temperature = 250°C, WHSV = 12 h^{-1}, Pressure = 5 MPa unless otherwise stated

Catalyst	Initial % Conversion[1]	1/2 life (h)[2]	Trend[3]	Run Time	SS[4] Conv.	wt% coke	H/S Coke[5]	C_{12}^+ wt%[6]
S11(1)	91	-	n	6	80	11.0	-	20.1
S11(2)	85	-	n	6	82	12.0	-	20.3
S11(3)	78	-	n	6	75	13.0	-	21.2
S11(3)DB	70	-	n	5	75	12.7	-	21.6
S11(3)[7]	92	-	ds	76	96	11.6	0.14	18.0
S11(3)[8]	94	-	ds	100	96	11.5	0.42	18.2
S11(3)[9]	36	-	ds	52	40	11.0	-	29.9
S11(3)[10]	74	-	ds	145	94	10.6	-	32.6
S11(3)[11]	75	-	ds	79	74	11.1	0.07	20.4
Acid-S11(3)	49	-	d	6	-	10.5	-	27.7
Silan-S11(3)	33	4	d	6	-	6.8	-	7.2
MS(2)-S11(3)[12]	73	-	n	8	80	8.0	-	23.1
MS(6)-S11(3)[14]	86	-	ds	162	88	9.4	0.14	18.6
$SS_{(250)}$-S11(3)[13]	86	-	n	6	95	7.0	-	14.9
$SS_{(120)}$-S11(3)[15]	84	-	ds	117	89	10.6	0.05	10.1
Ext-S11(3)	85	-	ds	57	79	10.2	0.11	13.6
Pell-S11(3)	82	-	ds	100	88	9.0	0.09	8.0
S11(4)	50	-	d	3	-	37.0	-	29.3
S11(5)	63	-	d	5	-	35.0	-	30.0
S11(6)	48	5	d	5	-	7.2	-	8.3
S11(7)	51	-	d	8	-	10.3	0.54	18.9
NiS11(1)	46	3	d	5	-	11.0	-	13.9
NiS11(2)	60	3	d	6	-	15.0	-	13.4
Ni(imp)	0	-	d	2	-	11.5	-	-
NiS11(2)IX	29	1	d	3	-	7.0	-	23.9
MnS11	72	-	n	12	65	27.0	-	24.2
MnS11-IX	16	4	d	4	-	-	-	-
CoS11	66	6	d	6	-	12.0	-	5.9
Co(imp)	0	-	d	2	-	-	-	-
CoS11-IX	23	2.5	d	4	-	10.0	-	11.0
FeS11	59	6	d	6	-	12.0	-	13.4
FeS11-IX	13	1	d	2	-	-	-	-

1. Initial conv.: conversion of propene to liquid after 1 hour on stream
2. Time to half of initial conversion
3. Trend: d-deactivating, n- not deactivating, ds-deactivating slowly
4. SS:-steady state conversion during first 6 hours on stream
5. H/S:-"hard" to "soft" coke ratio
6. C_{12}^+-from GC analysis of liquid product
7. 280°C, WHSV = 12 h^{-1}
8. 310°C, WHSV = 12 h^{-1}
9. 250°C, WHSV = 24 h^{-1}
10. 250°C, WHSV = 6 h^{-1}
11. 250°C, WHSV = 12 h^{-1} (reproducibility)
12. 60 Torr H_2O, 100 ml/min, 2 h
13. 60 Torr H_2O, 100 ml/min, 6 h
14. 250 Torr H_2O, 100 ml/min, 6 h
15. 120 Torr H_2O, 100 ml/min 12 h

Table 3.19 SAPO liquid product analysis[1] and cetane numbers

Catalyst	Dimer C_6-C_8	Trimer C_9-C_{11}	Tetramer C_{12}-C_{14}	Pentamer C_{15}-C_{17}	Hexamer C_{18}-C_{20}	Heptamer + C_{21} +	Cetane no.
S11(1)	58.5	21.4	13.6	5.7	0.6	0.2	-
S11(2)	57.8	21.9	14.3	5.4	0.5	0.1	-
S11(3)	56.3	22.3	14.8	5.6	0.6	0.2	39.9
S11(3)[2]	60.3	21.8	13.3	3.9	0.7	0.1	46.5
S11(3)[3]	48.5	33.3	15.3	2.7	0.1	0.1	48.7
S11(3)[4]	37.9	32.2	23.1	5.9	0.7	0.2	38.3
S11(3)[5]	34.9	32.5	24.2	7.9	0.4	0.1	38.6
S11(3)[6]	57.4	22.1	14.6	5.3	0.5	0.0	-
S11(4)	35.4	35.2	21.5	7.2	0.6	0.0	-
S11(5)	38.0	32.0	19.3	8.3	2.4	0.0	-
S11(6)	64.3	27.3	6.7	1.5	0.1	0.0	-
S11(7)	39.8	41.3	14.0	4.6	0.2	0.1	-
Acid-S11(3)	47.9	24.4	19.5	6.7	1.4	0.1	-
Silan-S11(3)	69.8	23.0	5.9	1.1	0.0	0.2	-
MS(2)-S11(3)[7]	57.3	19.6	15.8	5.8	1.2	0.3	-
MS(6)-S11(3)[8]	53.7	27.7	14.3	3.8	0.4	0.1	48.6
$SS_{(250)}$-S11(3)[9]	67.7	17.5	10.3	3.4	0.9	0.3	-
$SS_{(120)}$-S11(3)[10]	70.3	19.5	8.5	1.3	0.2	0.1	41.2
Ext-S11(3)	57.5	28.9	11.2	2.2	0.1	0.1	39.7
Pellet	65.0	27.0	5.4	2.5	0.1	0.0	37.6
NiS11(1)	53.2	32.9	10.8	2.9	0.1	0.1	-
NiS11(2)	56.2	30.4	10.6	2.7	0.1	0.0	34.9
NiS11(2)IX	31.0	45.0	16.9	5.9	1.0	0.1	-
MnS11	54.9	20.9	14.2	9.2	0.6	0.2	35.3
MnS11-IX	-	-	-	-	-	-	-
CoS11	73.3	20.8	4.9	0.8	0.1	0.1	-
CoS11-IX	46.3	42.8	8.9	1.9	0.1	0.1	-
FeS11	60.4	26.2	8.8	3.4	1.2	0.0	-

1. Product analysis after 3 hours on stream
2. 280°C, WHSV = 12 h^{-1}
3. 310°C, WHSV = 12 h^{-1}
4. 250°C, WHSV = 24 h^{-1}
5. 250°C, WHSV = 6 h^{-1}
6. 250°C, WHSV = 12 h^{-1}
7. 60 Torr H_2O, 100 ml/min, 2 h
8. 60 Torr H_2O, 100 ml/min, 2 h
9. 250 Torr H_2O, 100 ml/min, 6 h
10. 120 Torr H_2O, 100 ml/min 12 h

3.4.2 Coke Analysis

m-Xylene isomerization

The amount of coke after *m*-xylene isomerization was less than 4 wt% of which the majority was "hard coke", i.e. could only be removed by combustion in air at 500°C. FT-IR showed that these catalysts had polyaromatic Type II coke as well as Type I coke (polyolefinic).

2-Methylpent-2-ene isomerization

The amount of coke after 2-methyl-2-pentene isomerization was less that 5 wt% for all the sieves. All of the coke could be desorbed below 500°C in nitrogen, i.e. no "hard coke" was present. FT-IR showed that these catalysts only had Type I coke present.

Propene oligomerization

The amount of coke, as determined by TG-DTA (Figure 3.39), after oligomerization is given in Table 3.18. For the majority of the unmodified sieves the amount of coke corresponded to the amount needed for pore filling, i.e. the same as LOI, irrespective of the run times. For S11(4), S11(5) and MnS11 the amount of coke exceeded that expected for pore filling indicating that coke may have also formed on the external surface. In all cases the majority of coke was "soft coke" (no "hard coke" for $t<10$ hours). The amount of "hard coke" increased slightly as the run times increased ($t>24$ hrs).

Metal impregnated and acid washed S11(3)DB only had slightly less coke than the parent material, S11(3)DB, even though these catalysts were essentially inactive for oligomerization. The ion-exchanged samples had only slightly less coke than the parent materials whereas silanized S11(3)DB had almost half the coke of S11(3)DB. Increasing the reaction temperature increased the amount of hard coke present but the total amount of coke remained the same. Pelletizing reduced the amount of coke formed compared to the powder form but the ratio of "hard" to "soft" coke remained the same. The extrudates contained 10.2 wt% coke. Since the extrudates consisted of *viz.* 75 wt% catalyst the amount of coke normalized

with respect to the amount of catalyst was 13.6 wt% compared to 13.0 wt% for the powdered catalyst. The steamed catalysts all had less coke than the parent material, S11(3). MS-S11(3) had significantly more "hard" coke than SS-S11(3) probably due to its longer run time (162 h versus 117 h).

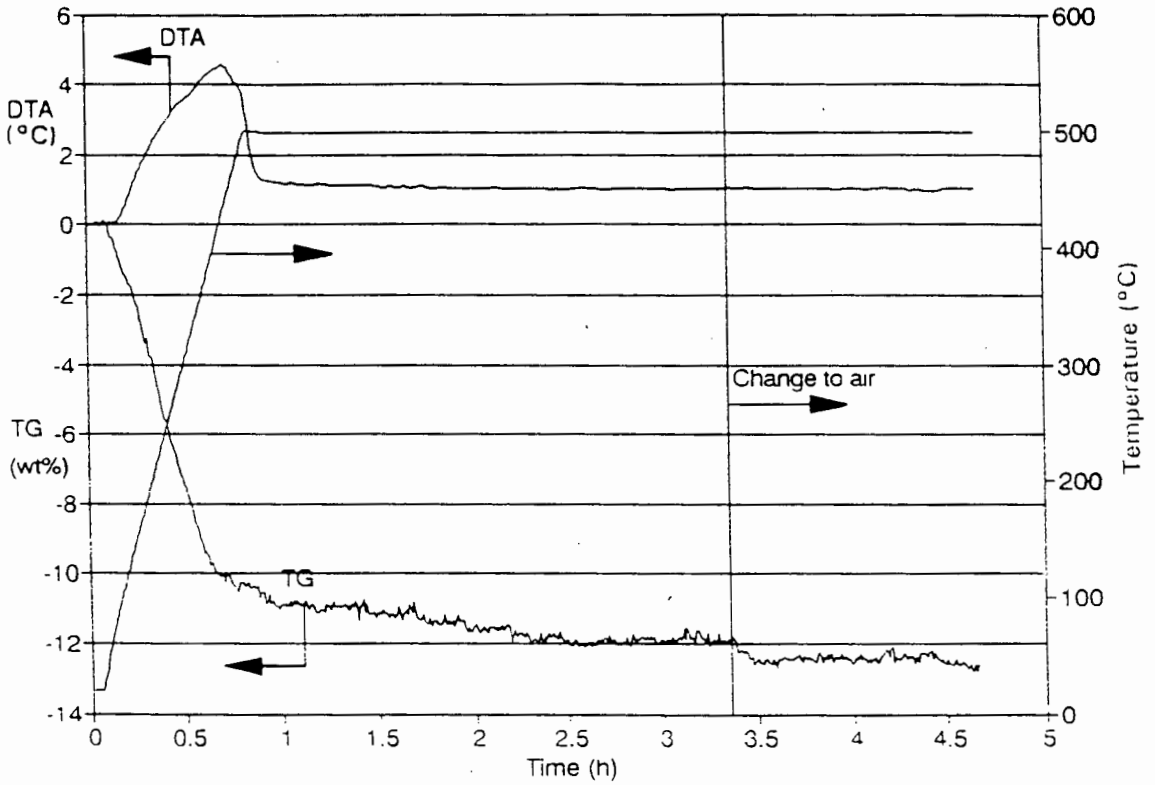

Figure 3.39 TG-DTA spectra of coked S11(3)

The desorption of the soft coke was accompanied by an exotherm (Figure 3.39). This exotherm may be due to the reaction of the trapped oligomers to form higher oligomers or coke species.

FT-IR showed that only Type I coke was present for all of the sieves after propene oligomerization (Figure 3.40). Analysis of coked S11(3) after long run times also only revealed the presence of Type I coke, which suggested that Type II coke formation was not a necessary condition for deactivation. FT-IR analysis of the coked MeAPSO-11, metal impregnated and ion-exchanged sieves showed only Type I coke.

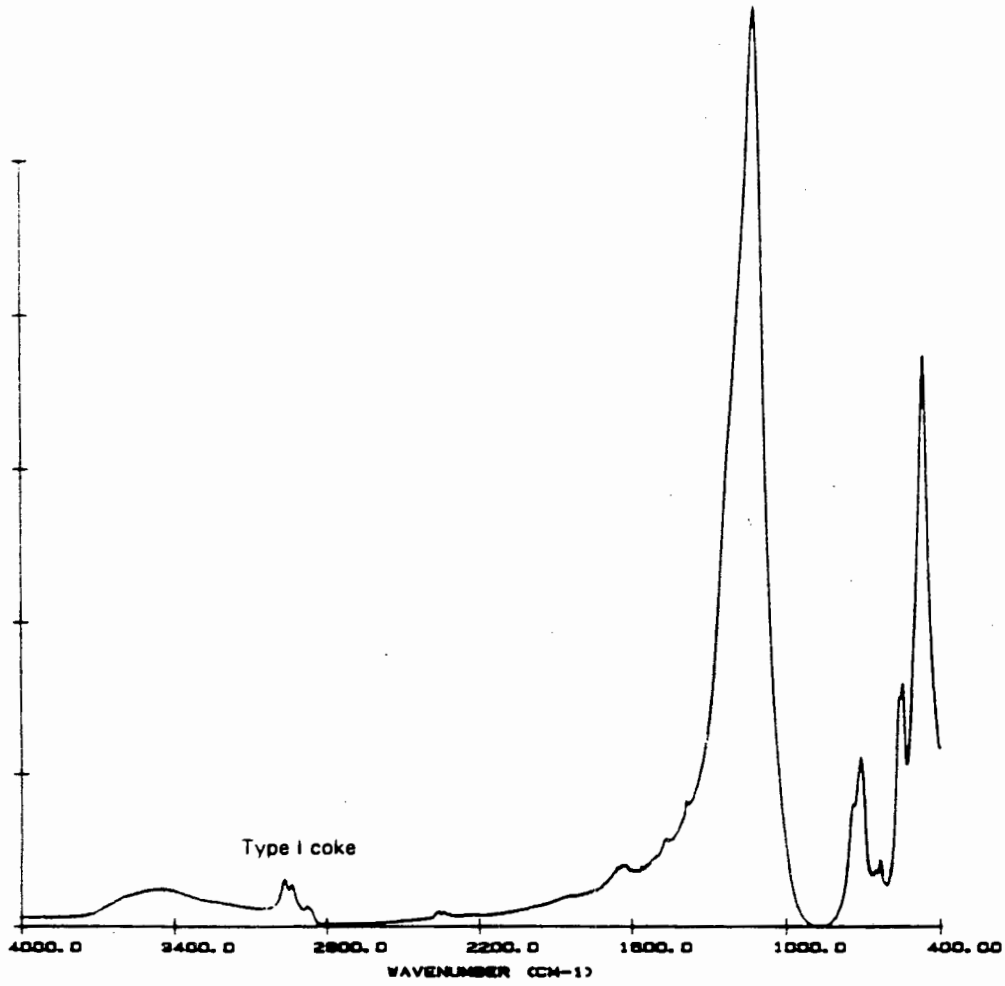

Figure 3.40 FT-IR spectra of coked S11(3), t = 79 h

Chapter 4
Discussion

4. DISCUSSION

4.1 HPA CHARACTERIZATION

4.1.1 Surface area, morphology and structure

The surface area results were similar to those reported by other workers [Hayashi and Moffat, 1982, 1983a; Akimoto *et al.*, 1981]. The NH_4PW salt had a lower surface area than that reported by Hayashi and Moffat (1983b) but was similar to that reported for NH_4PMo by Akimoto *et al.* (1981). The higher surface areas of the Type B salts may be due to their smaller crystallite size, as suggested by Misono (1987). The electronmicrographs (Figure 3.5) clearly showed that the Type B crystallites were an order of magnitude smaller than the Type A crystallites and hence an order of magnitude increase in their surface areas per gram of HPA would be expected. The higher surface areas of NH_4PW and other Type B salts may also be a result of the microporosity of these salts [McGravey *et al.*, 1988; Taylor *et al.*, 1985]. These micropores are not uniform like those in zeolites and are between 8 to 13Å in diameter.

The existence of multiple dehydration endotherms for Type A HPA salts has been previously reported [Tsigdinos, 1974; Niiyama *et al.*, 1981]. For HPW and other parent acids it has been stated that the first endotherm (in this case Endo(1) between 100 and 150°C) is due to loss of water of crystallization [Tsigdinos, 1974; Misono 1987]. The second endotherm, (in this case Endo(2) between 230 and 250°C) is due to the loss of water held deep within the bulk of the HPW [Hodnett and Moffat, 1984; Matsuda *et al.*, 1981]. This water is believed to be hydrogen bonded to the structural protons [Brown *et al.*, 1977; Mioc *et al.*, 1991]. For divalent metal salts of HPAs a second mass loss and endotherm at 200°C has been attributed to the interaction between water and the metal ions [Misono, 1987]. Hodnett and Moffat (1984) have also proposed, from their water-TPD data, that before complete decomposition of HPW (i.e. between 300-600°C), water may be desorbed as follows:

$$H_3PW_{12}O_{40} \rightarrow PW_{12}O_{38.5} + 1.5\ H_2O \quad (1).$$

The above reaction was not accompanied by an endo- or exotherm. For all the Type A HPW salts used in this study Endo(1) occurred at a higher temperature than that of the parent acid HPW. As these salts were pre-dried at 80°C overnight it is unlikely that the water desorbed during Endo(1) was water of crystallization as this water is known to be desorbed in flowing helium at 25°C [Hodnett and Moffat, 1984]. The higher temperature of Endo(1) compared to HPW is proposed to be a result of metal-water interactions. The temperature of the Endo(2) peak for the metal salts was within 10°C of that of HPW and may be due to water desorbing from a HPW-rich phase (see below). For all the Type A salts of HPW the number of water molecules desorbing which were associated with Endo(2) was between 5-6 per Keggin unit. This was to be expected as HPW (Type A) is also known to exist in the hexahydrate state after desorption of water of crystallization [Brown *et al.*, 1977]. AlPW:nitrate had a third endotherm, Endo(3), at 280-300°C, which also occurred during the second mass loss. This endotherm may be due to the desorption of either water of hydration associated with aluminium ions, or else water which is hydrogen-bonded to residual protons. Endo(4) for the AlPW salts and Endo(3) for NiPW, CePW and FePW, occurred at the end of the second mass loss, and since there was no simultaneous mass loss the endotherm is ascribed to a high temperature phase rearrangement. The presence of a small exotherm at 626°C for all the salts suggests that some HPW type material was present along with that of the salts (see Section 4.1.2 for further comment).

HPW and other freshly prepared parent acids have been shown to have 29, 24, 21, 13 or 6 molecules of water of hydration and are also known to exist as combinations of these hydrates [Hayashi and Moffat, 1982; Konishi *et al.*, 1982; Mioc *et al.*, 1991]. The freshly prepared Type A HPA salts and HPW had very irregular XRD patterns, most probably as a result of the presence of multiple hydration states [Black *et al.*, 1987]. Regular XRD patterns of the parent acids have only been obtained after calcination at or above 100°C [Konishi *et al.*, 1982; Mioc *et al.*, 1991]. At higher calcination temperatures it is known that the XRD peaks become broader and less intense due to loss of crystallinity [Black *et al.*, 1987] and this was shown for HPW after calcination at 325°C (Figure 3.3). Since the XRD pattern of the Type B salts did not change significantly on heating to 325°C it can be concluded that the secondary structure (the three dimensional arrangement of Keggin ions, water of crystallization and counter cations) is thermally

quite stable. This different thermal stability of the secondary structure of Type A salts and Type B salts has been reported elsewhere [Misono, 1987; Misono *et al.*, 1982; Highfield and Moffat, 1984]. In both instances however the primary structure (Keggin ions) remains intact at temperatures below 400°C as was evident from FT-IR data [Misono *et al.*, 1981; Konishi *et al.*, 1982] for Type A salts in particular, which showed that the Keggin ion bands remained essentially unchanged.

4.1.2 Acidity of HPAs

Ammonia and other oxygen and nitrogen containing polar molecules are readily adsorbed into the bulk of the HPA [Okuhara *et al.*, 1981; Misono, 1987]. Consequently the ammonia TPD results are representative of the bulk as well as surface acidity (i.e. total acidity). The broad LTD peak between 120 and 300°C (Figure 3.6) implies that there is some weak acidity present. The number of LTD sites varied depending on which counter cations were present and these sites may be weak Lewis acid sites resulting from metal-ammonia interactions. There was however no correlation between the number and strength of LTD sites and the electronegativities of the cations.

Comparing the data in Tables 3.1 and 3.3 it can be seen that the HTD1 peak positions of the HPAs corresponded to within 15°C of their respective major exotherms from TG-DTA. Therefore this peak is most probably due to the release of ammonia when the salt decomposes, since infra-red spectra of the catalysts after TPD to 600°C showed that the Keggin ion bands were absent. This decomposition must occur fairly rapidly as evidenced by the sharp nature of the HTD1 peak. The HTD2 peaks, present only in the M^{3+} salts, occurred some 40°C lower than their respective decomposition temperatures as determined from TG-DTA. This HTD2 peak is also very sharp and is therefore associated with a structural rearrangement or decomposition.

The baseline TPD spectra (water-TPD) of AlPW also showed two sharp desorption peaks, confirmed by mass spectrometry as water, at temperatures corresponding to HTD1 and HTD2. TPD-MS of ammonia on AlPW also showed water was desorbed when ammonia was released at HTD1 and HTD2. Since water is produced when HPAs decompose [Tsigdinos, 1974] these peaks in the baseline spectra seem to indicate that

there are two decompositions occurring in the trivalent metal HPA salts. This leads to the conclusion that two different phases exist in these salts. The existence of multi-phases or partial salts has been reported elsewhere by Highfield and Moffat, (1984a,b).

It has been suggested that for the metal salts of HPAs a large number of protons or HPW rich material are present on or near the surface [Misono *et al.*, 1981]. These workers have also stated that stoichiometric salts of HPAs are very difficult, if not impossible to synthesize. Hence there is always residual free acid phase present in HPA salts. Black *et al.* (1987) have prepared $K_{2.5}H_{0.5}PMo$ and shown that this salt existed as an HPMo phase on the surface of a pure K_3PMo phase. It is possible then that for the M^{3+} salts the HTD2 and HTD1 peaks represent the decomposition of the two different phases. NH_3-TPD spectra of AlPW catalysts synthesized with increasing amounts of aluminium, showed a shift in the HTD temperature to lower values (Figure 4.1). It should be noted that the differences in the spectrum below and those of Figure 3.6 are due to differences in desorption time of ammonia (2 hrs for Figure 3.6 and 24 hrs for Figure 4.1). Hence the HTD1 peak in Figure 3.6 is most likely to be associated with an HPW-rich phase decomposing and the HTD2 peak is most probably representative of a metal-rich phase decomposing.

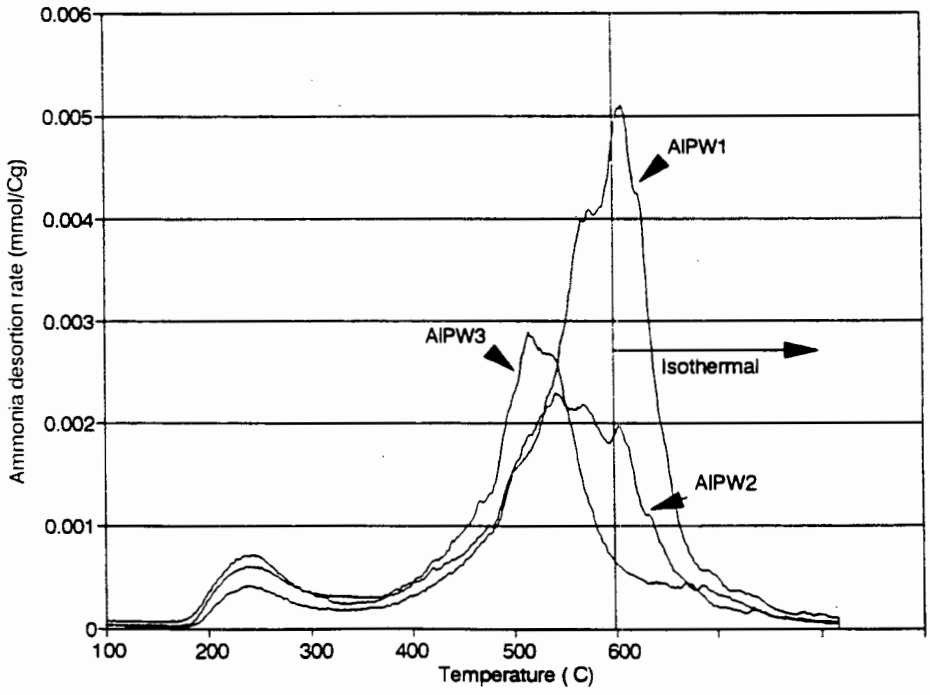

Figure 4.1 NH_3-TPD of AlPW with increasing amounts of aluminium.

Strength of acid sites

It was clear that for both the Type A and B salts, adsorbed ammonia was held at temperatures as high as 600°C and was released only when the salts decomposed. This suggested that there were strong acid sites present but that any further comment on their strength or distribution is impossible due to the associated decomposition of the salt, although it has been suggested that these sites are of fairly uniform strength [Misono *et al.*, 1981]. The presence of strong acid sites has been confirmed by Nowinska *et al.* (1991) who have shown that NH_4PW and HPW/HSiW supported on SiO_2 or alumina are capable of cracking cumene and of toluene disproportionation at low temperatures. Both these reactions require strong acid sites. As non-polar molecules such as n-butane, 1-butene and propene are not adsorbed into the bulk of the HPA, reactions of these molecules are regarded as surface type reactions and can therefore be used to probe the surface acidity of HPAs. It was apparent from the n-butane cracking and 1-butene isomerisation results in this present study that few or no strong acid sites existed on the surface of the Type A salts since none of the products observed are associated with reactions on strong acid sites. The presence of a small but measurable amount of coke (<1 wt%) on the catalysts after n-butane cracking did indicate though that some reaction had occurred but any strong acid sites on the surface must have been rapidly deactivated due to this coke formation. Thus the majority of the strong acid sites observed from ammonia TPD of the Type A salts were probably located within the bulk of the salts and were not accessible to the non-polar hydrocarbons. There were however acid sites present on the surface of the Type A HPAs which were capable of forming products typical of the double bond shift reaction of 1-butene.

The Type B salts, which had similar 1-butene isomerization conversion levels to the Type A salts (85%), were able to crack n-butane and 1-butene thus indicating that the Type B salts had stronger acid sites present on the surface than did the Type A salts. When 1-butene was passed over the Type B catalysts the cracking and skeletal isomerization products decreased after 30 minutes on stream. As these two reactions both require strong acid sites such sites may be deactivated quite rapidly due to coke formation, with the remaining weak acid sites only being capable of producing the cis- and trans-isomers. Baba *et al.* (1983) have reported a similar deactivation

behaviour for *o*-xylene conversion over Type A AlPW salts with the amount of disproportionation products decreasing to zero after 3.5 hours on stream.

From the n-butane cracking and 1-butene isomerization data it was clear that the ammonia TPD results gave no information about the nature of the surface acidity. Hence it is not surprising that there were no clear correlations between the ammonia TPD results and the propene oligomerization results. For example, in the case of FePW and AlPW:nitrate(2), although they had similar numbers and strengths of acid sites the latter was far more active for propene oligomerization. Type B salts, which n-butane cracking experiments had shown to have strong acid sites, had low propene oligomerization activities. It is possible that, as in the case of 1-butene isomerization, the strong acid sites deactivated due to rapid coke formation.

The characterization results of this study show that Type A and B HPAs have different properties which are outlined in Table 4.1 below.

Table 4.1. Comparison between Type A and B HPA salts

Property	Type A		Type B
Surface area	low (<15 m^2/g)		high (>35 m^2/g)
TG-DTA	multiple endotherms		single endotherm
XRD (2nd structure)	multi-crystalline		crystalline
SEM (morphology)	large crystallites		small crystallites
Water of hydration	high (>6)		low (<6)
Bulk Acidity (NH_3-TPD)			
No of bulk acid sites	A	>	B
Strength of bulk acid sites	A	≈	B
Surface acidity (strength)	A	<	B

4.2 OLIGOMERIZATION ACTIVITY OF HETEROPOLY ACIDS

4.2.1 Effect of Surface area

By far the most active of the undiluted catalysts was the AlPW:nitrate(2) salt and as a result this salt was studied in more detail to determine the possible reasons for its greater activity. AlPW has also been shown to be more active than HPW and CuPW for *o*-xylene isomerisation [Baba *et al.*, 1983] and of the metal salts of HPW it produced the greatest yield of C_4 hydrocarbons for the MTO reaction [Hayashi and Moffat, 1983]. Several batches of AlPW were synthesized and depending on the synthesis route and crystallization time the surface areas ranged between 2 and 12 m^2/g. Other workers have also synthesized salts with different surface areas by varying the amount of counter cation [Misono *et al.*, 1984]. Surprisingly the activity of the AlPW salts decreased as the surface areas increased (Figure 3.10). AlPW:nitrate(2) was as active for propene oligomerization as the zeolite ZSM-5, which has an appreciably higher surface area. The turn over numbers (TON) of propene per Keggin ion on the surface for the AlPW:nitrate(2) salt were approximately 2 orders of magnitude higher than those calculated per acid site of ZSM-5 (TON calculations shown in Appendix IX). As oligomerization is an exothermic reaction it was suspected that there may be difficulties in transferring the heat from such a low surface area catalyst to the bulk. During start-up (within the first hour on stream) the bed temperature of the higher surface area AlPW:nitrate(12) rose faster than that of the lower surface area AlPW:nitrate(2). At no time however did the bed temperature increase in such a way as to indicate that temperature runaway conditions were present. For both AlPW:nitrate(2) and AlPW:nitrate(12) the exotherms experienced on contact with the propene feed were approximately 30°C over 30 and 60 minutes respectively.

4.2.2 Effect of sand dilution

The catalyst bed was diluted with sand to act as a heat dissipator and to essentially eliminate temperature runaways or the formation of hot-spots which have been known to be responsible for the formation of hard coke and subsequent deactivation of catalysts [Verstappen and Waterman, 1955]. Figure 3.12 illustrated that the oligomerization performance of sand diluted AlPW:nitrate(2) was far greater than that of undiluted AlPW:nitrate(2). Similarly the performance of sand diluted AlPW:nitrate(12) (very similar performance to

sand diluted AlPW:nitrate(2)) was far greater than undiluted AlPW:nitrate(12). The increase in oligomerization performance of both salts when diluted with sand compared to their pure catalyst forms indicated clearly that there was poor heat transfer in the undiluted bed. It is thus clear that, when evaluating the catalytic activity of HPA catalysts, extreme care needs to be taken to maintain strictly isothermal conditions in the reactor. Since the conversion levels of sand diluted AlPW:nitrate(2) and sand diluted AlPW:nitrate(12) were both 100% it is not possible to make any statement regarding the effect of surface area on the activity of the sand diluted AlPW salts. To compare the true performance or activities of these salts their CUVs should be determined and compared, however due to the remarkable lifetimes of these catalysts, no sign of deactivation after 150 hours on stream, this was abandoned.

As mentioned above, in order to determine the true catalytic performance of the salts the catalyst utilization values (CUVs) of the sand diluted catalysts should be compared, and for AlPW, CuPW and FePW they followed the trends obtained when they were undiluted, i.e. AlPW >> CuPW > FePW. These results suggests that although the experimental conditions for the undiluted catalysts were clearly not optimal and subject to external factors such as temperature runaways or hotspots, the activity trend which was predicted using these conditions remains under isothermal (sand diluted) conditions.

4.2.3 The effect of water

Water plays an essential role in the generation of Brönsted acidity in the metal salts of HPAs [Baba *et al.*, 1983; Matsuda *et al.*, 1981) and the generation of acid sites has been proposed as follows:

$$M^{n+} + mH_2O \rightarrow (M(H_2O)m)^{n+} \rightarrow (M(H_2O)_{m-1}(OH))^{(n-1)} + H^+ \quad (2).$$

Brönsted acid sites have been shown to form when AlPW was steamed [Baba *et al.*, 1983; Ono *et al.*, 1984; Saito *et al.*, 1985] and these sites were responsible for an increase in *o*-xylene isomerisation activity. Water pulsed into the *o*-xylene feed also enhanced the activity of AlPW for isomerization. For propene oligomerization, steaming undiluted AlPW:nitrate(2) halved its activity. Steaming sand diluted AlPW:nitrate(2) however resulted in no activity loss with the catalyst remaining active for 150 hours without any sign of deactivation. But by comparing the pure catalyst data it seems that steaming may have enhanced the acidity as

the "apparent" loss in activity of the steamed pure AlPW:nitrate(2) salt due to coke formation was an indication of strong acid sites present.

The presence of water in the hydrocarbon feed mixture either at the start of a run, or by introduction during a run, had a detrimental effect on the activity of the undiluted AlPW:nitrate(2) catalyst. However in the case of sand diluted catalysts when wet feed was used the or the feed was changed to wet conditions during the run there were no losses in activity. The sudden increase in activity of the undiluted AlPW:nitrate(2) when the feed conditions were changed to "wet" may have been due to water interacting with aluminium to produce more acid sites as described above. This resulted in a sudden but temporary increase in activity thereafter these sites deactivated due to hot-spot formation.

4.2.4 The effect of calcination temperature

As mentioned above water plays an important role in the acidity of HPAs and several studies have concentrated on determining the relationship between water loss and acidity by looking at the effect of increasing the calcination temperature [Matsuda *et al.*, 1981; Hayashi and Moffat, 1982]. For 1-butene isomerization, a surface type reaction for HPAs, increasing the calcination temperature of the catalyst did not increase the conversion but did affect the cis- trans-isomer ratios [Matsuda *et al.*, 1981]. Hayashi and Moffat (1982) have shown that the yields of hydrocarbons were strongly dependent on the calcination temperatures of HPW for MTO, with the highest yields being observed after calcination at 350°C. The conversion of methanol remained quite similar however for all the catalysts. Calcining at temperatures higher than 400°C resulted in lower activities and yields, most probably due to loss of protons from HPW, via equation 1. The activity of AlPW:nitrate(2) or HPW was unchanged when calcined at 200, 325 or 425°C and hence it is unlikely that, within these temperature ranges, the strength or numbers of their surface acid sites changed significantly. HSiW was certainly affected by the amount of water present as its oligomerization activity decreased markedly as the calcination temperature increased. As HSiW is thermally less stable than HPW, calcination at 325°C may have caused partial decomposition of the catalyst (see equation 3 below) resulting in lower activity due to the loss of protons.

$$H_4SiW_{12}O_{40} \rightarrow H_2SiW_{12}O_{39} + H_2O \quad (3)$$

4.2.5 The effect of high surface area supports

Increasing the surface area available for reaction by supporting the HPA catalysts on suitable high surface area supports should result in increased activity for surface type reactions [Misono, 1987; Nowinska *et al.*, 1991]. The thermal stability of supported HPA catalysts has also been reported to increase [Kasztelan and Moffat, 1987], as well as decrease [Thouvenot *et al.*, 1991a,b]. The role of the support is often quite complex and the activity of the supported HPA is dependent not only on the type of support but also the extent of loading [Nowinska *et al.*, 1991]. In our case the loadings were kept constant at 25 wt% and α-alumina supported HSiW, when calcined at 325°C, was active for propene oligomerization. This activity cannot be ascribed to increased thermal stability compared to unsupported HSiW (which was inactive when calcined at 325°C) since it is well known that alumina supports reduce thermal stability [Izumi *et al.*, 1983]. The activity is probably due to the presence of an aluminated SiW (AlSiW) phase on the surface of the α-alumina since AlSiW was active when calcined at 325°C. Nowinska *et al.* (1991) have postulated that the active species for alumina supported HPAs is a proton rich phase since the activity for hexane cracking increased at loadings of greater than 36%. At lower loadings the HPA reacts with the surface of the alumina support to form a pure (and less active) AlPW/AlSiW phase.

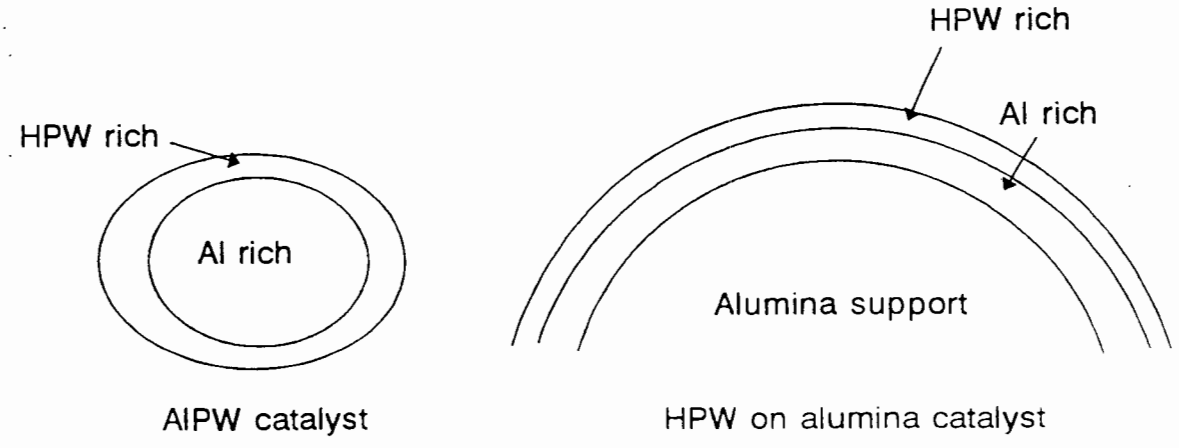

Figure 4.2 Active proton rich surface phase for salts and supported HPA catalysts

In this study when AlPW:nitrate and AlSiW were supported on α-alumina (25 wt%) their activity for propene oligomerization was much lower than their parent forms. The reduction in activity was probably due to reaction of the active HSiW/HPW phase present in AlSiW/AlPW with the alumina support to form the less reactive pure AlPW/AlSiW phase (i.e. proton deficient stoichiometric aluminium salt). The possibility also exists that the increased activity of the HPW and HSiW supported catalysts may also be due to a dilution effect of the support phase incurring isothermal behaviour.

Since it has been observed that HPAs are degraded by the presence of any basic residual material on the alumina support [Izumi *et al.*, 1983], the less acidic nature of HSiW compared to HPW may be advantageous as the extent of degradation due to any basic material present on the α-alumina would be less pronounced. This may account for the activity of α-alumina supported HSiW being greater than that of α-alumina supported HPW and the fact that HPW on α-alumina degrades with shelf time whereas HSiW on alumina remains as active.

HSiW on SiW support (acidic support) was more active than HSiW. Its activity increase was probably due to increased surface area available for reaction and a dilution effect of the support to incur more isothermal behaviour.

4.2.6 Liquid product selectivity

The various HPAs did not have any intrinsic selectivity properties as they all produced the trimer as the major oligomer group and, as seen in Figure 3.16, it was evident that the higher the conversion the greater the yield of heavier products. With increasing reaction temperature the selectivity to higher oligomers decreased, with a subsequent increase in the amount of cracking type products (C_5 and C_7). At 225°C the Type A salts showed no 1-butene cracking activity, however at higher temperatures it would be expected that for strongly acidic catalysts, cracking higher olefins to lighter olefins would occur. Likewise increasing the reaction temperature would promote cracking.

Quite large differences in the values of the cetane numbers of the liquid products obtained using pure powdered catalysts. This suggested that the counter cation may be responsible for changes in linearity of the product. The low cetane number of the liquid product using NH_4PW (Type B salt) may be a result of this catalyst's ability to skeletally isomerize olefins as was evident from the 1-butene

isomerisation results and thus increasing the degree of branching of the liquid product. The Type A salts on the other hand are unlikely to produce skeletal isomers as they only showed double bond shift activity for 1-butene isomerization at 225°C, and hence they would be expected to yield more linear product than the Type B salts.

Analysis of the liquid products using sand diluted Type A catalysts indicated that they all had identical amounts of C_{12}+ and therefore the counter cation did not appear to affect the product selectivity of these catalysts. The cetane numbers of the liquid products of the sand diluted catalysts were quite similar which also indicated that when isothermal conditions were employed no changes in product linearity for the Type A salts were present. Hence the differences in cetane numbers observed for the pure catalyst powder were probably due to temperature run aways which would have caused cracking or skeletal isomerization to occur thus yielding less linear olefins.

4.2.7 Coke analysis

FT-IR showed that Type II coke only existed after long run times and when non-isothermal conditions were employed for oligomerization. The Keggin unit bands were severely distorted by coke deposition, particularly the M-O-M_{edge} site. This leads to the conclusion that the active site for oligomerization is the so-called "cup-site" shown in Figure 4.3 below.

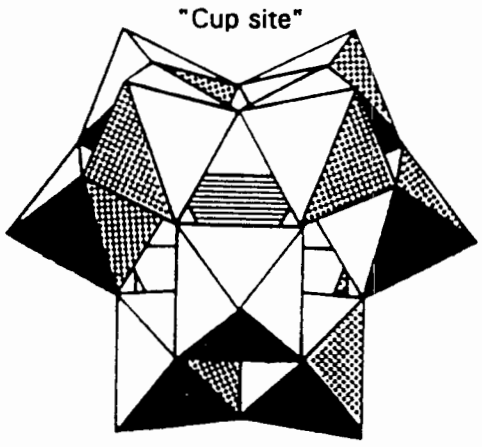

Figure 4.3 Proposed active site "cup-site"

This "cup-site" has been proposed to be the site at which ammonia adsorbs. Addition of ammonia to coked HPA catalysts with predominantly Type I coke showed that Type I coke could be displaced by ammonia, indicating that the Type I coke in the "cup-site" was probably not causing deactivation. However, ammonia addition to catalysts coked with Type II coke did not show much ammonia adsorption or Type I coke desorption which suggests that the Type II coke blocks/poisons the acid sites.

From the coke analysis results it can be concluded that Type II coke causes deactivation by poisoning or chemisorbing to the acid site ("cup-site"), thus preventing any other molecules from reacting. Type II coke is formed when non-isothermal conditions (i.e. when local temperature runaways or hot-spots are present) are employed and after long run times. The latter finding is consistent with the postulate of the ageing of Type I to Type II [Karge, 1991].

4.3 SAPO-11 AND MEAPSO-11 CHARACTERIZATION

4.3.1 Structure, composition, morphology and pore volume of SAPO-11

As synthesized SAPO-11 sieves

Although XRD confirmed that the only crystalline phase present was that of the AEL type, chemical analysis revealed that there was excess aluminium present for the SAPO-11 sieves (Table 3.8). Similar findings for $AlPO_4$-11 were also observed by Khouzami *et al.* (1988). This aluminium has been proposed to be occluded within the pores. The sieve with the highest Al/(P+Si) ratio, *viz.* S11(4), had a lower surface area and hexane adsorption value compared to S11(3) which suggested that the excess aluminium was possibly occluded within the pores and responsible for pore blockage and/or constriction. Of course aluminium present as amorphous alumina would also result in a lowering of the surface area or pore volume, however no separate amorphous species were seen by electron microscopy.

Higher stirring speeds have been shown to produce smaller crystallites of ZSM-5 [Schwarz *et al.*, 1991b]. In this study however, no differences were observed in the crystallite size of "fast" and "slow" stirred SAPO-11. The surface area of mechanically stirred (400 rpm) SAPO-11, i.e. S11(3) (236 m^2/g), was however, slightly higher than of the magnetically stirred (80 rpm) SAPO-11, i.e. S11(1) and S11(2) (200 and 212 m^2/g respectively). These values are similar those reported by Tapp *et al.* (1988b) for crystalline $AlPO_4$-11 of 200 m^2/g.

SAPO-11 synthesized with fumed silica was more crystalline than when synthesized with Ludox HS-40 as the Si source. Wilson (1991) has suggested that there is no clear preference between the various Si sources used for SAPO syntheses. Clearly however in this system Ludox HS-40 is not as efficient as fumed Si for high quality SAPO-11 synthesis. One possible explanation for such a result may have something to do with relative degree of reactivity of Si sources or it may have something to do with the rate of dissolution of the Si source which is known to affect the rate of crystallization and nucleation [Mertens, 1987].

Increasing the synthesis temperature (and decreasing synthesis time) of low and high Si content gels resulted in a SAPO-11 product with reduced % relative crystallinities. Weyda and Lechert (1990) have shown however that

increasing the synthesis temperature of SAPO-5 synthesis gels increased only the crystallization rate but did not change the % crystallinity of the product. An increase in the Si content however may be expected to reduce % crystallinity of SAPO sieves as this has been observed by Khouzami *et al.* (1988) and Mertens *et al.* (1990) for SAPO-11 as well as Weyda and Lechert (1990) for SAPO-5. A possible explanation for the reduction in % crystallinities of the SAPO-11 samples may be due to the presence of amorphous extra-framework aluminium occluded within the pores causing crystal disorder. Increased synthesis temperatures would be expected to increase the crystallization rate and this may facilitate the occlusion of extra-framework aluminium. Weyda and Lechert (1990) also observed that SAPO-5 samples with decreased % crystallinity had increased Al/P ratios, i.e. extra-framework aluminium. These same workers have also shown that at increased Si gel contents extra-framework SiO_2 was present for SAPO-5 sieves. This may also be a possible reason why our high Si gel SAPO-11 crystallites were less crystalline, i.e. there was extra-framework SiO_2. These sieves also appeared to be less crystalline on their surface as was seen from SEM.

The electron micrographs showed that SAPO-11 sieves synthesized with low Si contents in the gel and increased synthesis temperatures [e.g. S11(6)] consisted of large single crystallite material as well as circular agglomerates of rod-like crystallites. Increasing the Si content and/or reducing the water content of the high temperature synthesis gel resulted in no large single crystallite production. Several workers have shown that decreasing the water content of SAPO-5 synthesis gels results in faster crystallization rates and that high water content gels promoted the synthesis of larger SAPO-5 crystal formation [Weyda and Lechert, 1990; Kessler, 1989; Finger *et al.*, 1991]. The results of this study indicate therefore that in the synthesis of SAPO-11 sieves at high temperatures and with low Si contents large crystallites are formed. Decreasing the water content of this gel or increasing the Si content however promotes smaller crystallite formation, indicating that water and Si content plays an important role in determining the crystallite size of the SAPO-11 sieve. It should be pointed out that these conclusions may be specific to the aluminium source used as Tapp *et al.* (1988b) and Weyda and Lechert (1990) have shown differences in the synthesis behaviour of $AlPO_4$-11 and SAPO-5 depending on the aluminium source used.

The FT-IR results showed no significant changes in the asymmetric T-O stretching frequencies. Significant shifts are only observed when incorporation of elements (metals included) is greater than 5% [Ione and Vosrikova, 1987], and as chemical analysis showed less than 2 wt% Si incorporation it is not surprising that no significant shifts were observed.

Post synthesis Modified sieves

Calcination

The 2θ shifts and reduction in % crystallinity after calcination and subsequent hydration at room temperature indicated a transformation from the as-synthesized body-centred orthorhombic (Imma/Icmm/Icm2) structure type [Bennet *et al.*, 1987; Pluth *et al.*, 1988] to the structure primitive orthorhombic ($Pna2_1/Pbn2_1$) structure type [Meinhold and Tapp, 1990, Tapp *et al.*, 1990]. The proposed structure for calcined AEL molecular sieves is the orthorhombic (Icmm/Ima2/Icm2) structure type [Richardson *et al.*, 1988]. Other workers have observed changes in 2θ values after calcination and hydration of their as-synthesized samples [e.g. Vedrine *et al.*, 1988] and have shown that the transformation from $Pna2_1$ (calcined hydrated) to Ima2 (calcined dehydrated) is reversible and is due to hydration after calcination and not template removal [Tapp *et al.*, 1990; Goepper *et al.*, 1989; Khouzami *et al.*, 1990]. The FT-IR data of this study and that of Tapp *et al.* (1990) has also shown that, after calcination, physisorbed water affects the T-O internal tetrahedra as evidenced by the appearance of multiple absorptions in 1000-1300 cm^{-1} region. These features disappear after drying the sample. It has been postulated that the physisorbed water coordinates with framework aluminium species in $AlPO_4$-11 and SAPO-11 to form octahedral complexes [Goepper *et al.*, 1989; Peeters *et al.*, 1992].

Silanization, acid washing steaming and metal impregnation.

Silanized S11(3) showed a reduction in pore volume but no change in % crystallinity compared to calcined S11(3). Theocharis *et al.* (1989) have also shown that $AlPO_4$-5 silanized with $SiCl_4$ showed no % crystallinity decrease but that mesoporosity developed at the expense of some adsorption sites. Choudhary *et al.* (1989) have also shown no crystallinity decrease after silanization of $AlPO_4$-5 with $SiCl_4$. Li and Davis (1992) have suggested that

using $SiCl_4$, silanized $AlPO_4$-5, had significantly reduced pore volumes due to deposition of amorphous material in the pores. The reduction in porosity of silanized S11(3) in this study is most likely due to pore blockage/constriction by amorphous extra-framework Si species on the external surface rather than inside the pores. Tetraethoxysilane would not be expected to enter the pores of SAPO-11 and therefore the Si deposits should be only on external surface of the SAPO-11 sieve [Niwa *et al.*, 1984].

Mildly acid washed S11(3) (0.01 M HNO_3) showed a reduction in pore volume without a loss in % crystallinity relative to calcined S11(3). Acid washing removed 8% of the aluminium from S11(3). It has been suggested that mild acid washing removes or clears extra-framework aluminium species from the pores of zeolites [Wang *et al.*, 1991; Scherzer, 1984; Chen, 1976], but severe acid washing can create further extra-framework aluminium species [Musa *et al.*, 1987]. Barrer (1988) has suggested that $AlPO_4$-n molecular sieves are only mildly resistant to acid attack. Likewise, Hampson *et al.*, (1989) and Choudhary *et al.*, (1988), have shown that crystallinity and porosity of $AlPO_4$-5 decreases when the calcined $AlPO_4$-5 sieves were exposed to mineral acids. Hampson *et al.* (1989) have also proposed that $AlPO_4$-11 was more resistant than $AlPO_4$-5 to acid attack. The crystallinity and porosity decreases observed by Hampson *et al.* (1989) were attributed to framework collapse due to P leaching from the framework. Clearly the acid washing conditions used in this study are not optimal for removal of extra-framework aluminium species since the acid washed sample had a lower pore volume than the calcined S11(3) sieve. In contrast to the observations of Hampson *et al.* (1989) and Choudhary *et al.* (1988) in the case of $AlPO_4$-5, no loss in crystallinity was observed after acid washing the calcined S11(3) sieve even though its porosity decreased. The greater stability of the $AlPO_4$-11 framework compared to that of $AlPO_4$-5 framework may explain why S11(3) showed no decrease in crystallinity after acid washing. The decrease in porosity of S11(3) after acid washing in nitric acid may be due to the incomplete removal of extra-framework species generated by the leaching (during acid washing) of the framework aluminium or P by the NO_3^- ion [Hampson *et al.*, 1989].

No reduction in crystallinity was observed after mild steaming of S11(3) [Sample MS(6)-S11(3)] but MS(6)-S11(3) did have a lower hexane adsorption value compared to S11(3) (3.5 wt% versus 4.5 wt%). Barger *et*

al. (1992) have shown that even after severe steaming conditions (700°C, 100% steam) the crystallinity of SAPO-34 is only reduced by 20%. Choudhary *et al.* (1988) have also shown that the crystallinity and pore volume of $AlPO_4$-5 decreases with increasing steaming time. The decrease in pore volume of S11(3) after hydrothermal treatment is consistent with the results of Choudhary *et al.* (1988). The fact that the steamed S11(3) sample of this study showed no loss in crystallinity suggests that the framework of SAPO-11 sieves are more resistant to steam/hydrothermal treatments than $AlPO_4$-5 but that steaming still removes framework species from the SAPO-11 structure which deposit in the channel system thus causing a reduction in pore volume.

Impregnating S11(3) with Ni and Co (*ca.* 4 wt%) did not change the % crystallinity relative to calcined S11(3) but dramatically decreased the surface area and adsorption capacity. This indicated that metal impregnation had resulted in Ni/Co occlusion at the entrance to or within the pores. Kraushaar-Czarnetzki and van Hooff (1989) have shown that after pore volume impregnations of $AlPO_4$-5 with cationic, anionic and neutral nickel species, that the nickel existed preferentially on the external surface (XRD showed $2\theta=44.5^\circ$ [111] reflection of nickel) of the $AlPO_4$-5. The pore volumes of their nickel-impregnated catalysts did not change dramatically after the nickel-impregnation procedures. Unlike $AlPO_4$-5, SAPO-11 is not neutral and hence there may be contributing driving forces for nickel ions to enter the pores and cause pore blockage. It should be pointed out however that very little nickel (<0.2 wt%) could be exchanged into S11(3) by ion-exchange in 2 M $Ni(NO_3)_2$ solution. Similarly Lee *et al.* (1991) have found that very little Cu^{2+} (0.3 wt%) could be exchanged into H-SAPO-11 and that after ion-exchange in $Cu(NO_3)_2$ the crystallinity was reduced by 33%. Therefore it is more likely that due to the low ion-exchange capacity of S11(3) that the Ni/Co species would be located at the pore mouth. Due to the smaller pore size of SAPO-11 (6.3Å) compared to $AlPO_4$-5 (8Å), the effect of pore mouth blockage by metal impregnated species is greater than for $AlPO_4$-5.

4.3.3 Acidity of SAPO-11 and modified SAPO-11 sieves

The acid site strength of all the SAPO-11 sieves as determined by NH_3-TPD was generally weaker (T_{max}<350°C) than for e.g., H-ZSM-5 [Anderson, 1991; Schwarz *et al.*, 1989], a finding also reported by other workers [Khouzami *et al.*, 1988; Lui *et al.*, 1991; Thomson *et al.*, 1990a, 1990b; Tapp *et al.*, 1988a]. Since the relative pore sizes of SAPO-11 and ZSM-5 are similar a comparison of their TPD peak

maxima should not be affected by diffusional constraints but rather by acid strength differences. It is known however that diffusional constraints in molecular sieves can cause the ammonia desorption peak to shift thus making it difficult to assign peak temperatures to acid site strengths [Gorte, 1984; Karge, 1991]. Diffusional constraints will not however effect the number of acid sites determined by the NH_3-TPD procedure. There was no change in the number or strength of acid sites for SAPO-11 whether the sieve was synthesized by mechanical or magnetic stirring (both have similar pore volumes and BET surfaces areas so comparison of acid site strengths should be valid).

Chemical analysis of S11(3) revealed that there was very little Si present (0.4 wt%). If every Si atom substituted for a P atom this amount of Si would at the most generate 0.16 mmol/g of acid sites. This accounts for only 40% of the acid sites as detected by NH_3-TPD. This discrepancy between the amount of acid sites generated due to Si substitution for P and the amount detected by NH_3-TPD is most probably due to the contributing effect of AlPO phases in the SAPO-11 sieve [Peeters *et al.*, 1992]. The number of strong acid sites decreased with increasing Si concentrations in the gel and higher synthesis temperatures. Khouzami *et al.* (1988) have synthesized SAPO-11 sieves with increasing amount of Si in the framework. They have shown that the activity for propanol dehydration increased with increasing Si content (of the sieve), but that beyond an (Al/P+Si) ratio of 0.86 the activity began to drop. For the SAPO-11 sieves synthesized in this study the reduction in the number of acid sites with increasing gel Si content (high temperature syntheses) indicates that less Si is being incorporated for P when higher gel Si concentrations are used. It has been shown that at higher Si content, Si substitutes for Al:P pairs [Martens *et al.*, 1990; Khouzami *et al.*, 1988]. This substitution mechanism would not be expected to increase the number of acid sites, and this may be the case for our SAPO-11 sieves. However, given the low Si contents of the SAPO-11 sieves this seems unlikely and the reduction in the number of acid sites may be due to pore blockage by extra-framework species.

Silanized and acid washed S11(3) showed a reduction in the number of acid sites compared to S11(3). The reduction in number of acid sites after silanization was most probably due to pore mouth blockage by extra-framework Si species. The reduction in the number of acid sites of silanized S11(3) will also be due to the fact that the actual mass of acidic SAPO-11 catalyst has been reduced by nature of the fact that Si has deposited on the sieve, therefore per mass of silan-SAPO-

11 the number of sites will decrease. It is estimated that *ca.* 5-10 wt% Si was deposited on the sieve and therefore the number of acid sites per g of silan-SAPO-11 catalyst should be at least 5-10% lower than S11(3). The number of acid sites however drops by *ca.* 50% suggesting that Si is not only on the surface but is also completely blocking the pores preventing NH_3 from entering to react with acid sites within. The loss in acidity after acid washing may also be due to pore blockage by extra-framework aluminium species preventing the ammonia from entering the pores to react with the acid sites.

Mild and severely steamed S11(3) showed a reduction in the number of strong acid sites compared to S11(3). This reduction in the number of strong acid sites after steaming was accompanied with the formation of new distinct HTD peaks. It is well known that steaming reduces the number of acid sites in zeolites and that under optimal conditions new strong acid sites may be generated [Lago *et al.*, 1986]. The reduction in the number of acid sites after steaming S11(3) is consistent with the results reported by Barger (1992) for SAPO-34, who showed that steaming reduced the number of strong acid sites of SAPO-34. The appearance of new stronger acid sites after hydrothermal treatments of SAPOs has not been reported. These strong sites may be due to electronic interactions between extra-framework and framework species resulting in strong acidity as has been suggested in the case of zeolites.

No reduction in the number of acid sites was observed for nickel and cobalt impregnated S11(3), even though hexane and N_2 adsorption data indicated pore restrictions. Since it is known that NH_3 (kinetic diameter=2.6Å) is smaller than N_2 (3.64Å) or hexane (4.3Å) [van Hoof and Roelofsen, 1991; Csicsery, 1984] the NH_3 may be able to diffuse past the extra-framework pore constricting metal species to probe the acid sites. Water (2.65Å), which also has a smaller diameter than N_2, would be expected to diffuse past the extra-framework metal ions, and as shown in Table 3.12, the water adsorption value is similar to that of the parent material, S11(3).

4.3.4 Location and reducibility of metals in MeAPSO-11 sieves

The location and state (i.e. oxidation state and coordination number) of the metals in MeAPSO-n sieves is of great importance since the incorporation of Me^{2+} for Al^{3+} introduces acidity which impacts on the catalytic activity of the sieve. The possible locations of the metal ions are listed below:

(i). Framework species (Me^{2+} or Me^{3+} in tetrahedral or octahedral coordination).

(ii). Ion-exchange positions or charge balancing positions (e.g. metals in 6-ring channels etc.).

(iii). Me^{2+} or Me^{3+} oxides, either internal (pores) or;

(iv.). external on the surface of crystallites or as a separate metal rich phase.

Table 4.2 lists the elements that have been reportedly substituted into the framework of $AlPO_4$-n molecular sieves. The location and state of each metal and its effect on the structure, morphology, porosity and acidity of the sieve will be discussed separately below. For all the sieves the substitution of Me^{2+} for P was not considered as this would have resulted in a positively charged framework and led to the formation of Me-O-Al bonds, both of which are unlikely possibilities, evidence for which has not been reported to date [Flanigen *et al.*, 1986; Shirlikar *et al.*, 1989; Kraushaar-Czarnetzki *et al.*, 1991a,b].

Table 4.2. Elements reportedly substituted into $AlPO_4$-n structures

	charge	ionic radius (nm)x10^3	Electronegativity (Pauling) (eV)
Li	1+	68	0.98
Be	2+	35	1.57
Mg	2+	66	1.31
Mn	2+	80	1.55
Co	2+	63	1.88
Zn	2+	74	1.65
Fe	2+	78	1.83
Sn	2+	93	1.80
Ni	2+	69	-
Fe	3+	64	1.96
Ga	3+	62	1.81
B	3+	23	2.04
As	3+	58	2.18
Si	4+	41	1.90
Ti	4+	61	1.54
Zr	4+	72	1.33
Ge	4+	53	2.01
Sn	4+	69	1.96
As	5+	50	2.18
V	5+	54	1.63
Al	3+	50-	-
P	5+	-	-

Nickel containing SAPO-11

To date only a few reports concerning nickel containing $AlPO_4$-n type molecular sieves have been published (Section 1.4.4.2). The majority of workers [Xu *et al.* (1992); Mavrodinova *et al.* (1991); Lechert *et al.* (1991)]

have suggested that both framework and extra-framework nickel species were present (e.g. ion-exchange Ni^{2+} or separate octahedral Ni). Rajic *et al.* (1991) have provided evidence that the Ni^{2+} in NiAPO-21 and NiAPO-12 had replaced hexacoordinate aluminium and was octahedrally coordinated by the oxygen atoms of the framework. For Ni^{2+} to exist in the framework of SAPO-11 it would be expected to be in tetrahedral coordination with oxygen, although, as shown by Rajic *et al.* (1991), Ni^{2+} prefers octahedral coordination.

The physicochemical characterization data from this study showed that NiS11(2) was of the AEL structure type and was 70% crystalline, relative to S11(3). The surface area of NiS11(2) was *ca.* 30 m^2/g lower than that of S11(3). The reduction in surface area and pore volume suggested that there were extra-framework species present. Chemical analysis also showed that extra-framework nickel and/or aluminium was present since the (Al+Me)/(Si+P) ratio was greater than 1. These results are consistent with those of Mavrodinova *et al.* (1991) who have shown that NiAPSO-5 was 90% crystalline relative to SAPO-5 and that the pore volume of NiAPSO-5 was *ca.* 67% of that of SAPO-5. The chemical analyses of Mavrodinova *et al.* (1991) for NiAPSO-5 showed the (Al+Me)/(Si+P) ratio to be 1.33, similar to the value observed in this study for NiS11(2) (1.23).

XRD spectra of calcined NiS11(2) showed no sign of any large Ni/NiO species (XRD is only expected to detect particles greater than 20Å) present in NiS11(2) (i.e. no 2θ peak 44°). Mavrodinova *et al.* (1991) have also observed that XRD spectra of calcined NiAPSO-5 (synthesized using Ni(Ac) as the nickel source) showed no 2θ peaks at 44.3° and 50.7° (Co-Kα) indicating that the extra-framework nickel species were highly/finely dispersed. These nickel species were proposed to be located within the pores of the sieve and responsible for pore blockage. No separate amorphous material was evident from SEM analysis which showed NiS11(2) to have similar morphology to S11(3). Mavrodinova *et al.* (1991) have observed separate single crystallites for NiAPSO-5 which were low in nickel compared to the other hexagonal crystallites. Xu *et al.* (1989) have observed highly crystalline NiAPO-5 consisting only of hexagonal prisms. The

SEM results of NiS11(2) are consistent with those of Xu *et al.* (1989), in that only single phase material is present. This suggests that the nickel is well dispersed and not present in separate crystals as observed by Lechert *et al.* (1991) for NiAPO-5.

Ion-exchange with ammonium nitrate succeeded in removing 30% of the nickel from NiS11(2). No structural or morphological changes were observed after this procedure (i.e. XRD, FT-IR and SEM remained the same) but the pore volume was reduced; hexane adsorption value decreased from 3.8 to 2.5 wt%. To date no work has been reported investigating the ion-exchange properties of NiAPSO-11 sieves. Hampson *et al.* (1989) have shown though that calcined $AlPO_4$-n molecular sieves show loss of crystallinity, via phosphorous extraction from the framework, when placed in salts solutions. Since ion-exchange in ammonium nitrate is essentially the same as placing the catalyst in a salt solution it is possible that P would also be extracted from NiS11(2). Indeed P analysis of the ammonium nitrate ion-exchange solution proved positive and chemical analysis of the sieves after ion-exchange showed that 8% of the P had been extracted from NiS11(2). Incomplete removal of this extra-framework P species may explain the reduction in pore volume after ion-exchange. Montes *et al.* (1990) have observed P removal from CoAPO-5 after ion-exchange and have proposed this extra-framework P may exist as $H_2PO_4^-$ (or HPO42- and PO43-) species present as charge balancing for extra-framework Co^{2+} or template+. Occluded P as $H_2PO_4^-$ has also been reported in the case of $AlPO_4$-52 [Bennet *et al.*, 1989]. The fact that at least 30% of the nickel could be removed by ion-exchange provides further evidence that the nickel added to the synthesis mixture did not incorporate into the framework but rather exists in extra-framework positions.

NiS11(2) had the same number of acid sites as S11(3) but the LTD peak position was slightly lower indicating a slight weakening of acidity compared to S11(3). Similarly Inui (1991) has also shown that NiAPSO-34 has weaker acid sites than SAPO-34. The weakening in acidity is probably due to nickel species occupying ion-exchange type positions as it is known that ion-exchange cations reduce/weaken the acidity of zeolites [Minachev and Isakov, 1976]. Since there was no decrease or increase in the number of acid sites after ion-exchange with ammonium nitrate it was assumed that the Ni^{2+} species that were removed by ion-exchange did not contribute towards the number of acid sites in NiS11(2).

TPD-MS showed that the majority of the template desorbed from as-synthesized NiS11(2) as undissociated template. TG-DTA also showed that the template decomposition occurred *ca.* 100°C lower than, for e.g., S11(3). The TPD-MS results of Tapp *et al.*, (1988a) showed that, in the case of weakly acidic $AlPO_4$-11, template desorbed undissociated. Gorte *et al.* (1991) have suggested that the decomposition temperature for organic amine probes did not appear to be sensitive to the strength of the acid site so long as the strength was above a certain minimum. In our case the acid strength of NiS11(2) may be below that minimum strength which would explain why decomposition of the template occurred some 100°C lower than for S11(3) and the other MeAPSO-11 sieves. The weaker acidity may also explain why the majority of the template desorbed undissociated.

TPR data suggested that the nickel was in ion-exchange type positions as evident from the similar reduction temperatures to those of nickel in ion-exchange positions of Zeolite-Y [Suzuki *et al.*, 1989]. The nickel species that were ion-exchanged were responsible for the T_{red}=640°C peak in the TPR spectra of NiS11(2).

Reduction of the calcined nickel-containing samples showed excess hydrogen consumption, based on 2 H^+ for every Ni^{2+} species. A high temperature reduction peak which appeared at 950°C accounted for this excess. The amount of hydrogen consumed after a second reduction, however, (i.e. TPR of previously reduced NiS11(2)) corresponded to the amount of nickel present as determined by AA. This unusual behaviour has not been reported to date. After reduction to 650°C, 800°C and 1000°C Ni/NiO species, as detected by XRD (2θ=44°), were present and thus suggested that during the reduction nickel had not surprisingly migrated to the outer surface of the crystallites [Minachev and Isakov, 1976; Hurst *et al.*, 1982]. It is proposed that the high temperature reduction at 950°C (Figure 3.26) may be associated with the reaction of surface Ni^0 species, as detected by XRD, with terminal P=O or P-OH groups [Sauer and Schirmer, 1988; Sauer, 1989] to form NiP which may then be reduced at 950°C to release phosphine as shown below:

$$Ni^0 + P{=}O/P\text{-}OH(t) \rightarrow Ni_2P/NiP_2 + H_2O \text{ (Below 950°C)}$$

$$NiP/NiP_2 + H_2 \rightarrow Ni^0 + PH_3 \text{ (950°C)}$$

This reaction would result in a loss of terminal P=O/P-OH groups and may explain why, after the second reduction, there was no high temperature reduction, since the terminal P-OH groups would have been consumed during the first reduction. Phosphine can be produced by the reduction of ammonium phosphates, orthophosphoric acid and metaphosphoric acid with hydrogen at temperatures above 600°C [Mellor, 1971].

Another possibility is that the hydrogen may be become activated by the Ni^0 at high temperature (i.e. a spillover effect) [Sermon and Bond, 1973] and that these $H^{\cdot}$ species may react with the terminal P=O/P-OH groups to either release water or possibly liberate phosphine.

Iron containing SAPO-11

XRD and FT-IR showed that FeS11 had the AEL structure type but that it was only 60% crystalline compared to S11(3). FeS11 had a much higher (Al+Me)/(Si+P) ratio compared to S11(3) indicating that extra-framework iron or aluminium was present. The surface area and hexane adsorption values of FeS11 were also much lower than those of S11(3) suggesting that these extra-framework iron or aluminium species were occluded within the pores. SEM analysis also showed that FeS11 had amorphous type material present in conjunction with crystalline material. This amorphous material may have been rich in iron or aluminium.

The green colour of as-synthesized FeAPSO-11 suggests that iron is not in framework since, in a study of FeZSM-5, only white Fe-ZSM-5 was shown to have tetrahedral framework iron and green FeZSM-5 had extra-framework iron [Meagher *et al.*, 1988]. Likewise the brown colour after calcination has been attributed to FeO species [Meagher *et al.*, 1988].

No iron could be exchanged from FeS11DB. Iron in the framework or FeO species would not be expected to be exchanged into solution. It has been found that Fe^{3+} in the 6-ring channels of ZSM-5 were non exchangeable [Kan *et al.*, 1991], and a similar effect may be present here since $AlPO_4$-11 type sieves also have 6-ring channels. XRD and FT-IR spectra of ion-exchanged FeS11 were similar to those of the as-synthesized FeS11 and not the calcined FeS11 as was the case for NiS11(2). Since it has been established that the changes in 2θ and the multiple T-O absorption features

were due to water interaction with the calcined sieves' framework, the changes after ion-exchange indicate that there are no water interactions after ion-exchange of calcined FeS11. FT-IR also showed that there was a large absorption at 1385 cm^{-1} due to the presence of the nitrate ion.

Garten *et al.* (1970) have shown that it is possible to differentiate between tetrahedral and octahedral iron species, and therefore framework and extra-framework iron, from room temperature Mössbauer spectroscopy. The parameter used is the isomer shift (I.S.) parameter and a value of less than 0.3 mm/s indicates tetrahedral ferric and I.S. > 0.3 mm/s octahedral ferric (Section 1.7). Using this criterion it can be concluded that no tetrahedrally coordinated iron was present in the FeS11 sample of this study. Furthermore the quadrupole splitting (Q.S.) values are also consistent with those of Fe^{2+}/Fe^{3+} species in octahedral coordination. The I.S. and Q.S. values obtained in this study for FeS11DB are similar to those obtained by Park *et al.* (1992) and were assigned as an FeO species and an iron aluminium phosphate species, i.e. iron is not in the framework.

The Mössbauer spectroscopy results of this study also showed that little Fe^{2+} was present in FeS11syn molecular sieve even though Fe(II)Acetate was used as the iron source in the synthesis gel. It has been suggested that Fe^{2+} species in a synthesis gel at a pH of *ca.* 10 are oxidized in the autoclave [Ojo *et al.*, 1989], which may explain why little Fe^{2+} was present in as-synthesized FeS11. Ojo *et al.* (1989) has shown that by purging the autoclave with nitrogen the amount of Fe^{2+} in the final product increases.

According to the Mössbauer results, after calcination in air at 500°C, only Fe^{3+} species were present. Other workers have reported similar behaviour for FAPO-5 after air calcination [Park *et al.*, 1992; Pang *et al.*, 1989; Schubert *et al.*, 1989]. It has also been shown that calcining at increasing temperatures or in the presence of steam results in the formation of α-Fe_2O_3, Fe-phosphates and Fe-Tridimite [Schubert *et al.*, 1989]. The formation of these phases was accompanied by a reduction in what was assigned as framework Fe^{3+}(tetrahedrally coordinated) [Schubert *et al.*, 1989].

In summary Mössbauer spectroscopy has shown that all of the iron species are in octahedral coordination, i.e. not in the framework of FeS11.

Furthermore, after calcination in air at 500°C, only Fe^{3+} octahedral species exist.

FeS11 had the same number and similar strength of acid sites as S11(3). The Mössbauer data showed that only extra-framework Fe^{3+} species exist and these would not be expected to contribute towards the acidity of the sieve. Therefore the acidity of the FeS11 must be due to the substitution of Si into the framework for P. The decrease in the number of acid sites after ion-exchange can possibly be explained by the incomplete removal of extra-framework P species or by structural collapse due to P removal from the sieve as will be discussed in the case of CoS11.

The TPR data also provides further evidence that some of the iron species in FeS11 exists as extra-framework FeO species. The low temperature reduction peaks correspond to those obtained by Unmuth *et al.* (1980) for α-Fe_2O_3 on Si shown below and were also similar to those of bulk Fe_2O_3 (Table 3.15):

$H_2 + 3\alpha\text{-}Fe_2O_3 - 2\ Fe_3O_4 + H_2O\ \alpha = 343°C.$
$4H_2 + Fe_3O_4 - 3\alpha\text{-}Fe + 4H_2O\ \beta = 472°C.$

TPR also showed that FeS11 had a high temperature reduction peak at *ca.* 1000°C and that excess hydrogen was consumed. The excess consumption during the first reduction may be due to the formation of FeP species and subsequent reduction of these species to release phosphine [Mellor, 1971] as was suggested for NiS11.

Cobalt containing SAPO-11

Although XRD confirmed that the only crystalline phase present was that of AEL type, chemical analysis showed that extra-framework aluminium or cobalt was present, i.e. the (Me+Al)/(Si+P) ratio was greater than 1. CoS11 had significantly lower surface area and hexane adsorption values compared to S11(3) and it seems most likely that this was due to pore blockage/constriction by extra-framework cobalt or aluminium species. Extra-framework cobalt or aluminium has been proposed to be occluded within the pores of CoAPO-11 and CoAPO-5 [Prasad and Balakrishnan, 1991; Kraushaar-Czarnetzki *et al.*, 1991a,b; Borade and Clearfield, 1992;

Shiralkar *et al.*, 1989]. Kraushaar-Czarnetzki *et al.* (1991) and Xu *et al.* (1989) showed that no separate aluminium or cobalt rich phases were present in CoAPO-5. SEM analysis of CoS11 showed that there was separate amorphous material present which may be cobalt or aluminium rich.

As-synthesized CoS11 had an intense blue colour which is normally associated with that of tetrahedral Co(II) species [Cotton and Wilkinson, 1988]. Octahedral Co(II) species are usually pink. Rajic *et al.* (1990) have synthesized CoAPSO-14 and -34 and shown that the amorphous materials, and hence those containing extra-framework octahedral cobalt, were pink in colour. The crystalline samples were blue. It should be pointed out however that X-Ray amorphous CoAPSO materials have also been shown to have an blue colour [Prasad and Balakrishnan, 1991] and therefore the colour of the sieve is not a significant enough result in itself to suggest Co^{2+} incorporation (i.e. tetrahedral coordination) into the framework. After calcination in air the colour of as-synthesized CoS11 changed from blue to green. This colour change after calcination been reported by other workers for various CoAPSO materials [Iton *et al.*, 1989; Chen *et al.*, 1992] and has been attributed to a redox reaction (Section 1.4.4.2). This reaction has been proposed to be reversible and can be induced by methanol adsorption i.e. Co^{3+} + MeOH → Co^{2+} [Kraushaar-Czarnetzki *et al.*, 1991a,b; Iton *et al.*, 1989].

After hexane adsorption the colour of calcined CoS11 (green) reverted to that of the as-synthesized material (blue). It is unlikely that hexane can donate or accept electrons therefore this colour change is not likely to be due to redox reaction. Pereira *et al.* (1992) have suggested that the colour change after calcination and subsequent adsorption with methanol is due to changes in the coordination number and not the oxidation state.

Ion-exchange showed that at least 45% of the cobalt was exchangeable. The colour of ion-exchanged CoS11 also reverted to blue. No further colour changes were observed after ion-exchange which indicated that either the relevant redox reaction was not reversible after ion-exchange or that the species that were exchanged were responsible for the colour changes.

NH_3-TPD showed that the number of acid sites of CoS11 increased compared to S11(3) which would be consistent with Co^{2+} substitution for Al^{3+} in the framework of SAPO-11 [Tapp *et al.*, 1985]. After ion-exchange however the number of acid sites decreased. This indicates that the Co species that were removed by ion-exchange may have been contributing towards the acidity of CoS11, unlike in the case of NiS11(2) were the the Ni^{2+} ions that were exchanged showed no contributing effect. Another possible explanation for this result may be that the P species removed either from the framework or from extra-framework positions may have resulted in either structural/pore collapse or remained in the pores to cause severe pore blocking and thus preventing NH_3 from chemisorbing to the acid sites. Certainly after ion-exchange the pore volume of CoS11 was reduced suggesting that more extra-framework material had been generated. If this were the case then the Co^{2+} ions that were removed by ion-exchange may in fact not have been contributing towards the number of acid sites and therefore the increase in acidity of CoS11 compared to S11(3) may be due to Co^{2+} substitution into the framework, consistent with the results of Tapp *et al.* (1985).

It was evident from the much higher reduction temperatures compared to bulk CoO that there were strong metal support interactions between extra-framework cobalt and the SAPO framework. Strong interactions have been proposed by Kraushaar-Czarnetzki *et al.*, (1991a,b) who have shown that cobalt whether impregnated or in the framework, affected the P-NMR spectra to the same extent. From our respective TPR profiles alone little could be distinguished between the reduction behaviour of cobalt whether in Co(imp)S11(3) or CoS11. TPR of Co(imp)$AlPO_4$-11 [Kraushaar-Czarnetzki *et al.*, 1991a,b] showed reductions at 300-450°C and the beginning of a reduction at 600-650°C for Co(imp)$AlPO_4$-11. These authors only reduced to 700°C and hence did not see the high temperature reductions observed in this work. Very little reduction up to 700°C was observed for CoAPO-11. The TPR results showed that strong interactions existed between cobalt and the SAPO-11 framework whether impregnated or incorporated into the framework. TPR to 1000°C also indicated excess hydrogen consumption during the first reduction. This may be due to the reduction of Co(II)phosphide and subsequent phosphine release as was explained for the NiAPSO-11 sieves.

Manganese containing SAPO-11

As was observed for the other MeAPSO-11 sieves used in this study, XRD and FT-IR spectra showed that MnS11 had the AEL structure type. Chemical analysis showed that of all the sieves MnS11 had the lowest (Al+Me)/(Si+P) ratio but that the ratio was still greater than 1, indicating that extra-framework aluminium or manganese was present. The surface area of MnS11 was 43 m^2/g lower than for S11(3) and the hexane adsorption value was also lower than that of S11(3). The decrease in porosity is most probably due to extra-framework manganese or aluminium. Various workers have shown that Mn^{2+} substitutes preferentially for Al^{3+} in MnAlPO-11 and MnAPSO-44 sieves [Brouet *et al.*, 1991; Goldfarb 1989; Kuperman *et al.* 1992] and that extra-framework Mn^{2+} species were present.

MnS11 had more acid sites compared to S11(3) which is consistent with Mn^{2+} incorporation into the framework of SAPO-11. Ion-exchange however, showed that there was extra-framework manganese present, since 50% of the loaded manganese could be exchanged.

The colour of MnS11 changed from white to pink, typical of octahedral Mn^{2+} species (i.e. not in the framework), after calcination in air. TPR showed that this extra-framework manganese could not be reduced but that the colour returned to white, the colour of $Mn(OH)_2$.

The above characterization results for the MeAPSO-11 sieves indicate that certainly in the case of NiS11(2) and FeS11 no tetrahedrally coordinated framework metal species existed. For CoS11 and MnS11 the increase in number of acid sites compared to S11(3) is consistent with Me^{2+} incorporation into the SAPO-11 framework. Both of these sieves however, have extra-framework metal species present that can be removed by ion-exchange.

4.4 PROBE REACTIONS

4.4.1 *m*-Xylene isomerization

m-Xylene isomerization has been used extensively to probe the shape selective and acidic properties of various medium pore molecular sieves [Jacobs and Martens, 1986; Corma *et al.*, 1993; Kumar and Ratnasamy, 1989; Joensen *et al.*, 1989; Richter *et al.*, 1989]. It is generally accepted that product *p*/*o*-xylene ratios of greater than 1 imply that the catalyst is shape selective [Richter *et al.*, 1989] since at 450°C, the reaction conditions used in this study, the thermodynamic equilibrium *p*/*o*-xylene ratio is 0.95 (Thermodynamic conversion *ca.*=50%). The *p*/*o*-xylene ratio is also a function of conversion due to the reversible nature of the reaction [Richter *et al.*, 1989, Corma, 1993]. It was proposed that this reaction would be able to show the influence of metals in the framework on the acidity and pore size of MeAPSO-11 sieves.

Steady state *p*/*o*-xylene ratios decreased as follows: MnS11 > S11(3)≅CoS11 > FeS11 > NiS11≅Acid-S11(3) (Table 3.16). The steady state *p*/*o*-xylene ratios for all of the sieves tested were greater than 1, and given that the thermodynamically expected ratio is 0.95, this implies that the sieves were para-selective. Since the steady state conversions were similar the *p*/*o*-xylene ratios can compared without the effect of conversion having to be taken into account. Yang *et al.* (1991) and Oh and Lee (1993) have also shown that SAPO-11 and various MeAPO-11 sieves are para-selective for the toluene alkylation (with methanol or ethanol) reaction. Oh and Lee (1993) showed CoAPO-11 to be the most para-selective of the sieves tested (49.2%). Considering the pore dimensions of SAPO-11 (6.3x3.9Å), i.e. medium pore size, it is not surprising that the sieves showed para-selectivity as other medium pore sieves are known to be para-selective due to diffusional constraints. Yang *et al.* (1991) have shown SAPO-11 to have similar diffusional properties to ZSM-5, a catalyst which has well known para-selective properties.

The steady state conversions of *m*-xylene were similar for all the sieves (Table 3.16). This reaction has been shown to correlate well with the amount of strong acid sites in zeolites [Vinek and Lercher, 1991; Babu *et al.*, 1983]. The activity trend seen for the sieves in this study may also

therefore be an indication of the amount of strong acid sites present. Although NH_3-TPD showed no distinct HTD features the amount of strong acid sites, i.e. those which held ammonia to 450°C or above, were similar for all the sieves (0.19-0.22 mmol/g). Since the conversions are similar and the amounts of strong acid sites are similar it seems possible that for SAPO-11 type catalysts the activity is reflecting the amount of strong acid sites present.

FeS11 had the highest initial conversion of all of the sieves and also produced the most disproportionation products (toluene and trimethylbenzenes). High selectivities for the disproportionation products have also been obtained by Pyke *et al.* (1985) for Fe-containing $AlPO_4$-5 samples. These workers showed that, for the *m*-xylene isomerization reaction, FAPO-5 produced toluene in greater amounts compared to SAPO-5. Szostak *et al.* (1988), have shown that framework and non-framework metals strongly influence the activity and selectivity of catalytic reactions. By reacting ortho- or para-ethyltoluene over Fe-ZSM-5 catalysts with increasing amounts of extra-framework iron (achieved by using pretreatment conditions such as steaming or high temperature calcination), the amount of methylstyrene in the reaction product increased. The increase in methylstyrene in the reaction product was attributed to the presence of the extra-framework iron species. Kan *et al.* (1992) have shown that for the dehydrogenation of ethylbenzene to styrene reaction, $AlPO_4$-5 had very little dehydrogenation activity (2% conversion). FAPO-5 (60.6%) and FAPSO-5 (84.2%) on the other hand were found to active, a result due not only to their increased acidity compared to $AlPO_4$-5 but also due to the presence of iron in extra-framework positions.

Corma *et al.* (1993) have shown that xylene adsorption capacity of the Zeolite-Y sieve influences the xylene isomerization reaction mechanism. Increased concentrations of xylenes in the zeolite channels can change the kinetic model so that xylene products are formed from bimolecular secondary reactions. These workers have subsequently urged that care be taken when analyzing results to ensure that the xylene products are primary products, i.e. from unimolecular mechanism and not produced as a result of secondary reactions. These bimolecular reactions are not likely to occur inside medium pore sieves due to size constraints: i.e. due to restricted transition state selectivity. It is interesting to note however that FeS11 had

a larger *m*-xylene adsorption value than NiS11(2) or MnS11 (Table 3.12) even though FeS11 had a lower pore volume as determined by hexane and nitrogen adsorption.

The *m*-xylene isomerization results showed that all the sieves were para-selective and hence had shape selective properties and that the steady state conversion/activity correlates well with the amount of strong acid sites present.

4.4.2 2-Methyl-2-pentene isomerization

The 2-methyl-2-pentene isomerization reaction has been shown to be a good reaction to probe the relative acidity of solid acid catalysts of medium strength [Kramer and McVicker, 1986]. The relative rates of conversion (or selectivity) to isomers requiring skeletal rearrangement of the hydrocarbon framework (*c*/*t*-3-methyl-2-pentene) as opposed to proton or 1,2 hydride shift (*c*/*t*-4-methyl-2-pentene) can be used to define the relative acidity scale [Kramer *et al.*, 1985]. Since the NH_3-TPD results showed that the SAPO-11 type sieves were of medium strength it was proposed that this reaction would be appropriate to probe the differences in acidity between the SAPO-11 and MeAPSO-11 sieves.

The relative steady state ratios of skeletal isomerization to double bond shift products decreased as follows: S11(3) > MnS11 > NiS11(2) > CoS11 ≃ FeS11 (Table 3.17). The steady state conversion trend for 2-methyl-2-pentene isomerization decreased as follows: S11(3) ≃ MnS11 ≃ NiS11(2) > CoS11 ≃ FeS11 (Table 3.17). For alumina catalysts this ratio varied between 0.1-3 [Kramer and McVicker, 1986] and for this study the ratios were similar and varied between 0.1-1.8.

The observed trend in the ratio of skeletal isomerization to double bond shift products of S11(3) > MnS11 > NiS11(2) indicates that S11(3) has more strong acid sites than MnS11 followed by NiS11(2). Their respective conversions were similar and therefore the selectivities (or ratio of selectivities) can be compared. NH_3-TPD however showed that MnS11 had *ca.* 26% more acid sites (of similar strength) compared to S11(3). It would be expected therefore that an increase in the number of sites would result in an increase in the conversion, but as this was not observed for MnS11

compared to S11(3) there was obviously another factor influencing the conversion, such as diffusional constraints. The kinetic diameter of 2-methyl-2-pentene (*ca.* 5.0Å) is close to that of the dimensions of the SAPO-11 (6.3x3.9Å) pores but at the reaction temperatures employed the diffusion of the molecule in the pores would be expected to be facile. Barrer (1988) has also shown that SAPO-11 is capable of adsorbing molecules with dimension of 6Å, such as cylcohexane. However if metal species were constricting the pores, such as the decreased hexane adsorption data showed was the case for the MeAPSO-11 sieves, it would be expected that the isomerization activity would be reduced since the 2-methyl-2-pentene molecules may not be able to reach the internal acid sites. However, the difference in the selectivity ratio of the skeletal isomers to double bond shift isomers, between MnS11 and S11(3) still reflects the relative amounts of strong acid sites as was probed by 2-methyl-2-pentene, i.e S11(3) has more stronger acid sites than MnS11.

NiS11 was more active for 2-methyl-2-pentene isomerization than CoS11, a result not expected considering their respective strength of acid sites as determined from NH_3-TPD (CoS11 >> NiS11). However considering that the pore volume of NiS11 is greater than that of CoS11 due to the effect of extra-framework material, the result is not expected for the reasons described in the case of S11(3) and MnS11. The presence of extra-framework material probably also explains the low activity of FeS11 compared to S11(3) even though the two have identical NH_3-TPD characteristics.

The ratio of 2-methyl-1-pentene to 2-methyl-2-pentene was constant suggesting that these products were at equilibrium as has been suggested by Kramer *at al.* (1985). Reactions involving double bond shifts (which are very fast reactions) are often at equilibrium [Csicsery, 1992].

The results of the two probe reaction studies show the importance of using reactions to probe available catalyst acidity rather than ammonia TPD. Due its small size the diffusion of ammonia in the pores is hardly affected by the presence of extra-framework species and hence all the acid sites are probed even though some of these sites may be inaccessible to reacting species. The 2-methyl-2-pentene probe reaction showed that diffusional constraints can be more important than the amount or strength of the acid sites. The *m*-

xylene isomerization probe reaction showed that steady state conversions correlate well with the number of strong acid sites but that extra-framework metal species could have resulted in the presence of large amounts of disproportionation products as was observed for FeS11.

4.5 PROPENE OLIGOMERIZATION OVER SAPO-11 TYPE SIEVES

4.5.1 Effect of Si and metal addition to the synthesis gel

The conversion trend after 3 hours on stream for oligomerization over the different SAPO-11 sieves decreased as follows: S11(1)≃S11(2)≃S11(3) > S11(5)≃S11(4) > S11(6)≃S11(7) (Figure 3.32). This conversion trend correlates well with the decrease in the number of acid sites of these sieves (S11(3) > S11(4)≃S11(5)≃S11(6) > S11(7)). It would be expected that a decrease in the number of acid sites would reduce the catalytic activity of the sieve. The trend may also be showing the effect of the greater crystallite size of S11(6) relative to the other samples. Crystallite size is known to affect the oligomerization activity of ZSM-5 catalysts as was shown by Schwarz *et al.* (1991a,b). Large crystals of ZSM-5 were less active than small crystals and the activity difference was attributed to the difference in the depth of effective reaction surface in the crystallite.

The oligomerization activity for the MeAPSO-11 sieves decreased as follows:

S11(3)≃MnS11 > CoS11≃FeS11 > NiS11(2) (Figure 3.33)

Although there are no reported studies on the activity of MeAPSO-11 sieves for high pressure propene oligomerization, Rabo (1988) has shown that for low pressure hexene isomerization that MnAPSO-11 and SAPO-11 had similar conversions and produced similar amounts of oligomerization products. FAPO-11 (FeS11 without Si) on the other hand also had similar conversions to MnAPSO-11 and SAPO-11 but produced less oligomerization products and significantly more skeletal isomerization products.

The characterization results of this study showed that MnS11 had more acid sites than S11(3) but a lower pore volume possibly due to the presence of extra-framework species. The fact that MnS11 and S11(3) had similar oligomerization activities, even though MnS11 had more acid sites, may indicate again that the diffusional constraints caused by the extra-framework species as indicated by the lower pore volume of this sieve, counteracted the effect of the increased number of acid sites. The extra-

material may of course also be preventing product molecules from desorbing from the constricted pores and hence reduce the activity.

CoS11 was also shown to have more acid sites than S11(3) but a substantially lower pore volume than either MnS11 or S11(3). Its lower activity compared to S11(3) and MnS11 is also therefore likely to be due to the reduction in pore volume due to extra-framework metal species, thus preventing oligomer products from desorbing out of the pores. Coke analysis of CoS11 showed that the amount of soft coke present was similar to the amount of template desorbed on loss on ignition. Considering the similarities in density of dipropylamine (the template ρ=0.738 g/cm^3) and soft coke (C_6-C_{12} oligomers, $\rho \cong$0.68-0.75g/cm^3) and the similarity between the amount of coke and the amount of template it is proposed that the pores are filled by slowly diffusing C_{12} oligomers or coke species. This implies that propene was able to diffuse into the pores of CoS11 and react to form oligomers. Once formed these oligomer products cannot diffuse out of the pores due to the presence of extra-framework material and hence the catalyst deactivates. Similarly the low oligomerization activity for FeS11, which had similar strength and number of acid sites to S11(3), can be explained by the inability of product oligomers to diffuse out of the constricted pores.

NiS11 had weaker acid sites compared to S11(3) and a slightly reduced pore volume, both of which would be expected to reduce the oligomerization activity compared to S11(3) as explained above. The lower activity of NiS11(2) compared to S11(3) is therefore expected.

Under the oligomerization conditions employed, 250°C, WHSV=12 h^{-1} and 5 MPa, all of the sieves, except S11(7) and NiS11(2)-IX, produced the dimer as the major oligomer product. This was unexpected since thermodynamically heavier oligomers are favoured at high reaction pressures [Quann *et al.*, 1988]. Other workers, for e.g. Pellet *et al.* (1988) and Long *et al.* (1985), have shown that SAPO-11 is capable of producing heavier oligomers but that the majority of the product was the dimer fraction. The high selectivity for dimer was attributed to the catalysts' weak acidity and shape selectivity. The results of this study are consistent with those of Pellet *et al.* (1988) and Long *et al.* (1985) in that although appreciable amounts of nonenes and dodecenes are produced the major product is the

dimer. Catalysts with strong acid sites are more likely to strongly adsorb hexene thus increasing the probability of chain growth and the formation of larger oligomers. Catalysts with weak or medium strength acid sites (i.e. SAPO-11 type catalysts) would therefore have more dimer product compared to catalysts with stronger acid sites, which is what was observed when comparing the results of this study with those over ZSM-5 [Schwarz *et al.*, 1989, 1991a,b]. Schwarz *et al.* (1989) have also observed that for ZSM-5 with increasing Si/Al ratios (>64), and therefore reduced number and strength of acid sites, the amount of dimer in the product increases.

The linear relationship between yield of heavier oligomers and increasing conversion indicated a consecutive reaction mechanism as has been proposed elsewhere [Tabak *et al.*, 1986; Quann *et al.*, 1988]. This relationship explains the changes in selectivity of the unmodified sieves with different conversions for propene oligomerization.

The amount of coke for all the sieves except MnS11 and S11(4) corresponded well with the amount required for pore filling, i.e. the same amount as mass loss on ignition. The majority of this coke was "soft" coke and determined by FT-IR to be Type I (polyalkenes), but with increasing time on stream, the amount of "hard" coke (coke that can only be burned off in air at 500°C) present on the SAPO-11 type catalysts increased. Although the amount of "hard" coke increased, no Type II polyaromatic coke could be detected by FT-IR. The deactivation of these sieves is therefore not related to Type II coke formation as was the case for HPAs but more to the formation of so called "hard" coke. Such "hard" coke species may consist of long chain highly branched oligomers. This "hard" coke probably constricts the pore mouth restricting access of propene or preventing product oligomers from desorbing. In the interpretation of the coke data the possibility that the TG-DTA procedure may have been responsible for producing the "hard" coke, i.e. by high temperature polymerization of the Type I or "soft" coke species, was considered. It was unlikely however that this effect was occurring since it was shown that for coked catalysts after short run times no "hard" coke was present, i.e. the "soft" Type I coke did not form "hard" coke by the TG-DTA procedure.

Long *et al.* (1985) have suggested that a significant feature of the high pressure oligomerization process is "liquid phase embodiment" involving

contact between the olefin feed and the SAPO-11 catalyst. It is proposed that by contacting the olefin feed and the SAPO-11 catalyst in the liquid phase (at supercritical conditions, for propene $T_c = 92°C$) products results in increased lifetimes since it is proposed that the liquid washes the surface of high molecular weight products preventing build up of these products and therefore reducing the possibility of these compounds forming coke and deactivating the catalyst. Long *et al.* (1985) have also suggested that due to the low hydrogen transfer ability of these sieves, as indicated by lack of alkanes in liquid product, the propensity for aromatic production and coke production is reduced. These products are produced by hydrogen transfer. No aromatic products were found to exist on the coked SAPO catalysts of this study, i.e. no Type II coke, supporting the argument that these type of catalysts have low hydrogen transfer ability.

The above results indicate that the activity of SAPO-11 and MeAPSO-11 sieves for propene oligomerization is a function of the acidity, pore volume and possibly crystallite size. Deactivation occurs either due to the inability of product oligomers to desorb from pores constricted with extra-framework metal species or from pores constricted with "hard" coke. The absence of Type II polyaromatic coke indicates that the sieves have low hydrogen transfer capabilities. The preference for dimer, even though thermodynamically heavier oligomers are favoured, is the most probably due to the weakly acidic nature of the SAPO-11 sieve.

4.5.2 Effect of post synthesis modifications

Pellets and extrudates

The effect of pelletizing and extruding S11(3) was investigated because these forms, as opposed to powders, are used industrially to improve ease of handling and crushing strength of the catalyst and to reduce pressure drop over the reactor. Pellets of S11(3) were found to the more active than either powdered S11(3) or extrudates of S11(3). Schwarz *et al.* (1991b) have shown the opposite for ZSM-5, i.e. that pellets had decreased lifetimes and that extrudates of ZSM-5 were slightly more active than ZSM-5 powder.

For oligomerization over HPA it was shown that there were difficulties in transferring the heat of reaction from the catalyst to the bulk phase and that

by adding quartz sand to act as a heat dissipator the activity and lifetimes were improved. This was due to more isothermal conditions being achieved and therefore the avoidance of Type II coke formation which caused deactivation. For SAPO-11 sieves however, deactivation is thought to be due, not to Type II coke, but rather to "hard" coke formation which constricts the pores and prevents desorption of product oligomers. It is postulated that the pellets of SAPO-11 will also have heat transfer difficulties and therefore temperature gradients in the pellet would be expected. For SAPO-11 this will not result in lower activities since increasing temperatures did not cause deactivation: in fact they increased activity and lifetime. For extrudates the aluminium binder may act as heat dissipator, thereby reducing temperature gradients and inducing more isothermal conditions, which in this case would reduce activity due to a reduction in the temperature difference between the surface and bulk of the catalyst.

Steaming

Mild and severe steaming enhanced the activity and lifetime of S11(3) even though NH_3-TPD showed a reduction in the total number of acid sites after the hydrothermal treatment. Steaming is known to introduce new acid sites responsible for the increased activity as was shown by Lago *et al.* (1986) for ZSM-5. It is proposed therefore that these same strong acid sites that are formed in zeolites could be formed in SAPO sieves and be responsible for the increased activity of steamed SAPO sieves. Martens *et al.* (1990) have shown that zeolitic or SiAl domains exist in SAPO-11 sieves and it is possible that the acidity of these domains is enhanced by the steaming treatment.

The cetane number of the liquid product increased dramatically for mild steaming compared to the parent material. The lower hexane adsorption value indicated that some extra-framework material maybe present, which is consistent with the fact that steaming is known to extract aluminium from the framework of zeolites. It is possible that these extra-framework species may be causing confinement effects within the pores resulting in more linear products. This effect is an example of enhanced product selectivity. The liquid product of severely steamed S11(3) however had a lower cetane number than MS(6)-S11(3) but was similar to that of S11(3). More severe

conditions would be expected to produce more extra-framework material as was shown by Choudhary *et al.* (1988) for $AlPO_4$-5 but for SAPO-11 may also produce stronger acid sites responsible for cracking. This may explain why the severely steamed catalyst had a higher selectivity for dimer than S11(3) and a lower cetane number than MS(6)-S11(3). It should be pointed out that the cetane number analysis was done on a fractionated +180°C cut of the hydrogenated liquid product and hence did not include the dimer fraction which would have reduced the cetane number.

Silanization and acid washing

Both silanized and acid washed S11(3) sieves showed lower oligomerization activities compared to S11(3). This was not surprising since the sieves had less acid sites and lower pore volumes after the respective modifications. Wilshier *et al.* (1987) has shown that ZSM-5 silanized with hexamethyldisilazane was less active than unmodified ZSM-5 but more shape selective due to pore constriction. Silanization or selective poisoning of the external acid sites has been proposed to reduce coke formation in ZSM-5 by reducing formation of external allylic coke precursor species. The amount of coke after silanization was less than for S11(3) but this may also have been due to the lower conversion caused by the lower pore volume of the silanized catalyst.

Metal impregnation

Metal impregnated S11(3) sieves were investigated in order to determine the effect of extra-framework metal species on their oligomerization performance. These sieves showed little activity for propene oligomerization (10 wt% dimer was in the effluent gas). The characterization results showed that the metal impregnated sieves had the same number and strength of acid sites as S11(3) but that the pore volume as determined by hexane and nitrogen adsorption was dramatically reduced. Coke analysis after oligomerization showed that the metal impregnated sieves had the same amount of coke as the parent material S11(3), i.e. pore filling by "coke" species had occurred. This "coke" was exclusively of the "soft" Type I coke. The low activity therefore of the metal impregnated sieves may be due to the inability of these trapped "coke" species to desorb from the metal constricted pores.

Ion-exchanged MeAPSO-11 sieves

The oligomerization activity of all the ion-exchanged MeAPSO-11 sieves were lower than their respective parent materials. Characterization of these sieves showed reductions in pore volumes and in the case of FeS11 and CoS11 reduced acidity. Both of these factors would be expected to contribute towards the lower activity compared to their parent materials. Coke analysis showed similar amounts of coke ("soft" Type I) were present compared to their respective parent sieves implying deactivation was due to the inability of product molecules to desorb.

4.5.3 Effect of reaction temperature and WHSV

Increasing the reaction temperature and reducing the WHSV increased the conversion for oligomerization. These effects were expected since it is well known that increasing the reaction temperature will increase the conversion of propene [Quann *et al.*, 1988; Occelli *et al.*, 1985; Schwarz *et al.*, 1991a]. Thomson *et al.* (1990a) have observed however that increasing the reaction temperature reduced the reaction rate for low pressure propene oligomerization (101 kPa, 16.2 kPa propene in nitrogen) over SAPO-11 sieves. The differences between our results and those of Thomson *et al.* (1990a) may have something to do with different reactor conditions. Our conditions favour the production of higher oligomers and at the reaction conditions these will be in a super critical phase which is proposed to wash the coke species from the surface. Since Thomson *et al.* (1990a) were operating at low pressures/gas phase the coke species may not have been able to desorb from surface thus causing deactivation.

Several workers have suggested that propene oligomerization over ZSM-5 occurs near or at the surface of the crystallite [Wilshier *et al.*, 1987; Schwarz *et al.*, 1991b, Miller, 1987]. Tabak (1985) has reported though that ZSM-5 is shape selective since the hydrogenated tetramer of propene was 2,6-dimethyldecane whereas the equivalent product over a non-shape selective catalyst is 2,3,4-trimethylnonane. Wishier *et al.* (1987) has also shown that increasing the reaction temperature results in the products become more linear. This was attributed to diffusivities in the pores increasing with increasing temperature and the pore effect becoming evident along with products from the surface. Schwarz *et al.* (1991) have also

shown increased linearity of product with increasing reaction temperature over ZSM-5. Since it has been shown that the diffusivities of various hydrocarbon molecules in SAPO-11 are similar to ZSM-5 [Yang *et al.*, 1991] the present results of increased linearity (i.e. higher cetane number) with increasing reaction temperature may be similar to those proposed by Wilshier *et al.* (1987) and Schwarz *et al.* (1991b) in the case of ZSM-5 and may imply greater penetration depth of the feed monomer.

Increasing the reaction temperature resulted in increased amounts of "hard" coke. It was proposed earlier that hard coke caused deactivation after long run times and that these "hard" coke species constricted the entrance of the pores and restricted access of reactant or diffusion of product, therefore reducing activity. Since it is known that at higher temperatures diffusivities are increased it is probable that the product molecules would be able to diffuse out of the constricted pores at higher temperatures. The constricted pores may also explain why product is more linear.

4.6 COMPARISON OF OLIGOMERIZATION PERFORMANCE OF HPA AND SAPO-11 WITH ZSM-5 AND CATPOLY

Table 4.3 below shows the catalyst utilization values and product properties of AlPW+Sand, SAPO-11, ZSM-5 and solid phosphoric acid (CATPOLY) catalysts. The differences in activity and product selectivity and quality are discussed below.

Table 4.3 Comparison of propene oligomerization activities over AlPW+Sand, SAPO-11, ZSM-5 and CATPOLY catalyst.

Catalyst	CUV	Cetane No.	C_{12}+ (wt%)	Reaction Conditions
AlPW+Sand[1]	1800+[3]	41	41	230-240°C, WHSV=12 h^{-1}, P=5 MPa
SAPO-11[1]	761*[4]	49	17	310°C, WHSV=12 h^{-1}, P=5 MPa
Ext-ZSM-5[1]	1100	36-44[5]	58	220-290°C, WHSV=12 h^{-1}, P=5 MPa
CATPOLY[2]	1000-1700+	33-35	28	191°C, WHSV=9 h^{-1}, P=1.5 MPa

1. Feed 86 wt% propene, 14 wt% propane
2. Feed 100 wt% propene, * McMohan 1963
3. "+" implies catalyst still had activity
4. "*" CUV of catalyst after 100 hrs, estimated CUV of 1960 g·(liquid)/g·(catalyst) for this catalysts assuming linear deactivation to 0% conversion.
5. Cetane number increases with increasing temperature, this value is for the whole fraction and therefore true cetane number of a diesel fraction would be estimated to be at least 4 cetane units higher.

AlPW, ZSM-5 and CATPOLY

AlPW and sand diluted AlPW, were surprisingly active oligomerization catalysts considering their low surface areas (<15m^2/g). The catalyst utilization value (CUV) of sand diluted AlPW is in excess of 1800 g·(liquid)/g·(catalyst) which is appreciably higher than the value for ZSM-5 [1100 g·(liquid)/g·(catalyst)] [Schwarz *et al.*, 1991b] and similar to the value for CATPOLY [1000-1700 g·(liquid)/g·(catalyst)] [Dry, 1993]. The yield of distillate product (i.e. C_{12}+ fraction) of AlPW+Sand was greater than that of CATPOLY but less than that of ZSM-5. The higher C_{12}+ fraction of AlPW+Sand compared to CATPOLY may be due to HPAs' stronger acidity [Misono, 1987]. AlPW and the CATPOLY catalyst are not microporous and hence are not expected to show any shape selective properties and may explain their lower cetane numbers compared to ZSM-5 and SAPO-11. AlPW+Sand produces a distillate product with higher cetane value than

CATPOLY probably due to the higher molecular weight of the product which increases cetane number.

SAPO-11s

The steamed SAPO-11 catalysts or those operated at higher reactions temperatures (310°C) showed good performance and had similar CUVs to ZSM-5 and CATPOLY catalyst. The SAPO-11 product selectivity however shows a preference for the dimer fraction and has the lowest distillate yield. Optimum conditions for good quality distillate production were high reaction temperatures and mild steaming. The distillate product is of higher quality than for both CATPOLY or ZSM-5.

The major disadvantage however of AlPW+Sand catalyst is that the catalyst cannot be regenerated by burning the coke in air as can the other catalysts. This procedure destroys the AlPW catalyst. The major drawback for SAPO-11 catalysts is their low selectivity to distillate product.

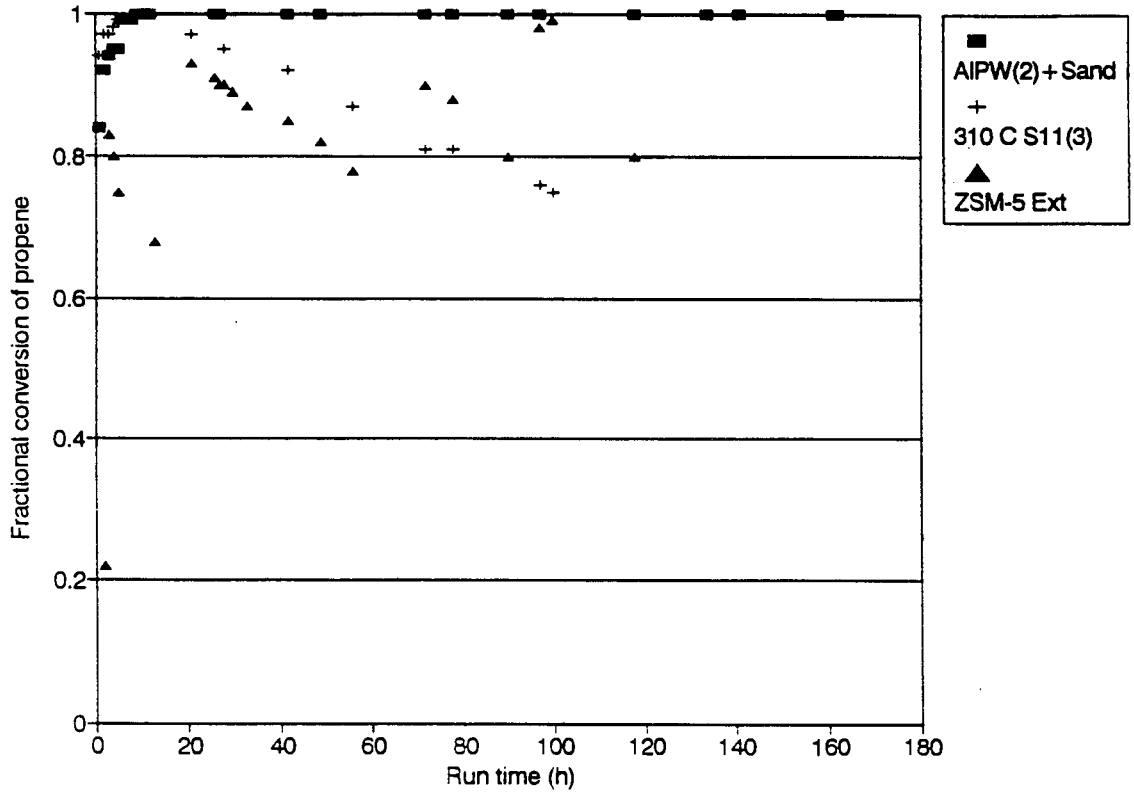

Figure 4.4 Oligomerization activity comparison of AlPW+Sand (230-240°C), SAPO-11 (310°C), and ZSM-5 (220-290°C), WHSV= 12h^{-1}, Pressure=5 MPa.

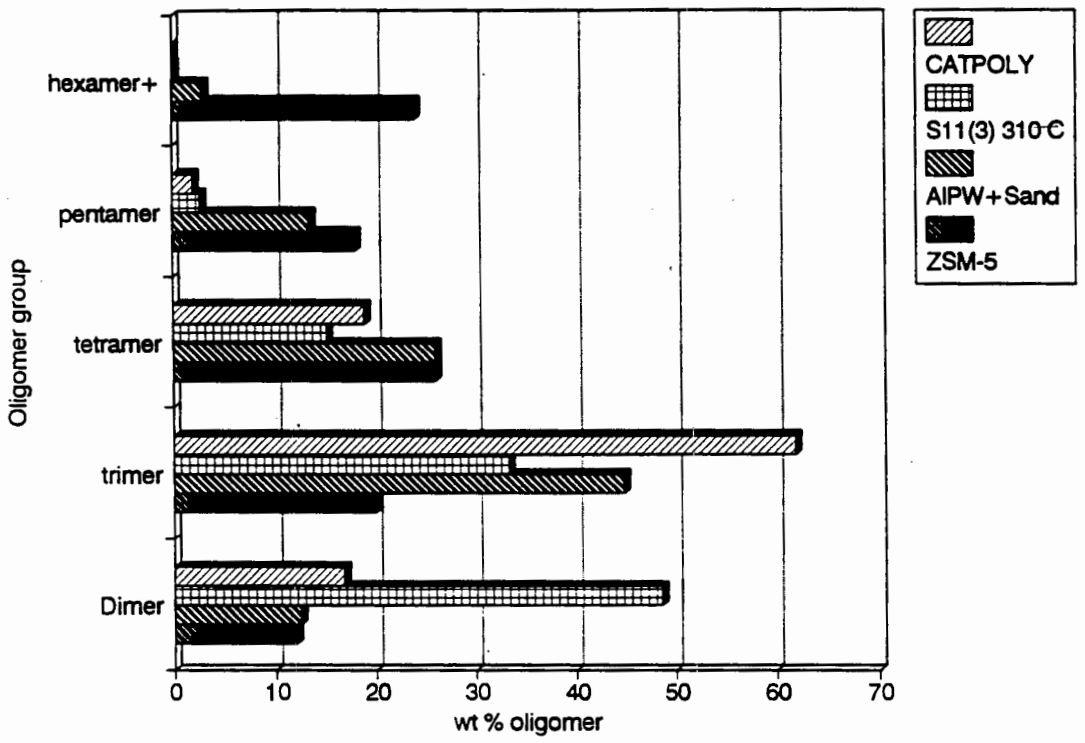

Figure 4.5 Product selectivity comparison of AlPW+Sand, SAPO-11 (310°C), ZSM-5 and solid phosphoric acid (CATPOLY) catalysts.

Chapter 5
Concluding remarks and recommendations

5. CONCLUDING REMARKS AND RECOMMENDATIONS

Thermal analysis and surface area characterization of the heteropoly acid (HPA) catalysts revealed that they could be divided into two types as was suggested by Niiyama *et al.* (1980), *viz.* **Type A**, consisting of multiple endothermic mass losses and low surface areas (<15 m^2/g); and **Type B**, consisting of a single endothermic mass loss and high surface areas (>35 m^2/g). Further characterization revealed that the Type A salts consisted of large irregular shaped crystallites (ca. 10 μm) and the Type B salts of small uniform rounded cubic crystallites (ca. 0.5 μm).

Acidity characterization by NH_3-TPD revealed that both Type A and Type B HPAs consisted of strong acid sites which were situated in the bulk of the HPA since NH_3 probes total bulk acidity. The majority of the absorbed ammonia was only released upon decomposition of the salt. Probe reaction studies such as n-butane cracking and 1-butene isomerization showed that the Type B salts had strong acid sites on the surface, but that these sites deactivated rapidly due to polyaromatic coke formation. The Type A salts had weaker acid sites on the surface compared to the Type B salts and were not capable cracking hydrocarbons (not a surface area effect).

The olgimerization activity of the parent HPAs was sensitive to alcination temperature. After calcination in nitrogen at 325°C the activity order for oligomerization was as follows: HPW >> HSiW≃HPMo. However, when calcined at 200°C, HSiW was more active than HSiW. The decrease in activity of HSiW with increasing calcination temperature was attributed to a loss of protons (as water) from the catalyst.

The propene oligomerization activity of the HPA salts decreased as shown: AlPW >> CoPW > NH_4PW≃NiPW > CuPW≃HPW > CePW≃FePW > KPW. By far the most active catalyst was the aluminium salt of 12-tungstophosphoric acid, AlPW. The counter cation had a large influence on the activity for oligomerization, indicating that the counter cation strongly influenced the surface acidity. The oligomerization activity could not be related to the NH_3-TPD results since these results are representative of the bulk acidity and the propene is unable to access all these sites since propene is only adsorbed on the surface of HPAs. Dilution of the catalyst

bed with inert quartz sand dramatically improved the activity and lifetime af all the Type A HPAs for propene oligomerization due to more isothermal conditions prevailing and this limited the formation of polyaromatic coke and subsequent deactivation of the catalyst. Polyaromatic and olefinic coke species are proposed to be located in the "cup-sites" and to cause perturbation of the Keggin structure.

Supporting heteropoly acids on α-alumina increased their oligomerization performance. This was possibly due to the formation of an active aluminium HPA salt phase on the surface of the α-alumina support.

The trimer of propene was the major oligomerization product. The product selectivity and cetane numbers of liquid product of the sand diluted Type A salts was not affected by counter cation type. Type B salts produced a lower cetane number liquid product due to their ability to crack and skeletally isomerize olefins. Cetane numbers of the sand diluted catalysts product were in the range 37-41. Increasing the reaction temperature from 230°C to 310°C reduced the distillate ($C_{12}+$) yield due to increased cracking. The catalyst utilization value of [AlPW+Sand] is in excess of 1800 g·(liquid)/g·(catalyst).

Of the SAPO-11s synthesized, the most crystalline was that synthesized using the conditions outlined in Example 15 of the patent by Lok *et al.* (1984b). XRD revealed that the only crystalline material present was that of the AEL type. Pore volume analysis of all the sieves indicated that the pores were constricted by extra-framework materials. Increasing the synthesis temperature of the low Si content synthesis gel increased the crystallite size and reduced the % crystallinity. Reducing the water content and increasing the Si content of the synthesis gel constrained the formation of large crystallites.

The acidity as determined from NH_3-TPD was mild ($T_{max}<350$°C) in comparison to HPA or zeolites such as ZSM-5. Post-synthesis modifications such as steaming, acid washing and silanization reduced the number of acid sites of SAPO-11 and reduced the pore volume. The reduction in pore volume was due to the formation of extra-framework species. Metal impregnation did not reduce the number acid sites but did significantly reduce the pore volume of SAPO-11.

Characterization using chemical analysis, NH_3-TPD and TPR of the MeAPSO-11 sieves showed that Ni was not incorporated into the framework of NiAPSO-11, but existed in ion-exchange type positions, 30% of which were easily exchangeable. The remaining Ni species are thought to exist in S_I sites or to be occluded in 6-membered rings. The Ni species in the ion-exchange positions weakened the acidity of NiS11 and reduced pore volume. No Fe was incorporated into the framework of FeAPSO-11 and Mössbauer spectroscopy showed that after calcination two octahedrally coordinated Fe^{3+} species were present. These were assigned to be an iron oxide and iron aluminium phosphate phase. The acidity of FeS11 was due to a SAPO-11 phase and the pore volume was significantly reduced by the iron oxide/iron aluminium phosphate phases. Manganese and cobalt were incorporated into the framework of the SAPO-11 sieves as evident by the increase in number of acid sites compared to SAPO-11 but ion-exchange showed that at least 50% and 45% of the Mn and Co respectively was in ion-exchange type positions.

The probe reaction (*m*-xylene and 2-methyl-2-pentene isomerization) studies showed that the catalytic activity of the sieves was affected by the presence of extra-framework metal species. These metals caused diffusional problems influencing the products formed and reducing the catalytic activity.

Propene oligomerization activity of the AEL type molecular sieves decreased as shown: S11≃MnS11 > CoS11≃FeS11 > NiS11. The oligomerization performance of SAPO-11 and MeAPSO-11 molecular sieves is significantly influenced by the acidity and pore volume of the sieve. Less and weaker acid sites resulted in lower activity and low pore volumes (a result of extra-framework species) resulted in deactivation. Except in the case of MnAPSO-11 and hydrothermally treated SAPO-11 the metal species in extra-framework positions reduced the oligomerization activity and caused rapid deactivation. This deactivation was not due to "hard coke" or Type II coke formation and was most likely due the inability of oligomer products to desorb from the constricted pores. Likewise post-synthesis modifications that reduced the pore volume and number of acid sites, such as acid washing and silanization, showed lower oligomerization activities. Metal

impregnation of sieves which showed no loss in number of acid sites but reduced pore volumes were inactive.

Steaming, which was shown to reduce pore volume and the number of acid sites, increased the oligomerization activity. The increase in activity may be due to the formation of new strong acid sites such as in the case of zeolites. Mild steaming resulted in improved cetane numbers whereas severe steaming showed no improvement in cetane number of the liquid product.

Increasing the reaction temperature increased the activity of the sieve and increased the linearity of the product. However increasing the reaction temperature also increased the amount of "hard" coke. Changes in residence time (WHSV) did not effect the cetane number but increasing the WHSV reduced conversion. Deactivation after long run times was due to "hard" coke formation, i.e. that can only be burned off in air and which possibly constricts the pores. No polyaromatic coke was formed, even at high temperatures, probably due to the low hydride transfer ability of SAPO-11 sieves. Increasing the reaction temperature possibly increases the desorption of oligomers out of constricted pores and may also increase the diffusion of coke species out of the pores.

Pellets of pure SAPO-11 performed better than the pure powder which performed better than extrudates of [SAPO-11 + alumina]. It is proposed that due to the higher temperatures gradients in the pellets the activity is enhanced. Extruding or pelletizing did not effect the cetane number of the liquid product.

Comparing solid phosphoric acid (CATPOLY) and ZSM-5 with HPA and SAPO-11 catalysts showed that AlPW + Sand achieved the highest catalyst utilization value but lower distillate selectivity compared to ZSM-5. The product quality of AlPW was similar to that of ZSM-5 and solid phosphoric acid and contained no aromatics. The cetane numbers were in the region of 40. SAPO-11 had similar activity to ZSM-5 when operated at higher reaction temperatures but the selectivity to distillate fraction was low. The cetane number of the distillate fraction was the highest especially when the SAPO-11 catalyst was mildly steamed or operated at higher temperatures. SAPO-11 liquid product contained no aromatics even at high reaction temperatures (310°C).

It is recommended that work be performed to investigate methods of regeneration of HPA catalysts without destroying their structure as this would be of great benefit if this type of catalyst was to be used commercially. Such methods may include washing the catalyst with organic solvents. Further investigations into the effect of sand dilution, water in the feed and steaming of the AlPW catalyst on the oligomerization performance would also provide useful information if such a catalyst were to be used industrially. The effects of synthesis variables such as increasing synthesis temperature on the crystallite size of SAPO-11 needs to be investigated in greater detail, the size of the crystallite being of obvious importance in catalytic reactions. Finally a study investigating the effect of varying the amount of metal added to the SAPO-11 synthesis gel with the objective being to reduce the amount of extra-framework metal species and maximize metal incorporation.

AlPW is a low surface area Type A HPA salt with no strong surface acid sites capable of cracking olefins or alkanes, yet this catalyst is extremely active for propene oligomerization. Its activity is such that without careful control of bed temperatures, achieved by addition of sand to the catalyst bed to act as a heat sink, the catalyst deactivates due to type II polyaromatic coke formation. The distillate fraction contains no aromatics and is therefore an environmentally friendly fuel, although the cetane number is only 40. Although this compares well to the product obtained over ZSM-5 and solid phosphoric acid (CATPOLY) and the yield of distillate is higher compared to the CATPOLY process, the yield of distillate is less than that of ZSM-5. The low distillate yield in comparison to ZSM-5 and the inability to regenerate AlPW makes this catalysts possible use, in an industrial context, unlikely. The recent claims of high cetane number distillate product (52) for olefin oligomerization over supported 12-tungstosilicic acid are more than likely due to the high distillate cut temperature employed (250°C). Such high temperatures would increase the cetane number of the distillate product and hence the high cetane number obtained is probably due to the distillate cut temperature and not any intrinsic property of the catalyst system.

Metal incorporation into the SAPO-11 framework by addition of metals to the SAPO-11 synthesis gel does not occur readily. Certainly for Fe and Ni

there does not seem to be any metal incorporation into the SAPO-11 framework. Although Co and Mn were incorporated in the framework, as evident by increased number of acid sites (determined by NH_3-TPD) compared to SAPO-11, these sieves still had significant amounts of metals present in extra-framework positions. The probe reaction results indicated that these extra-framework species caused diffusional constraints, preventing access of reactant to acid sites or desorption of products from constricted pores. It was these diffusional constraints that were most likely to be the reason for the NH_3-TPD data and the catalytic activity data not correlating well.

Although Long *et al.* (1985) have suggested that SAPO-11 sieves may be used for the production of distillate fuels via propene oligomerization, it is clear from the results of this study that although the activity may acceptable, the yield of distillate product is low compared to ZSM-5 and solid phosphoric acid. The distillate product contains no aromatics even at high reaction temperatures (310°C) and has an acceptable cetane number of 48, the low distillate yield however makes such a catalyst unlikely to be used industrially for the production of distillate fuels.

References

Akimoto, M., Tsuchida, Y., Sato, K., and Echigoya, E., *J. Catal.* **72**, 83 (1981).

Alberty, R.A., *Chem. Eng. Sci.* **42** (10), 2325 (1987).

Anderson, B., PhD Thesis, University of Cape Town, 1991.

Argauer, R.J., and Landolt, G.R., U.S. Patent, 3702 886, 1972.

Avidan., A.A., *in "Methane Conversion"* (D.M. Bibby, C.D. Chang, R.F., Howe and S. Yurchak, Eds.) p. 307. Elsevier, Amsterdam, 1988.

Baba, T., Sakai, J., and Ono, Y., *Bull. Chem. Soc. Japan.* **55**, 2657 (1982).

Baba, T., Watanabe, H., and Ono, Y., *J. Phys. Chem.* **87**, 2406 (1983).

Baba, T., Nomura, M., Ono, Y., and Kansaki, Y., *J. Chem. Soc. Faraday Trans. 1* **88**, 71 (1992).

Babu, G.P., Hedge, S.G., Kulkarni, S.B., and Ratnasamy, P., *J. Catal.* **81**, 471 (1983).

Balakrishnan, I., and Prasad, S., *Appl. Catal.* **62**, L7 (1990).

Barger, P.T., U.S. Patent, 5 095 163, March 10, 1992.

Barrer, R.M., *in "Methane Conversion"* (D.M. Bibby, C.D. Chang, R.F. Howe and S. Yurchak, Eds.) p. 537. Elsevier, Amsterdam, 1988.

Bauer, R.S., Ching, H., Glockner, P.W., Kei, W., and van Zwet, H., U.S. Patent, 3 635 937, 1972.

Bennet, J.M., Richardson, J.W., Pluth, J.J., and Smith, J.V., *Zeolites* **7**, 160 (1987).

Bennet, J.M., and Marcus, B.K., *in "Innovations in Zeolite Materials Science"* (P.J. Grobet, W.J. Mortier, E.F. Vansant and G. Schulz-Ekloff, Eds.) p. 269. Elsevier, Amsterdam, 1988.

Bennet, J.M., Kirchner, R.M., and Wilson, S.T., *in "Zeolites: Facts, Figures, Future"* (P.A. Jacobs and R.A. van Santen, Eds.) p. 731. Elsevier, Amsterdam, 1989.

Bethea, S.R., and Karchmer, J.H., *Ind. Eng. Chem.* **48** (3), 370 (1956).

Beyer, H.K., and Belenykaja, I., *in "Catalysis by Zeolites"* (B. Imelik, C. Naccache, Y. Ben Taarit, G. Coudier and H. Praliaud, Eds.) p. 303. Elsevier, Amsterdam, 1980.

Black, J.B., Clayden, N.J., Gai, P.L., Scott, J.D., Serwicka, E.M., and Goodenough, J.B., *J. Catal.* **106**, 1 (1987).

Borade, R.B., and Clearfield, A., *Appl. Catal. A:General* **80**, 59 (1992).

Bourdillon, G., Gueguen, C., and Guisnet, M., *Appl. Catal.* **61**, 123 (1990).

Breck, D.W., *in "Zeolite Molecular Sieves"* p. 2. Wiley, New York, 1984.

Brinen, J.L., and White, M.G., *J. Catal.* **124**, 133 (1990).

Brink, A., and Swart, J.S. de K., *"The Fischer-Tropsch Synthesis as applied at Secunda with special reference to Product Work-up and Product Quality"* International Coal Conversion Conference, CSIR, South Africa, 1982.

Brouet, G., Chen, X., and Kevan, L., *J. Phys. Chem.* **95**, 4928 (1991).

Brown, G.M., Noe-Spirlet, M.R., Busing, W.R., and Levy, H.A., *Acta. Crystallogr. Sect. B* **33**, 1038 (1977).

Calis, G., Frenken, P., de Boer, E., Swolfs, A., and Hefni, M.A., *Zeolites* **7**, 319 (1987).

Cardile, C.M., Tapp, N.J., and Milestone, N.B., *Zeolites* **10**, 90 (1990).

Chang, C.D., Chu, C.T-W., and Socha, R.F., *J. Catal.* **86**, 289 (1984).

Chao, K.J., Sheu, S.P., Shue, H.W., *J. Chem. Soc. Faraday Trans. 1* **88**, 2949 (1992).

Chen, J., Sankar, G., Thomas, J.M., Xu, R., Greaves, G.N., and Waller, D., *Chem. Mater.* **4**, 1373 (1992).

Chen, N.Y., *J. Phy. Chem.* **80**, 60 (1976).

Cheng, W-C., and Luthra, N.P., *J. Catal.* **109**, 163 (1988).

Cotton, F.A., Wilkinson, G., and Gaus, P.L., *"Basic Inorganic Chemistry"* 2nd Edition, Wiley, New York, 1987.

Choudhary, V.R., Akolekar, D.B., Singh, A.P., and Sansare, S.D., *J.Catal.* **111**, 254 (1988).

Choudhary, V.R., Pandit, M.Y., and Sansare, S.D., *J. Chem. Soc. Commun.* p. 1343 (1989).

Choung, S.J., and Butt, J.B., *Appl. Catal.* **64**, 173 (1990).

Corma, A., Llopis, F., and Monton, J.B., *in "New Frontiers in Catalysis"* (L. Guczi *et al.*, Eds.) p. 1145. Elsevier, Amsterdam, 1993.

Csicsery, S.M., *Zeolites* **4**, 202 (1984).

Csicsery, S.M., Catalyst Consultant Publishing Company, (1991).

Davis, M.E., *Chem. Ind.* Feb 17, p. 137. (1992).

Delafosse, D., *J. Chim. Phys.* **83**, 791 (1986).

Derouane, E.G., Maistriau, L., Gabelica, Z., Tuel, A., Nagy, J.B., and van Ballmoos, R., *Appl. Catal.* **51**, L13 (1989).

Dry., M.E., Cat: Sci & Tech., *1*, (J.R. Anderson and M. Boudart, Eds.) p. 159. Springer Verlag, N.Y., 1981.

Dry, M.E., in "High Yield, High Quality Diesel from Fischer-Tropsch" Int. Coal Conversion Conference, CSIR, South Africa, 1982a.

Dry, M.E., *Chemtech*, 744 (1982b).

Dry, M.E., Catalysis Today, 6, (3), 183, 1990.

Ernst, S., Puppe, L., and Weitkamp, T., *in "Zeolites: Facts, Figures, Future"* (P.A. Jacobs and R.A. van Santen, Eds.) p. 447. Elsevier, Amsterdam, 1988.

Ehwald, H., Fiebig, W., Jerschkewitz, H-G., Lischke, G., Parlitz, B., Reich, P., and Öhlmann, G., *Appl. Catal.* **34**, 23 (1987).

Finger, G., Kornatowski, J., Richter-Mendau, J., Jancke, K., Bulow, M., and Rozwadoski, M., *in "Catalysis and Adsorption by Zeolites"* (G. Öhlmann, H. Pfeifer and R. Fricke, Eds.) p. 501. Elsevier, Amsterdam, 1991a.

Finger, G., Richter-Mendau, J., Bulow, M., and Kornatowski, J., *Zeolites* **11**, 443 (1991b).

Flanigen, E.M., *in "Zeolite Chemistry and Catalysis"* (J.A. Rabo, Ed.), p. 80. ACS Monograph 171, Am. Chem. Soc., Washington, D.C., 1976.

Flanigen, E.M., Lok., B., Patton, R.L., and Wilson, S.T., *Pure Appl. Chem.* **58**, 1351 (1986).

Flanigen, E.M., Patton, R.L., and Wilson, S.T., *in "Innovations in Zeolite Materials Science"* (P.J. Grobet, W.J. Mortier, E.F. Vansant and G. Schulz-Ekloff, Eds.), p. 13. Elsevier, Amsterdam, 1988.

Fricke, R., and Öhlmann, G., *J. Chem. Soc. Faraday Trans. 1* **82**, 263 (1986a).

Fricke, R., and Öhlmann, G., *J. Chem. Soc. Faraday Trans. 1* **82**, 273 (1986b).

Gadja, G.J., U.S.Patent 5,132,484, Jul 21, 1992.

Garbowski, E.D., and Vedrine, J.C., *Chem. Phys. Lett.* **48**, 550 (1977a).

Garbowski, E.D., and Primet, M., *Chem. Phys. Lett.* **49**, 247 (1977b)

Garten, R.L., Delgass, W.N., and Boudart, M., *J. Catal.* **18**, 90 (1970).

Gautier, S., Diplome-Ingenieur Thesis, Conservatoire National des Arts et Matiers, Paris, (1988).

Gentry, S.J., Hurst, N.W., and Jones, A., *J. Chem. Soc. Faraday Trans. 1* **75**, 1688 (1979).

Goepper, M., Guth, F., Delmotte, L., Guth, J.L., and Kessler, H., *in "Zeolites: Facts, Figures, Future"* (P.A. Jacobs and R.A. van Santen, Eds.) p. 857. Elsevier, Amsterdam, 1989.

Goldfarb. D., *Zeolites* **9**, 509 (1989).

Gorte, R.J., Kokotailo, G.T., Biaglow, A.I., Parrillo, D., and Pereira, C., *in "Zeolite Chemistry and Catalysis"* (P.A. Jacobs, N.I. Jaeger, L. Kubelkova and B. Wichterlova, Eds.) p. 181. Elsevier, Amsterdam, 1991.

Guisnet, M., *Chemica Stosowana*, XXVIII, 369 (1984).

Guisnet, M., and Magnoux, P., *Appl. Catal.* **54**, 1 (1989).

Guisnet, M., and Magnoux, P., *in "Zeolite Microporous Solids: Synthesis, Structure and Reactivity"* (E.G. Derouane *et al.*, Eds.) p. 457. Kluwer Academic Press, Netherlands, 1992.

Halik, C., Chaudhuri, S.N., and Lercher, J.A., *J. Chem. Faraday Trans. 1* **85**, 3879 (1989).

Hampson, B., Leach, H.F., Barrie, B.M., Lowe, M., and Williams, C.D., *Zeolites* **9**, 521 (1989).

Hasha, D., de Saldarriaga, L.S., Saldarriaga, C., Hathaway, P.E., Cox, D.F., and Davis, M.E., *J. Am. Chem. Soc.* **110**, 2127 (1988).

Hayashi, H., and Moffat, J.B., *J. Catal.* **77**, 473 (1982).

Hayashi, H., and Moffat, J.B., *J. Catal.* **81**, 61 (1983).

Hayashi, H., and Moffat, J.B., *J. Catal.* **83**, 192 (1983).

Highfield, J.G., and Moffat, J.B., *J. Catal.* **88**, 177 (1984a).

Highfield, J.G., and Moffat, J.B., *J. Catal.* **89**, 185 (1984b).

Hocevar, S., and Levec, J., *J. Catal.* **135**, 518 (1992).

Hocevar, S., Batisa, J and Kaucic, V., *J. Catal.* **139**, 351 (1993).

Hodnett, B.K., and Moffat, J.B., *J. Catal.* **88**, 253 (1984).

Hoffmeister, M., and Butt, J.B., *Appl. Catal.* **A 82**, 169 (1992).

Hunger, M., Anderson, M.W., Ojo, A., and Pfeifer, H., *Micrporous Materials* **1**, 17 (1993).

Hurst, N.W., Gentry, S.J., and Jones, A., *Catal. Rev.-Sci. Eng.* **24**, 233 (1982).

HYSIM., Hyprotech Ltd., April 1991, Ver. C1.05.

Ione, K.G., and Vostrikova, L.A., *Russ. Chem. Rev.* **56(3)**, 231 (1987).

Ipatieff, V.N., *Ind. Eng. Che.*, 1067 (1935).

Inui, T., European Patent, 0418142 A1, 11.09.90, 1990.

Inui, T., Matsuda, H., Okaniwa, H., and Miyamoto, A., *Appl. Catal.* **58**, 155 (1990).

Inui, T., *in "Structure-Activity and Selectivity Relationships in Heterogeneous Catalysis"* (R.K. Grasselli and A.W. Sleight, Eds.) p. 233. Elsevier, Amsterdam, 1991.

Iton, L.E., Choi, I., Desjardins, J.A., and Maroni, V.A., *Zeolites* **9**, 535 (1989).

Izumi, Y., Hasebe, R., and Urabe, K., *J. Catal.* **84**, 402 (1983).

Jacobs, P.A., Linart, J-P., Nijs, H., and Uytterhoeven, J.B., *J. Chem. Soc. Faraday Trans 1* **73**, 1754 (1977).

Jacobs, P.A., Nijs, H., and Verdonck, J., *J. Chem. Soc. Faraday Trans 1* **75**, 1196 (1979).

Jacobs, P.A., and Mertens, J.A., *Pure & Appl. Chem.* **58**, 1329 (1986).

Jager, B., Holtkamp, W., and Gaensellen, H., "Opportunities for Low Temperature Fischer-Tropsch Processing" International Coal Conference, CSIR, South Africa, 1982

Jahn, E., Muller, D., Wieker, W., and Richter-Mendau, J., *Zeolites* **9**, 177 (1989).

Jahn, E., Muller, D., and Becker, K., *Zeolites* **10**, 151 (1990).

Joensen, F., Blom, N., Tapp, N.J., Derouane, E.G., and Fernandez, C., *in "Zeolites: Facts, Figures, Future"* (P.A. Jacobs and R.A. van Santen, Eds.) p. 1131. Elsevier, Amsterdam, 1989.

Kan, Q., Wu, Z., Xu, R., Wei, Q., Peng, S., Xiong, G., Seng, S., and Huang, J., *in " Zeolite Chemistry and Catalysis"* (P.A. Jacobs, N.I. Jaeger, L. Kubelkova and B. Wichterlova, Eds.) p. 241. Elsevier, Amsterdam, 1991.

Kan, Q., Wu, Z., Xu, R., Lui, X., and Peng, S., *J. Molec. Catal.* **74**, 223 (1992).

Karge, H.G., *in* "Introduction to Zeolite Science and Technology" (H. van Bekkum E.M. Flanigen and J.C. Jansen Eds.) Chpt. 14, p. 531. Elsevier. Amsterdam, 1991.

Kasztelan, S., and Moffat, J.B., *J. Catal.* **116**, 82 (1987).

Kessler, H., *in "Recent Advances in Zeolite Science"* (J. Klinowski and P.J. Barrie, Eds.) p. 17. Elsevier, Amsterdam, 1989.

Khouzami, R., Coudurier, G., Mentzen, B.F., and Vedrine, J.C., in *"Innovations in Zeolite Materials Science"* (P.J. Grobet, W.J. Mortier, E.F. Vansant and G. Schulz-Ekloff, Eds.) p. 355. Elsevier, Amsterdam, 1988.

Khouzami, R., Coudurier, G., Lefebvre, F., Vedrine, J.C., and Mentzen, B.F., *Zeolites* **10**, 183 (1990).

Kock, A.J.H.M., Fortuin, H.F., and Gues, J.W., *J. Catal.* **96**, 261 (1985).

Konishi, Y., Sakata, K., Misono, M., and Yonenda, Y., *J. Catal.* **77**, 169 (1982).

Kozhevnikov, I.V., and Matveev, K.I., *Appl. Catal.* **5**, 135 (1982).

Kramer, G.M., McVicker, G.B., and Ziemiak, J.J., *J. Catal.* **92**, 355 (1985).

Kramer, G.M., and McVicker, G.B., *Acc. Chem. Res.* **19**, 78 (1986).

Kraushaar-Czarnetzki, B., and van Hoof, J.H.C., *in "Zeolites: Facts, Figures, Future"* (P.A. Jacobs and R.A. van Santen, Eds.) p. 1063. Elsevier, Amsterdam, 1989.

Kraushaar-Czarnetzki, B., Hoogervorst, W.G.M., Andrea, R.R., Emeis, C.A., and Stork, H.J., *in "Zeolite Chemistry and Catalysis"* (P.A. Jacobs, N.I. Jaeger, L. Kubelkova and B. Wichterlova, Eds.) p. 231. Elsevier, Amsterdam, 1991a.

Kraushaar-Czarnetzki, B., Hoogervorst, W.G.M., Andrea, R.R., Emeis, C.A., and Stork, H.J., *J. Chem Soc. Faraday Trans 1* **87**, 891 (1991b).

Kuhl, G.H., and Schmitt, K.D., *Zeolites* **10**, 2 (1990).

Kumar, R., and Ratnasamy, P., *J. Catal.* **118**, 68 (1989).

Kuperman, A., and Ozin, G.A., in abstract proceedings of 9th IZC, RP242, (1992).

Kustov, L.M., Zubkov, S.A., Kazansky, V.B., Bondar, L.A., *in "Zeolite Chemistry and Catalysis"* (P.A. Jacobs, N.I. Jaeger, L. Kubelkova and B. Wichterlova, Eds.) p. 303. Elsevier, Amsterdam, 1991.

Lago, R.M., Haag, W.O., Mokovsky, R.J., Olson, D.H., Hellring, S.D., Schmitt, K.D., and Kerr, G.T., *in "Proceedings of the 7TH International Zeolite Conference"* (Y. Murakami, A. Lijima and J.P. Ward, Eds.) p. 677. Elsevier, Amsterdam, 1986.

Lazar, K., Borbely, G., and Beyer, H., *Zeolites* **11**, 214 (1991).

Lechert, H., Weyda, H., Hess, M., Kleinworth, R., Penchev, V., and Minchev, C.H., *in "Zeolites Chemistry and Catalysis"* (P.A. Jacobs, N.I. Jaeger, L. Kubelkova and B. Wichterlova, Eds.) p. 145. Elsevier, Amsterdam, 1991.

Lee, C.W., Chen, X., and Kevan, L., *J. Phys. Chem.* **95**, 8626 (1991).

Li, H-X., Martens, J.A., Jacobs, P.A., Schubert, S., Schmit, F., Zeithen, H.M, and Trautwein, A.X., *in "Innovations in Zeolite Materials Science"* (P.J. Grobet, W.J. Mortier, E.F. Vansant and G. Schulz-Ekloff, Eds.) p. 75. Elsevier, Amsterdam, 1988.

Li, H-X., and Davis, M.E., *J. Phys. Chem.* **96**, 331 (1992).

Lok, B.M., Cannan, T.R., Messina, C.A., *Zeolites* **3**, 282 (1983).

Lok, B.M., Messina, C.A., Patton, R.L., Gajek, R.T., Cannan, T.R., and Flanigen, E.M., *J. Am. Chem. Soc.* **106**, 6092 (1984a).

Lok, B.M., Messina, C.A., Cannan, T.R., Patton, R.L., Gajek, R.T., and Flanigen, E.M., U.S.Patent. 4,440,871, Apr. 3 (1984b).

Lok, B.M., Marcus, B.K., Vail, L.D., Flanigen, E.M., Patton, R.L., and Wilson, S.T., European Patent 0 159 624, Oct. 30, (1985).

Long, G.N., Pellet, R.J., and Rabo, J.A., European Patent, 0 142 154, 1985.

McGarvey, G.B., McMonagle, J.B., Nayak, V.S., Taylor, D., and Moffat, J.B., "Proceedings of the 9th International Congress on Catalysis, Calgary, 1988" (M. J. Phillips and M. Ternan, Eds.), p. 1804. Chem. Institute of Canada, Ottawa, 1988.

Mahoney, F., Rudham, R., and Summers, J.V., *J. Chem. Soc. Faraday Trans 1* **75**, 314 (1979).

Man, P.P., Briend, M., Peltre, M.J., Lamy, A., Beaunier, P., and Barthomeuf, D., *Zeolites* **11**, 563 (1991).

Marchi, A.J., and Froment, G.F., *Appl. Catal.* **71**, 139 (1991).

Martens, J.A., Verlinden, B., Mertens, M., Grobet, P.J., and Jacobs, P.A., in "Zeolite Synthesis" ACS Symposium Series 398 (M.L. Occelli and H.E. Robson Eds.) p. 305. 1989.

Martens, J.A., Janssens, C., Grobet, P.J., Beyer, H.K, and Jacobs, P.A., *in "Zeolites: Facts, Figures, Future"* (P.A.Jacobs and R.A. van Santen Eds.) p. 215. Elsevier, Amsterdam, 1989.

Martens, J.A., Mertens, M., Grobet, P.J., and Jacobs, P.A., ##.

Martens, J.A., Grobet, P.J., and Jacobs, P.A., *J. Catal.* **126**, 299 (1990).

Mavrodinova, V., Neinska, Y., Minchev, C., Lechert, H., Minkov, V., Valtchev, V., and Penchev, V., *in "Zeolites Chemistry and Catalysis"* (P.A. Jacobs, N.I. Jaeger, L. Kubelkova and B. Wichterlova Eds.) p. 395. Elsevier, Amsterdam, 1991.

Matsuda, T., Sato, M., Kanno, T., Miura, H., and Sugiyama, K., *J. Chem. Soc. Faraday Trans. 1* **77**, 3107 (1981).

Maxwell, W.E., and Stork, W.H.J., in "Intridcution to Zeolite Science and Practice" (H. van Bekkum, E.M. Flanigen and J.C. Jansen, Eds.), p. 571. Elsevier, Amsterdam, 1991.

McMahon, J.F., Bednars, C., and Solomaon, E., *in "Advanced Petrochemical Chemical Refining. 1"* (J.J. McKetta, jr., Ed.) Chpt. 5, Interscience Publishers, 1963.

McMonagle, J.B., and Moffat, J.B., *J. Colloid Int. Sci.* **101**, 479 (1984).

Meagher, A., Nair, V., and Szostak, R., *Zeolites* **8**, 3 (1988).

Meagher, A., *Zeolites* **9**, 87 (1989).

Meier, W.M., *in "Molecular Sieves"* p. 12. Soc. Chem. Ind., London, 1968.

Meinhold, R.H., and Tapp, N.J., *J. Chem. Soc. Chem. Commun.*, 219 (1990).

Mellor, J.W., in "Mellors comprehensive treatise on Inorganic and Theoretical Chemistry", Vol. VII Ser. III, Longman, 1971.

Mertens, M., Martens, J.A., Grobet, P.J., and Jacobs, P.A., *in "Guidelines for Mastering the Properties of Molecular Sieves"* (D. Barthomeuf E.G. Derouane and W. Holderich, Eds.) p. 1. NATO ASI Series B: Physics Vol 221, Plenum Press. New York, 1990.

Meusinger, J., Vinek, H., Dworeckow, G., Goepper, M., and Lercher, L., *in "Zeolites Chemistry and Catalysis"* (P.A. Jacobs, N.I. Jaeger, L. Kubelkova and B. Wichterlova, Eds.) p. 373. Elsevier, Amsterdam, 1991.

Mile, B., Stirling, D., Zammitt, M.A., Lovell, A., and Webb, M., *J. Catal.* **114**, 217 (1988).

Minachev, Kh.M., and Isakov, Ya.I., *in "Zeolite Chemistry and Catalysis"* (J.A. Rabo, Ed.), p. 171. ACS Monograph 171, Am. Chem. Soc., Washington, D.C., 1976.

Mioc, U., Davidovic, M., Tjapkin, N., Colomban, Ph., and Novak, A., *Solid State Ionics* **46**, 103 (1991).

Misono et al., 1978. ##

Misono, M., Sakata, K., and Yonenda, Y., Studies in Surface Science and Catalysis, *in* "Proceedings of the 7th International Congress on Catalysis, Tokyo, 1980" (T. Seiyama and K. Tanabe, Eds.), p. 1047. Kodansha-Elsevier. Tokyo-Amsterdam, 1981.

Misono, M., Mizuno, N., Katamura, K., Kasai, A., Konishi, Y., Sakata, K., Okuhara, T., and Yonenda, Y., *Bull. Chem. Soc. Japan.* **55**, 400 (1982).

Misono, M., Mizumo, N., and Komaya, T., *"Proceeding of the 8th International Congress on Catalysis, West Berlin, 1984."* Vol. 5, p. 487. Verlag-Chemie, Weinheim, 1984.

Misono, M., *Catal. Rev. Sci. Eng.* **29**, 269 (1987).

Misono, M., Okuhara, T., and Mizuno, N., *in "Successful Design of Catalysts"* (T. Inui, Ed.) p. 267. Elsevier. Amsterdam, 1988.

Misono, M., *in "New Frontiers in Catalysis"* (L. Guczi *et al.*, Eds.) p. 69. Elsevier, Amsterdam, 1993.

Montes, C., Davis, M.E., Murray, B., and Narayana, M., *J. Phys. Chem.* **94**, 6425 (1990).

Monti, D.A.M and Baiker, A., *J. Catal.*, **83** (1983) 323.

Muller, U., Brenner, A., Reich, A., and Unger, K.K., *in "Zeolite Synthesis"* ACS Symposium Series 398 (M.L. Occelli and H.E. Robson, Eds.) Chpt 24, p. 346., 1989.

Musa, M., Tarina, V., Stoica, A.D., Ivanov, E., Postinaru, D., Pop, E., Pop, Gr., Ganea, R., Birjega, R., Musca, G., and Paukshtis, E.A., *Zeolites* **7**, 427 (1987).

Nakamura, S., and Ichihashi, H., *in "New Horizons in Catalysis"* (T. Seiyama and K. Tanabe, Eds.) p. 755. Elsevier, Amsterdam, 1980.

Nayak, V.S., and Moffat, J.B., *Appl. Catal.* **36**, 127 (1988).

Nayak, V.S., and Moffat, J.B., *Appl. Catal.* **47**, 97 (1989).

Niiyama, H., Saito, Y., and Echigoya, E., *in "Proceedings of the 7th International Congress on Catalysis, Tokyo, 1980"* (T. Seiyama and K. Tanabe, Eds.), p. 1416. Kodansha-Elsevier, Tokyo-Amsterdam, 1981.

Niwa, M., Morimoto, S., Kato, M., Hattori, T., and Murakami, Y., in "Preprint of 8th ICC" p. 701. 1984.

Nowinska, K., *J. Chem. Soc., Chem. Commun.*, 44 (1990).

Nowinska, K., Fiedorow, R., and Adamiec, J., *J. Chem. Soc. Faraday Trans. 1* **85**, 749 (1991).

O'Connor, C.T., and Kojima., *S.A.J. Inst. Chem. Eng.* **1**, 23 (1989).

Oh, S.H., and Lee, W.Y., *in "New Frontiers in Catalysis"* (Guczi *et al.*, Eds.), p. 1693. Elsevier, Amsterdam, 1993.

Ojo, A.F., Dwyer, J., and Parish, R.V., *in "Zeolites: Facts, Figures, Future"* (P.A.Jacobs and R.A. van Santen, Eds.) p. 227. Elsevier, Amsterdam, 1989.

Ojo, A.F., Dwyer, J., Dewing, J., and Karim, K., *J. Chem Soc. Faraday Trans. 1* **87**, 2679 (1991).

Okuhara, T., Kasai, A., Hayakawa, N., Misono, M., and Yonenda, Y., *Chem. Lett. Chem. Soc. Japan.*, 391 (1981).

Ono, Y., and Baba, T., *"Proceedings of the 8th International Congress on Catalysis, West Berlin, 1984"* Vol. 5, p. 405. Verlag-Chemie. Weinheim, 1984.

Otake, M., and Onoda, T., *in "New Horizons in Catalysis"* (T. Seiyama and K. Tanabe, Eds.) p. 780., Elsevier, Amsterdam, 1980.

Owen, H., Marsh, S.K., and Wright, B.S., U.S. Patent, 4 456 779, 1984.

Pang, W., Qiu, S., Kan, Q., Wu, Z., Peng, S., Fan, G., and Tian, D., *in "Zeolites: Facts, Figures, Future"* (P.A.Jacobs and R.A. van Santen Eds.) p. 281. Elsevier, Amsterdam, 1989.

Park, J.W., and Chon, H., *J. Catal.* **133**, 159 (1992).

Peeters, M.P.J., de Haan, J.W., van de Ven, J.M., and van Hooff, J.H.C., *J. Chem. Soc. Chem. Commun.* p. 1560 (1992).

Pellet, R.J., Coughlin, P.K., Shamshoum, E.S., and Rabo, J.A., *in "Perspectives in Molecular Sieve Science"* ACS, Toronto, Canada, 1988, (W.H. Flank and T.E. Whyte, Eds.) p. 512. 1988.

Pereira, C., Parrillo, D.J., Kokotailo, G.T., and Gorte, R.J., RP125, in abstract proceedings 9th IZC, 1992.

Perry, R.H., and Green, D., *in "Perry's Chemical Engineers' Handbook"* 6th Edition, McGraw-Hill, New York, 1984.

Pines, H., in *"Chemistry of Catalytic Hydrocarbon Conversions"* Chpt. 1, Academic Press, New York, 1981.

Pluth, J.J, Smith, J.V., and Richardson, J.W., *J. Phys. Chem.* **92**, 2734 (1988).

Pluth, J.J., and Smith, J.V., in *"Zeolites: Facts, Figures, Future"* (P.A.Jacobs and R.A. van Santen Eds.) p. 835. Elsevier, Amsterdam, 1989.

Prasad, S., and Balakrishnan, I., *Cat. Lett.* **11**, 105 (1991).

Pyke, D.R., Whitney, P., and Houghton, H., *Appl. Catal.* **18**, 173 (1985).

Quann, R.J., Green, L.A., Tabak, S.A., and Krambeck, F.J., *Ind. Eng. Chem. Res.* **27**, 565 (1988).

Qui, S., Tian, W., Pang, W., Sun, T., and Jiang, D., *Zeolites* **11**, 371 (1991).

Quinwei, Z., and Jingfa, D., *J. Catal.* **116**, 298 (1989).

Rabo, J.A., *in "Zeolite Chemistry and Catalysis"* (J.A. Rabo, Ed.), p. 332. ACS Monograph 171, Am. Chem. Soc., Washington, D.C., 1976.

Rabo, J.A., Bezman, R.D., and Poutsma, M.L., *Acta. Phys. Chem* **24**, 39 (1978).

Rabo, J.A., in *"New Advances in Molecular Sieve Science and Technology"* Periodica Polytechnica, Technical University, Budapest, p. 211. 1986.

Rabo, J.A., in *"Zeolite Microporous Solids: Synthesis, Structure, and Reactivity"* Sintra, Estoril Portugal, 1991, (E. Derouane, F. Lemos, C. Naccache and F.R. Ribeiro) p. 531. NATO ASI Series, Series C: Mathematical and Physical Sciences - Vol. 352, Kluwer Academic, Dordrecht/Boston/London, 1991.

Rabo, J.A., in *"Zeolites as Catalysts, Sorbents and Detergent Builders"* (H.G. Karge and J. Weitkamp Eds.) p. 1. Elsevier, Amsterdam, 1989.

Rajic, N., Kaucic, V., and Stojakovic, D., *Zeolites* **10**, 169 (1990).

Rajic, N., Stojakovic, D., and Kaucic, V., *Zeolites* **11**, 612 (1991).

Ratnasamy, P., and Sivasanker, S., U.S.Patent. 4,950,821, Aug 21 1990.

Reid, R.C., in *"Chemical Applications of Graph Theory"* (A.T. Balaban, Ed.) Chpt. 4. Academic Prèss, New York, 1976.

Ren, X., Komarneni, S., and Roy, D.M., *Zeolites* **11**, 142 (1991).

Richter, M., Fiebig, W., Jerschkewitz, H.-G., Lischke, G., and Öhlmann, G., *Zeolites* **9**, 238 (1989).

Robertson, S.D., McNicol, B.D., De Baas, J.H., Kloet, S.C., and Jenkins, J.W., *J. Catal.* **37**, 424 (1975).

Rocchiccioli-Deltcheff, C., Thouvenot, R., and Franck, R., *Spectrochim. Acta Part A* **32**, 587 (1976).

Rocchiccioli-Deltcheff, C., Amirouche, M., Herve, G., Fournier, M., Che, M and Tatibouet, J-M., *J. Catal.* **126**, 591 (1990).

Saito, Y., Cook, N.P., Niiyama, H., and Echigoya, E., *J. Catal.* **95**, 49 (1985).

Sauer, J., *in "Recent Advances in Zeolite Science"* (J. Klinowski and P.J. Barrie, Eds.) p. 73. Elsevier, Amsterdam, 1989.

Sauer, J., and Schirmer, W., *in "Innovations in Zeolite Materials Science"* (P.J. Grobet, W.J. Mortier, E.F. Vansant and G. Schulz-Ekloff, Eds.) p. 323. Elsevier, Amsterdam, 1988.

Schubert, S., Ziethen, H.M., Trautwein, A.X., Schmidt, F., Lee, H-X., Martens, J.A., and Jacobs, P.A., *in "Zeolites as Catalysts, Sorbents and Detergent Builders"* (H.G. Karge and J. Weitkamp, Eds.) p. 735. Elsevier, Amsterdam, 1989.

Schooneydt, R.A., de Vos, R., Pelgrims, J., and Leeman, H., *in "Zeolites: Facts, Figures, Future"* (P.A.Jacobs and R.A. van Santen, Eds.) p. 559. Elsevier, Amsterdam, 1989.

Schwarz, S., Kojima, M., and O'Connor, C.T., *Appl. Catal.* **56**, 263 (1989).

Schwarz, S., Kojima, M., and O'Connor, C.T., *Appl. Catal.* **73**, 313 (1991a).

Schwarz, S., Kojima, M., and O'Connor, C.T., *Appl. Catal.* **68**, 81 (1991b).

Scherzer, J., A.C.S. Symp. Sre. Vol. 248, (T.E. Whyte *et al.*, Eds.) p. 157. Am. Chem. Soc., Washington DC, 1984.

Sermon, P.A., and Bond, G.C., *Catal. Rev.* **8(2)**, 211 (1973)

Serwicka, E.M., and Grey, C.P., *Colloids and Surfaces* **45**, 69 (1990).

Serwicka, E.M., Bruckman, K., Haber, J., Paukshtis, E.A., and Yurchenko, E.N., *Appl. Catal.* **73**, 153 (1991).

Shihabi, D.S., Garwood, W.E., Chu, P, Miale, J.N., Chu, C.T-W., and Chang, C.D., *J. Catal.* **93**, 471 (1985).

Shiralkar, V.P., Saldarriaga, C.H., Perez, J.O., Clearfield, A., Chen, M., Anthony, R.G., and Donohue, J.A., *Zeolites* **9**, 474 (1989).

Skupinska, J., *Chem. Rev.* **91**, (1991).

Smith, B.P., *AlChe. J.* **5**, 26 (1959).

Smith, J.M, and Van Ness, H.C., *in "Introduction to Chemical Engineering Thermodynamics"* 4th Edition, McGraw-Hill, New York, 1987.

Stencel, J.M., Diehl, J.R., D'Este, J.R., Makovsky, L.E., Rodrigo, L., Marcinkowska, K., Adnot, A., Roberge, P.C., and Kaliaguine, S., *J. Phys. Chem.* **90**, 4739 (1986).

Suzuki, J., Kiyozumi, Y., Matsuzaki, K., and Shin, S., *Appl. Catal.* **42**, 35 (1988).

Suzuki, M., Tsutsumi, K., Takahashi, H., and Saito, Y., *Zeolites* **9**, 98 (1989).

Szostak, R., Nair, V., Simmons, D.K., Thomas, T.L., Kuvadia, R., Dunson, B., and Shieh, D.C., *in "Innovations in Zeolite Materials Science"* (P.J. Grobet, W.J. Mortier, E.F. Vansant and G. Schulz-Ekloff, Eds.) p. 403. Elsevier, Amsterdam, 1988.

Szostak, R., Nair, V., and Thomas, T.L., *J. Chem. Soc. Faraday Trans. 1.* **83**, 487 (1987).

Szostak, R., *in "Guidelines for mastering the properties of molecular sieves"* (D. Barthomeuf, E.G. Derouane and W. Holderich, Eds.) p. 95. NATO ASI Series B: Physics Vol 221, Plenum Press. New York, 1990.

Szostak, R., *"Handbook of Molecular Sieves"*, Van Nostrand Reinhold, New York, 1992.

Tabak, S.A., U.S. Patent, 4547612, 1985.

Tabak, S.A., Krambeck, F.J., and Garwood, W.E., *AlChe. Journal* **32**, (9), 1526 (1986).

Tabak., S.A., and Yurchak, S., *in "Cat. Sci & Tech."* (J.R., Anderson and M. Boudart, Eds.) p. 307. Springer Verlag, New York, 1990.

Tang, R-Y., Zhang, S., Wang, C., Liang, D., and Lin, L., *J. Catal.* **106**, 440 (1987).

Tapp, N.J., Milestone, N.B., and Wright, L.J., *J. Chem Soc. Chem. Commun.*, 1801, 1985.

Tapp, N.J., Milestone, N.B., and Bibby, D.M., *in "Innovations in Zeolite Materials Science"* (P.J. Grobet, W.J., Mortier E.F. Vansant, and G. Schulz-Ekloff, Eds.) p. 393. Elsevier, Amsterdam, 1988a.

Tapp, N.J., Milestone, N.B., and Bibby, *Zeolites* **8**, 183 (1988b).

Tapp, N.J., Milestone, N.B., Bowden, M.E., and Meinhold, R.H., *Zeolites* **10**, 105 (1990).

Taylor, D.B., McMonagle, J.B., and Moffat, J.B., *J. Colloid Interface Sci.* **108**, 278 (1985).

Theocharis, C.R., Gelsthorpe, M.R., and Yeates, D., *J. Chem. Soc. Faraday Trans. 1*. **85**, 2641 (1989).

Thomson, R., Noh., N.M., and Wolf, E.E., Chpt. 7. ACS, p. 75. (1990a).

Thomson, R., Montes, C., Davis, M.E., and Wolf, E.E, *J. Catal.* **124**, 401 (1990b).

Thouvenot, R., Rocchiccioli-Deltcheff, C., and Fournier, M., *J. Chem. Soc., Chem. Commun.*, 1352 (1991).

Thouvenot, R., Fournier, M., and Rocchiccioli-Deltcheff, C., *J. Chem. Soc. Faraday Trans. 1* **87**, 2829 (1991).

Tsigdinos, G.A., *Ind. Eng. Chem. Prod. Res. Develop.* **13**, 267 (1974).

Tsigdinos, G.A., *Methodicum Chimicum* **8** *in* "Preparations of Transition Metal Derivatives" (Niedenzu and Zimmer, Eds.) p. 553. Acadenic Press, 1976.

Tsigdinos, G.A., *Topics in Current Chemistry* **76**, 1 (1978).

Uytterhoeven, J.B., *Acta. Phys. Chem.* **24**, 53 (1978).

Unmuth, E.E., Schwartz, L.H., and Butt, J.B., *J. Catal.* **61**, 242 (1980).

Van Ballmoos, R and Higgins, J.B., *Zeolites* **10**, (1990), Butterworth-Heinemann.

Van Hooff, J.H.C., and Roelofsen, J.W., *in "Introduction to Zeolite Science and Practice"* (H. van Bekkum, E.M. Flanigen and J.C. Jansen, Eds.) p. 241. Elsevier, Amsterdam, 1991.

Van Koningsveld, H., *in "Introduction to Zeolite Science and Practice"* (H. van Bekkum, E.M. Flanigen and J.C. Jansen, Eds.) p. 35. Elsevier, Amsterdam, 1991.

Van Niekerk, M., PhD Thesis, University of Cape Town, 1992.

Van't Blik, H.F.J., and Prins, R., *J. Catal.* **97**, 188 (1986).

Van't Blik, H.F.J., Koningsberger, D.C., and Prins, R., *J. Catal.* **97**, 210 (1986).

Vedrine, J.C., Coudurier, G., and Mentzen, B.F., *in "Perspectives in Molecular Sieve Science"* (W.H. Flank and T.E. Whyte Jr., Eds.) p. 66. Chpt. 4. ACS Series 368, 1988.

Verstappen, J.J., and Waterman, H.I., *J. Inst. Petrol.* **41**, 343 (1955a).

Verstappen, J.J., and Waterman, H.I., *J. Inst. Petrol.* **41**, 347 (1955b).

Vinek, H., and Lercher, J.A., *J. Mol. Catal.* **64**, 23 (1991).

Wang, Q.L., Giannetto, G., Torrealba, M., Perot, G., Kappenstein, C., and Guisnet, M., *J. Catal.* **130**, 459 (1991).

Ward, J.W., *in "Zeolite Chemistry and Catalysis"* (J.A. Rabo, Ed.), p. 118. ACS Monograph 171, Am. Chem. Soc., Washington, D.C., 1976.

Weyda, H., and Lechert, H., *Zeolites* **10**, 251 (1990).

Wielers, A.F.H., Kock, A.J.H.M., Hop, C.E.C.A., Geus, J.W., and Van der Kraan, A.M., *J. Catal.* **117**, 1 (1989).

Wilshier, J.G., Smart, P., Western, R., Mole, T., and Behrsing, T., *Appl. Catal.* **31**, 345 (1987).

Wilson, S.T., Lok, B.M., Messina, C.A., Cannan, T.R., and Flanigen, E.M., *J. Am. Chem. Soc.* **104**, 1146 (1982).

Wilson, S.T., Lok, B.M., Messina, C.A., and Flanigen, E.M., *"Proceedings of 6TH International Zeolite Conference"* (D. Olson and A. Basio, Eds.) p. 97. Butterworths, Guildford, 1984.

Wilson, S.T., and Flanigen, E.M., *"Zeolite Synthesis"* ACS Symposium Series 398 (M.L. Occelli and H.E. Robson, Eds.) Chpt 23. p. 329. 1989.

Wilson, S.T., *in "Introduction to Zeolite Science and Practice"* (H. van Bekkum, E.M. Flanigen and J.C. Jansen, Eds.) p. 137. Elsevier, Amsterdam, 1991.

Wohlrab, S., Rademacher, O., and Scheler, H., O5, in abstract proceedings 9th IZC, (1992).

Xu, Y., Maddox, P.J., and Thomas, J.M., *Polyhedron* **8**, 819 (1989).

Xu, W., Li, R., Ma, J., and Fan, B., RP72, in abstract proceedings of 9TH IZC, 1992.

Yang, L., Aizhen, Y., and Qinhua, X., *Appl. Catal.* **67**, 169 (1991).

Appendices

Appendix I. 1-Butene isomerization data work-up

The following data was recorded or collected during a 1-butene isomerization run:

Flow 1-butene = 15 ml/min
Flow nitrogen (N_2) = 45 ml/min
Mass catalyst = 1.0 g, (bed volume = 0.5 cm^3) determined by placing 1 g of HPA catalyst in a 10 ml measuring cylinder.
Room temperature = 23°C

WHSV and GHSV calculation

Total flow rate of 1-butene = 15 ml/min (20°C)
Volume of catalyst bed = 0.5 cm^3

GHSV = volume of feed/volume of catalyst bed·h
GHSV = 15 × 60/0.5 = 1800 h^{-1}

WHSV = mass of 1-butene/mass catalyst·h
WHSV = [(0.015 × 56 × 60 × 101.325)/(8.314 × 293)]/1
WHSV = 2.1 (g.1-butene)/(g.catalyst)·h

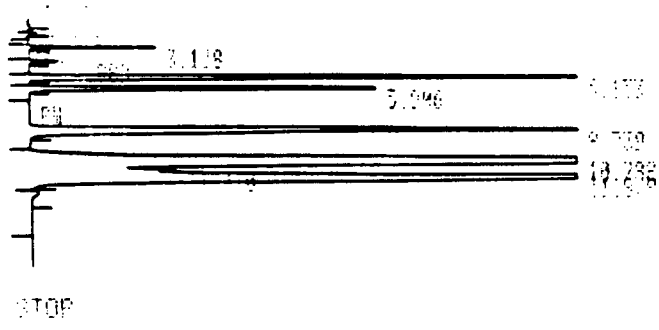

Figure Appendix I. 1-Butene isomerization GC printout.

Gas analysis (off-line)

Compound	RT(min)[1]	Area	Area%	RF[2]	Mass %
Methane	2.189	694	0.05	1.211	0.05
Ethane	3.138	10119	0.71	1.022	0.72
Ethene	4.083	3694	0.26	0.994	0.25
Propane	5.153	173150	12.19	1.000	11.99
Propene	5.906	56331	3.97	0.988	3.85
1-butene	8.739	172390	12.14	1.022	12.20
cisbutene	10.782	611980	43.09	0.949	44.70
isobutene	11.410	30711	2.16	1.055	2.02
transbutene	11.878	361050	25.42	0.969	24.22
Total	-	1420119	100.00	-	100.00

1. RT-retention time of compound
2. RF-response factor of compound

Conversion calculation:

From GC printout

mass % Conv = (100 - wt% 1-$C_4^=$ in product)
= 100 - 12.2 = 87.8 wt%

Selectivity to double bond shift (DBS) isomerization products
= (cis + trans $C_4^=$)/Conversion
= ([44.7 + 24.22]/87.8) × 100 = 78.5 %

Selectivity to skeletal isomerization = (iso-butene)/Conversion
= (2.02/87.8) × 100 = 2.3 %

Selectivity to cracking = ($C_1 + C_2 + C_3$)/Conversion
= ([0.05 + 0.72 + 0.25 + 11.99 + 3.85]/87.8) × 100 = 19.20 %

Mass balances was checked by monitoring the total GC area count, only those spectra with area counts within 5 % of each other were used (10 μl gas samples). The apparatus was also pressure tested before each run to ensure no leaks were present (pressure = 200 kPa for atmospheric apparatus).

Appendix II. *M*-xylene isomerization data work up

The following data was recorded or collected during a *m*-xylene isomerization run:

Mass of catalyst = 0.5 g
Flow N_2 = 100 ml/min (wet)
Room temperature = 24°C
T_{sat} = 20°C (temperature of top stage of the double stage saturator)
pp(*m*-xylene) at 20°C = 1 kPa (7.5 Torr) [Perry and Green, 1984]
Reactor temperature = 450°C
Reactor pressure = 115 kPa

WHSV calculation

Raoults law for ideal gas behaviour: $pp_m = y_m \times P_m^{sat}$
P_m^{sat} = from correlation or tables [e.g. Perry and Green, 1984]
$pp_m \times V = n_m \times R \times T$

mass *m*-xylene = $MW_{m\text{-}xyl} \times n_m$
WHSV = mass *m*-xylene/mass catalyst·h
$WHSV = pp_m \times V \times MW_{m\text{-}xyl}/R \times T \times m_{cat}$
$WHSV = [(1 \times 0.100 \times 60 \times 106)/(8.314 \times 297)]/0.25 = 1.05$
(g.feed)/(g.catalyst·h)

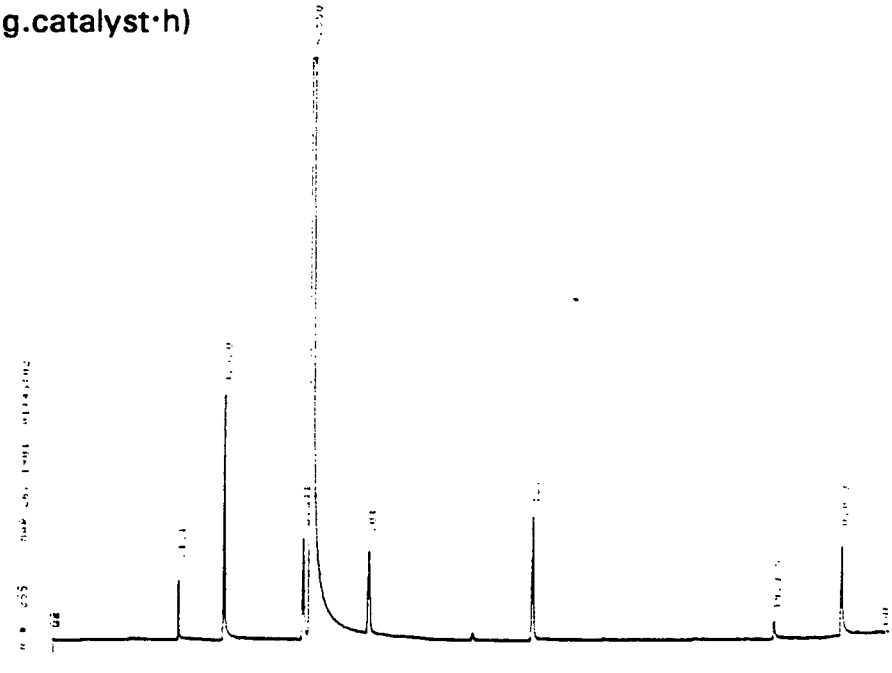

Figure Appendix II. *m*-xylene GC printout.

Conversion calculation to products other than m-xylene:

For the GC trace above (R6 *m*-xylene isomerization)

Compound	RT(min)[1]	Area	RF[2]	Mass%
Benzene	3.181	1238	1.12	0.52
Toluene	4.320	7127	1.07	2.87
p-xylene	6.341	4214	1.00	1.59
m-xylene	6.550	229632	1.04	89.84
o-xylene	8.017	3869	1.02	1.48
135TMB[3]	12.225	5484	0.98	2.02
TetraMB[4]	18.375	728	1.00	0.27
TetraMB	20.088	3724	1.00	1.40
Total	-	256016	-	100.00

1. RT = Retention time of component
2. RF = Response factor of component
3. TMB = trimethyl benzene
4. Tetra/MB = tetramethyl benzene

Conversion = (100 - 89.84) = 10.16 wt%

Selectivity to isomerization = (*o*-xylene + *p*-xylene)/Conversion

$$= [(1.48 + 1.59)/(10.16)] \times 100 = 30.2\ \%$$

Selectivity to disproportionation products

$$= (\text{Benzene} + \text{Toluene} + \text{TMB} + \text{TetraMB})/\text{Conversion}$$
$$= (0.52 + 2.87 + 2.02 + 0.27 + 1.40)/(10.16) = 67.0\ \%$$

Mass balances were checked by monitoring the total GC area count, only those spectra with area counts within 5 % were used. The apparatus was also pressure tested before each run to ensure no leaks were present (pressure = 200 kPa for atmospheric apparatus).

Appendix III. 2-Methylpent-2-ene (2M2P) isomerization data work-up

The following data was recorded or collected during a 2-methylpent-2-ene isomerization run:

Catalyst mass = m_{cat} = 0.25 g
Reactor temperature = 200°C
Total pressure = 115 kPa
Saturator temperature = 18°C
Room temperature = T = 20°C
Partial pressure of 2M2P [pp(2M2P)] at 18°C = 15.38 kPa
Volumetric flowrate N_2 = V = 100 ml/min (wet)

The partial pressure of 2-methyl-2-pentene was calculated using the process package HYSIM (1991).

WHSV calculation

$WHSV = [pp(2M2P) \times MW_{2M2P} \times V/R \times T]/m_{cat}$
$WHSV = [15.38 \times 84 \times (0.100 \times 60)/(8.314 \times 293)]/(0.25) = 11.02$
(g.2M2P)/(g.catalyst)·h

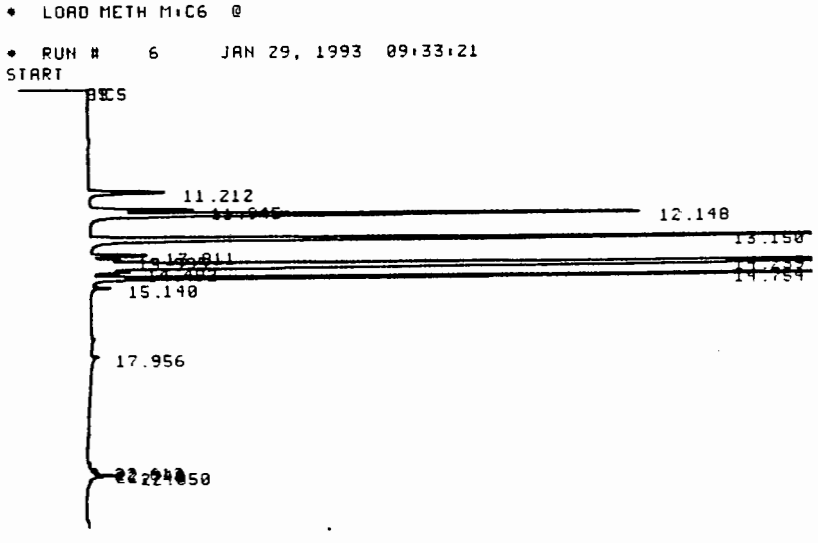

Figure Appendix III. 2-methyl-2-pentene isomerization GC printout.

Conversion and selectivity calculations

Compound	RT	Area	RF	mass %
$DMC_4^=$	11.212	12210	1.0	1.57
c-2M3P	11.945	15135	1.0	1.94
t-2M3P	12.148	78212	1.0	10.05
2M1P	13.150	123603	1.0	15.88
$C_6^=$	13.811	6809	1.0	0.87
$C_6^=$	13.995	3101	1.0	0.40
2M2P	14.239	449500	1.0	57.75
$C_6^=$	14.492	4121	1.0	0.53
4M2P	14.754	77572	1.0	9.97
$C_6^=$	15.140	1675	1.0	0.22
Oligomers	-	6461	1.0	0.83
Total	-	778399	--	100.00

Conversion = (100 - 57.75) = 42.25 wt%

Ratio of selectivity to double bond shift products (DBS) to selectivity to methyl shift products

$$= (9.97/(10.05 + 1.94)) = 0.83$$

Ratio of 2M2P to 2M1P

$$= (57.75/15.88) = 3.64$$

Nomenclature of compounds

$DMC_4^=$ - dimethyl butene
c-2M3P - cis-2-methyl-3-pentene
t-2M3P - trans-2-methyl-3-pentene
2M1P - 2-methyl-1-pentene
$C_6^=$ - linear C_6 alkene
2M2P - 2-methylpent-2-ene
4M2P - 4-methyl-2-pentene

Mass balance calculation:

The amount of liquid product collected at 5°C in the catchpot was collected after each run and weighed and the volume of 2-methyl-2-pentene used during the run determined by measuring the drop in the liquid (2M2P) level in the saturator (I.D. = 35 mm). Knowing the density of 2-methyl-2-pentene ($\rho = 0.69$ g/cm^3) and the volume consumed during the run a simple mass balance can be done:

Mass collected (after 121 min) = 5.38 g
Volume loss = 8.18 cm^3 ($\Delta h = 0.85$ cm) = 5.64 g

Mass balance = (5.38/5.6) × 100 = 95.4%

A further check on the mass balance was done by monitoring the total area count of each GC spectrum. Each total area was within 5 % of each other. The apparatus was pressure tested before each run to ensure that no leaks were present (pressure = 200 kPa)

Appendix IV. Propene oligomerization data work-up

The following data was recorded or collected during a propene oligomerization run (see run sheet shown below):

Liquid sample masses (M_L) over a time interval Δt (g)
Wet gas flow meter (WGFW) reading over the time interval (t1 to t2), $WGFM^1$ and $WGFM^2$ (ℓ)
Temperature of WGFW (°C)
GC analysis of gas sample (analyzed off-line), taken at $t = \Delta t/2$ or $t = (t2-1/2)$ h
Reactor jacket temperature (°C)
Bed temperature (at hot spot) (°C)
Reactor pressure (MPa)
Pump setting (vernier scale 0-10)
Mass of catalyst (g)
mass of gas cylinder and contents at start and end of run (kg)

Calculation of Conversion

The conversion quoted is the mass of propene converted to liquid (collected in a catchpot at 5°C). To determine the conversion the mass of gas and mass of liquid exiting the catchpot have to be determined. The calculations are shown below.

Calculation of mass of gas exiting during time interval, Δt:

From the WGFM:

$$V = c_f \times (WGFM^2 - WGFM^1)/\Delta t$$

where

V = volumetric flowrate (dm^{-3}/h)
c_f = correction factor for WGFM (0.942)
$WGFM^1$, $WGFM^2$ = WGFM reading (ℓ)
Δt = time interval in hours

Then by using Raoults law

$P \times V = z \times n \times R \times T$, where T = (K) and z = compressibility factor of exiting gas stream (0.95) (see below for detailed calculation)

and knowing the average molecular weight, MW_{av}, of the exiting gas

$$M_g = P \times V \times MW_{av}/(z \times n \times R \times (T + 273.15))$$

M_g = gas flow rate (g/h)
P = atmospheric pressure (101 325 Pa)
R = universal gass constant (8.314 J/K·gmol)
T = WGFM temperature (°C)

Calculation of compressibility factor

	MW	Mass%	Mol%	T_c(K)	P_c(bar)	T_r	P_r	Z
Ethane	30.07	3.33	2.21	305.4	48.8	0.959	2.05	0.978
Propane	44.09	72.10	70.36	369.8	42.5	0.792	2.35	0.960
Propene	42.08	14.41	13.43	365.0	46.2	0.803	2.16	0.964
Butanes	58.00	1.15	4.37	425.0	38.0	0.689	2.63	0.887
Butenes	56.00	4.43	2.53	419.6	40.2	0.698	2.49	0.941
Pentenes	70.00	1.83	2.83	464.7	40.5	0.631	2.47	0.924
Hexenes	84.00	2.75	4.26	500.0	40.8	0.586	2.45	0.908

where $T_r = T/T_c$ and for gas mixtures $P_r = P/P_c$ where P = 1 atm for our system. Knowing T_c and P_c the compressibility factor for each component i, Z_i, can be calculated from generalized charts or correlations (e.g. Smith and Van Ness, 1987).

The mean compressibility factor, Z_m, can be calculated from:

$Z_m = \Sigma(Z_i \times y_i)$ so for the above mixture, Z_i is the individual compressibility of component i and y_i = mol fraction of component i.

$$Z_m = 0.022 + 0.675 + 0.129 + 0.039 + 0.024 + 0.026 + 0.039$$
$$Z_m = 0.95$$

Calculation of average molecular weight of gas stream

From the previous table the average molecular weight is then calculated from

$MW_{av} = \Sigma\ (y_i \times MW_i)$ where y_i is the mol fraction of *i* in the gas phase. For the table above the $MW_{ave} = 45$ g/mol

For a typical oligomerization run

Mass cat = 1 g
$\Delta t = 1$ h
$WGFM^2 = 72.9$ *l*
$WGFM^1 = 71.9$ *l*
$T_{WGFM} = 26°C$
$M_L = 9.46$ g (collected in $\Delta t = 1$ h)
$MW_{av} = 45$ g/mol

$\therefore\ M_g = 1.0 \times 101.325 \times 45/(8.314 \times (26 + 273.15))$
$M_g = 1.83$ g/h

Then conversion is as follows

$M_L = 9.46$ g/h

Conversion of feed
$= Conv_f = M_L/(M_g + M_L) \times 100 = 9.46/(9.46 + 1.83) \times 100 = 84$

since the feed consists of 86 % propene

Conversion of propene = Conv. = $Conv_f/0.86 = 97.4$ %

(data may also be presented as fractional conversion of propene which is simply Conv./100)

$WHSV = (M_L + M_g)/\text{mass cat} = 11.29$ (g.feed)/(g.catalyst)·h

Selectivity and Yield calculations

Selectivity (ratio of amount of one product to the amount of another)

From the liquid product GC spectra, C_{12} wt% fraction = 15 wt%.

Selectivity to C_{12} = Yield/Conversion = (0.15 × 0.75)/0.75

Yield of C_{12}(fraction of reactant converted to product)

Yield C_{12} = Conversion × wt% C_{12}

Therefore yield C_{12} = 0.75 × 0.15 = 0.11 $(g \cdot C_{12})/(g \cdot C_3^=)$ converted

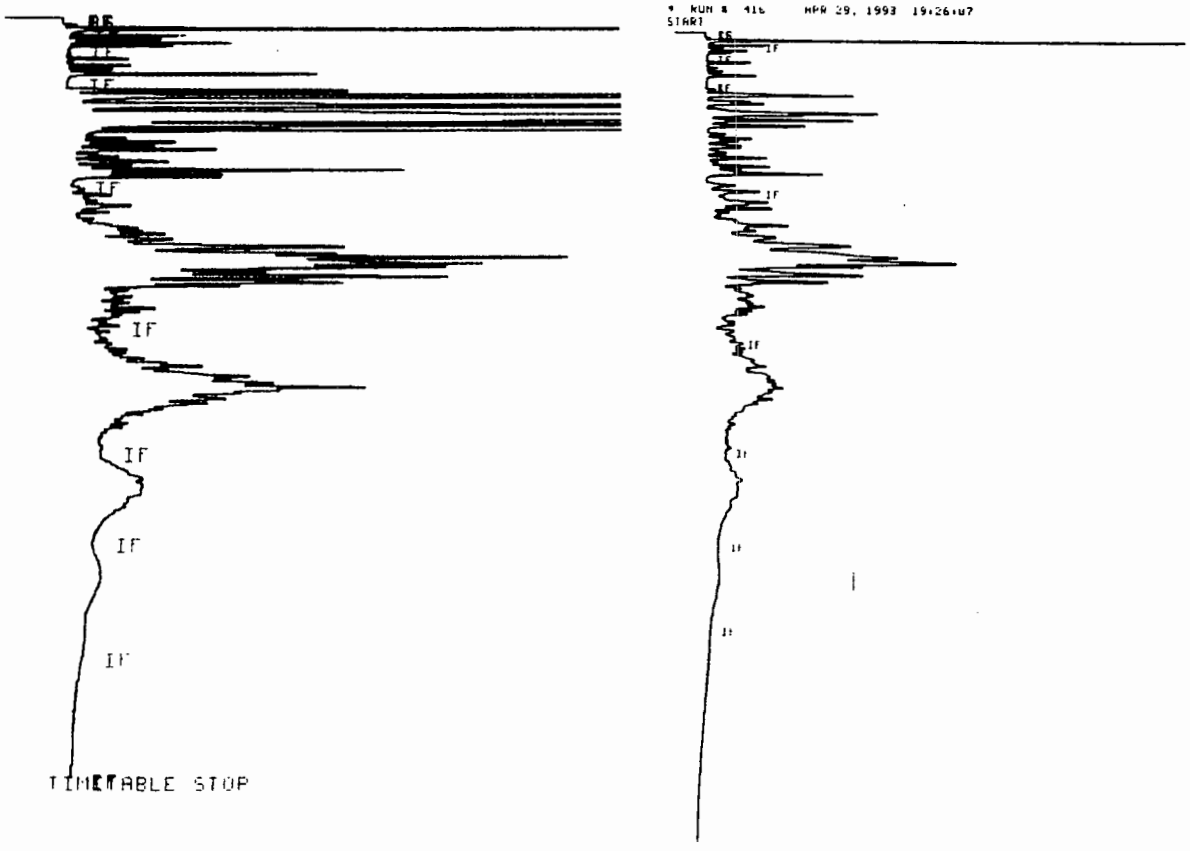

Figure Appendix IV. GC LP trace of SAPO and HPA product.

Catalyst utilization value (CUV) calculation

CUV is defined as mass of liquid produced per mass of catalyst. For the run sheet provided

$CUV = \Sigma\ (M_L) = 1231.44$ (g.liquid)/(g.catalyst)

Mass balance check

The overall mass balance was checked by comparing the total calculated mass exiting versus the mass loss from the gas cylinder, e.g.

Weight of gas cylinder before run: $M_{cyl} = 7.546$ kg
Weight of gas cylinder after the run: $M_{cyl} = 5.439$ kg.

$\therefore$ Mass loss of feed from cylinder = 7.546 - 5.439 = 2.107 kg

Total Mass exiting the rig = $\Sigma(M_L + M_g) = 2058$ g

Mass balance = 2058/2107 x 100 = 97.7 %

Runs were only reported/accepted when the mass balance tie was greater than 95 %. Values less than 95 % were usually due to leaks prior to the reactor.

Run Sheet MS(6)-S11(3) Run Time (h)	WGFM (l)	T(WGFM) (deg C)	Pump setting	Mass Liquid (g/hr)	Ave MW = 50 Mass gas (g/hr)	WHSV	Feed Conv %	Propene Conv %	Total Mass Exiting (g)	Mass Liquid Exiting (CUV)
0.0	79.6	25	3.2	-	-	-	-	-	0	
1.0	81.3	25	3.2	9.26	3.47	12.7	72.7	84.6	13	9
2.0	82.5	25	3.2	9.93	2.45	12.4	80.2	93.2	12	10
3.0	84.1	25	3.2	10.81	3.27	14.1	76.8	89.3	14	11
18.0	110.7	25	3.2	10.84	3.62	14.5	74.9	87.1	217	163
19.0	112.7	25	3.2	9.47	4.09	13.6	69.8	81.2	14	9
20.0	114.5	25	3.2	8.82	3.68	12.5	70.6	82.1	12	9
27.0	127.5	26	3.2	9.10	3.78	12.9	70.6	82.1	90	64
46.0	166.5	24	3.2	8.78	4.21	13.0	67.6	78.6	247	167
48.0	170.8	24	3.2	8.27	4.41	12.7	65.2	75.8	25	17
49.0	173.2	24	3.2	8.35	4.92	13.3	62.9	73.2	13	8
69.0	219.6	23	3.2	7.81	4.77	12.6	62.1	72.2	252	156
70.0	221.9	23	3.2	7.40	4.73	12.1	61.0	70.9	12	7
92.0	278.0	23	3.2	7.39	5.25	12.6	58.5	68.0	278	163
93.0	280.4	23	3.2	6.82	4.94	11.8	58.0	67.4	12	7
112.0	333.3	22	3.2	6.87	5.75	12.6	54.4	63.3	240	131
113.0	336.1	23	3.2	6.58	5.76	12.3	53.3	62.0	12	7
114.0	339.1	23	3.2	6.42	6.17	12.6	51.0	59.3	13	6
119.0	354.0	24	3.2	6.39	6.11	12.5	51.1	59.4	63	32
120.0	357.0	24	3.2	6.33	6.15	12.5	50.7	59.0	12	6
139.0	416.7	22	3.2	6.30	6.49	12.8	49.3	57.3	243	120
141.0	422.7	23	3.2	5.93	6.17	12.1	49.0	57.0	24	12
161.0	478.9	23	3.2	5.65	5.78	11.4	49.4	57.5	229	113
162.0	481.7	22	3.2	5.77	5.78	11.6	50.0	58.1	12	6
					Average	12.7		Total	2058	1231

Appendix V. Cetane number calculation

The H^1-NMR spectra of two hydrogenated liquid products are shown in the following pages.

According to Gautier (1988), the Cetane number (CN) can be calculated from the formula shown below:

$$CN = -0.0571\ H_3 + 0.935\ H_2 - 0.454\ H - 0.718\ H_a + 0.102\ H_d$$

where,

H_3 = relative amount of H in CH_3 groups range 0.5-1.06 ppm
H_2 = relative amount of H in CH_2 groups range 1.06-1.8 ppm
H = relative amount of H in CH groups range 1.8-4.0 ppm
H_a = relative amount of H in aromatic rings range 6.5-7.05 ppm
H_d = relative amount of H attached to aromatic ring-junction carbon range 7.05-9.0 ppm

From the spectra it can be seen that no aromatic hydrogens exist and the relative amounts of CH_3 and CH_2 are 40 and 60% respectively.
Therefore for the two H^1-NMR spectra shown:

For AlPW:nitrate(2)

$CN = (47.6 \times 0.935) - (52.4 \times 0.0571)$
$CN = 41.5$ and,

For S11(3)

$CN = (46.7 \times 0.935) - (53.3 \times 0.0571)$
$CN = 40.6$

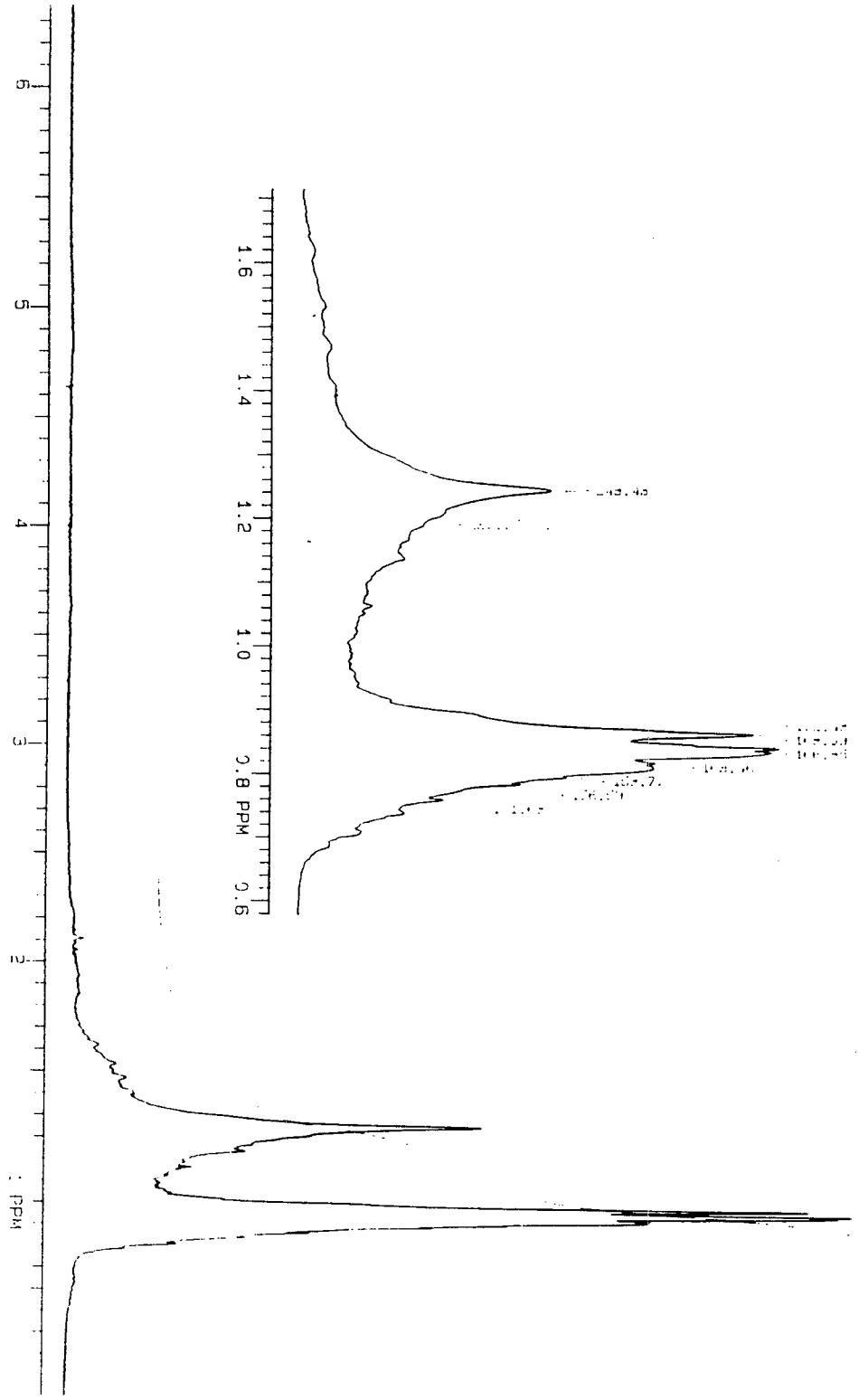

Figure Appendix V. H^1-NMR spectra of liquid product of AlPW:nitrate(2).

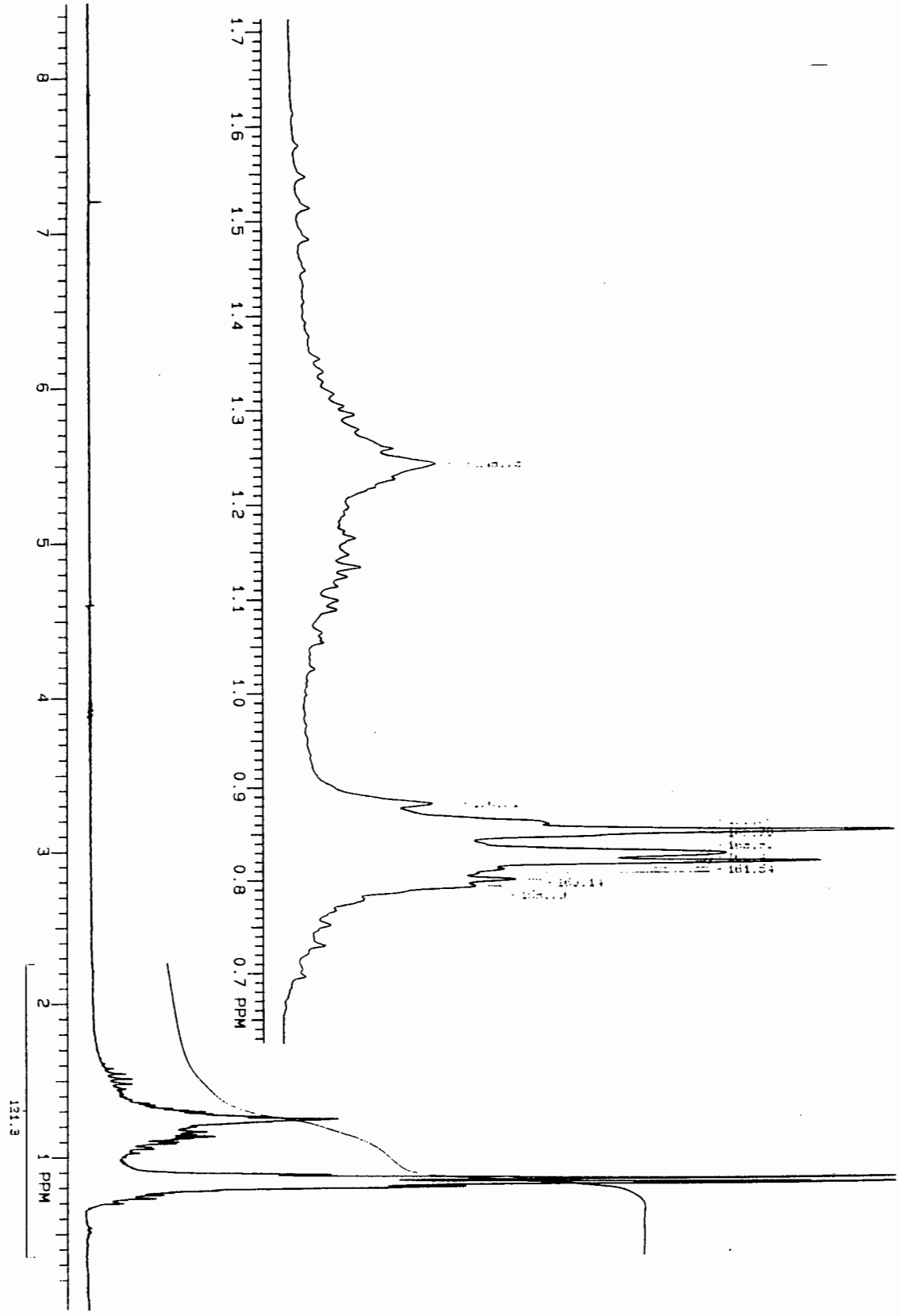

Figure Appendix V. H^1-NMR spectra of liquid product of S11(3).

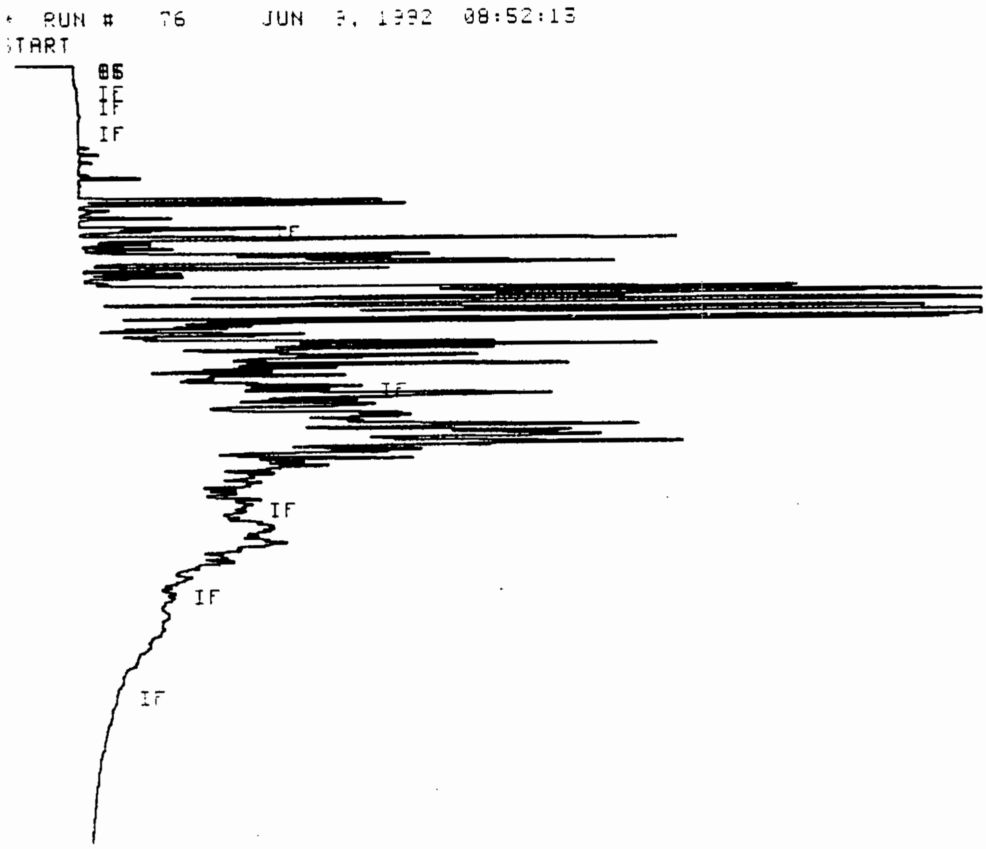

Figure Appendix V. GC trace of total hydrogenated product (AlPW:nitrate(2)).

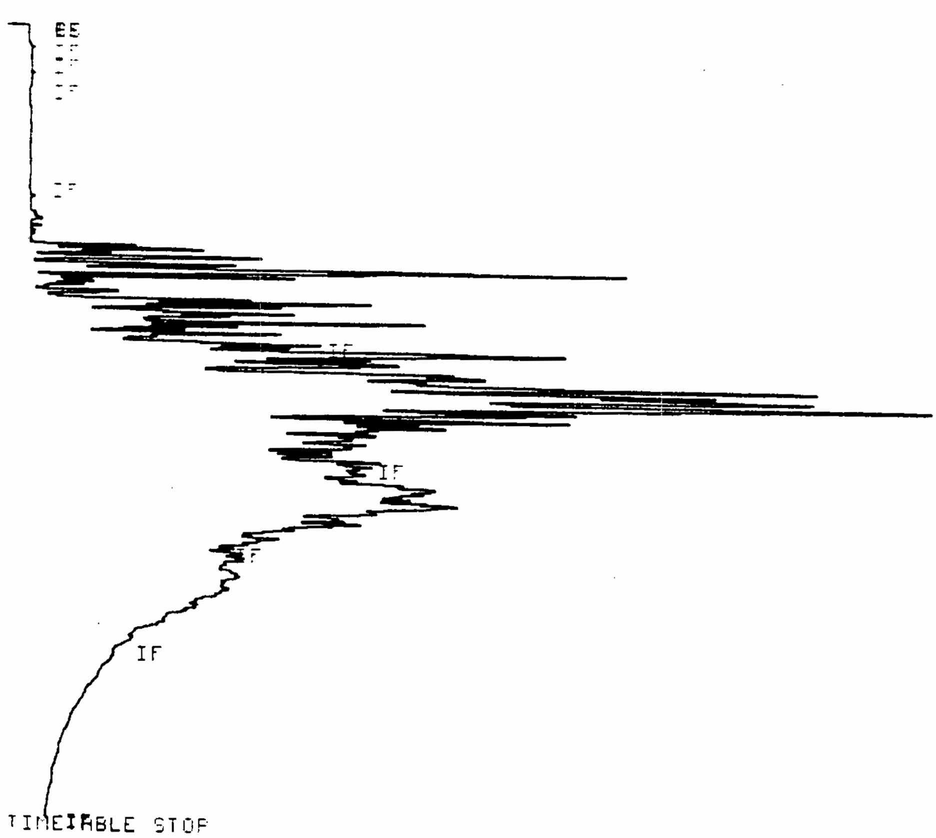

Figure Appendix V. GC trace of fractionated (+180°C) hydrogenated distillate (AlPW:nitrate(2)).

Appendix VI. TPR K-value determination

Monti and Baiker (1983) have proposed the use of a characteristic number, K, to assist in the selection of appropriate operating variable for TPR. They have suggested that for commonly used heating rates, between 0.1 and 0.3 K/s the limiting values of K are $55 < K < 140$ s.

$K = S_o/(V^* \cdot c_o)$ where

S_o = amount of reducible metal (μmol)
V^* = total volumetric flowrate of H_2 in N_2 (cm^3(NPT)/s) and
c_o = concentration of hydrogen ($\mu mol/cm^3$)

For the system used in this study the flowrate and hydrogen concentration were kept constant and the amount of catalyst varied to obtain the required K value (typically 65 s).

Sample calculation:

Concentration of reducing gas = 5 % H_2 in N_2, 60 ml/min (20°C), 3.7 wt% Ni on catalyst (0.25 g)

$c_o = 2.231$ $\mu mol/cm^3$
$V^* = 0.93$ cm^3/s
$S_o = (0.037 \times 0.25/58.71) = 157.5$ μmol

$K = 157.5/(0.93 \times 2.231) = 75.8$ s

Appendix VII. FT-IRs spectra of HPAs

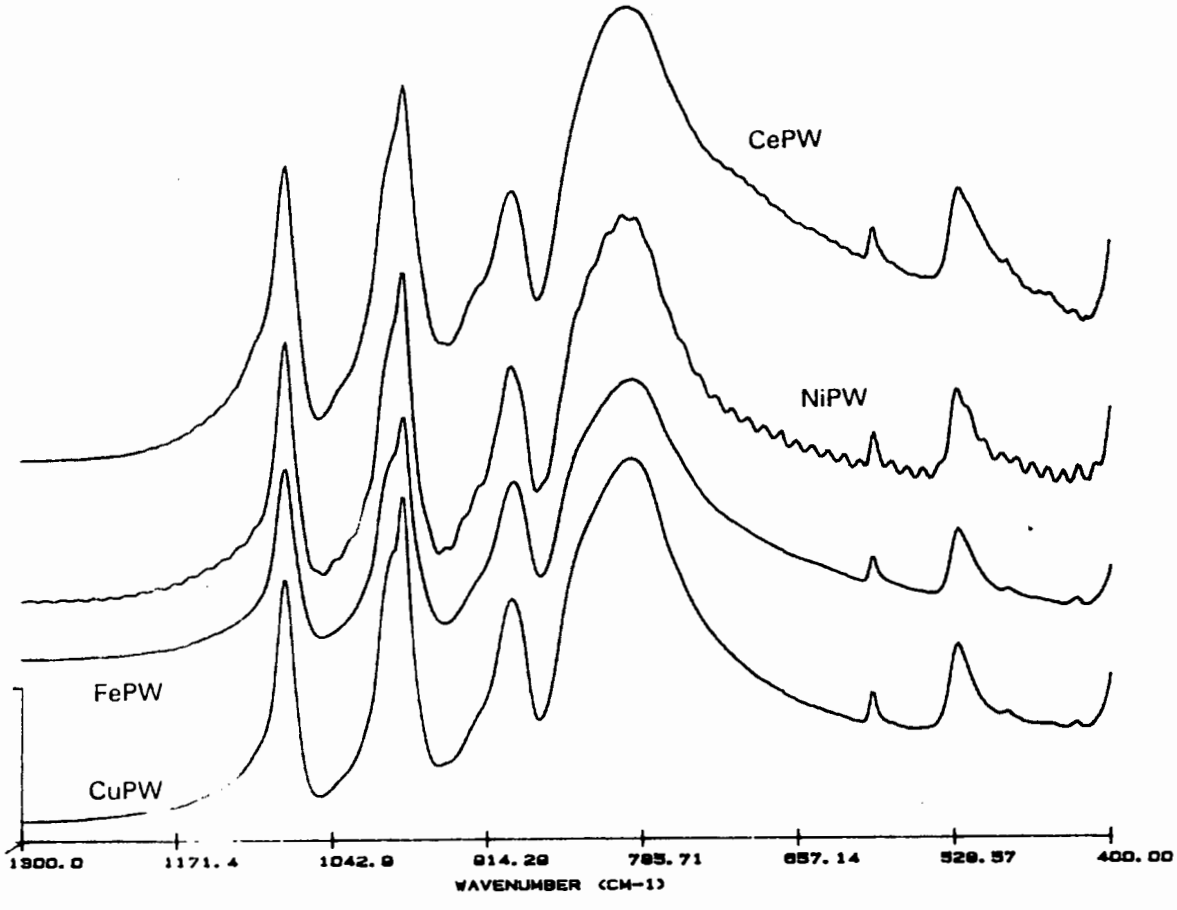

Appendix VII. FT-IR spectra of SAPOs

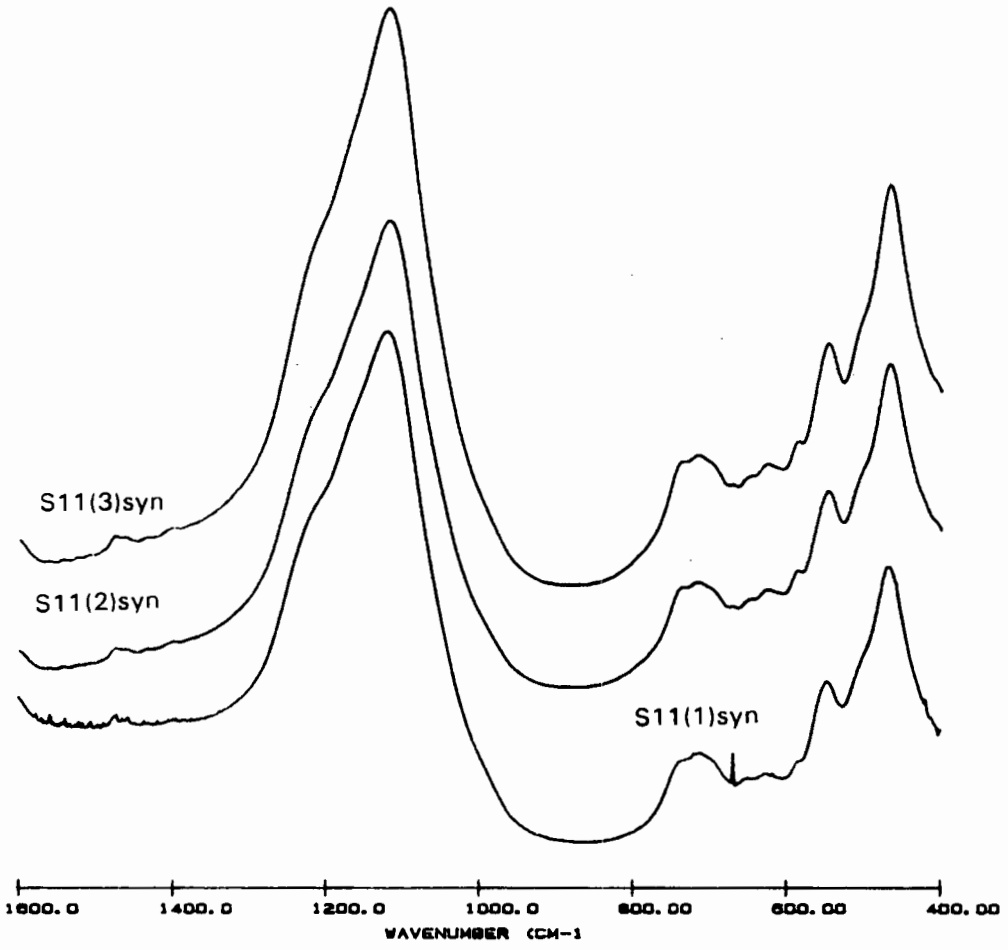

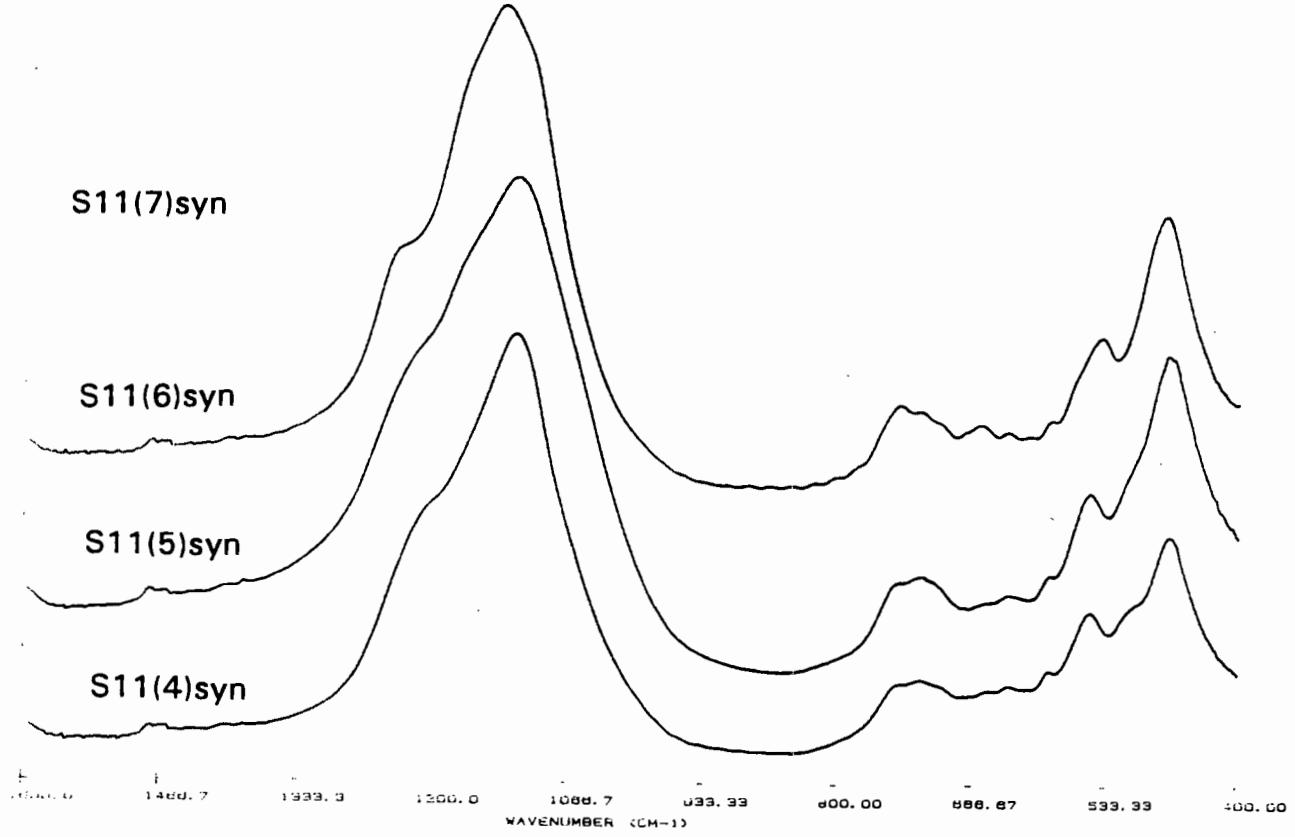

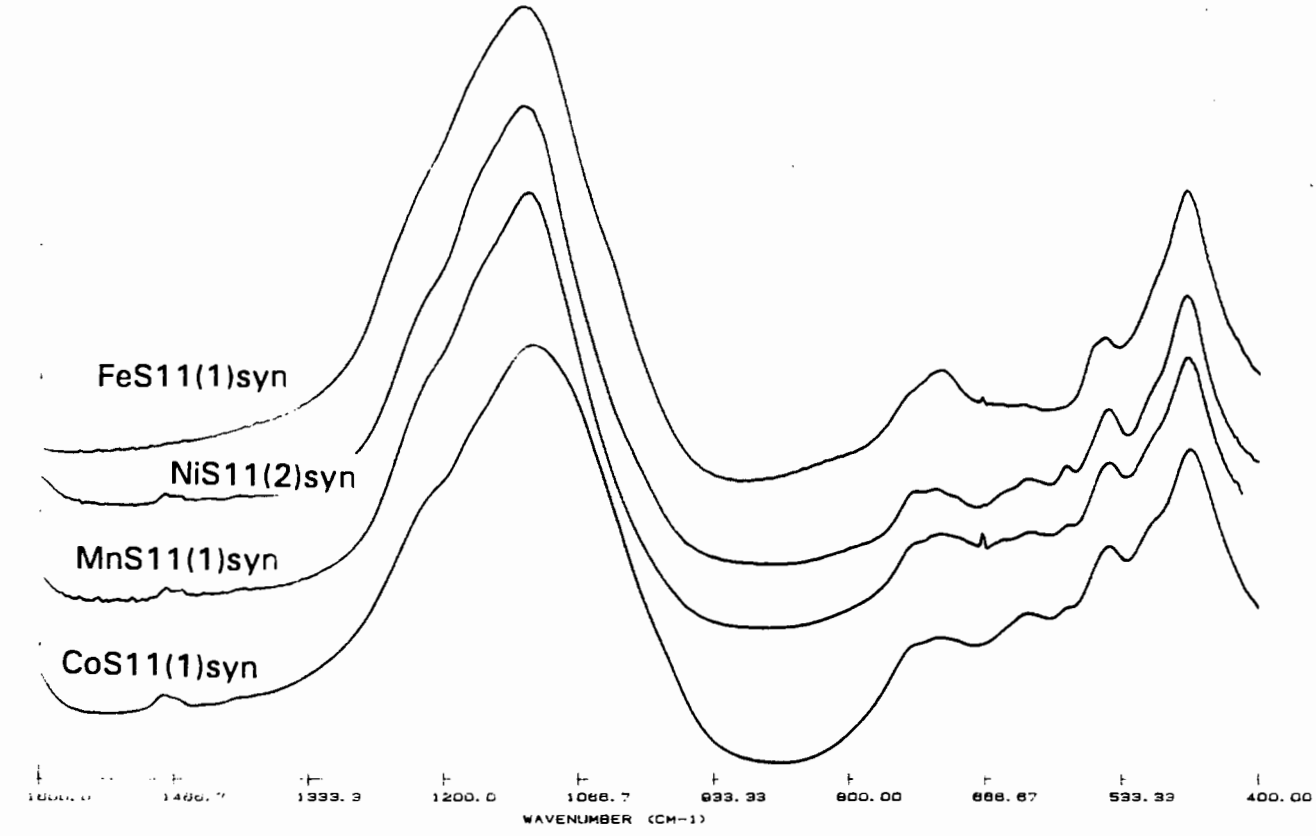
FeS11(1)syn
NiS11(2)syn
MnS11(1)syn
CoS11(1)syn
1933.3
1200.0
1066.7
933.33
800.00
666.67
533.33
400.00
WAVENUMBER (CM-1)

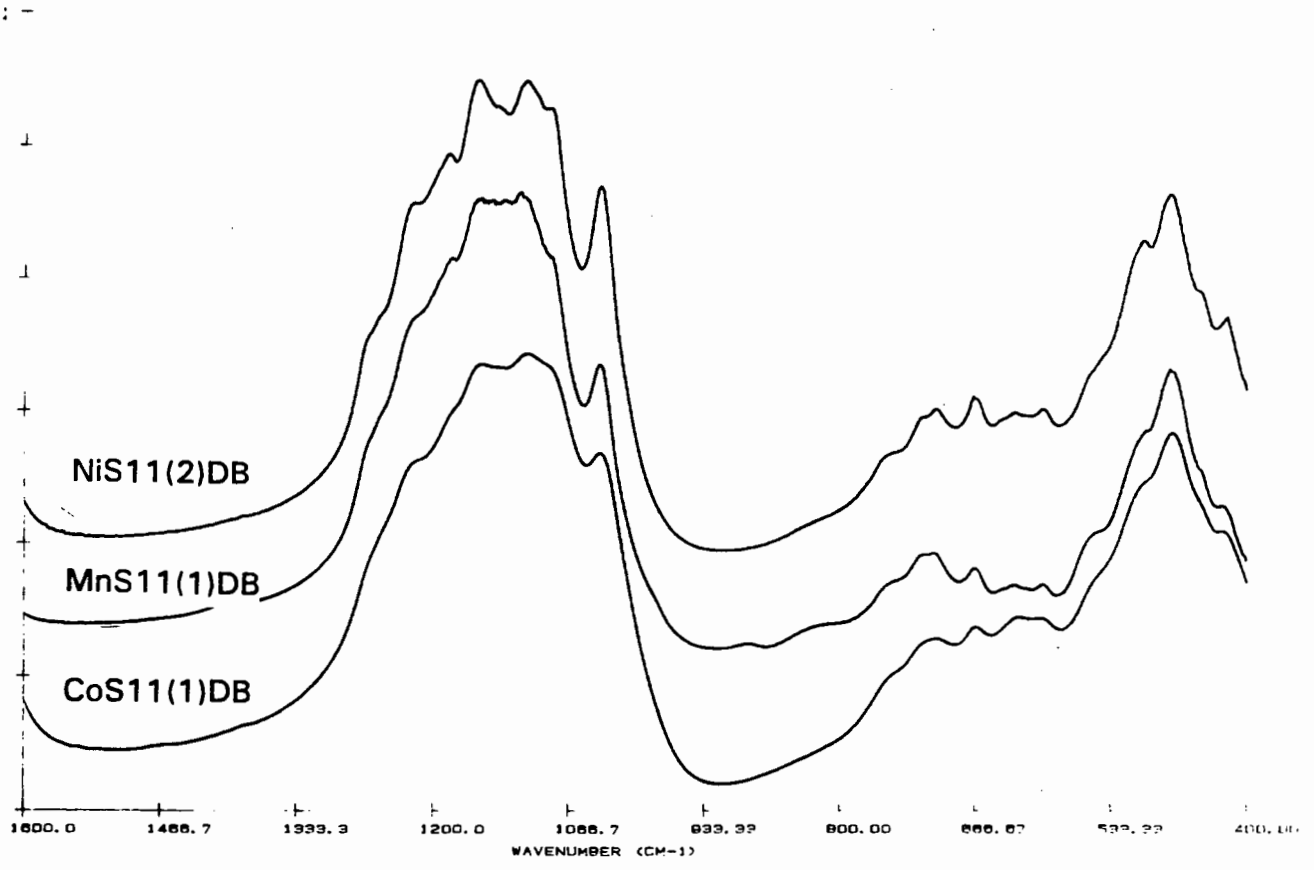
NiS11(2)DB
MnS11(1)DB
CoS11(1)DB
1600.0
1466.7
1933.3
1200.0
1066.7
933.33
800.00
WAVENUMBER (CM-1)

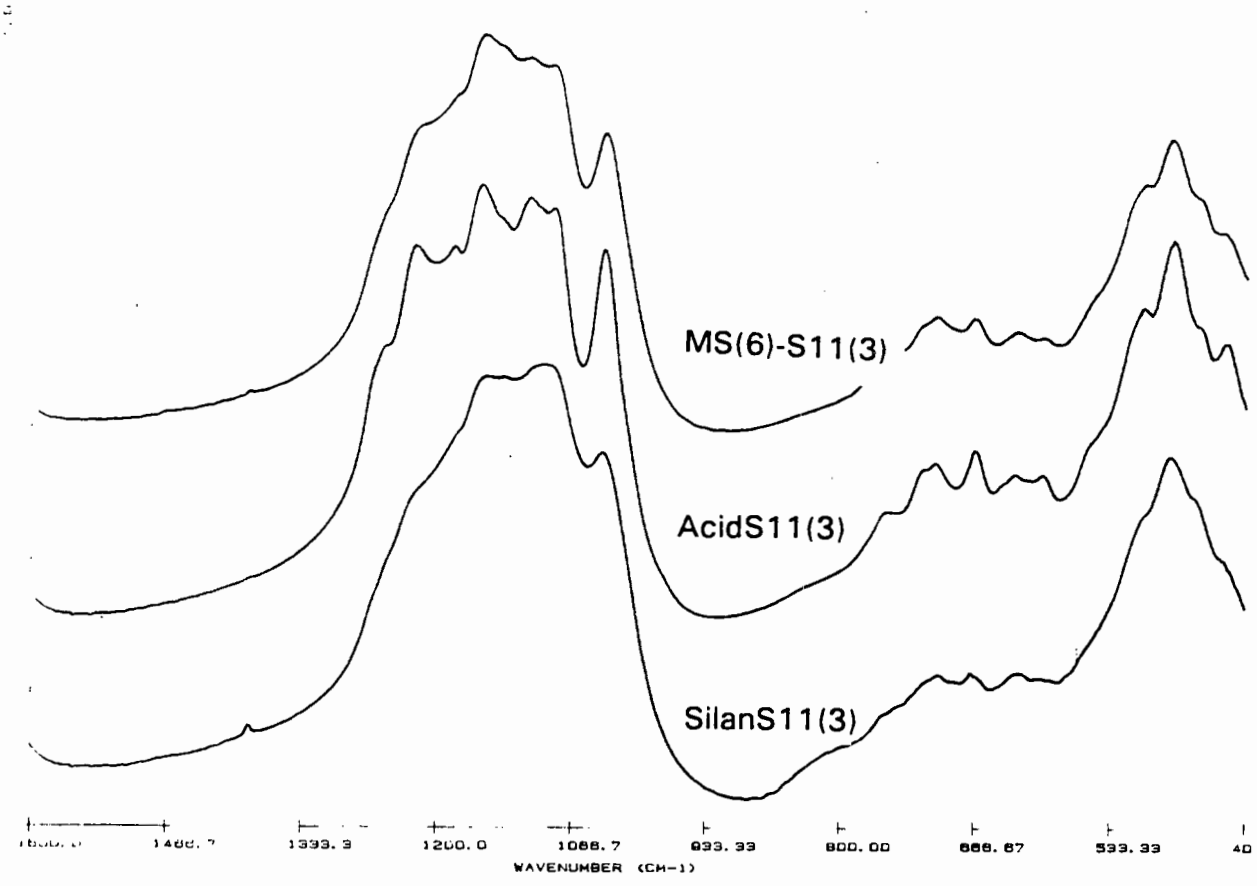
MS(6)-S11(3)
AcidS11(3)
SilanS11(3)
1466. 7
1333. 3
1200. 0
1066. 7
933. 33
800. 00
666. 67
533. 33
WAVENUMBER (CM-1)

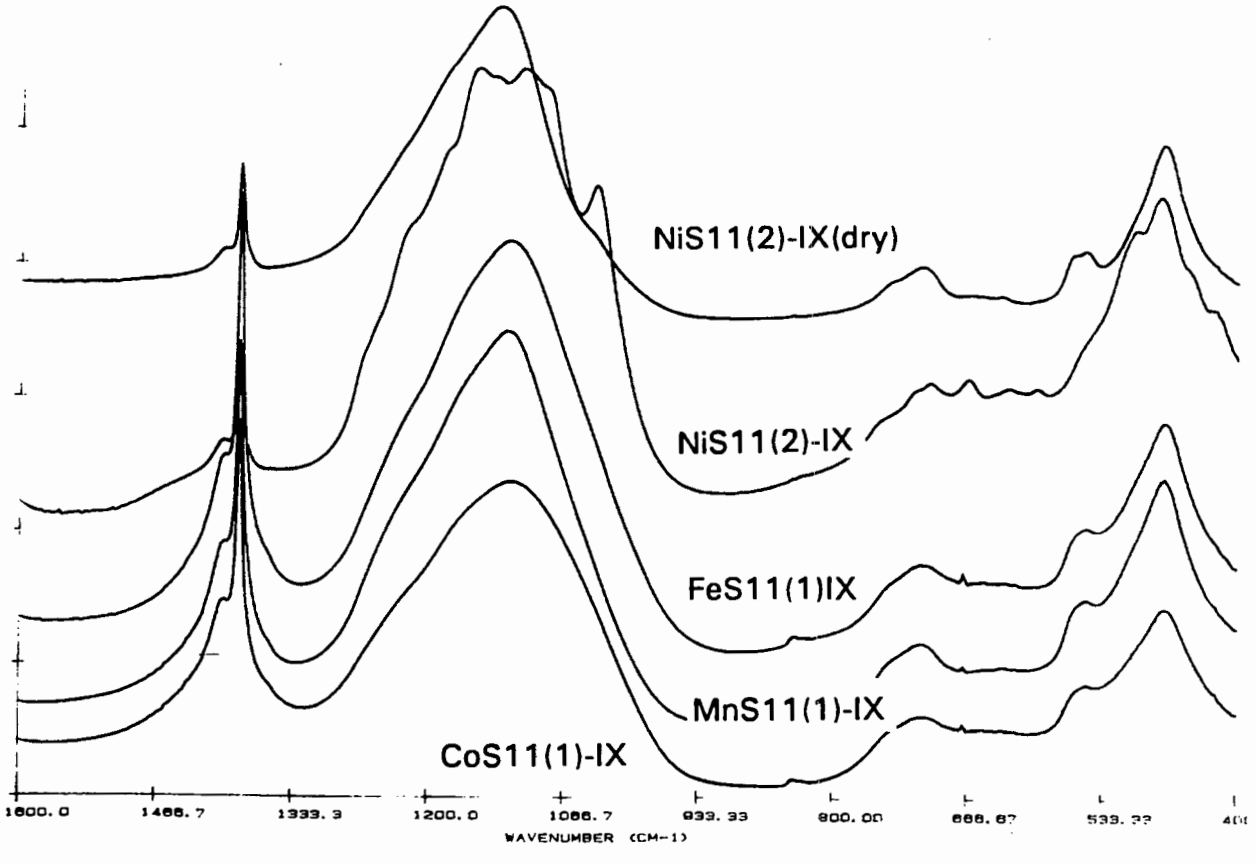
NiS11(2)-IX(dry)
NiS11(2)-IX
FeS11(1)IX
MnS11(1)-IX
CoS11(1)-IX
1600. 0
1466. 7
1333. 3
1200. 0
1066. 7
933. 33
800. 00
666. 67
533. 33
WAVENUMBER (CM-1)

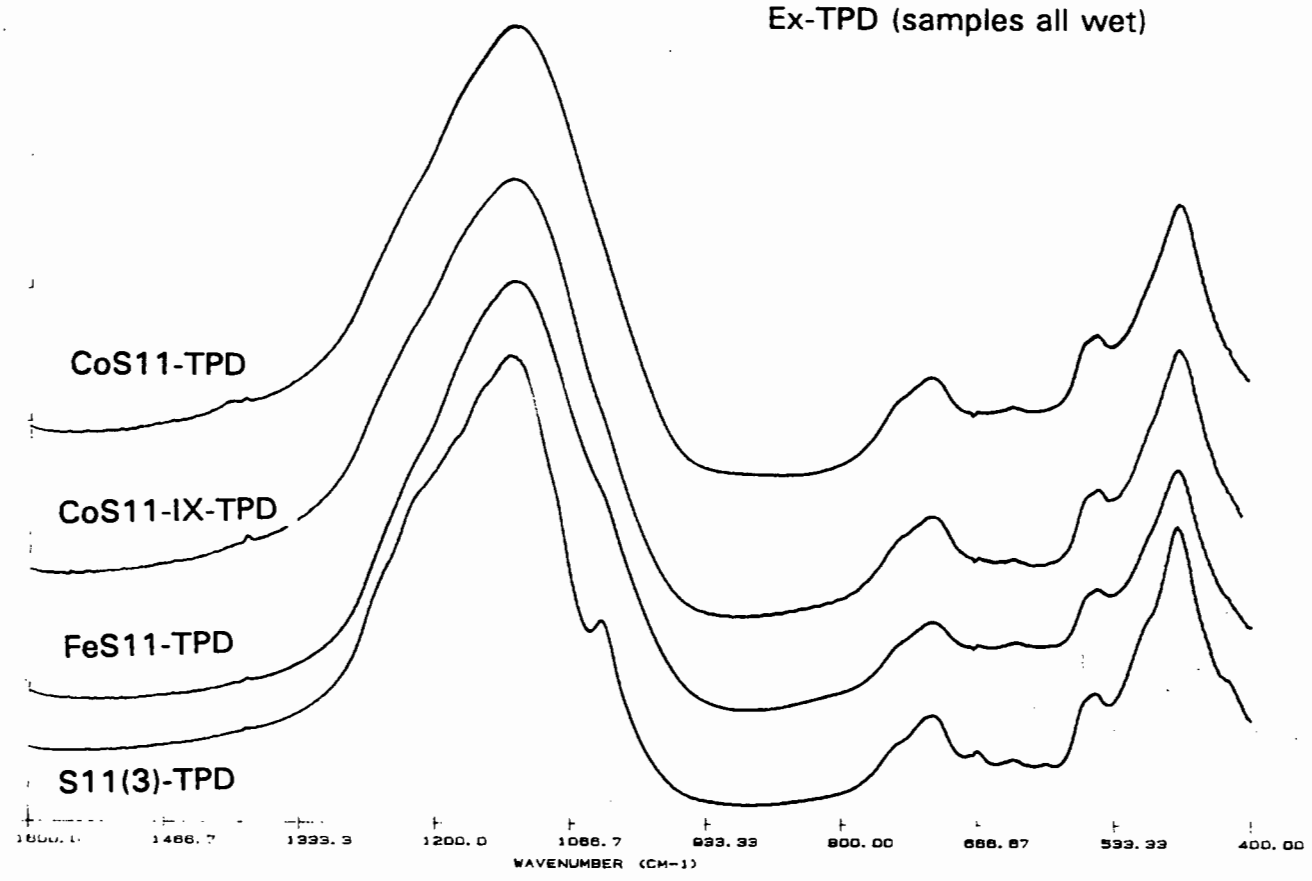
Ex-TPD (samples all wet)
CoS11-TPD
CoS11-IX-TPD
FeS11-TPD
S11(3)-TPD
1600.0
1466.7
1333.3
1200.0
1066.7
933.33
800.00
666.67
533.33
400.00
WAVENUMBER (CM-1)

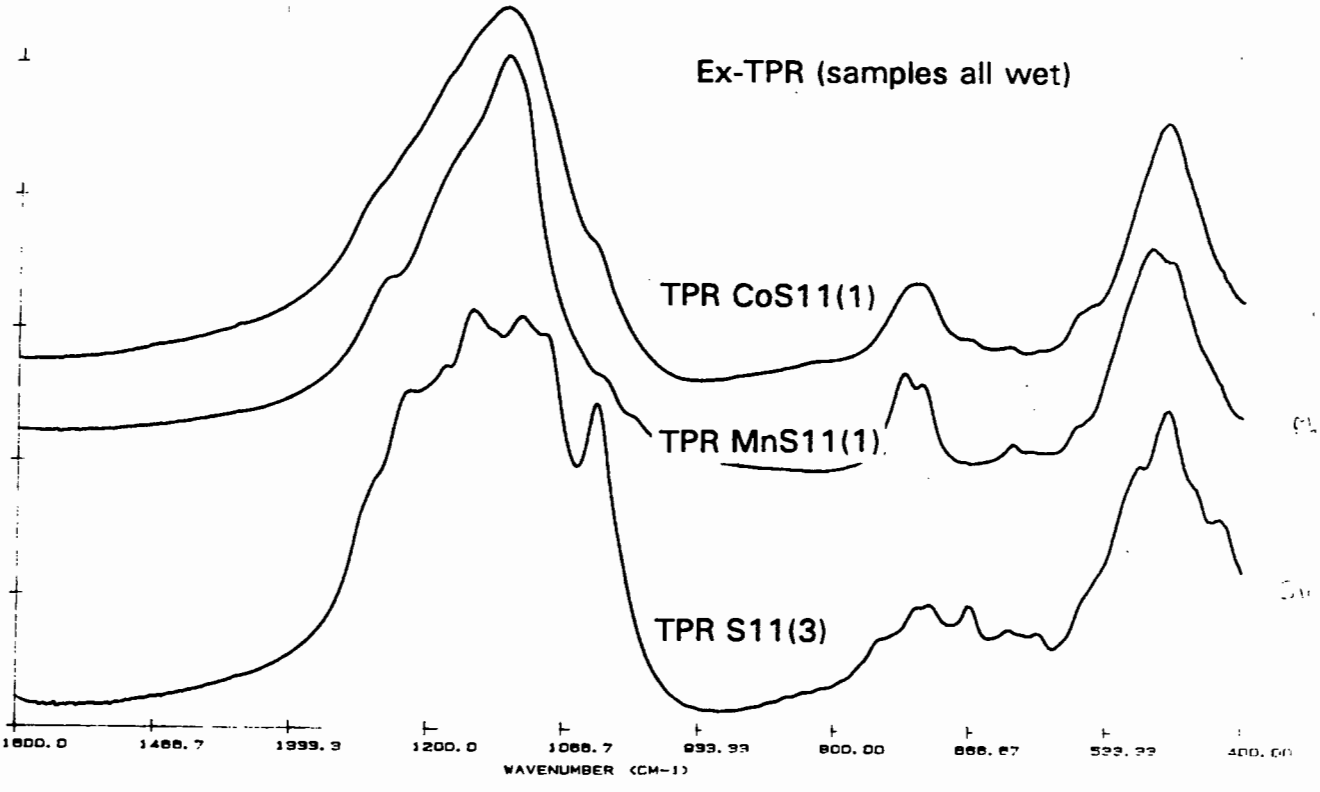
Ex-TPR (samples all wet)
TPR CoS11(1)
TPR MnS11(1)
TPR S11(3)
1600.0
1466.7
1333.3
1200.0
1066.7
933.33
800.00
666.67
533.33
400.00
WAVENUMBER (CM-1)

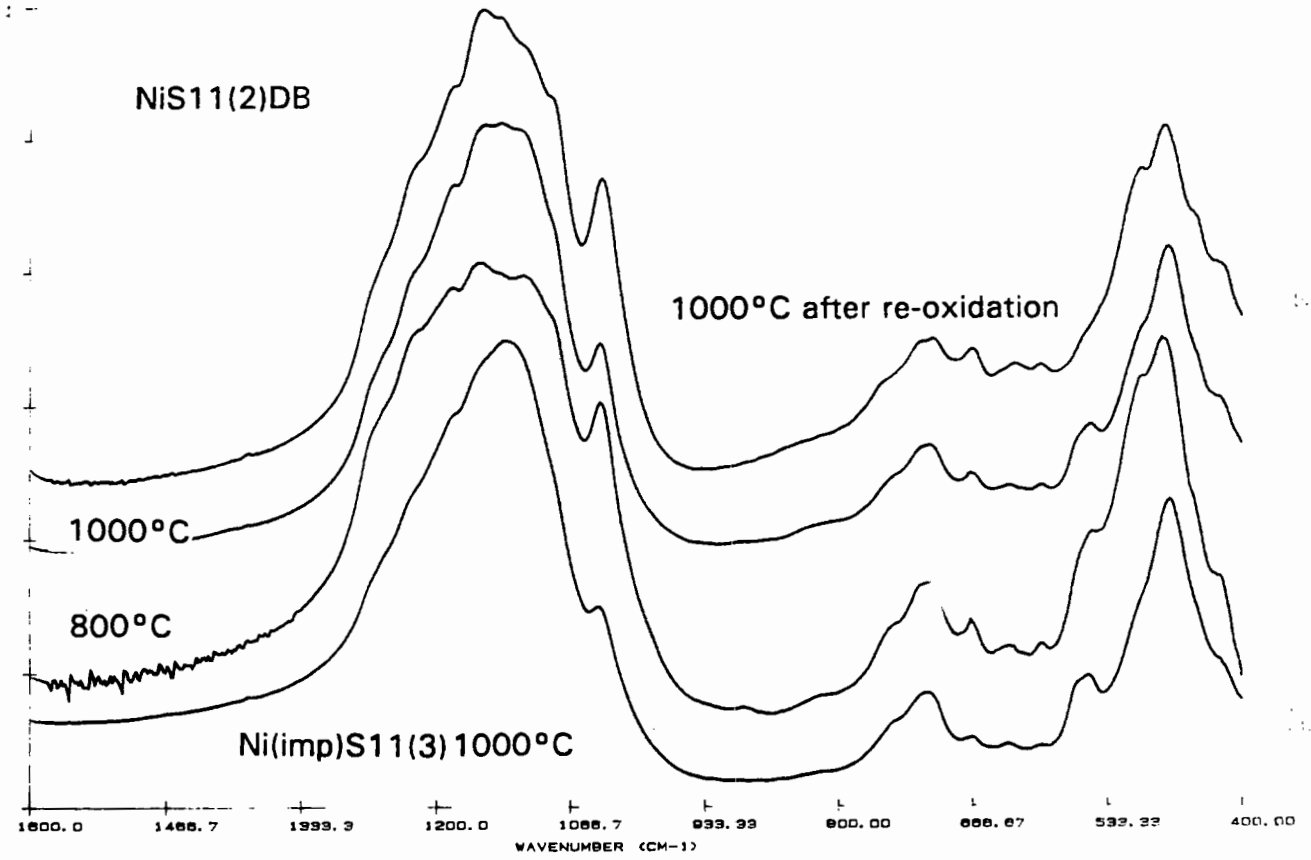
NiS11(2)DB
1000°C after re-oxidation
1000°C
800°C
Ni(imp)S11(3) 1000°C
1600.0
1466.7
1333.3
1200.0
1066.7
933.33
800.00
666.67
533.33
400.00
WAVENUMBER (CM-1)

Appendix VIII. XRDs of HPAs

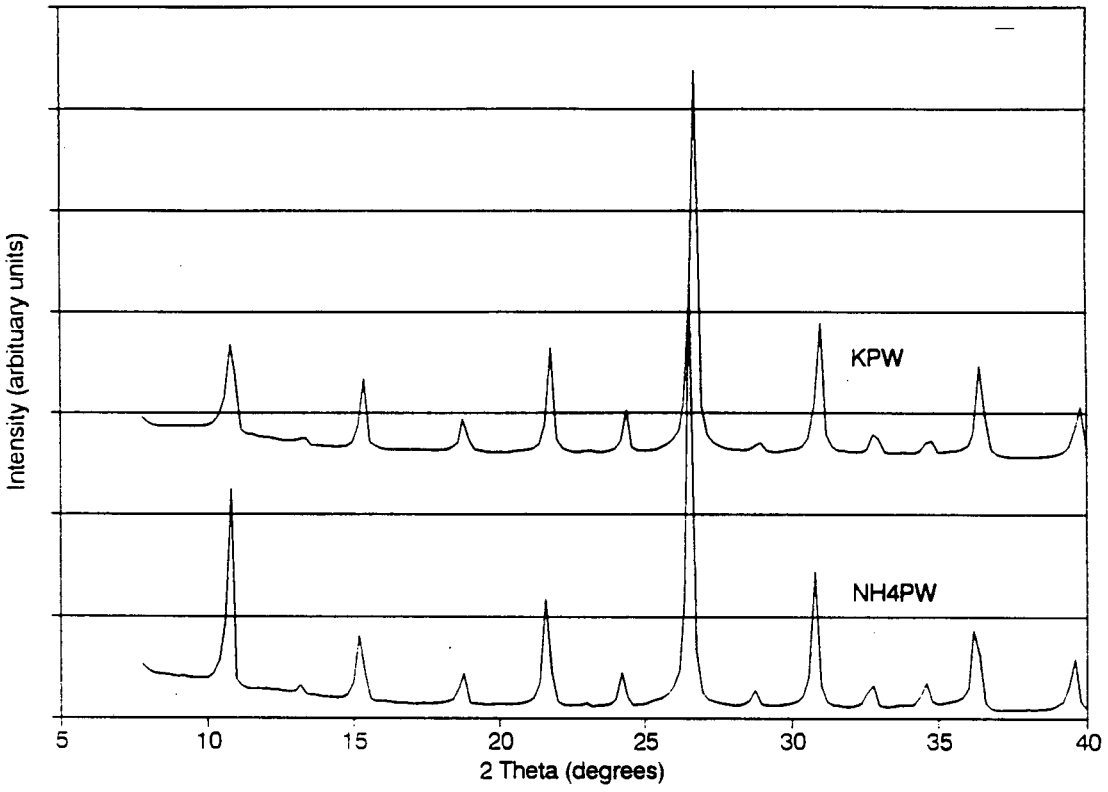

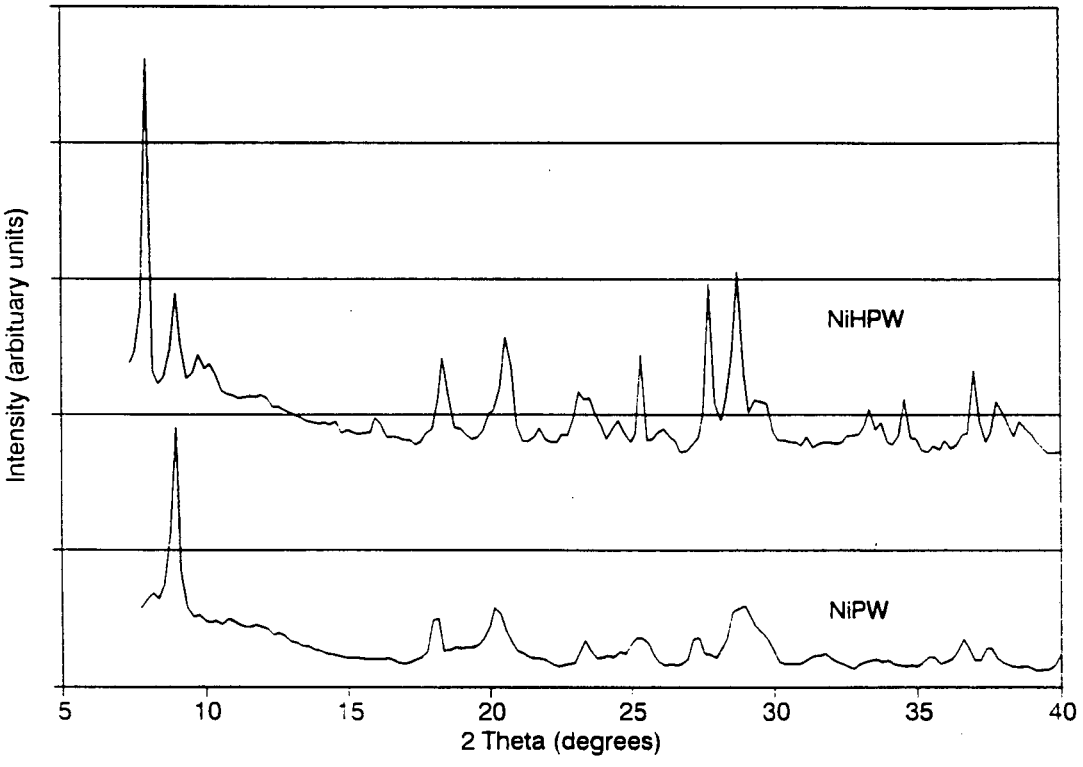

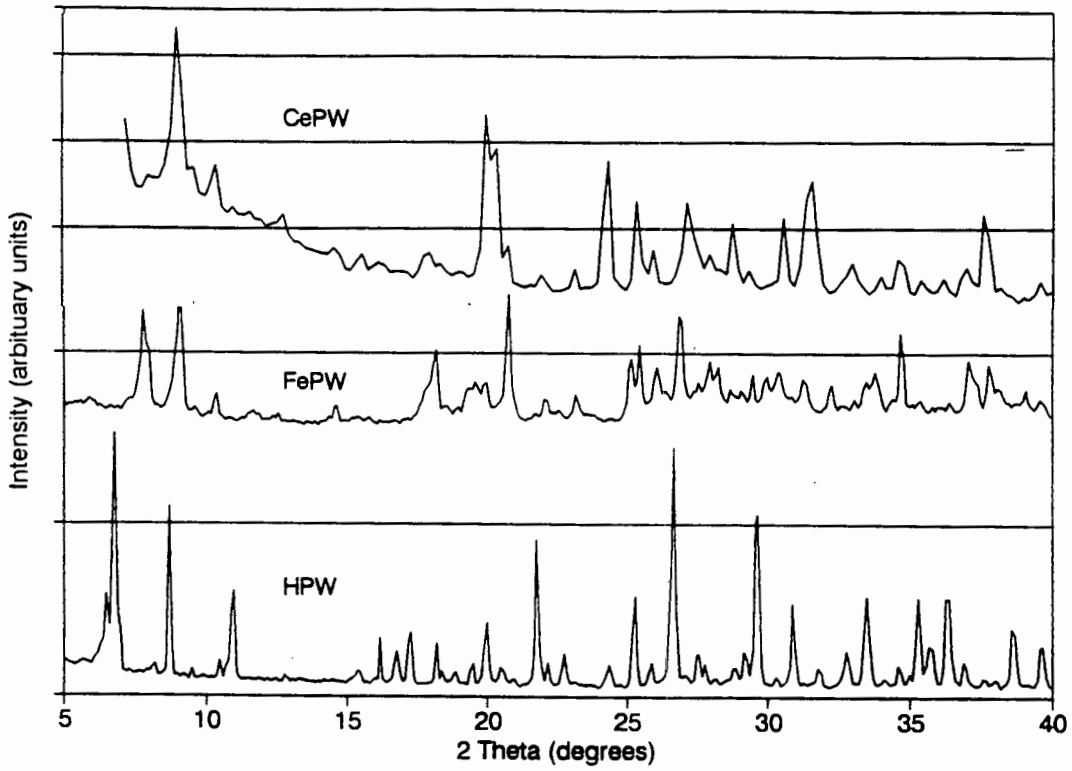
CePW
FePW
HPW
Intensity (arbituary units)
5
10
15
20
25
30
35
40
2 Theta (degrees)

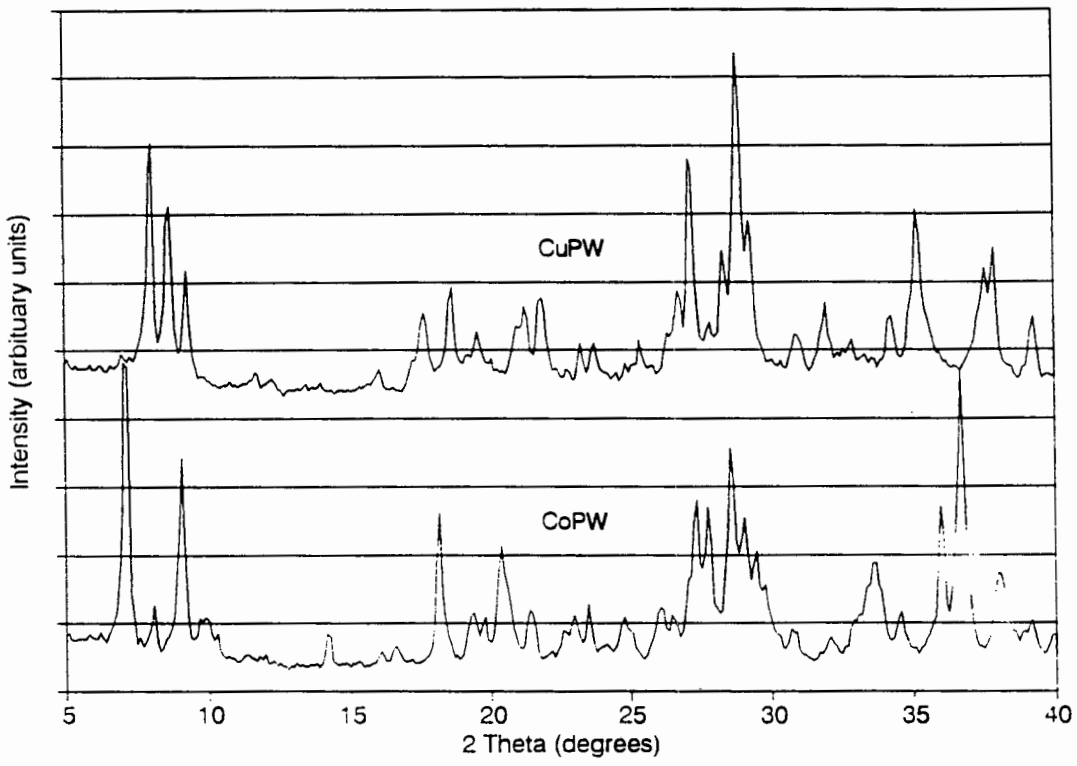
CuPW
CoPW
Intensity (arbituary units)
5
10
15
20
25
30
35
40
2 Theta (degrees)

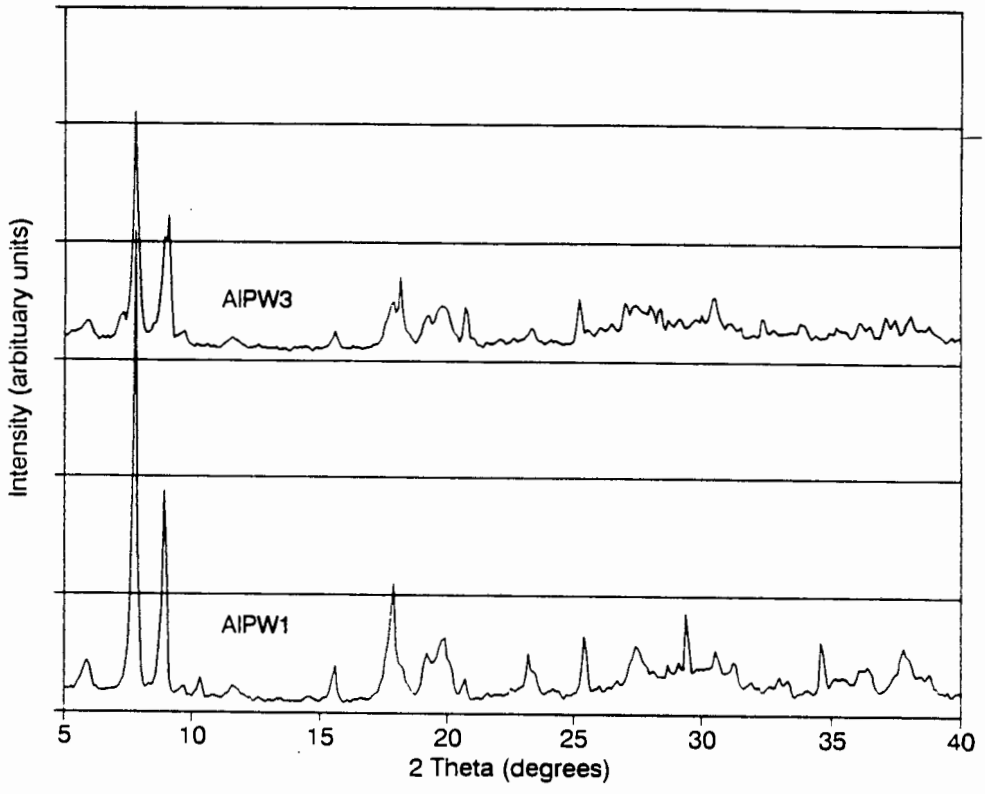
Intensity (arbituary units)
AlPW3
AlPW1
5
10
15
20
25
30
35
40
2 Theta (degrees)

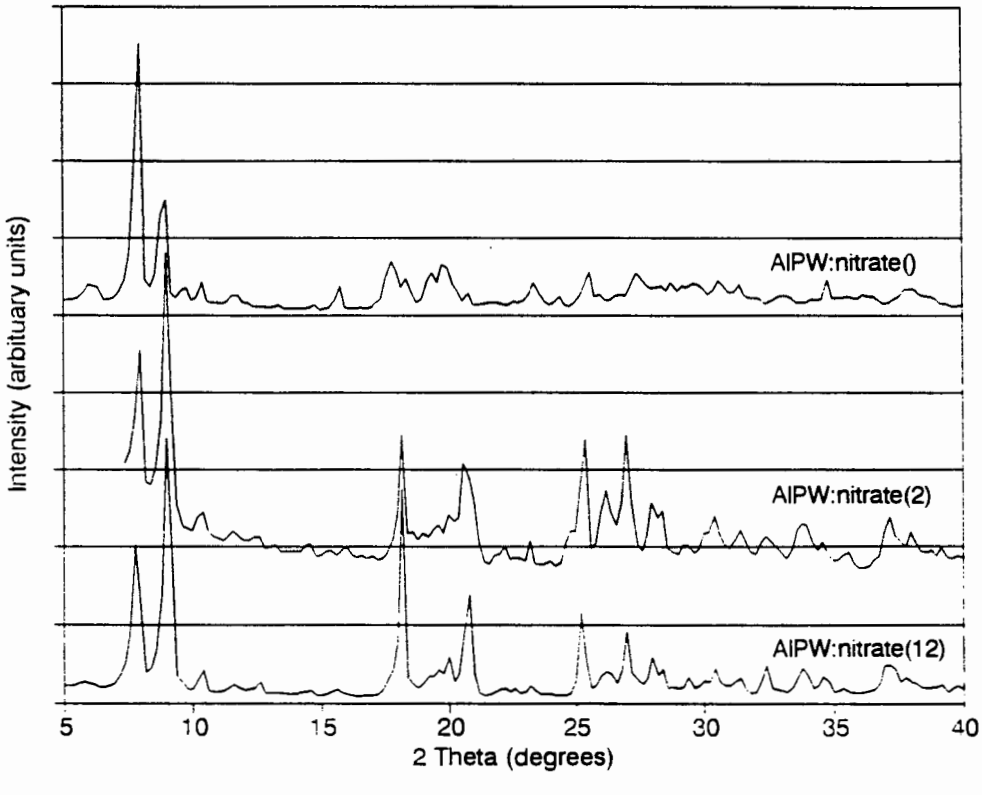
Intensity (arbituary units)
AlPW:nitrate()
AlPW:nitrate(2)
AlPW:nitrate(12)
5
10
15
20
25
30
35
40
2 Theta (degrees)

Appendix VIII. XRDs of SAPOs

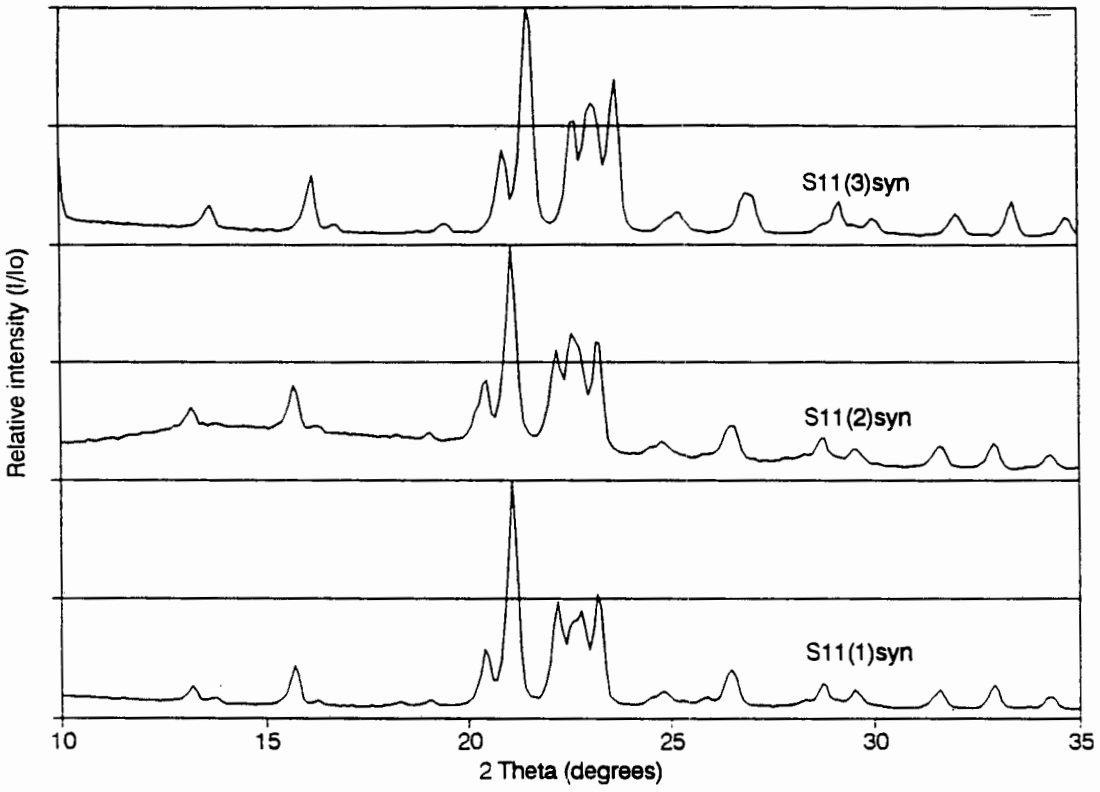

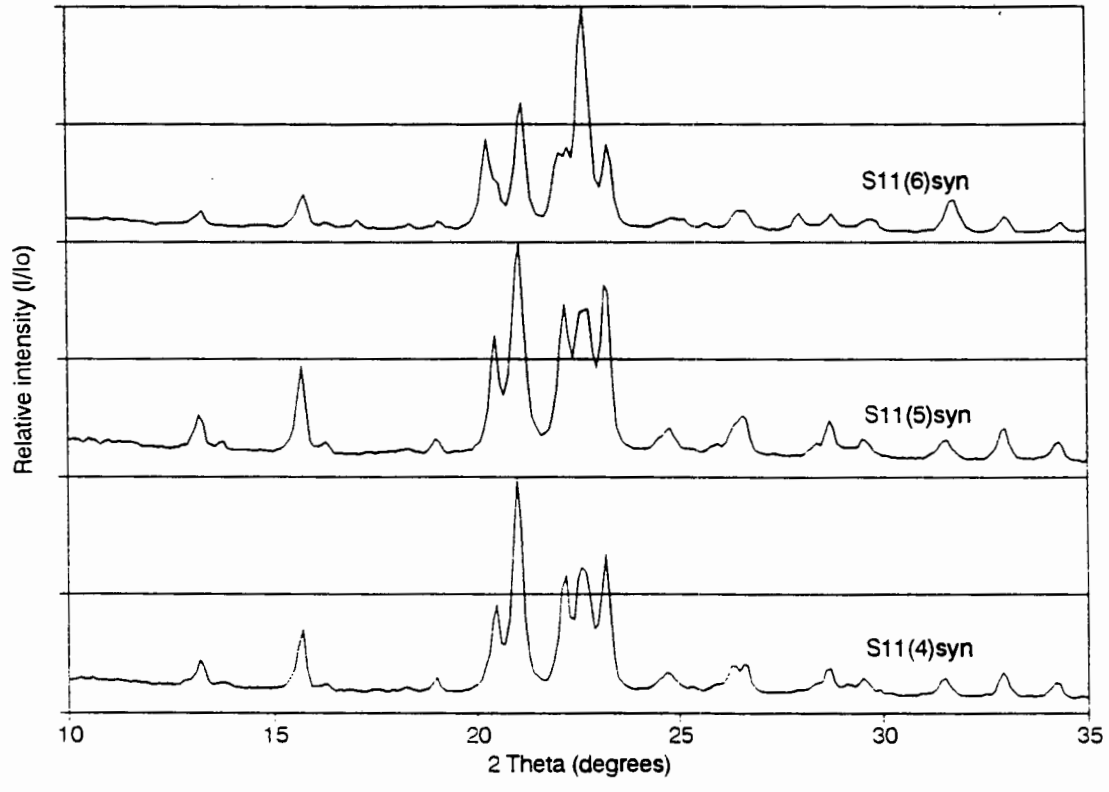

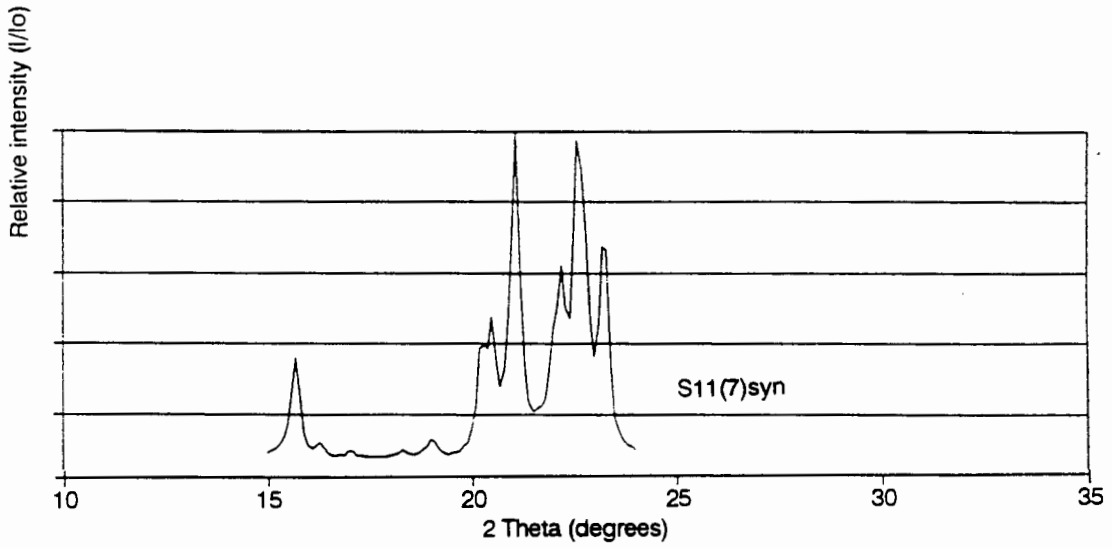
Relative intensity (I/Io)
S11(7)syn
10
15
20
25
30
35
2 Theta (degrees)

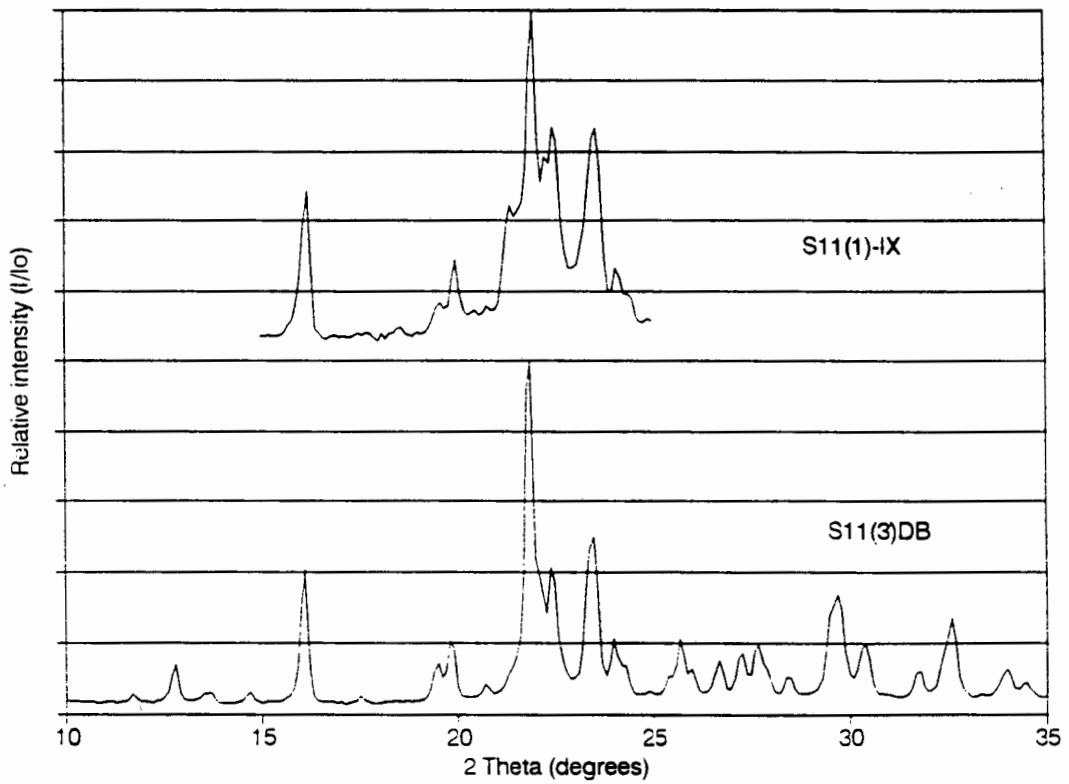
Relative intensity (I/Io)
S11(1)-IX
S11(3)DB
10
15
20
25
30
35
2 Theta (degrees)

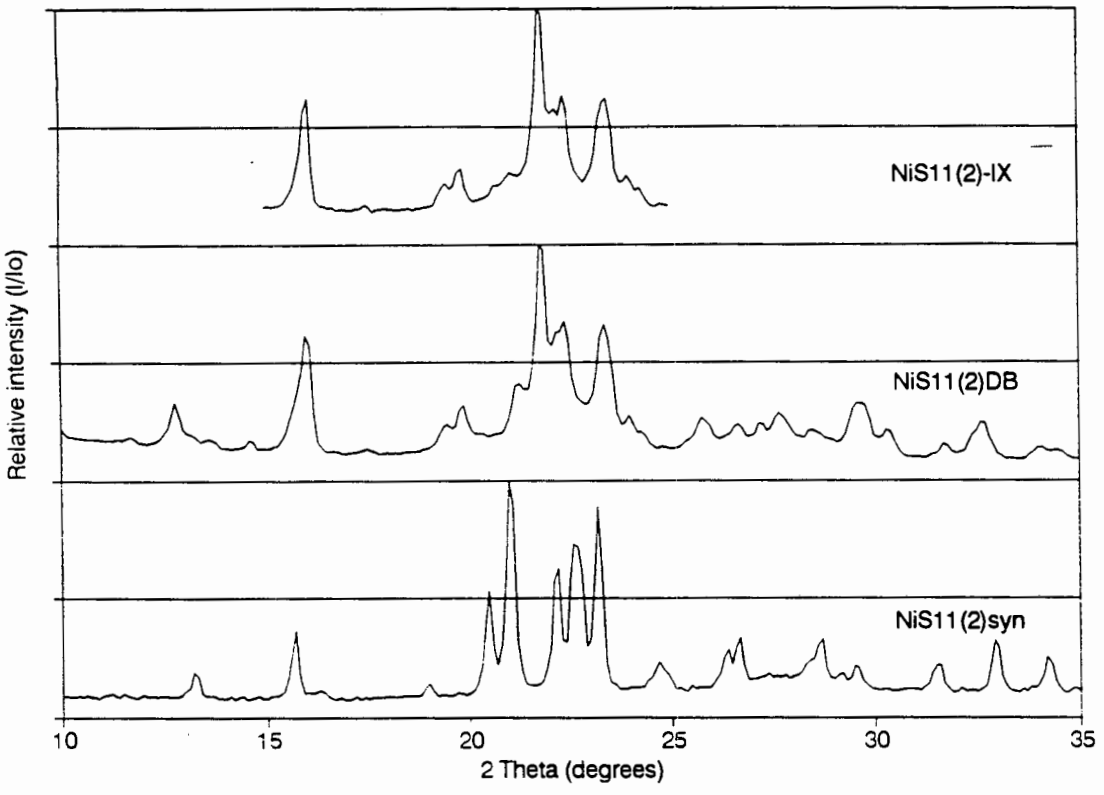
NiS11(2)-IX
NiS11(2)DB
NiS11(2)syn
Relative intensity (I/Io)
10
15
20
25
30
35
2 Theta (degrees)

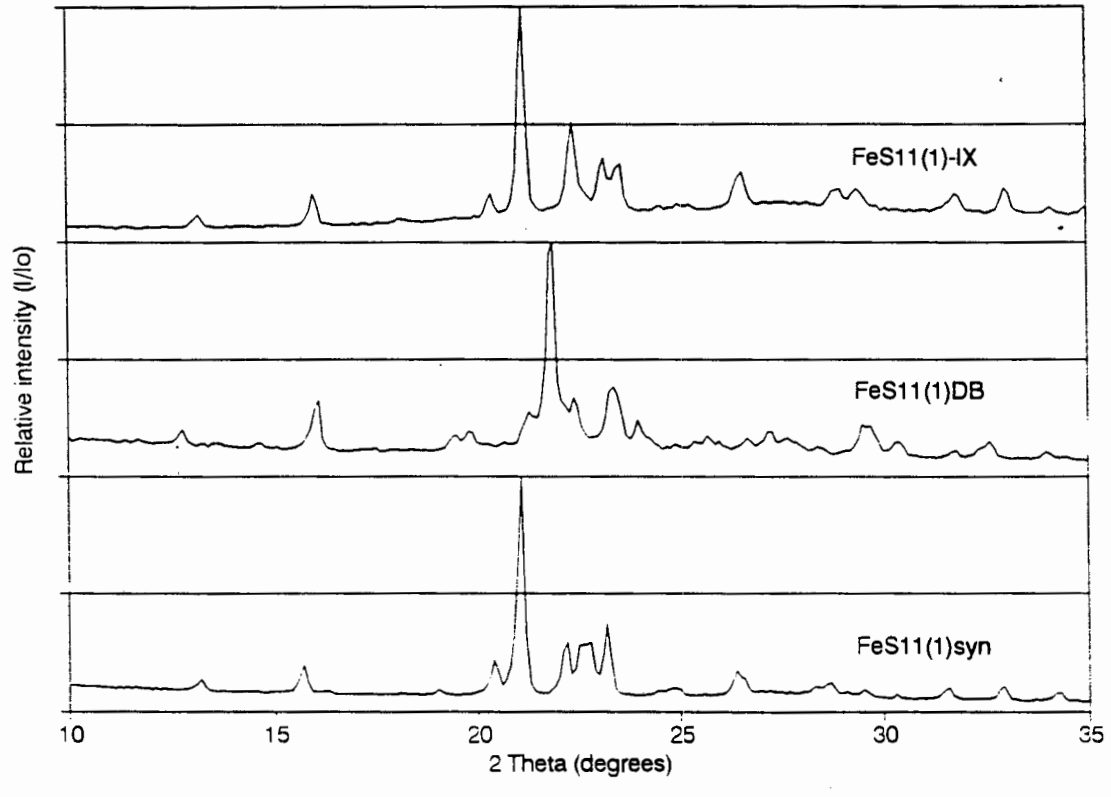
FeS11(1)-IX
FeS11(1)DB
FeS11(1)syn
Relative intensity (I/Io)
10
15
20
25
30
35
2 Theta (degrees)

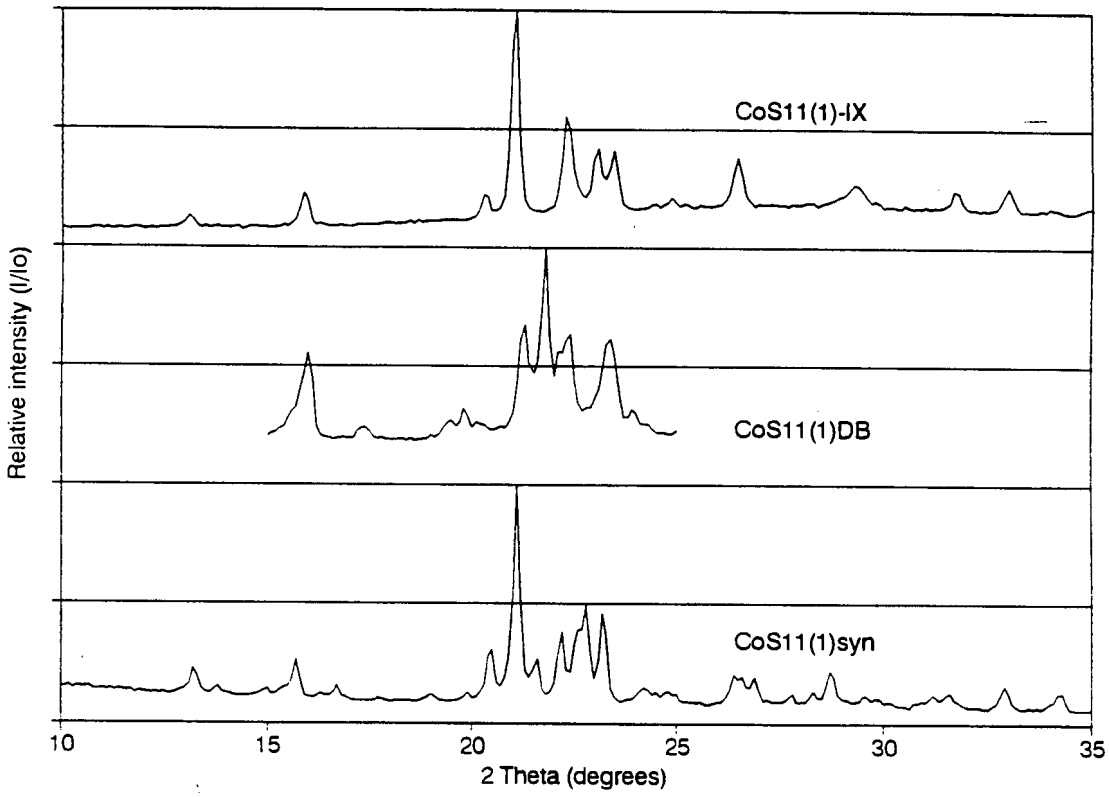
CoS11(1)-IX
CoS11(1)DB
CoS11(1)syn
Relative intensity (I/Io)
10
15
20
25
30
35
2 Theta (degrees)

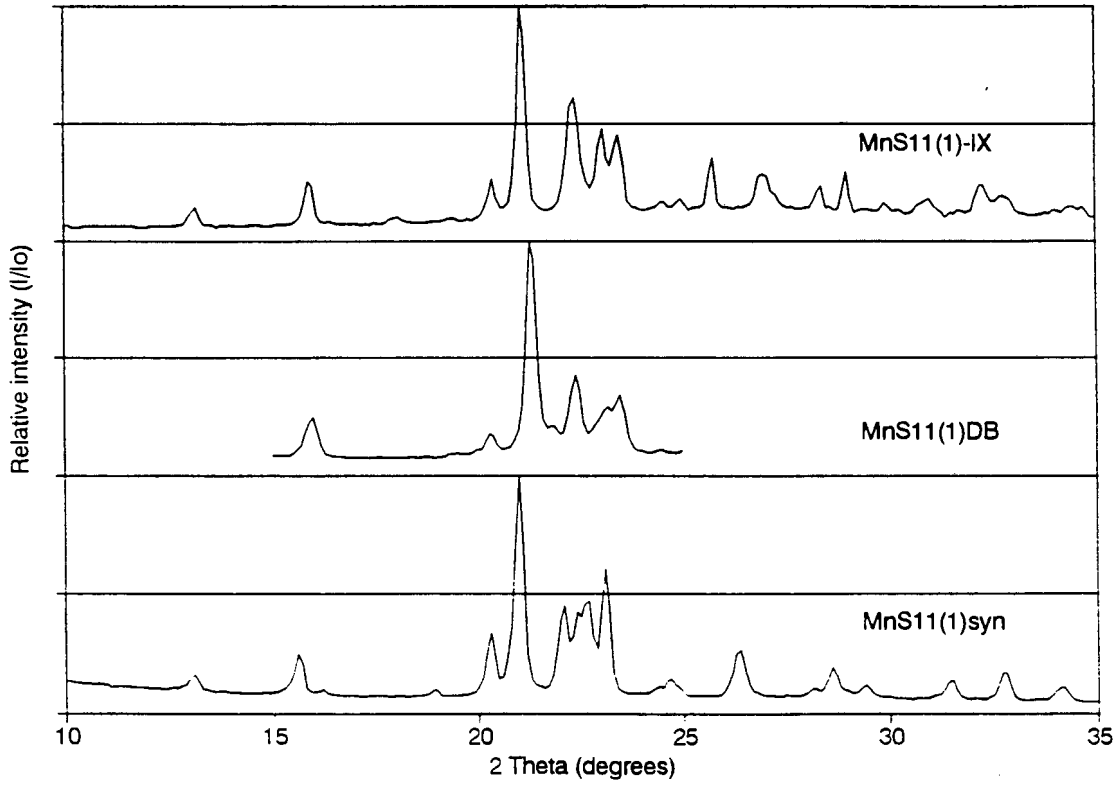
MnS11(1)-IX
MnS11(1)DB
MnS11(1)syn
Relative intensity (I/Io)
10
15
20
25
30
35
2 Theta (degrees)

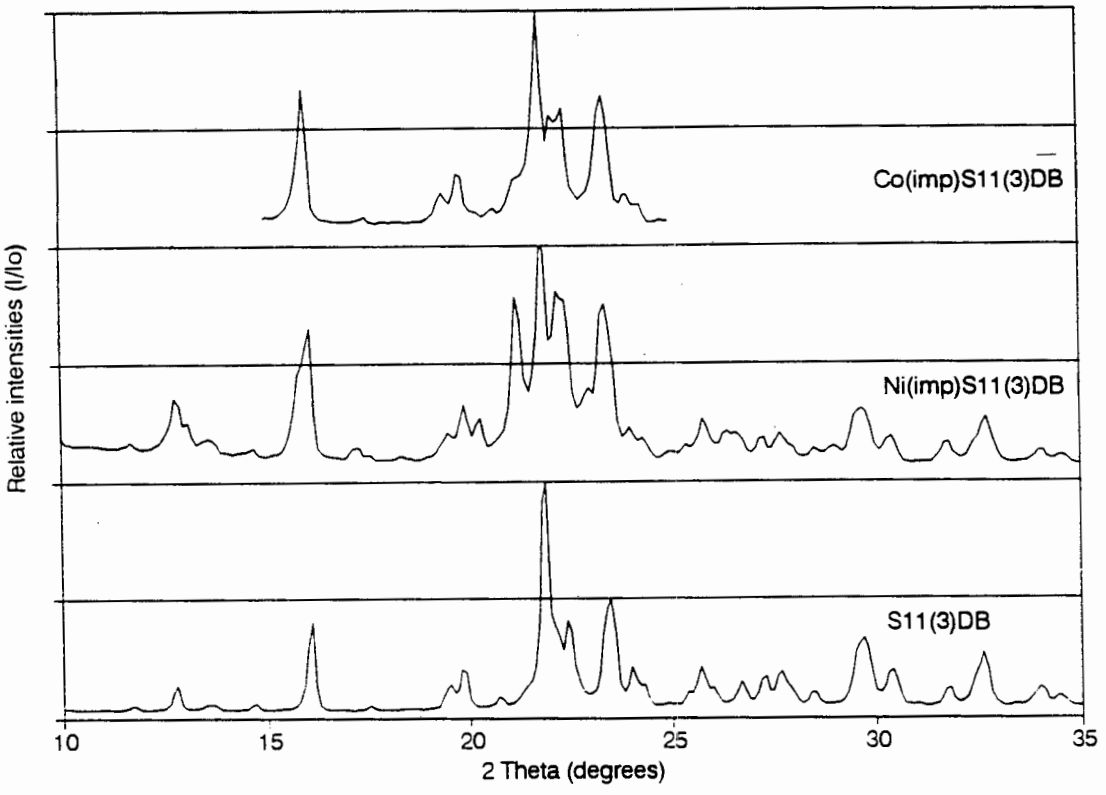
Co(imp)S11(3)DB
Ni(imp)S11(3)DB
S11(3)DB
Relative intensities (I/Io)
10
15
20
25
30
35
2 Theta (degrees)

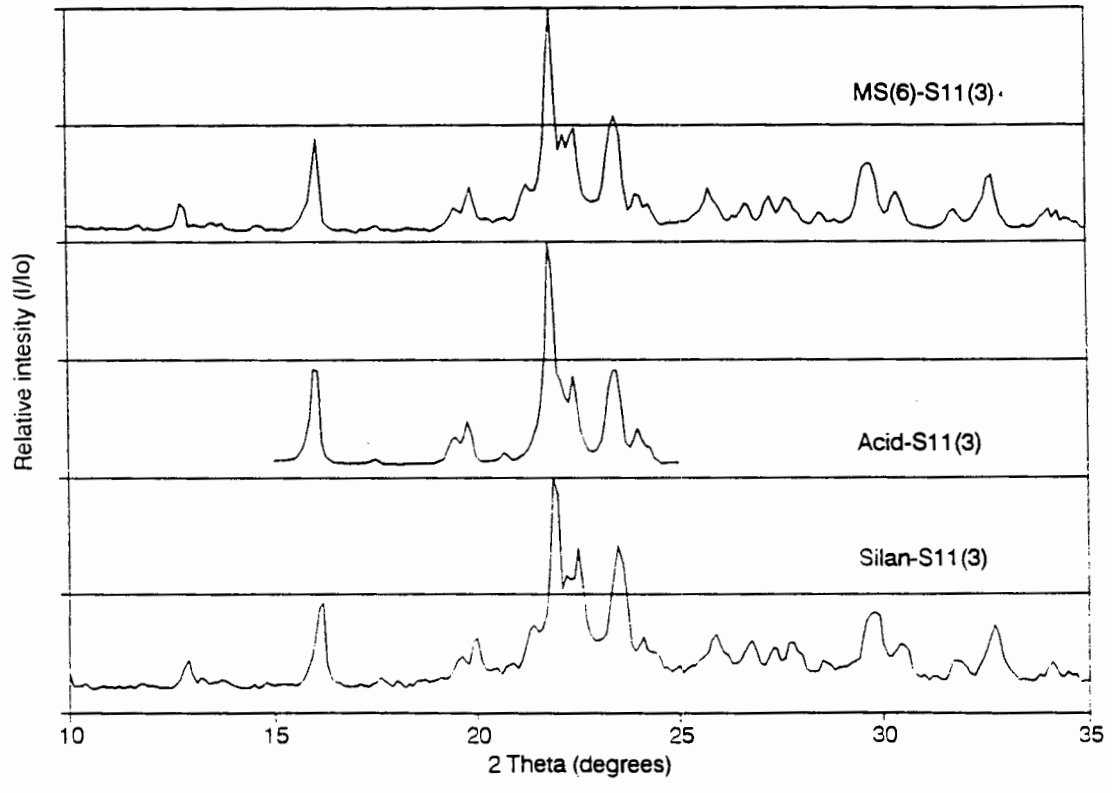
MS(6)-S11(3)
Acid-S11(3)
Silan-S11(3)
Relative intesity (I/Io)
10
15
20
25
30
35
2 Theta (degrees)

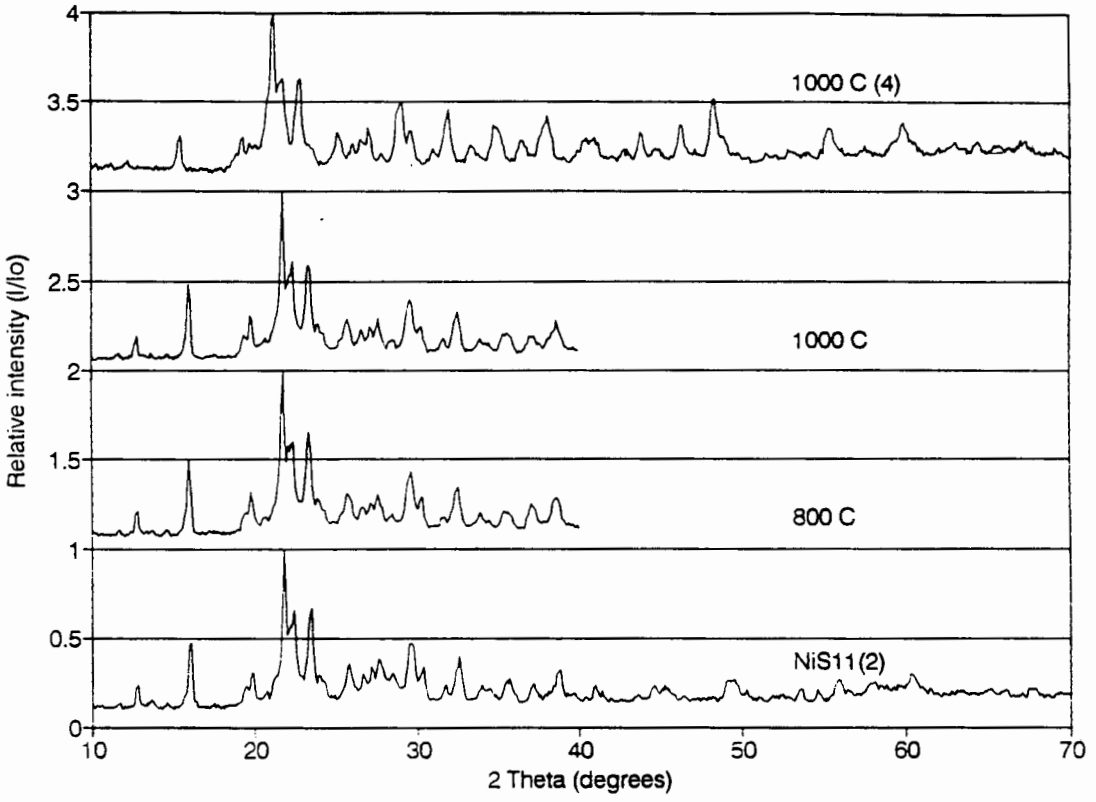
1000 C (4)
1000 C
800 C
NiS11(2)
Relative intensity (I/Io)
2 Theta (degrees)
0
0.5
1
1.5
2
2.5
3
3.5
4
10
20
30
40
50
60
70

Appendix IX. Turn over number (TON) calculations for AlPW and ZSM-5

As it was not possible to determine the number of protons at the surface of the HPA the TON is calculated per Keggin ion at the surface. The approximate size of a Keggin ion is 12Å, and therefore the area occupied by one Keggin ion is 144Å^2.

Knowing the surface area of AlPW:nitrate(2) = 2 m^2/g the number of Keggin ions ate the surface can be calculated as shown below:

No of Keggin units on the surface = $2/1.44 \times 10^{-18} = 1.3888 \times 10^{18}$ KUs

No of propene molecules converted assuming a conversion of 85% of the propene (WHSV = 12h^{-1} of total feed, 86 wt% propene)

number of moles propene converted per hour is

0.86*12*0.86/42 = 0.2113 gmoles/h and therefore number of propene molecules converted per Keggin ion per second is as follows:

= $0.2113*6.023*10^{23}/3600$ = molecules s^{-1}
= $3.6569 * 10^{19}$ molecules of propene per s
TON = $3.6569 * 10^{19}/1.3888 * 10^{18}$
TON = 26.33 molecules of propene/KU s

For ZSM-5, which has a surface area of 350 m^2/g the number of acid sites at the surface are known, for this example a ZSM-5 with a Si/Al ratio of 40 was used and has approximately 0.6 mmol/g.

For 1 g of ZSM-5 and 95% conversion the number of propene molecules converted per second is:

= $4.0395 * 10^{19}$ propenes per s and the no of acid sites
= $0.6 * 10^{-3} * 6.023 * 10^{23} = 3.6138 * 10^{20}$ H

Therefore
TON = $4.0395 * 10^{19}/3.6138 * 10^{20}$
TON = 0.111 moles propene per acid sites per s.

Comparing the TON for AlPW of 26.33 with that for ZSM-5 of 0.11 it can be seen that the TON is ca. 2 orders of magnitude higher for AlPW.

Based on the assumption of propene converting per Keggin ion the number of acid sites at the surface is estimated to be 0.0023 mmol/g for AlPW:nitrate(2) or *ca.* 0.4 % of the total number of acid sites as determined by NH_3-TPD. Note NH_3-TPD probes all sites as it absorbs into the bulk, whereas propene will only desorb on the surface of HPAs.